

ISSN 2458-973X



JSCMT

Journal of
Sustainable Construction
Materials and Technologies

Volume 7
Issue 3
Year 2022

YTU
PRESS

www.jscmt.yildiz.edu.tr



Journal of Sustainable Construction Materials and Technologies
Web page info: <https://jscmt.yildiz.edu.tr>

JSCMT
Journal of Sustainable Construction
Materials and Technologies

Editor In Chief

Prof. Dr. Orhan CANPOLAT
Yildiz Technical University, Türkiye

Assistant Editor

Ekin Paylan
Kare Publishing, Türkiye

Contact

Journal of Sustainable Construction
Materials and Technologies (JSCMT)
Yildiz Technical University
Civil Engineering Department, 34220 Esenler
Istanbul – Türkiye
Web: <https://dergipark.org.tr/en/pub/jscmt>
E-mail: jscmt@yildiz.edu.tr



Honorary Editorial Advisory Board

Tarun R. NAIK
University of Wisconsin-Milwaukee, USA

Editor-In Chief

Orhan Canpolat
Yildiz Technical University, Türkiye

Co-Editors

Rakesh KUMAR
Central Road Research Institute, India

Benchaa BENABED
University of Laghouat, Algeria

Editorial Board

Messaoud SAIDANI
Coventry University, UK

Xiaojian GAO
Harbin Institute of Technology, China

Muammer KOÇ
Hamad bin Khalifa University (HBKU), Qatar

Mohiuddin M KHAN
Washington State University, USA

Mustafa ŞAHMARAN
Hacettepe University, Türkiye

Sudharshan N. RAMAN
Monash University, Malaysia

Roman RABENSEIFER
Slovak University of Technology in Bratislava, Slovakia

Shengwen TANG
Wuhan University, China

Soofia Tahira Elias ÖZKAN
Middle East Technical University, Türkiye



A.S.M. Abdul AWAL
Universiti Teknologi Malaysia, Malaysia

Ghazi G. AL-KHATEEB
Jordan University of Science and Technology, Jordan

Murat ATEŞ
Tekirdag Namik Kemal University, Türkiye

Asad-ur-Rehman KHAN
NED University of Engineering & Technology, Pakistan

Mohammed ARIF KEMAL
Aligarh Muslim University, India

Aravind Krishna SWAMY
Indian Institute of Technology Delhi, India

Mohammed Mosleh SALMAN
College of Engineering Al-Mustansiriya University, Iraq

Ali Najji ATTIYAH
University Of Kufa, Iraq

Sepanta NAIMI
Altinbas University, Türkiye

Siyu REN
School of Economics, Nankai University, China

Language Editors

Mohiuddin M KHAN
Washington State University, USA

Ömer Faruk KURANLI
Yildiz Technical University, Türkiye

Assistant Editor

Ekin Paylan
Kare Publishing, Türkiye



TABLE OF CONTENTS

Title	Pages
Research Articles	
<i>Performance of dredged sediments based controlled low-strength material</i> <i>Pranshoo SOLANKI</i> DOI: 10.47481/jscmt.1119330	119-127
<i>Natural pozzolan-based green geopolymer foam for thermal insulation</i> <i>Kübra EKİZ BARIŞ, Leyla TANAÇAN</i> DOI: 10.47481/jscmt.1142100	128-144
<i>Characterization of carbon fiber reinforced conductive mortars filled with recycled ferrochrome slag aggregates</i> <i>Fatih DOĞAN, Heydar DEHGHANPOUR, Serkan SUBAŞI, Muhammed MARAŞLI</i> DOI: 10.47481/jscmt.1157026	145-157
<i>Effect of fiber type, shape and volume fraction on mechanical and flexural properties of concrete</i> <i>Mahmut BAŞSÜRÜCÜ, Cenk FENERLİ, Ceren KINA, Şadiye Defne AKBAŞ</i> DOI: 10.47481/jscmt.1137088	158-171
<i>An evaluation of vertical dynamic stress attenuation for compacted coarse-grained soils</i> <i>Kuangbiao SUN, Mingjing FANG, Donglin SHU, Yang PU, Wenbing WANG</i> DOI: 10.47481/jscmt.1142438	172-183
<i>Assessment of the adoption of 3D printing technology for construction delivery: A case study of Lagos State, Nigeria</i> <i>Akintayo OPAWOLE, Betty Oluwafunso OLOJEDE, Kahilu KAJÍMO-SHAKANTU</i> DOI: 10.47481/jscmt.1133794	184-197



Review Articles

- Bibliographic analysis on 3D printing in the building and construction industry: Printing systems, material properties, challenges, and future trends* 198-220
Qamar SHAHZAD, Muhammad UMAIR, Saad WAQAR
DOI: [10.47481/jscmt.1143239](https://doi.org/10.47481/jscmt.1143239)
- Effect of thermal variances on flexible pavements* 221-230
Michael Toryila TIZA, Kavnen JIRGBA, Habibu Abubakar SANI, Terlumun SESUGH
DOI: [10.47481/jscmt.1136848](https://doi.org/10.47481/jscmt.1136848)
- A review on engineering biocomposites and natural fiber-reinforced materials* 231-249
Ataberk BAYSAL, Paşa YAYLA, Halit Süleyman TÜRKMEN
DOI: [10.47481/jscmt.1136018](https://doi.org/10.47481/jscmt.1136018)



Research Article

Performance of dredged sediments based controlled low-strength material

Pranshoo SOLANKI*^{ID}

Department of Technology, Construction Management Program, Illinois State University, Illinois, USA

ARTICLE INFO

Article history

Received: 20 May 2022

Accepted: 18 July 2022

Key words:

Concrete, dredged, excavatability, flowable fill, stabilization

ABSTRACT

The process of depleting the natural sources of virgin sand and aggregate makes it challenging to satisfy the demand for construction work. Therefore, in a context of sustainable construction, this study examined the feasibility of utilizing dredged sediments (DS) as a substitute for sand in non-structural controlled low-strength materials (CLSM). A total of two types of dredged sediments, coarser and finer, were collected from two different sources. Then, nine CLSM mixtures were prepared by using different proportions of natural sand (virgin sand) and dredged sediments. Each mixture was tested for flowability, unconfined compressive strength, density and excavatability. Flow consistency decreased with the amount of dredged sediments and presence of finer material in CLSM. Strength results were found within required specification for all nine CLSM tested in this study. Overall, flow consistency, strength and excavatability were found dependent on the characteristics of dredged sediments. This study showed that up to 50% of substitution of sand with DS in CLSM improved strength and density. Furthermore, flow consistency was found to decrease with increase in the amount of DS in CLSM mixtures.

Cite this article as: Solanki, P. (2022). Performance of dredged sediments based controlled low-strength material. *J Sustain Const Mater Technol*, 7(3), 119–127.

1. INTRODUCTION

Dredging of sediments is a critical operation to maintain and improve the global and national water navigation [1], recreation, and defense systems [2]. Additionally, this operation is of great significance for flood prevention by reducing sea level [3], and coastal protection [4]. The materials excavated from waterbodies including waterways and harbors through dredging activities are recognized as dredged sediments (DS). DS is composed of high amount of water and various sizes of solid particles. In terms of the DS's physical and chemical properties, it is significantly different from the natural sand used for construction due to its content of not only salt, but the presence of heavy metals and organic matter [5]. Specifically, DS consists

of a mixture of solid particles, organic/inorganic matter, contaminants (heavy metals and toxic substances), and a high content of liquid (interstitial water). The solid particles include sand, silt, clay, and shells. Moreover, heavy metals (e.g., mercury, cadmium, arsenic, etc.) and toxic substances (e.g., benzene, dioxins, pesticides, naphthalene, etc.) have also been found in DS [6].

According to the United States Army Corps of Engineers [7], the average annual quantity of material removed from waterways and channels in the United States is approximately 152 million m³ (212 million yd³) during fiscal years 2008–2012. In many countries, dredged sediments are considered as waste material. In most of the countries, only about 10% of dredged materials were reused, and 90% were either dumped into the sea or used for land reclamation [5, 8, 9].

*Corresponding author.

*E-mail address: psolanki@ilstu.edu



According to McNeil [10], USACE dredge 152 million m³ (200 million yd³) of DS per year nationwide to maintain channels' navigation. Approximately, 38 million m³ (50 million yd³) DS are beneficially reused and 116 million m³ (150 million yd³) provide opportunity [10]). This 116 million m³ (150 million yd³) DS are enough for covering 1 m (1.1 yard) of approximately 10,918 soccer fields. Some of the beneficial applications of dredged material are for beach nourishment, topsoil creation/enhancement, land creation/enhancement, habitat restoration and construction materials [11].

Literature review indicates that several researchers studied beneficial use of DS as a sand substitute in concrete materials. However, DS has not been widely used in concrete materials in the US. There appears to be three barriers. Barrier #1) The first is that concrete utilized in pavements or structures must meet tight specifications/standards, and only frequently tested/used materials are relied upon to meet those specifications/standards. Barrier #2) Contamination of DS could potentially impact performance of concrete materials. If DS is used directly then low pH and high salinity may corrode the reinforcement and increase the possibility of chloride attack [12, 13]. Barrier #3) The variability of DS due to spatial location, dredging operation, and material placement is also a concern in receiving consistent quality of material for reusing in concrete [14]. Physically, DS particles can range from sand to fine clay sizes. Chemically, DS may be clean or may contain any variety of contaminants as well as valuable nutrients [11].

The current research investigated an innovation that has the potential to address all four of these barriers from environmental and economic standpoints. Controlled low-strength material (CLSM) (also known as "flowable fill") is a concrete material which is used for backfilling utility trenches and excavations. It is applied as a flowable liquid, allowing voids to be easily filled and avoiding labor costs associated with compacted fill, yet is sufficiently low in strength to allow easy re-excavation [15]. Any ready-mix concrete plant can produce CLSM. These characteristics have resulted in increasing popularity of flowable fill [16].

The use of DS in CLSM could potentially address all three aforementioned barriers of utilizing dredged material in construction. First, CLSM mix is non-structural and specified by contractors or local agency [15]. Therefore, use of DS in CLSM imposes less risk compared to structural concrete. This will allow ready-mix plants to gain confidence and experience with DS, encouraging its use in other concrete mixtures in future. Second, CLSM requires low performance standards due to which it could tolerate contaminated DS materials. Third, inferior quality of sand that do not meet structural and pavement concrete standards are often acceptable in CLSM [15].

2. BRIEF REVIEW OF PREVIOUS STUDIES

Tarabdkar [17] created artificial aggregates using the accelerated carbonation technique, in which a mixture of sediments, water, and Portland cement were carbonated in a 100% carbon dioxide atmosphere. The accelerated carbonation technique improved the material's properties by facilitating carbon dioxide sequestration. Various artificial aggregate mixtures were analyzed using a statistical technique. Small scale experiments were carried out to determine the key process parameters for process optimization. The optimal mixture was composed of 55% sediments, 25% Portland cement, and 20% water. The mixture was carbonated in a tumbler for 2 hours to produce artificial aggregates. Full-scale experiments on the optimal mixture were carried out while key process parameters were considered. Artificial aggregates were uniformly graded, according to particle size analysis. Scanning Electron Microscopy (SEM) and thermogravimetric analysis revealed that a higher percentage of clay in the sediments caused the formation of two distinct layers in an aggregate, obstructing the uniform formation of CaCO₃. The results of the pH-dependent leaching tests revealed that metals were released at a lower rate in carbonated artificial aggregates than in uncarbonated raw sediments. Finally, it was determined that artificial carbonation of contaminated sediments can produce artificial aggregates that can be used for beneficial purposes.

Kim and Pradhan [18] evaluated stabilized organic dredged soils by conducting unconfined compression tests, pH tests, and seed germination experiments. To assess the impact of the organic content on the mechanical and germination characteristics of the stabilized soils, several mixtures with organic contents ranging from 0 to 30% by mass and binder contents ranging from 5 to 15% were prepared. It was found that a stabilized organic soil's strength and pH fall as its organic content rises, creating ideal germination circumstances. With an increase in organic content, both the germination rate and plant growth rate dramatically increased. The soil's strength was boosted by adding binder to mixtures, but the pH was also raised. As the organic content increased, the stability of the soils became weaker. This was explained by humic acid's affinity for the calcium in the soil. Increased soil nitrogen concentration was associated with a lower pH. Higher seed germination rates in mixtures with more organic material resulted in plants with more height and biomass overall. Shorter seed germination rates brought for plants with lower heights and less total biomass when binder levels were higher. This was related to both the increased soil strength, which inhibits root growth, and the decreased availability of nutrients at the higher pH with increased binder levels.

Kaliannan et al. [19] demonstrated that the addition of ground granulated blast furnace slag could minimize the cement content in solidification of dredged marine soils. Dredged marine soils had extremely low stiffness,

low load-bearing capacity, high compressibility, and low permeability in the absence of solidification. The properties of the dredged marine soil were enhanced by the cement and slag mixture. The mix containing binder content of 3% cement and 7% slag was found to show greatest solidification outcome.

Rabbanifar [20] stabilized dredged material using hydrated lime (HL) and fly ash (FA) type F. The mechanical and physiochemical properties of the dredged material stabilized with HL and FA were evaluated after 7, 28, and 90 days of curing. The results revealed that the combination of HL and FA could effectively increase the compressive strength and decrease plasticity index of stabilized dredged material. SEM imaging revealed formation of gel covers on smaller particles, holding them together to form larger clusters. New compounds were formed, according to X-ray diffraction tests. A non-linear multi variable model was developed based on the experimental results of the study using the software R (R Studio) for predicting properties such as density and strength of the stabilized dredged material mix. The findings showed that dredged material could be successfully stabilized using HL and FA with predictable properties, transforming it into an environmentally friendly high-quality construction material.

Do et al. [21] investigated CLSM developed using a blend of natural sand, marine dredged soil (MDS), and binders, in geothermal systems. This study looked at flowability, fresh density, unconfined compressive strength, thermal conductivity, bleeding rate, and environmental impacts, among other factors. To evaluate total cost, a bleeding-rate-based volume compensation premise for an actual large-scale geothermal system was described. In terms of general and environmental properties, all the prepared CLSM mixtures performed well. Furthermore, the developed CLSM-based grout showed significantly higher thermal conductivity than conventional grouts. More importantly, an extremely positive effect of MDS was discovered: an appropriate addition of MDS to CLSM-based grout can result in a significant reduction in bleeding rate, resulting in only a small volume compensation of required boreholes.

In a recent study, Abidi et al. [22] investigated the viability of employing different percentages of dredged sediments from the Bouhanifia dam as an additive to calcareous tuff which is a natural material commonly used in road construction in Algeria. The physical, chemical, and mineralogical features of the sediments and tuff, as well as short-term mechanical performance tests, were used to make a general estimate of their long-term mechanical behavior. The study suggested that tuff admixed sediments could be used as an embankment or subgrade material; however, long-term mechanical behavior testing of these materials is required, and mechanical stabilization is recommended to improve their geomechanical behavior, as sediments are expected to have lower strength than tuff.

In another recent study, Shi et al. [23] investigated the effects of moisture content, maximum steel slag particle size, curing age, and cement and steel slag ratio on the compressive strength of dredged silty clay in a plastic flow condition. By contrasting the results of relevant earlier investigations, the performance enhancement of dredged silty clay stabilized with cement and steel slag was examined. Microstructural observation was used to investigate the strengthening process of dredged soils stabilized with cement and steel slag. The findings demonstrated that the strength qualities of dredged silty clay stabilized by cement and steel slag could guarantee the minimum requirements of the project larger than 100 kPa when the ratio of cement to steel slag was 9:6; specifically, utilizing steel slag to replace 40% of cement. The stabilizing effect improved with increasing steel slag particle fineness. With particle sizes of less than 0.075 mm, dredged silty clay stabilized with cement and steel slag showed compressive strengths that were 1.06, 1.10, and 1.16 times greater than those of 0.25 mm, 1 mm, and 2 mm, respectively. Additionally, the compressive strength increased linearly over curing ages up to 28 days. Dredged silty clay stabilized by cement and steel slag showed a compressive strength that was 2.44 times, 1.59 times, and 1.36 times greater than that of 3, 7, and 14 days, respectively. Due to the formation of more calcium silicate hydrate and other agglomerated flocculent gel materials because of the continued reaction between steel slag and cement hydration products, the structural compactness of dredged soil.

3. MATERIALS AND METHODS

3.1 Dredged Sediments and Natural Sand

The DS samples were obtained from two sources in coordination with USACE. The first sample, called as DS#1 in this study, was randomly collected from stockpiles located close to Illinois River in Glasford, Illinois. It was sitting in two piles with approximate height of forty feet. The top of the pile was washed away by rain revealing large quantities of clam shells, but the collection of material was deeper into the pile to make sure not to get washed-out material. The second sample, called as DS#2 in this study, was the stockpile next to Calumet Harbor (south side of Lake Michigan) in Chicago, Illinois. Specifically, DS#2 samples were collected from three separate stockpiles and then remixed in the laboratory before testing.

The sand used was naturally collected, not manufactured, from a pit located in Heyworth, IL. This sand was named as natural sand (NS) in this study. NS was collected by dredging under water and then sieved on US#200 (0.075 mm) for removing fines. Other than this, the sand is kept natural in most part. Figure 1 shows a photographic view of NS, DS#1 and DS#2. It is evident from Figure 1 that NS looks coarser than DS. Also, chunks of clumped clayey material are visible in DS#2.



Figure 1. Leftmost pan shows natural sand, middle pan shows DS#1 and rightmost pan shows DS#2.

For gradation analysis, sieve analysis was performed on two samples of NS, DS#1 and DS#2 in accordance with ASTM C136 test method. The results were compared to the upper limit (UL) and lower limit (LL) sieve sizes recommended by the Illinois Department of Transportation (IDOT) (2016) for CLSM sand (fine aggregates), called as FA-1 by IDOT. Figure 2 shows gradation of NS, DS#1 and DS#2. Additionally, IDOT UL and LL are also plotted for comparison on Figure 2. It is evident from Figure 2 that NS gradation is within IDOT’s LL and UL ranges, as expected. However, DS#1 and DS#2 gradation is out of limits established by the IDOT for the FA-1 material. Specifically, for percent passing#200 sieve (0.075 mm size), DS#2 passed more through this sieve (7.6%) compared to natural sand and DS#1. This indicates that DS#2 has more finer clayey type material compared to natural sand. For percent passing#10 sieve (2 mm size), DS#1 passed more through this sieve (99.6%) compared to natural sand (86.2%). This indicates that DS#1 is finer than natural sand.

Besides above-mentioned materials, other materials used were Portland cement Type 1 and class C fly ash which were collected from Prairie Materials, a local ready-mix concrete plant, located in Normal, Illinois.

3.2 Mix Design

In this study, a total of nine CLSM mixtures, containing different amount of cement, fly ash, NS, DS#1 or DS#2, and water. The proportions of each ingredient was selected based on IDOT (2016) CLSM specifications, as presented in Table 1. In accordance with ACI229R, the amount of water was selected based on the flow consistency of CLSM mixtures. One control CLSM was prepared by mixing only cement, fly ash, NS and water (no DS). A total of four mixtures (three specimens in each group) were prepared by substituting 25%,

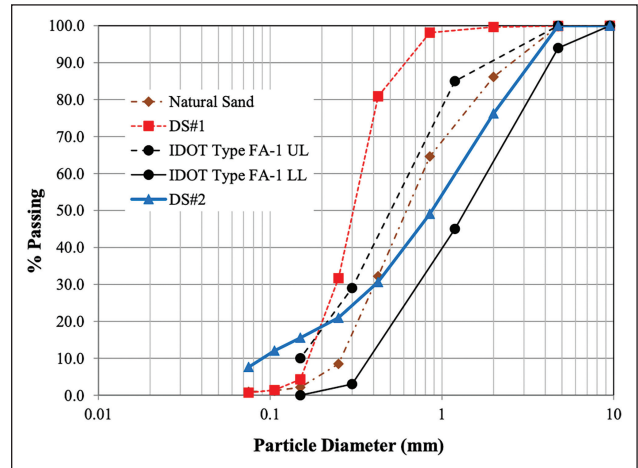


Figure 2. Sieve analysis results.

50%, 75% and 100% of natural sand with DS#1 by weight. Further, four mixtures were prepared by substituting 25%, 50%, 75% and 100% of natural sand with DS#2 by weight.

3.3 Specimen Preparation and Testing

All nine mixtures were prepared by adding required amount of dry ingredients in a five-gallon stationary vertical mixer (Fig. 3a). Then, all ingredients were mixed for 7 minutes followed by a 3 minutes rest, followed by a 5 minutes final mixing. The flow consistency of all nine CLSM mixtures was evaluated just after mixing in accordance with ASTM D 6103 test method. In this test, a 7.62 cm (3 in) by 15.24 cm (6 in) open-ended cylinder is used to spread CLSM on a flat non-absorbent surface and diameter of spread is measured.

For evaluating unconfined compressive strength (UCS) of CLSM mixtures, cylindrical specimens 10 cm x 20 cm (4 in x 8 in) were casted in accordance with ASTM D 4832 test method. To keep low strength CLSM specimens intact during preparation, special plastic molds were designed and manufactured in the laboratory (Fig. 3b). These molds can be split open into two halves for easy extraction of hardened CLSM specimen. Plastic molds were tied to a wooden board for easy transportation and handling. A total of three replicates were casted using each CLSM mixture. After casting, specimens were placed inside a plastic box under controlled temperature of 21°C (69.8 °F) and relative humidity of greater than 95% for four days. Then,

Table 1. Design of flowable fill mix proportions

Tag	% Natural sand	% DS	Cement (kg)	Fly ash (kg)	NS (kg)	DS (kg)	Water (kg)	Water/cementitious
CONTROL (NS-100 DS-0)	100	0	0.41	1.22	10.61	0.00	2.40	5.9
NS-75 DS-25	75	25	0.41	1.22	7.96	2.65	2.40	5.9
NS-50 DS-50	50	50	0.41	1.22	5.31	5.31	2.40	5.9
NS-25 DS-75	25	75	0.41	1.22	2.65	7.96	2.40	5.9
NS-0 DS-100	0	100	0.41	1.22	0.00	10.61	2.40	5.9



Figure 3. (a) CLSM mixer; (b) Specimen mold; and (c) Unconfined compressive strength test setups.

Table 2. A summary of results of dredged sediment containing specimens

Mix#	Tag	% DS	Flow		Compressive strength		Density		Excavatability (RE)
			inch	cm	psi	kPa	psi	kN/m ³	
1	Control	0	13.5	34.3	72.3	498.3	117.6	1885	0.95
2	NS-75 DS#1-25	25	12.8	32.4	84.3	581.0	116.3	1863	0.98
3	NS-50 DS#1-50	50	9.0	22.9	132.1	909.8	119.6	1916	1.31
4	NS-25 DS#1-75	75	9.5	24.1	102.7	707.9	117.9	1889	1.14
5	NS-0 DS#1-100	100	8.0	20.3	78.2	538.7	117.5	1882	0.97
6	NS-75 DS#2-25	25	9.0	22.9	85.6	589.9	113.7	1822	0.96
7	NS-50 DS#2-50	50	9.0	22.9	130.3	898.0	116.6	1869	1.25
8	NS-25 DS#2-75	75	9.5	24.1	65.9	454.2	112.8	1807	0.84
9	NS-0 DS#2-100	100	0.0	0.0	76.3	525.8	114.9	1841	0.93

specimens were demolded, wrapped with plastic film and then placed back in the storage box until the time of testing. Specimens were tested after 28 days of curing using a Universal Testing Machine in accordance with ASTM D 4832 test method (Fig. 3c). Specifically, specimens were subjected to load at a constant rate such that the cylinder failed in not less than 2 min.

4. RESULTS AND DISCUSSIONS

Table 2 shows a summary of results of all specimens tested in this study. A total of three replicates were tested for each mix and average was reported in Table 2.

4.1 Flow Consistency

Flow consistency enables CLSM to flow into a void and be self-consolidating which is a major benefit of CLSM compared to conventional fill materials. Variation of flow consistency with percent dredged material substitution is graphically presented in Figure 4 and tabulated in Table 2. In general, introducing more dredged sediments showed a decrease in the flow consistency values. Mixtures prepared by using 100% DS#1 and DS#2 substitution showed decrease in flow consistency by 14 cm (5.5 in) and 34.3 cm (13.5 in), respectively. One of the reasons for decrease in flow could be increase in finer particles in DS containing CLSM mixtures. As discussed in Materials and Methods section, gradation

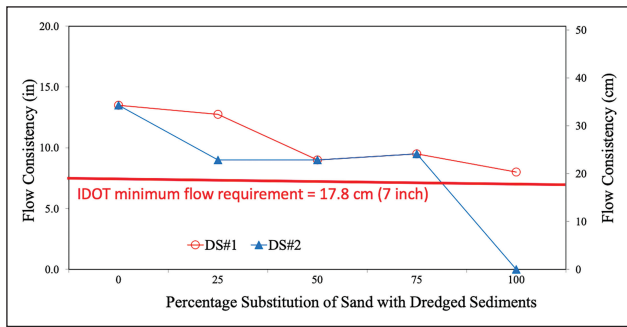


Figure 4. Variation of flow consistency with percentage substitution of sand with dredged sediments.

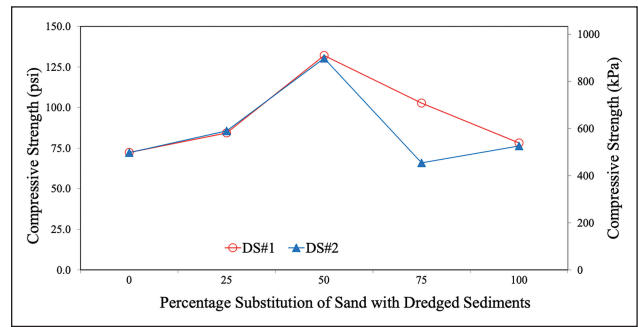


Figure 6. Variation of unconfined compressive strength with percentage substitution of sand with dredged material.

analysis showed relatively higher amount of fines in DS compared to NS. More fines results in larger surface area which will require more water for lubrication and flow of particles. Further, all CLSM mixtures tested, except Mix#9 prepared by substituting 100% sand with DS#2, showed a flow consistency of greater than 17.8 cm (7 in), as required by IDOT [24] specification for CLSM. According to ACI 229R [25], flowability can be expressed based on the diameter of CLSM material spread: low flowability (less than 15.2 cm, i.e., 6 in), normal flowability (15.2 cm to 20.3 cm, i.e., 6 to 8 in), and high flowability (greater than 20.3 cm, i.e., 8 in). Based on the results presented in Table 2 and Figure 4, all mixtures showed high flowability except Mix#5 (normal flowability) and Mix#9 (no flowability). Figure 5 shows photographic

comparison of flow consistency of control mix (Mix#1), mix containing 100% DS#1 (Mix#5) and 100% DS#2 (Mix#9). It is evident from Figure 5 that control mix is highly flowable compared to 100% dredged sediments containing mixes. Bleeding of water in Mix#5 and caky type behavior of Mix#9 with no flow is visible from Figure 5. In general, water is released to the CLSM surface (i.e., owing to its high water content) as bleed water or absorbed by dredged sediments (Fig. 5b). More interestingly, an outstandingly positive effect of DS#2 was discovered: The addition of DS#2 to the CLSM decreased bleeding rate, as shown in Figure 5c. This could be attributed to finer and more cohesive nature of DS#2 which could hold excess amount of capillary water, leading to a reduction in the bleeding water.

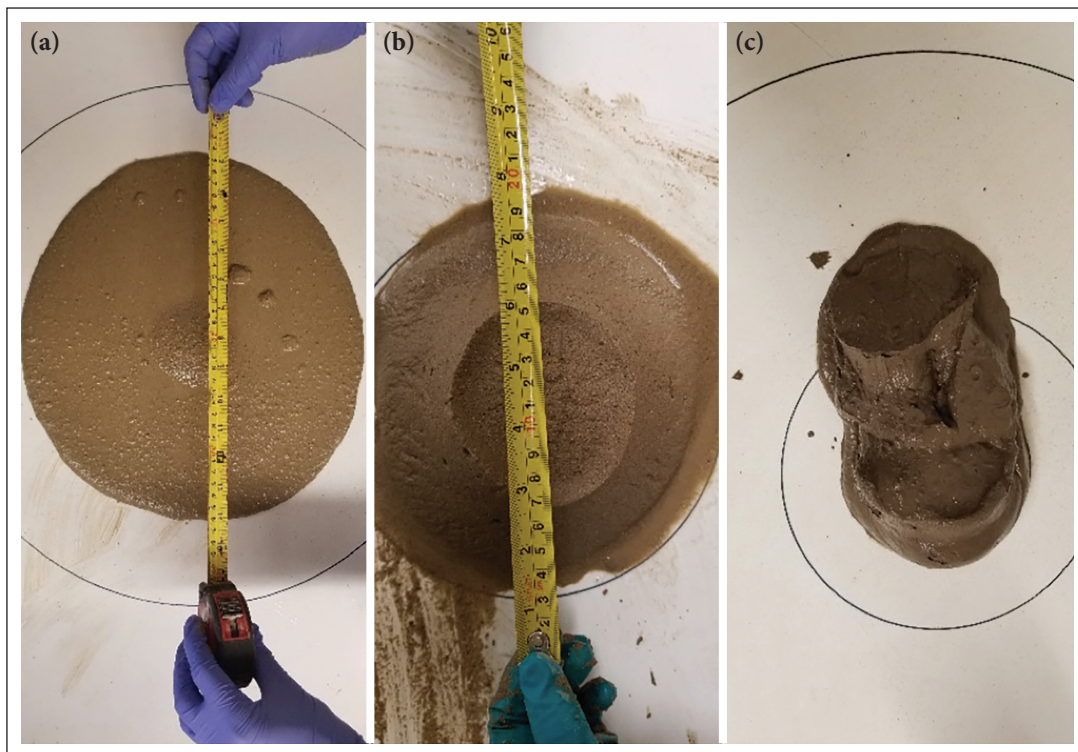


Figure 5. Photographic view of (a) Control (Mix#1), (b) 100% DS#1 containing (Mix#5) and (c) 100% DS#2 containing (Mix#9) containing mixes.

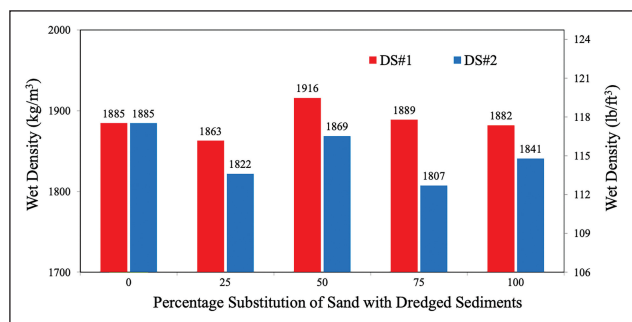


Figure 7. Variation of wet density with percentage substitution of sand with dredged material.

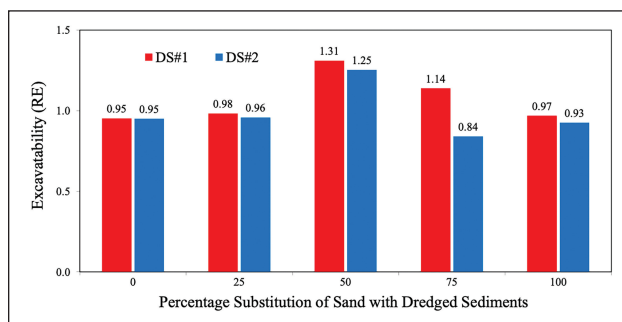


Figure 8. Variation of excavatability with percentage substitution of sand with dredged material.

4.2 Unconfined Compressive Strength

CLSM is designed with low unconfined compressive strengths which is a major objective for projects where later excavation is needed. Figure 6 shows UCS results of all mixes tested in this study. The strength values of CLSM specimens increases with percent substitution of NS with DS up to 50%. Beyond 50% substitution of NS with DS, decrease in strength of CLSM specimens was noticed. For example, substitution of sand with 50% DS#1 and 50% DS#2 provided an increase in strength by approximately 83% and 80%, respectively. Similar observations were reported by Do et al. [21] where strength of CLSM mixture decreased with increase in the amount of marine dredged sediments. This behavior of decrease in strength of CLSM mixtures with increase in DS was attributed to very small particle size of marine dredged sediments.

The behavior of increase in strength up to 50% can be rationalized using density of casted CLSM specimen, as shown in Figure 7. The CLSM containing 50% NS and 50% DS provided maximum density in case of both DS#1 and DS#2 which resulted in highest strength among all the mixtures tested in this study. The compressive strength of all CLSM mixtures tested in this study was found within IDOT requirements. Specifically, IDOT [24] specifies compressive strength value between 207 kPa (30 psi) and 1034 kPa (150 psi) for CLSM mixtures.

4.3 Density and Excavatability

Wet density results of all nine CLSM mixtures are presented in Figure 7. It is evident from Figure 7 that wet density of all nine mixtures varies between 1807 and 1916 kg/m³ (113 and 120 lb/ft³) which is within the range recommended by ACI 229R [25]. According to ACI 229R [25], wet density of CLSM in place is in the range of 1840 to 2320 kg/m³ (115 to 145 lb/ft³). Further, it was found that wet density improved with percentage of substitution of NS with DS up to 50% beyond which decrease in wet density was noticed. However, all mixtures prepared by substituting sand with DS#2 showed wet density lower than control. This could be attributed to finer clayey nature of DS#2 which resulted in lower density values.

The ability to excavate in future is an important property of CLSM. In general, CLSM with a compressive strength of 0.7 MPa (100 psi) or less can be excavated manually. According to ACI 229R [25], a removability modulus (RE) can be used to determine the excavatability of CLSM. The RE can be calculated as follows in metric units:

$$RE = (W^{1.5} \times 0.619 \times C^{0.5}) / 106 \quad (1)$$

Where, W is the dry mass density in kg/m³ and C is the 28-day unconfined compressive strength in kPa. If the RE is less than 1.0, the CLSM is removable, while CLSM with RE values greater than 1.0 are not easily removed. The type and content of cementitious materials is important in determining excavatability of CLSM. Literature review shows that acceptable long-term performance can be achieved with cement contents from 24 to 59 kg/m³ (40 to 100 lb/yd³) and class F fly ash quantity up to 208 kg/m³ (350 lb/yd³) [25].

RE values of all nine mixtures are plotted in Figure 8. A total of three out of nine mixtures showed RE values of greater than 1.0. Specifically, Mix#3, Mix#4 and Mix#7 resulted in RE values of 1.31, 1.14 and 1.25, respectively. This could be attributed to higher compressive strength values (greater than 700 kPa, i.e., 100 psi) of Mix#3, Mix#4 and Mix#7. According to ACI 229R [25], CLSM with a compressive strength of 700 kPa (100 psi) or less can be excavated manually.

5. CONCLUSIONS AND RECOMMENDATIONS

Based on the results presented in this study following conclusions could be drawn:

- 1) Flow consistency decreased with the amount of DS and presence of finer material in CLSM.
- 2) Unconfined compressive strength and wet density was found to improve with amount of DS in CLSM up to 50% beyond which strength and wet density started decreasing.
- 3) Based on flow consistency, unconfined compressive strength, wet density and excavatability, 100% substitution of sand with DS#1 and 75% substitution of sand with DS#2 could be used in preparing CLSM mixtures.

As noticed in this study, source and gradation of dredged sediments could influence the properties of CLSM. Therefore, it is recommended to investigate properties of DS in the laboratory before using it for CLSM projects.

ACKNOWLEDGMENTS

The author would also like to thank Harsh Chauhan, Mobi Singh, Xi Hu and Harshvardhan Jain for assisting in sample collection and specimen preparation. Also, assistance provided by Dr. Charles Theiling (Aquatic Research Ecologist, US Army Corps of Engineers) for sample collection is acknowledged.

DATA AVAILABILITY STATEMENT

The authors confirm that the data that supports the findings of this study are available within the article. Raw data that support the finding of this study are available from the corresponding author, upon reasonable request.

CONFLICT OF INTEREST

The authors declare that they have no conflict of interest.

FINANCIAL DISCLOSURE

This work was supported in part by the Illinois-Indiana Sea Grant (IISG) College Program, grant number NA18OAR4170082.

PEER-REVIEW

Externally peer-reviewed.

REFERENCES

- [1] Sheehan, C., & Harrington, J. (2012). Management of dredge material in the Republic of Ireland - A review. *Waste Management*, 32(5), 1031–1044. [CrossRef]
- [2] USEPA & USACE (2007). *Identifying, planning, financing beneficial use projects using dredged material: beneficial use planning manual*. Epa842-B-07-001, (U.S. Environmental Protection Agency & U.S. Army Corps of Engineers), p. 81.
- [3] Dia, M. (2014). Effect of chemical and thermal treatment on the geotechnical properties of dredged sediment. *Procedia Engineering*, 83(5), 159–169.
- [4] Costa-Pierce, B. A. and Weinstein, M. P. (2002). Use of dredge materials for coastal restoration. *Ecological Engineering*, 19(3), 181–186.
- [5] Limeira, J. (2011). Mechanical and durability properties of concrete made with dredged marine sand. *Construction and Building Materials*, 25(11), 4165–4174. [CrossRef]
- [6] United States Environmental Protection Agency (USEPA). (1991). *Handbook - Remediation of Contaminated Sediments*. United States Environmental Protection Agency.
- [7] United States Army Corps of Engineers (USACE) (2015). Dredging and dredged material management, U.S. *Environmental Protection Agency*, p. 920. http://www.publications.usace.army.mil/Portals/76/Publications/EngineerManuals/EM_1110-2-5025.pdf
- [8] Lim, Y. C., Lin, S-K., Ju, Y-R., Chen, C-W., Dong, C-D. (2019). Reutilization of dredged harbor sediment and steel slag by sintering as lightweight aggregate. *Process Safety and Environmental Protection*, 107, 2411–2502. [CrossRef]
- [9] Mostafa, Y. E. S. (2012). Environmental impacts of dredging and land reclamation at Abu Qir Bay, Egypt. *Ain Shams Engineering Journal Faculty of Engineering, Ain Shams University*, 3(1), 1–15. [CrossRef]
- [10] McNeil, D. (2019). *Private Sector Perspective, Beneficial Use of Dredged Material Workshop*. September 4, 2019, Peoria, IL. [CrossRef]
- [11] Great Lakes Commission (2001), *Waste to resource: beneficial use of great lakes dredged material, habitat and coastal, library, soil erosion and dredging*, Aug. 2001, Ann Arbor, MI, <https://www.glc.org/library/2001-waste-to-resource-beneficial-use-of-great-lakes-dredged-material>
- [12] Medeiros, M. H. F. (2013). Reinforced concrete in marine environment: Effect of wetting and drying cycles, height and positioning in relation to the sea shore. *Construction and Building Materials*, 44, 452–457. [CrossRef]
- [13] Park, J. (2016). The suitability evaluation of dredged soil from reservoirs as embankment material. *Journal of Environmental Management*, 183, 443–452. [CrossRef]
- [14] Lee, C. R., Brandon, D. L., & Price, R. A. (November 30, 2020). *Manufactured soil field demonstration for constructing wetlands to treat acid mine drainage on abandoned Minelands, U.S. Army Corps of Engineers*. <https://apps.dtic.mil/sti/pdfs/ADA474492.pdf>
- [15] NRMCA (2006), *Guide Specification for Controlled Low Strength Materials (CLSM), Specification Guide*, National Ready Mixed Concrete Association, 2006. Retrieved from <http://www.flowablefill.org/downloads/CLSMSpecifications1.pdf>
- [16] Naik, T.R., Kraus, R.N., Carty, R.H. (2002). *Use of ponded fly ash and crushed sand for flowable slurry* (Report No. CBU-2002-10). Center for By-Product Utilization, University of Wisconsin, Milwaukee, Wisconsin.
- [17] Tarabadkar K. (2009). *Accelerated carbonation of contaminated sediments and its application*. (Publication No. 1481717) [Master Thesis, Bachelor of Engineering, Pune University]. ProQuest Dissertations Publishing.
- [18] Kim, & Pradhan, B. (2016). Mechanical and germination characteristics of stabilized organic soils. *Marine Georesources & Geotechnology*, 34(7), 681–688. [CrossRef]
- [19] Kaliannan, Chan, C.-M., & Suratkon, A. (2017). 1D Compressibility of DMS Treated with Cement-GGBS Blend. The 9th International Unimas Stem Engineering Conference (ENCON 2016) “Innovative Solutions for Engineering and Technology Challenges. MATEC Web of Conferences, 87, 1004. [CrossRef]

- [20] Rabbanifar S. (2018). *Stabilization of organic silty clayey dredged material for beneficial use, a macro-micro study on physio-chemical properties*. Lamar University.
- [21] Do, T. M., Do, A. N., Kang, G. O., & Kim, Y. S. (2019). Utilization of marine dredged soil in controlled low-strength material used as a thermal grout in geothermal systems. *Construction and Building Materials*, 215, 613–622.
- [22] Abidi, I., Benamara, L., Correia, A. A. S., Pinto, M. I. M., & Cunha, P. P. (2021). Characterization of dredged sediments of Bouhanifia dam: potential use as a raw material. *Arabian Journal of Geosciences*, 14(23), 2631. [\[CrossRef\]](#)
- [23] Shi, J., Wang, S., Cao, W., Su, J., & Zhang, X. (2022). Mechanical properties and strengthening mechanism of dredged silty clay stabilized by cement and steel slag. *Materials*, 15(11), 3823. [\[CrossRef\]](#)
- [24] IDOT. (2016). Standard specification for road and bridge construction, illinois department of transportation. Springfield, Illinois.
- [25] ACI 229R. (2013). *Report on controlled low-strength materials*. American Concrete Institute, Farmington Hills, MI.



Research Article

Natural pozzolan-based green geopolymer foam for thermal insulation

Kübra EKİZ BARIŞ^{*}, Leyla TANAÇAN

Department of Architecture, İstanbul Technical University, İstanbul, Türkiye

ARTICLE INFO

Article history

Received: 07 July 2022

Accepted: 18 August 2022

Key words:

Alkali activator, geopolymer foam, natural pozzolan, optical microscopy, porosity, thermal conductivity

ABSTRACT

The current study investigates the possibility of volcanic Tuff of Earth of Datça (ED) in Turkey to be used as an aluminosilicate source in producing a geopolymer foam for thermal insulation. An extensive evaluation of the effects of fine sand-to-pozzolan and Al powder-to-pozzolan ratios on the physical, mechanical, and thermal properties and morphology (porosity, average and maximum pore diameter, pore size distribution) of the pores were carried out. The sodium silicate and potassium hydroxide (12.5 M) solutions with an activator ratio of 2.5 were used as alkali activators, and Al powder was used as a foaming agent. Research results reveal that Earth of Datça is a suitable precursor for producing a geopolymer foam. Fine sand and aluminum powder contents are critical to the optimum foam structure. The addition of finely ground silica sand ensured the volumetric stability of the binder and prevented the collapse after swelling of the binder. The optimum Al powder-to-pozzolan ratio was determined as 0.5% because it gives higher physical, mechanical, and thermal properties due to the more homogenous microstructure with finer pore size and narrower pore size distribution lower degree of interconnectivity between the pores. Research results also show that the natural volcanic Tuff of Datça Peninsula as an aluminosilicate source gives promising results in the field of producing highly porous geopolymers with low thermal conductivity (0.087–0.134 W/mK), high porosity (72.3–82.6%) and an adequate compressive strength (0.40–2.09 MPa). This study contributes to the literature that Earth of Datça-based geopolymer foam may function well as an insulation material for building enclosures.

Cite this article as: Ekiz Barış, & K., Tanaçan, L. (2022). Natural pozzolan-based green geopolymer foam for thermal insulation. *J Sustain Const Mater Technol*, 7(3), 128–144.

1. INTRODUCTION

The building industry is one of the fastest growing industries [1], and buildings are liable for approximately 40% of the total energy consumption [2]. Generally, thermal insulation materials decrease the energy consumption of buildings by decreasing the energy loss. But organic thermal insulation materials are flammable, inorganic thermal

insulation materials need complex processing conditions, and high sintering temperature results in higher costs [3] and embodied energy. To reduce the energy consumption and consequently the energy requirement of buildings, apart from using thermal insulation materials, the development of new materials with higher thermal performance is of the utmost importance.

*Corresponding author.

*E-mail address: ekizk@itu.edu.tr



Cellular or lightweight aggregate concrete materials have been produced to provide energy savings. However, their raw material is Ordinary Portland Cement (OPC), whose production process is energy intensive and emits approximately 1 ton of CO₂ in a ton of production [4]. Recently, geopolymer foams have been produced by creating the gas bubbles into the binder during the chemical reactions between the foaming agent and alkali activator or by incorporating a large volume of readily-prepared air bubbles into the mixture [5], have been produced to replace foamed cementitious materials. Commonly used foaming agents such as finely divided metallic aluminum, hydrogen peroxide, sodium peroxide, sodium perborate, metal silicon, silica fume, and silicon carbide are in the field of promising research [6]. Due to the high volume of pores, they could contribute to the material's thermal performance. Furthermore, they are more sustainable than OPC-based foams since their process emits 0.19–0.24 tonnes of CO₂ in a ton of its production [5], and up to 80% energy savings could be achieved [7].

Up until the present, scores of works have focused on producing highly porous geopolymers (porosity $\geq 50\%$ or bulk density ≤ 0.7 g/cm³ [8]) having low thermal conductivity with different types of aluminosilicate sources. For example, ultrafine perlite-based geopolymer, activated with sodium hydroxide (NaOH) and foamed with hydrogen peroxide (H₂O₂, 0.5–3.0% by weight of aluminosilicate source), exhibits thermal conductivity, porosity, and compressive strength ranging between 0.03–0.06 W/mK, 74–89%, and 0.2–0.8 MPa, respectively [9]. Porous fly ash-based geopolymer was produced using sodium silicate (Na₂SiO₃) as an alkali activator and H₂O₂ (0.05–0.1% by weight of aluminosilicate source) as the foaming agent. The test results reveal that the values of thermal conductivity (0.07–0.09 W/mK), porosity (74–81%), and compressive strength (0.4–1.4 MPa) show promise as thermal insulation material [3]. In another study, biomass fly ash-based-geopolymers were activated by a mixture of NaOH and Na₂SiO₃ and were foamed using H₂O₂ as a pore-forming agent. Foamed geopolymers exhibit thermal conductivity as low as 0.10 W/mK, porosity up to 72.5%, and compressive strength in a range of 1.2–6.6 MPa, depending on the content of the pore-forming agent (0.03–1.20% by weight of aluminosilicate source) [10]. In another research, fly ash-based geopolymer foams were produced by using H₂O₂ or Al powder foaming agents. The specimens containing H₂O₂ have 0.31–0.97 g/cm³ density and 0.083–0.174 W/mK thermal conductivity, whereas the specimens with Al powder have 0.50–0.77 g/cm³ density and 0.099–0.159 W/mK thermal conductivity. Study results state that these foams can be used as thermal insulation materials [11]. Fly ash was also foamed with sodium perborate foaming agent in the literature. The study results reveal that the density, thermal conductivity, and compressive strength of geopolymer foams

are in the range of 0.64–0.82 g/cm³, 0.27–0.32 W/mK, and 4.2–4.8 MPa, respectively [12].

Metakaolin-based geopolymer foam, activated with a mixture of potassium hydroxide (KOH) and potassium silicate (K₂SiO₃) and foamed with silica fume blowing agent, has a thermal conductivity between 0.12 and 0.33 W/mK, and porosity in a range of 65–85% [13]. The characterization of metakaolin-based geopolymer foam contains KOH and K₂SiO₃ as alkali activators and H₂O₂ (5–20%, by weight) as a forming agent, shows that the material with low thermal conductivity (0.11–0.17 W/mK), high porosity (60.2–83.1%), and acceptable compressive strength (0.3–11.6 MPa) could be successfully produced [14]. The pore morphology, density, porosity, thermal conductivity, and compressive strength of metakaolin-based porous geopolymers (containing H₂O₂ chemical pore-forming agent) were researched in another study. These geopolymers have 0.35–1.20 g/cm³ density, 0.4–5.65 MPa mechanical strength and improved thermal conductivity (0.13–0.32 W/mK) [15]. The influence of the Al powder content (3–12%, by weight) on the properties of the KOH/NaOH+Na₂SiO₃ activated metakaolin-based geopolymer foam was investigated. Material with improved insulating behavior, thermal conductivity of 0.15 W/mK, and porosity of 70% was produced depending on increasing Al powder content [16]. The possibility of using metakaolin-based geopolymer foams foamed with Na₂O₂ to be applied for fire protection was investigated. The foamed material with 0.30–0.46 g/cm³ density, 0.085–0.115 W/mK thermal conductivity, and 0.6–1.6 MPa compressive strength possess a stable porous structure and excellent fire resistance [17]. The effects of sodium lauryl ether sulfate (SLES) foaming agents on pore types and properties of lightweight kaolinite-based geopolymers were also investigated in the literature. The results show that the lightest geopolymer foam has a porosity of 72.34% and a compressive strength of 4.69 MPa with low thermal conductivity of 0.197 W/mK [18].

Waste glass-based porous geopolymers with thermal conductivity of 0.21 W/mK, porosity of 55%, and compressive strength of 7.3 MPa were produced using a combination of KOH and K₂SiO₃ activators and H₂O₂ (5%, by weight) as pore foaming agent [19]. NaOH-activated bottom ash with varying amounts of Na₂SiO₃ (25–55%, by weight) as the foaming agent has 0.075 W/mK thermal conductivity, 72% porosity, and 3.55 MPa compressive strength and could be used as a thermal insulation material [20]. Waste metakaolin, recycled glass, and steel-plant waste were activated with NaOH+Na₂SiO₃ solutions and foamed with aluminum scrap recycling waste (50% by weight). The results showed that highly porous, lightweight building materials could be obtained with thermal conductivity, porosity, and compressive strength ranging between 0.14–0.15 W/mK, 83–86%, and 1.1–2.0 MPa, respectively [21]. Consequently, geopolymer foams show good insulating properties with thermal

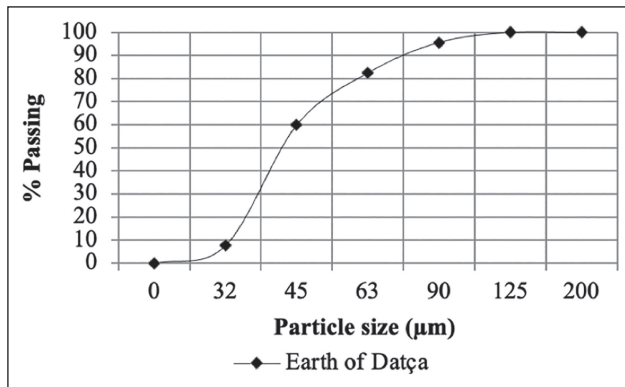


Figure 1. Particle size distribution of volcanic Tuff of Earth of Datça.

conductivities, porosities, and compressive strengths ranging between 0.03–0.33 W/mK, 55–89%, and 0.2–11.6 MPa, respectively, depending on the type and quantity of aluminosilicate source, pore foaming agent, pore foaming agent-to-pozzolan ratio and fine sand-to-pozzolan ratio.

Although much of the research carried out has been based on producing artificial pozzolan-based highly porous geopolymers with improved thermal performance, investigations regarding the production of natural pozzolan-based geopolymer foams are scarce. The natural pozzolan resources of Turkey are at a level that cannot be ignored. Approximately 155,000 km² of the country consists of volcanic rocks [22]. Datça pozzolan used in this research is the natural soil of Datça Peninsula. It was formed due to strong volcanic eruptions in Nysiros and Yelli Islands [23].

This research aims to investigate the possibility of volcanic Tuff of Earth of Datça (ED) to be used as an aluminosilicate source in the production of geopolymer foam for thermal insulation. In the scope of the study, key factors such as fine sand-to-pozzolan (FS/P) and Al powder-to-pozzolan (Al/P) ratio affect the physical, mechanical, and thermal characteristics of ED-based geopolymer foam are researched. Optimizing the test results, a new porous material with low thermal conductivity is proposed as an alternative to the existing thermal insulation materials in the building industry.

2. EXPERIMENTAL TECHNIQUES

2.1. Raw Materials

For the production of geopolymer foam, natural Datça pozzolan was used as an aluminosilicate source, and its specific gravity is 2.52 g/cm³. The specific surface area of the pozzolan, determined using the Blaine method [24], is 5467.75 cm²/g, and the particle size distribution is shown in Figure 1.

Semi-quantitative element (XRF) and quantitative XRD analysis of the ED and lime-pozzolan mortar (ED)T produced for the pozzolanic activity test were performed in the

Table 1. Oxide Composition of ED, quicklime, and hardened mortar (ED)T determined by XRF

	Quicklime (%)	ED (%)	(ED)T mortar (%)
SiO ₂	–	75.289	58.934
Al ₂ O ₃	–	15.991	11.510
Fe ₂ O ₃	–	0.984	0.829
Na ₂ O	–	2.211	1.361
K ₂ O	–	3.026	2.408
CaO	85	1.222	21.377
CO ₂	5	–	–
MgO	1.5	0.622	2.870
P ₂ O ₅	–	0.072	0.077
TiO ₂	–	0.149	0.148
MnO ₂	–	0.047	0.050
Cr ₂ O ₃	–	0.005	–
NiO	–	0.004	0.005
CuO	–	0.002	–
ZnO	2.23	0.002	0.006
Rb	–	0.006	0.007
SrO	–	0.015	0.019
V ₂ O ₅	–	–	0.022
Y ₂ O ₃	–	0.002	0.006
ZrO ₂	–	0.010	0.015
Nb ₂ O ₅	–	0.001	0.008
BaO	–	0.097	0.075
Cl	–	0.092	0.078
SO ₃	0.8	0.1	0.194
PbO	–	–	–
ThO ₂	–	–	–
L.O.I.	–	0.15	–
Total	93.8	100.00	–

previous research [22] using Philips 71 PW–2404 XRF and Shimadzu XRD–6000 (Cu X-ray tube 1.5405 Angstrom) equipment, respectively. XRF analysis indicated that (Table 1) Earth of Datça fulfills the requirements of T.S. 25 [25] to be used as a natural pozzolan in cement and other types of binders because its SiO₂+Al₂O₃+Fe₂O₃ content (92.26%) is higher than 70.0%, and its SO₃ and Cl contents (0% and 0.092%) are lower than 3.0% and 0.1%, respectively. Furthermore, the pozzolanic activity test results (1.43 MPa flexural strength and 6.12 MPa compressive strength) provide the requirements of T.S. 25, which are ≥1 and 4 MPa, respectively. XRD patterns have shown that (Fig. 2) ED contains cristobalite, quartz, feldspar, and an amorphous compound, and (ED)T has hydration products, cristobalite, quartz, feldspar, portlandite, and an amorphous compound.

Solid KOH with a molecular weight of 56.1 g/mol was

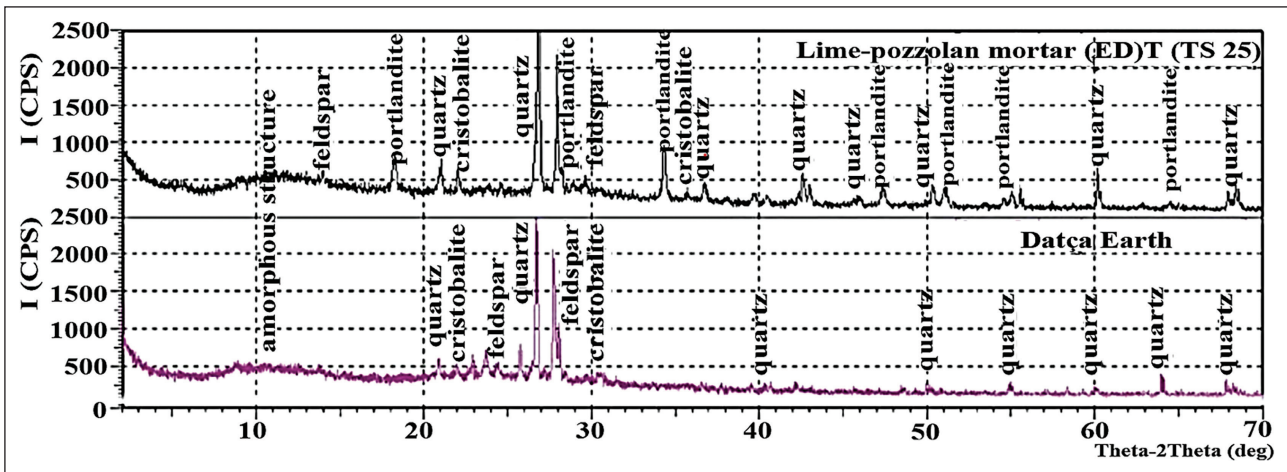


Figure 2. XRD data of ED and hardened mortar (ED)T.

dissolved in deionized water for 24 hours before use and kept at ambient temperature. The mass of solid KOH in the solution is expressed as Molar (M). 12.5 molar KOH solution contains $12.5 \times 56.1 = 701$ grams of solid KOH in a one-liter solution. The sodium silicate solution's molar ratio ($\text{SiO}_2/\text{Na}_2\text{O}$) is 3.4. Finely ground silica sand with 211 μm maximum grain size and 2.63 g/cm^3 specific gravity and aluminum powder foaming agent with 99% purity and 50 μm mean particle diameter was supplied from Ytong A.Ş.

2.2. Mixing, Molding, and Curing Process

The effects of activator types (NaOH, KOH, S+NaOH, and S+KOH), molar concentrations of the NaOH and KOH (7.5, 10, 12.5, and 15), and activator ratio (1.0, 1.5, 2.0, 2.5, by weight) on the geopolymeric reactivity were investigated in the previous research [26]. The combination of sodium silicate solution with potassium hydroxide (SK) as the activator type; 12.5 M as the concentration of KOH, and 2.5 as the activator ratio was selected for their better performance gain in physical and mechanical properties. In this research, the effectiveness of the following parameters, which may affect the development of the physical, mechanical, and thermal properties of the natural pozzolan-based geopolymer foam, was investigated:

- i The effect of acceptable sand-to-pozzolan ratio (FS/P);
- ii The effect of Al powder-to-pozzolan ratio (Al/P).

Fine aggregate/filler is generally not added to highly porous geopolymers having low thermal conductivities in the literature [3, 9–10, 13–16, 19–21]. It converts cementitious binders to mortars, gives mortars their volumetric stability, rigidity, and stiffness [27], and has a restraining effect on drying shrinkage due to the stability in shape [28]. Acceptable sand use as a filler may also decrease the production cost by reducing the amount of binder (pozzolan and chemical activators). In the preliminary tests of this research, and was not added to the ED-based geopolymer binder. The new binder expanded approximately 3.5 times within 10 minutes after the binder was poured

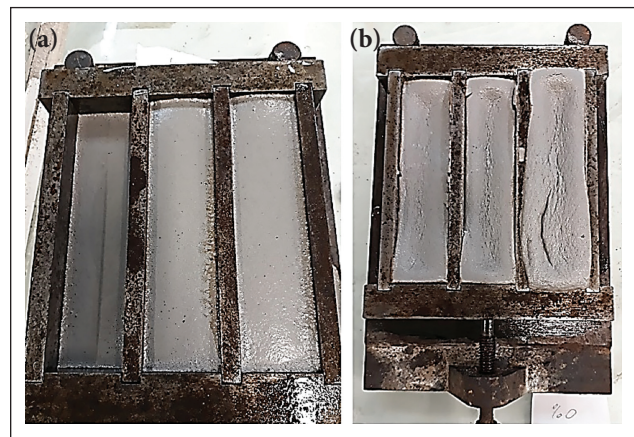


Figure 3. (a) The specimens 10 minutes after placing the molds; (b) The existence of collapse 30 minutes after placing the molds.

into the molds (Fig. 3a). However, after 30 minutes, separation of solid and gas phases was observed, and the foam collapsed (Fig. 3b). The reason for this result may be the lower plastic density ($\leq 0.5 \text{ g/cm}^3$) of the porous binder which results in a significant decrease in the bubble confinement force (F_c) and leads to more giant and more closely spaced bubbles. Increasing bubble diameter causes an increase in the bubble buoyancy force (F_b). When F_b overcomes the surrounding F_c , bubbles become buoyant and float towards the surface of the porous binder, displace the surrounding solids, reach the surface, and collapse occurs [29]. Thus, in the first stage, the effects of the FS/P ratio (20/100, 25/100, 33/100, 50/100, and 100/100, by weight) on the properties of the foam were researched. The Al/P ratio was kept constant at 0.5% in this stage. The workability of the binder was determined by the flow table test performed according to ASTM C 1437 [30]. The water/total solid ratio, which results in optimum workability, was 0.4, and flow was found to be 100.

Table 2. The specimen codes, mixing ratios, and curing conditions of the ED-based geopolymer foams according to the experiment stages

Stage	Code	Activator ratio	Activator-to-pozzolan (by weight)	Total water-to-solid (by weight)	FS/P (by weight)	Al/P (% by weight)	Curing conditions
i	SK-20/100-0.5	2.5	0.3	0.40	20/100	0.5	
	SK-25/100-0.5				25/100		
	SK-33/100-0.5				33/100		
	SK-50/100-0.5				50/100		
	SK-100/100-0.5				100/100		
ii	SK-20/100-0	2.5	0.3	0.40	20/100	0	95±5 %
	SK-20/100-0.25				0.25	R.H. for	
	SK-20/100-0.5				0.5	24 h	
	SK-20/100-1.0				1.0		
	SK-20/100-1.5				1.5		

Specimen codes consist of XX-X-X format. The first symbol shows the alkali activator type (S: Sodium silicate, K: Potassium Hydroxide); the second shows the FS/P ratio, and the third points out the Al/P ratio.

According to the results of the first stage experiments, the FS/P ratio was selected as 20/100 because it has consistent properties for the following study stage. In the second stage, the effects of the Al/P ratio (0, 0.25, 0.50, 1.0, and 1.5%, by weight) on the foam's physical, mechanical, and thermal properties were tested. The specimen codes, mixing ratios, and curing conditions according to the experiment stages are shown in Table 2.

The solid components (ED and fine sand) were mixed in a plastic bowl and then added to previously homogenized alkali activators and mixed for 5 minutes. Afterward, Al powder was added and mixed for additional 2 minutes. The mixture was then poured into 40 x 40 x 160 mm molds. It should be noted that foaming started immediately after Al powder was added to the mix. The reaction time for volume expansion of the mixture took approximately 10 minutes. Since the volume expansion ratio of the foam differs depending on the quantity of the added Al powder, in each increment of the Al powder addition, the volume expansion ratio of the mortar was determined by using a 500 ml glass test tube. The produced fresh mortar was filled in this test tube up to the level of 100 ml. After the expansion was completed, the volume expansion ratio (R_{ve}) was calculated by Eq. (1):

$$R_{ve} = (V_f - V_i) / V_i \quad (1)$$

where V_i is the initial volume of the fresh mortar (ml); V_f is the final volume of the mortar (ml). Thus, the least amount of mixture was poured into the molds, and overflowing of the mixture from the mold during the expansion was prevented. The molded blend was covered with Polyethylene (P.E.) film to prevent rapid evaporation and cured at 70 °C and 95±5% R.H. for 24 h. Cured specimens were then taken from the oven and were kept at ambient temperature (20±2 °C, 50±5% R.H.) for seven days.

2.3. Testing Methods

Throughout the study, the relevant standards applied each physical and mechanical test to 9 prismatic specimens of 4 x 4 x 16 cm dimensions.

Bulk density was calculated as the ratio of the dry mass to volume of the samples dried to a constant weight in a ventilated oven at 105 °C (TS EN 1015–10 [31]).

The water absorption ratio (A_b) was calculated by considering the amount of water absorbed by the specimens, which were dried to a constant mass (m_d). The specimens were wholly immersed in water at 20°C for 48 hours, removed from the water, and weighed again (m_s). The water absorption ratio was calculated according to the following equation (2) (TS EN 13755 [32]):

$$A_b = [(m_s - m_d) \times 100] / m_d \quad (2)$$

The ultrasound pulse velocity (U.P.V.) test was applied according to TS EN 14579 [33] with a portable Proceq ultrasonic non-destructive device.

The flexural strength was specified by using a machine (Universal) with a 300 kN capacity and 50 N/s loading rate (TS EN 196–1 [34]). The specimen was put on the machine with one side face on the supporting rollers and its longitudinal axis normal to the supports. The load was applied vertically using the loading roller to the opposite side face of the specimen and increased until fracture. The flexural strength (R_f) was according to the following equation (3):

$$R_f = (1.5 \times F \times l) / b^3 \quad (3)$$

where b is the side of the square section of the specimen, (mm); F is the load applied to the middle of the specimen at fracture, (N); l is the distance between the supports, (mm).

Eighteen samples, broken into two pieces in the flexural strength test, were subjected to the compressive strength test (TS EN 196–1 [34]). The specimen was centered laterally to the machine's plates, and the load was increased at a 2400 N/s rate until fracture. Compressive strength (R_c) was calculated from Eq (4):

Table 3. Test results of the ED-based geopolymer foam

Stage	Code	Bulk density (g/cm ³)	Water absorption by weight (%)	Porosity (%)	UPV (km/s)	Flexural strength (MPa)	Compressive strength (MPa)
i	SK-20/100-0.5	0.51	69.63	76.80	1.25	0.90	1.39
	SK-25/100-0.5	0.55	66.09	72.72	1.28	1.02	1.63
	SK-33/100-0.5	0.59	59.15	70.62	1.32	1.15	1.76
	SK-50/100-0.5	0.64	54.04	68.47	1.44	1.37	1.95
	SK-100/100-0.5	0.85	48.02	64.01	1.60	1.62	2.52
ii	SK-20/100-0	1.29	28.69	43.72	1.95	3.92	5.69
	SK-20/100-0.25	0.60	63.68	72.31	1.41	1.22	2.09
	SK-20/100-0.5	0.51	69.63	76.80	1.25	0.90	1.39
	SK-20/100-1.0	0.48	74.75	79.69	0.91	0.33	0.85
	SK-20/100-1.5	0.46	79.32	82.66	0.65	0.12	0.40

$$R_c = (F_c / 1600) \tag{4}$$

where F_c is the maximum load at fracture, (N); 1600 is the area of the plates (40 mm × 40 mm), (mm²).

Thermal conductivity was measured using the heat flow meter apparatus in steady-state conditions per ASTM C518–17 [35]. The heat flow meter apparatus consists of two copper plates, one heat flux transducer, and a protective casing with thermal insulation to prevent heat loss. The specimen (100 mm diameter and 10 mm thickness) was positioned between two copper plates, and the heat flow passing through the plates was recorded. The difference in temperature between the copper plates ($\Delta T = T_1 - T_2$) and the heat flux (Q) was obtained with conventional sensors. Fourier's law of heat conduction was used to calculate thermal conductivity by using Eq. (5):

$$Q = \lambda \frac{\Delta T}{\Delta x} = \lambda \frac{T_1 - T_2}{d} \tag{5}$$

where Q is heat flux flowing through the specimen (W/m²), λ is thermal conductivity (W/mK), ΔT is the temperature difference across the specimen (K), x and d are the thickness of the specimen (m), T/x is temperature gradient (K/m).

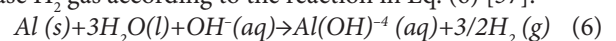
Optical analysis, which gives a detailed two-dimensional picture of the pores, was carried out to characterize the morphology of macroscale pores (>10 μ m). The specimens were cut from geopolymer foams using a cutting machine. Three samples were prepared for each analysis, and four images of a fracture section of each sample were observed by optical microscope (1×). However, it is difficult to determine the pore size distribution solely by analyzing the microscopic images. Therefore, image analysis was conducted using Image-Pro Plus Image Analysis Software to analyze better the morphology of macroscale pores (air pores with >10 μ m). The pore dimensions were quantified with equivalent circle diameter. Porosity, average pore diameter, maximum pore diameter, and pore size distribution were determined. The distribution of

mesoscale pore (100 nm – 10 μ m) was not considered because they are assumed to be insignificant in affecting the properties of geopolymer foams [36]. The test results are given in Table 3.

3. RESULTS AND DISCUSSION

3.1. Influence of the Fine Sand-to-Pozzolan Ratio on the Properties of the ED-Based Geopolymer Foam

Pores are generated by a gas-releasing reaction in the geopolymer mixture, which results in a cellular structure when set. After Al powder is added to the homogeneous geopolymer mixture, in the alkali environment, reactive metal powders are oxidized in the presence of water to release H₂ gas according to the reaction in Eq. (6) [37]:



The hydrogen gas bubbles generated led to the ED-based geopolymer binder's expansion, which continued for the next 10 minutes. The influence of the FS/P ratio on the volume expansion ratio of the mortar was investigated together with the observation of the surface properties of the expanded specimens (Table 4). According to this, the volume of the first series prepared with a 20/a 100 FS/P ratio increased 3.0 times compared to their initial volume. Volume expansion ratios of the specimens, for each fine sand–pozzolan ratio increment, decreased by 2.8, 2.5, 2.2, and 1.1 times respectively. Especially in the specimens with the highest sand content (100/100 FS/P ratio), Al powder could not swell the binder, and almost no volume expansion (Table 4–Fig. e). The higher the amount of sand, the lower the alkali activator, Al powder, and pozzolan ratio, which are responsible for foaming the binder. In addition, light gray material precipitation looking like aluminum was observed on the top open surfaces of the sand-rich specimens (33/100, 50/100, and 100/100 FS/P ratio) after oven curing at 70 °C. This causes surface deformation; accordingly, the color and texture homogeneity of the specimens was impaired (Table 4–Fig. c–e).

Table 4. The effects of the FS/P ratio on the volume expansion ratio and surface properties of the swollen specimens

FS/P (by weight)	Volume expansion ratio	Surface properties	The specimens after 70 °C ovens curing for 24 h
20/100	3.0 times	Homogenous surface and color	
25/100	2.8 times	Homogenous surface and color	
33/100	2.5 times	Non-homogenous surface and color	
50/100	2.2 times	Non-homogenous surface and color	
100/100	1.1 times	Non-homogenous surface and color	

The influence of the FS/P ratio on the physical and mechanical properties of ED-based geopolymer foam is given in Figure 4.

The gradual increase of the FS/P ratio from 20 to 100% decreased porosity and water absorption by 0.83 and 0.68, respectively. Parallel to this decrease, there was an almost two-fold increase in the bulk density of the specimens (1.66 times). Notably, this becomes significant in the region between 50 to 100% FS/P ratio, where the increment ratio of the sand is two-

fold. U.P.V., flexural and compressive strengths of the specimens increased 1.28, 1.80, and 1.81 times, respectively. When the increment of the sand ratio is twofold in the region between 50 to 100% FS/P ratio, the material's compressive strength increases significantly parallel to the increase of its bulk density.

Figure 5 shows the microscopic images of ED-based geopolymer foams in each FS/P ratio. The sand ratio increases lead to a decrease in the pore volume (porosity) and the number of pores, which is also consistent with physical

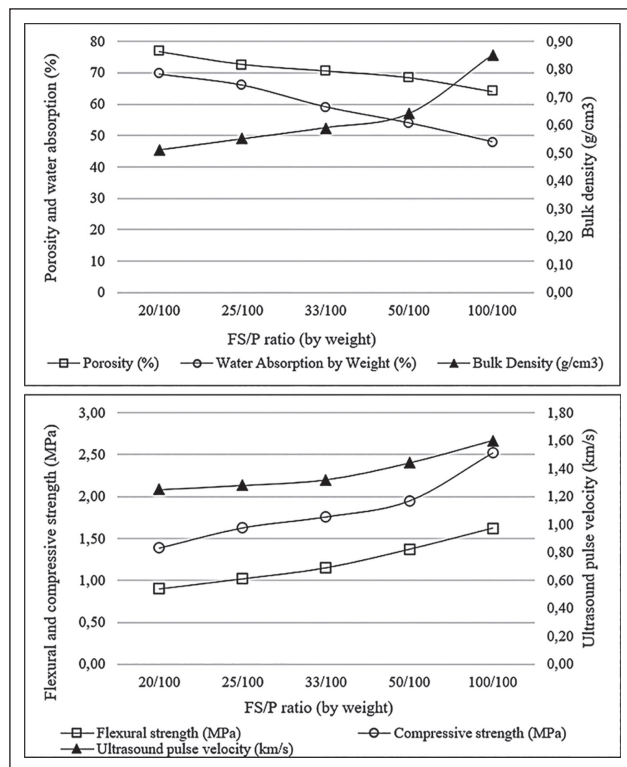


Figure 4. Effects of the FS/P ratio on the physical and mechanical properties of ED-based geopolymer foam.

test results. Frequency distribution diagrams of the pore diameters were prepared and given in Figure 6. Accordingly, the diameter of the specimens' pores ranged from 61 μm to 2038 μm (2.038 mm). The gradual increase of the FS/P ratio from 20/100 to 100/100 reveals that the distribution of pore size shifts towards the larger pore size distribution. The specimens with a 20/100 FS/P ratio are more homogeneous with finer pore sizes, regular (narrower) pore size distribution, and a maximum 1217 μm pore diameter. When the sand content of the binder increases, the porous matrix shows the non-homogeneous distribution of larger pores, and the maximum pore diameter increases up to 2038 μm . The average pore diameter is 280 μm in the specimens having a 20/100 FS/P ratio, while the average pore diameter increases up to 407 μm depending on the increase of the FS/P ratio (100/100). These findings may be due to a higher proportion of pores between fine sand particles and at the fine sand–binder interface. In addition, the pores of sand-rich specimens have a higher degree of interconnectivity, whereas the specimens having lower sand content have a relatively lower degree of interconnectivity between pores. Furthermore, while the number of pores per mm^2 is the highest in samples with a 20/a 100 FS/P ratio, increasing sand content decreased the number of pores per mm^2 . From these findings, it can be inferred that the total amount of fine sand in the porous geopolymer mixture controls the pores' total volume, dimension, and size distribution.

Total pore areas and porosities of the specimens as a function of the FS/P ratio are given in Figure 7. According to this, both the porosities of the specimens (obtained by experiments) and total pore areas per mm^2 (obtained by image analysis) decrease with the increase of sand content of the mixture. This decreasing trend is significantly similar for both factors, which may also denote that the image analysis is a suitable method for determining the pore volume of the geopolymer foams.

3.2. Influence of the Al Powder-to-Pozzolan Ratio on the Properties of the ED-Based Geopolymer Foam

The effects of the Al/P ratio on the physical and mechanical properties of ED-based geopolymer foam having 20% find sand content are given in Figure 8.

When the Al/P ratio increases gradually from 0% to 1.5%, two distinct regions become apparent in the evolution of the properties. At first, adding 0.25% Al/P into the mixture was quite effective in pore-forming, and the bulk density of the material dropped by 53%. Beyond this level to the 1.5% Al/P, even though there was a 1.25 times increment in the Al powder ratio, the same property only decreased by 23%, which may show the influence of Al powder in pore-forming became lower. Other properties of the material as a function of Al/P ratio increment displayed almost a coherent change with the bulk density. At 0.25% Al/P ratio, the porosity, and the water absorption ratio increased sharply by 1.65 and 2.21 times, and parallel to this increase in U.P.V., flexural and compressive strengths of the specimen decreased by 0.72, 0.31, and 0.36 times, respectively. The gradual decrease in U.P.V. (54%) in the whole aluminum powder increment range may have resulted from the porous structure's gradual formation. The decreasing tendency of physical and mechanical properties with the increasing pore foaming agent content is also consistent with other study results [3, 5, 38].

Figure 9 shows the microscopic images of ED-based geopolymer foams with various Al/P ratios, and Figure 10 shows frequency distribution diagrams of the pore diameters and average and maximum values of pore diameters of ED-based geopolymer foams with various Al/P ratios.

Increasing the Al/P ratio from 0 to 1.5% led to an increase in the total pore volume of the ED-based geopolymer and was consistent with the physical test results (Fig. 9 and 10). Pore diameters of the specimens ranged between 72 μm and 1787 μm (1.787 mm). Specimen with 0.25% Al/P ratio has homogenous, fine pore size with regular (narrower) pore size distributions. Average and maximum pore diameter was detected as 268 μm and 1200 μm , respectively. Gradually increase in the Al/P ratio from 0.25 to 1.5% shifted the pores of the specimen towards broader pore size distribution. Non-homogeneous distribution of larger pores with an average pore diameter of 411 μm and maximum pore diameter of 1787 μm were detected in its porous matrix. In addition, the pores showed a higher degree of interconnectivity than the specimens, with a 0.25%

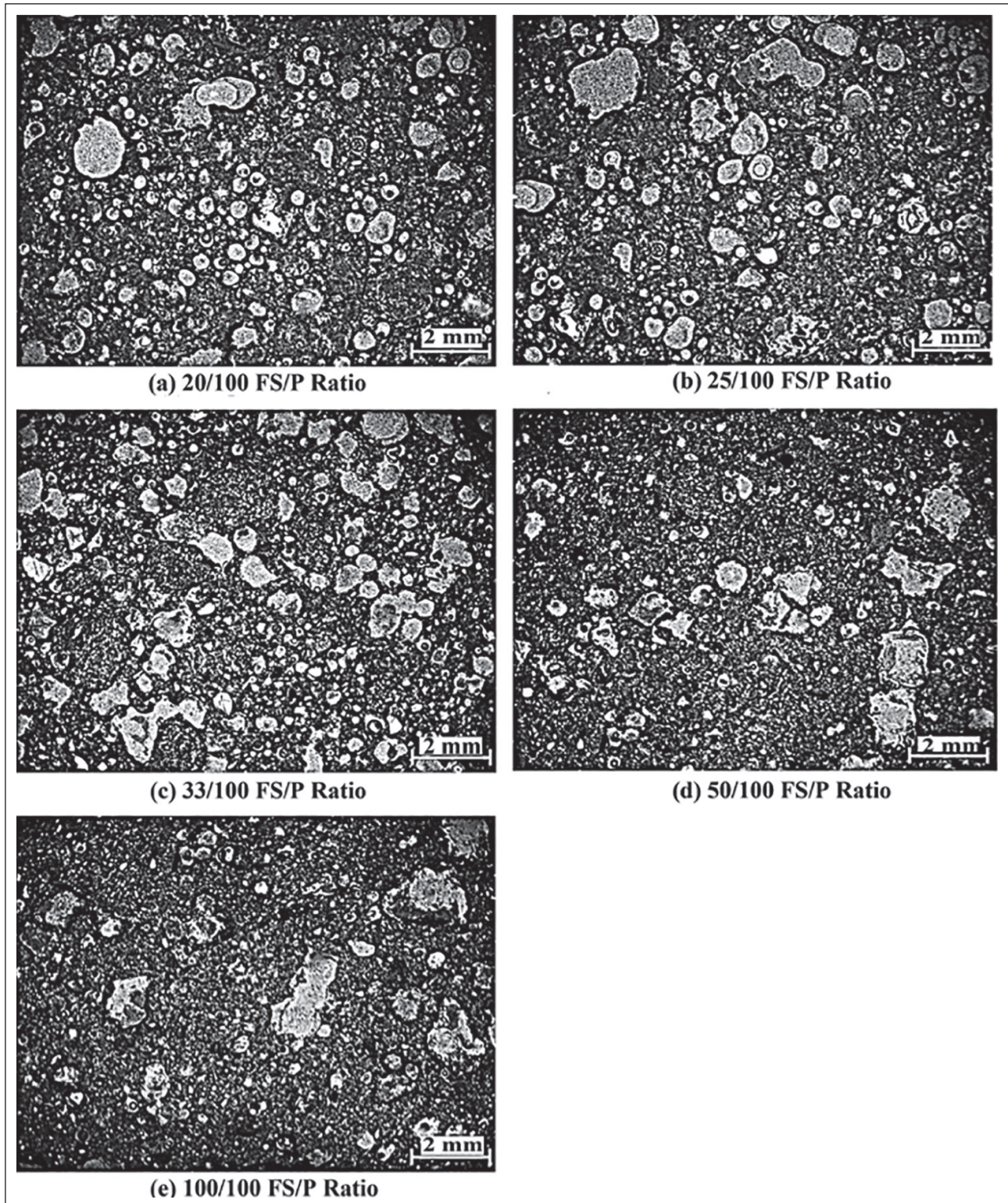


Figure 5. Microscopic images of ED-based geopolymer foams having various FS/P ratios.

Al/P ratio. This degree of pore coalescence may have led to a non-homogeneous pore structure and caused the least number of pores per mm^2 , compared to other samples. Similar results were obtained by various studies [16, 39].

Thus, it can be stated that in the porous geopolymer mixtures, the content of Al powder is decisive in determining the total volume, dimension, size distribution of the pores, and the degree of interconnectivity between them.

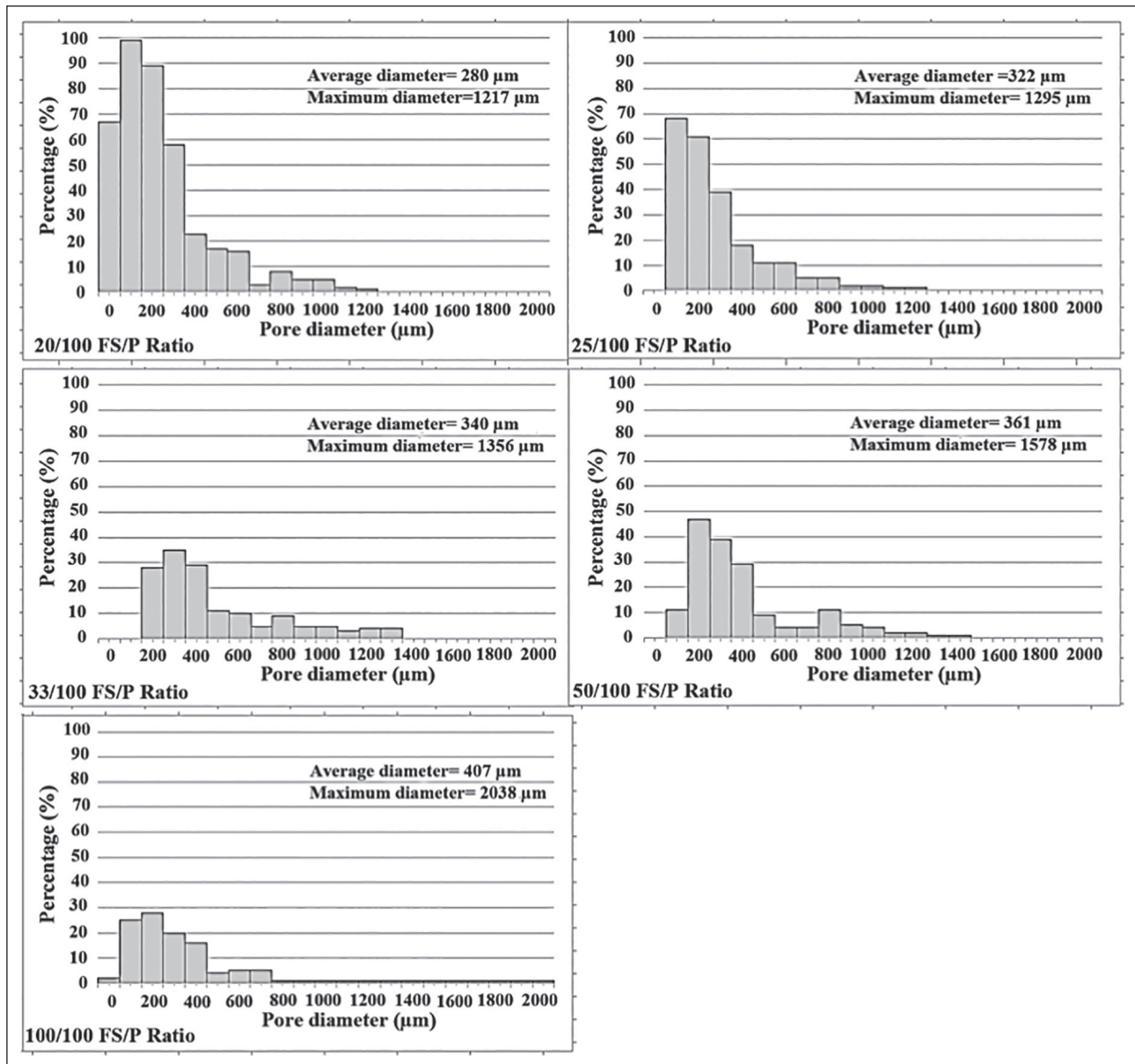


Figure 6. Frequency distribution diagrams of the pore diameters, average and maximum values of pore diameters of ED-based geopolymer foams having various FS/P ratios.

The ultrasound pulse velocity (U.P.V.) is a non-destructive test method used to measure the homogeneity of concrete [40]. The pores and cracks in the concrete reduce the U.P.V. of the material, which aids in specifying the quality of concrete [41]. In this study, the homogeneity of the pore distribution of the material is determined by measuring the U.P.V. in two different regions of the sample (Fig. 11a), and the homogeneity percentage is calculated according to the standard deviation of U.P.V. results (Fig. 11b). The highest homogeneity (99.3%) was obtained from the specimens which do not have any Al powder content as expected. Increasing the Al powder content led to a decrease in the homogeneity of the ED-based geopolymer

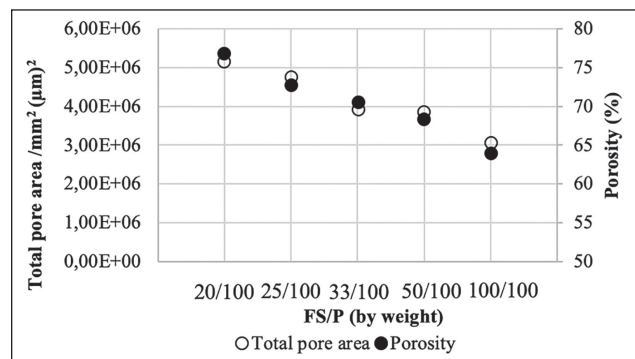


Figure 7. Total pore area and porosity of ED-based geopolymer foams as a function of FS/P ratio.

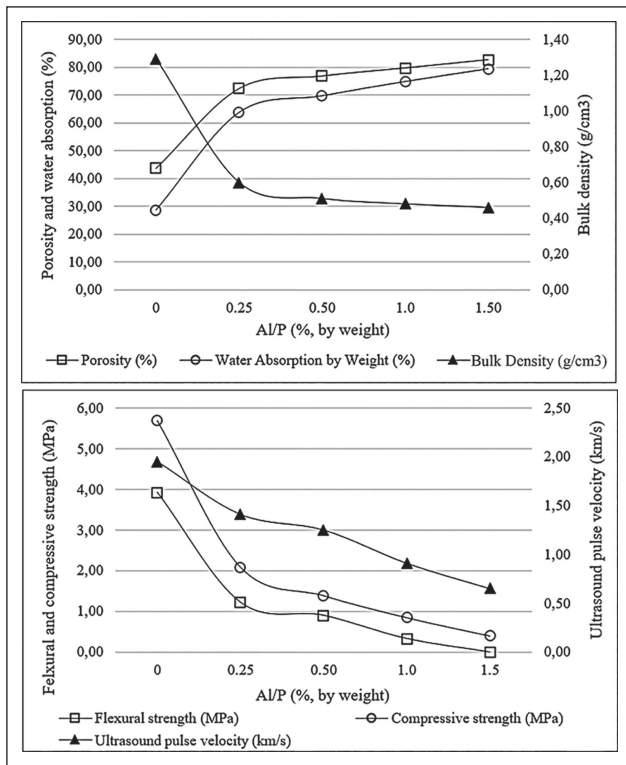


Figure 8. Effects of Al/P ratio on the physical and mechanical properties of ED-based geopolymer foam.

foams. Mainly, the least level of homogeneity (85.8%) was observed in the specimens having a 1.5% Al/P ratio, which may have resulted from the larger pore size distribution. This result confirms the findings that adding more Al powder may cause a microstructure with larger pores and irregular pore size distribution.

The effects of the Al/P ratio on porosity, average pore diameter, thermal conductivity, and compressive strength are given in Figure 12.

The porous microstructure of ED-based geopolymer mortar by adding Al powder in various proportions caused lower compressive strength than the sample without Al powder content. The specimens containing lower amounts of Al powder (0.25 and 0.50%) have found higher strengths due to the paste's being more homogenous with finer pore size and narrower pore size distribution. In addition, these specimens have a relatively lower amount of interconnectivity between pores. Thus, regularly formed air pores increase the compressive strength [42]. However, in the specimens with a 1.5% Al/P ratio, pores were interconnected, and a higher degree of pore interconnectivity and foam coalescence (merging of bubbles) led to a wide distribution of pore size and lower strength [42]. When the pore wall is too thin to bear incoming shrinkage, and if there are excessive bubbles in the matrix, during the drying process, the films between them become weak, and the bubbles start to co-

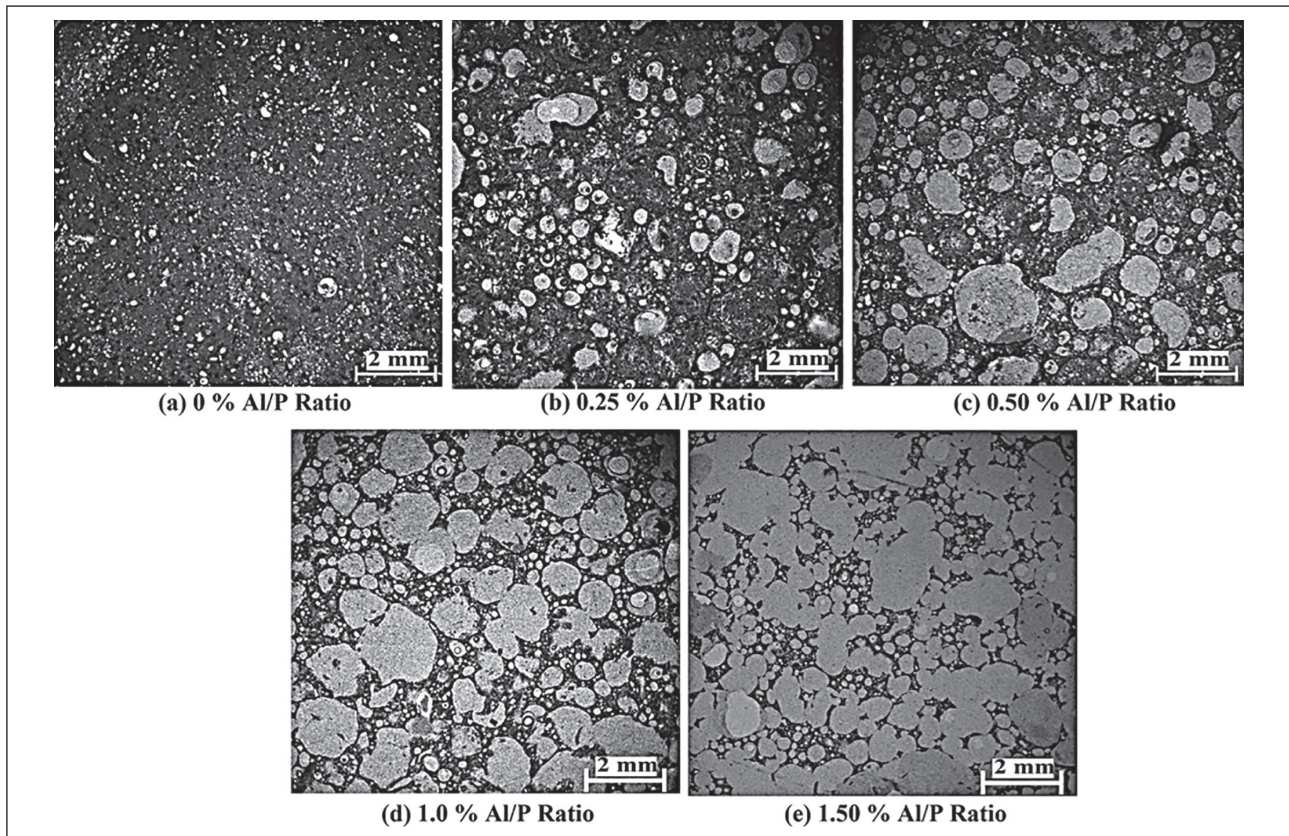


Figure 9. Microscopic images of ED-based geopolymer foams having various Al/P ratios.

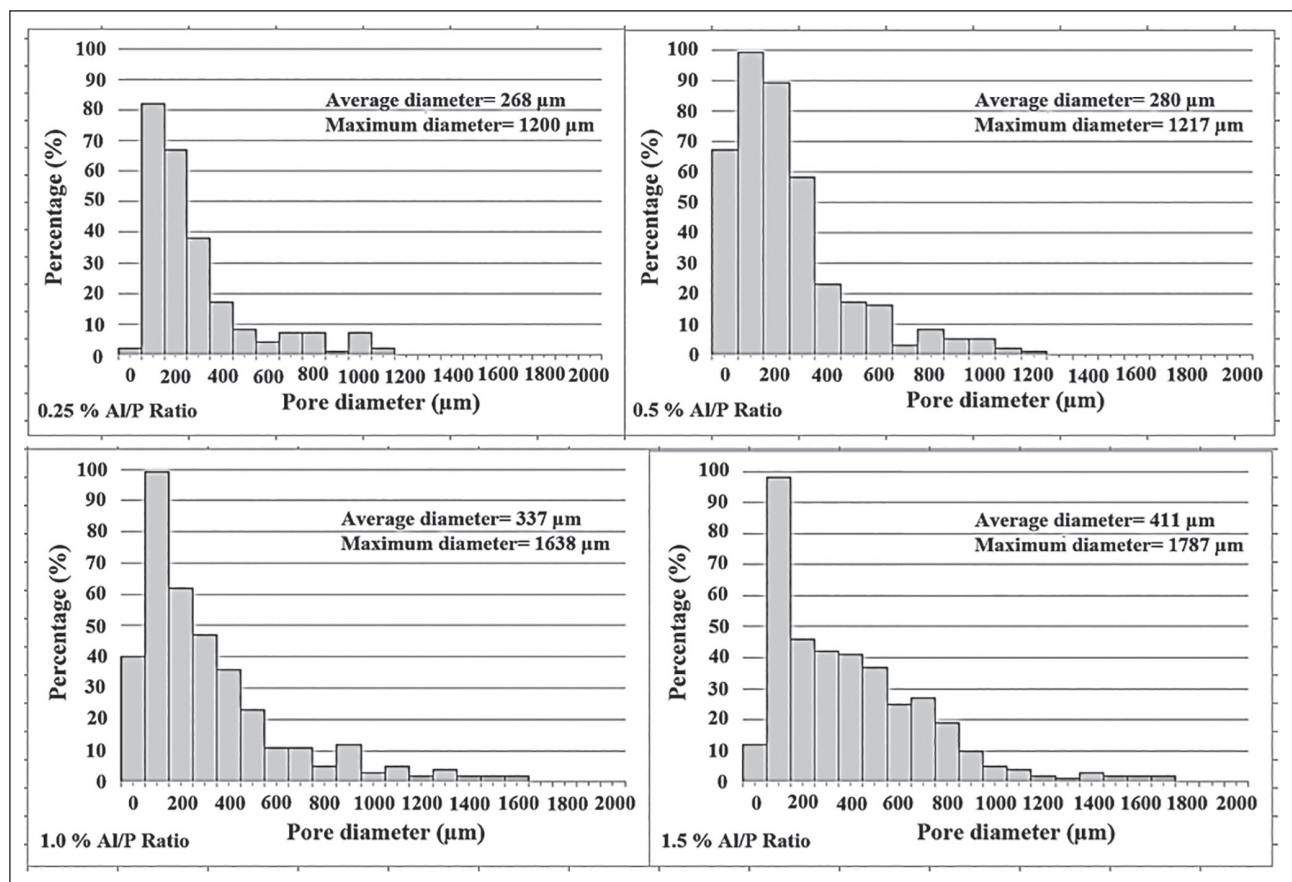


Figure 10. Frequency distribution diagrams of the pore diameters, average and maximum values of pore diameters of ED-based geopolymer foams having various Al/P ratios.

alesce, giving rise to much more connected pores with larger overall pore size. Accordingly, the mechanical properties of the material decrease [43–46].

3.3. Thermal Properties of the ED-Based Geopolymer Foam

In the current study, Al powder was added to the geopolymer mortar to reduce its thermal conductivity without compromising the physical and mechanical performance requirements required for the material to be used in partition walls. The gradual increase of the Al/P ratio from 0% to 1.5% is directly proportional to the increase in porosity (1.89 times), but it is inversely proportional to the thermal conductivity, where it decreased from 0.312 W/mK to 0.087 W/mK (0.27 times) (Figure 12). A higher degree of porosity means more pores that may act as thermal insulation [47] since the thermal conductivity of still-air is lower than that of the solid matrix [48]. The most significant decrease in the thermal conductivity of the material occurred between 0–0.25% Al/P ratio, which highlights the positive effect of Al powder addition on lowering the thermal conductivity of the solid matrix. By increasing the Al/P ratio from 0.25 to 0.50, the porosity and average pore diameter increased approximately 1.1 times, while the thermal conductivity de-

creased 0.75 times. By increasing the Al/P ratio from 0.50 to 1.50, although the porosity and pore diameter increased approximately 1.50 times, the decrease in the thermal conductivity was only 0.86 times (Figure 12). Increasing the amount of Al/P ratio by more than 0.50 did not give the expected effect in reducing the thermal conductivity. This may be due to the contrasting effect of the non-homogeneous pore size distribution with larger pores (Figure 9). Therefore, it can be stated that the development of the thermal insulation capacity of a geopolymer foam is not only affected by the porosity and hence density, but also by the pore size, shape, and interconnectivity between pores [49, 50]. Smaller, more circular, and less interconnected pores increase the insulation capacity in porous structures [51].

In the case of higher thermal performance is expected, the specimen with the lowest thermal conductivity (0.087 W/mK) having the highest Al/P ratio can be selected as optimum. However, mechanical properties cannot be ignored during practical implementations [43]. Indeed, it is expected that these porous materials have the least strength that could maintain their stability under loads of non-load bearing wall sections. The criteria in the production of ED-based geopolymer foam are determined to have a thermal

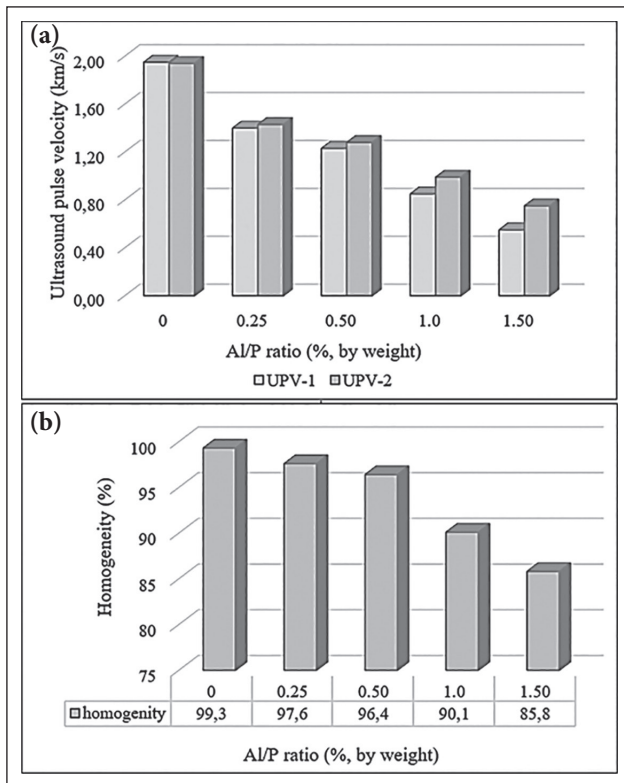


Figure 11. (a) Ultrasound pulse velocity obtained from two different regions in a sample; (b) calculated homogeneity percentage.

conductivity of ≤ 0.1 W/mK and compressive strength of ≥ 1.0 MPa [48]. According to this, the optimum Al/P ratio of 0.5% meets the determined criteria.

3.4. Comparison with Other Current Inorganic Ceramic Wall and Insulation Materials

Bulk density, thermal conductivity, and compressive strengths of ED-based geopolymer foams are compared with those of various inorganic ceramic wall and insulation materials used in the building sector (Table 5, Fig. 13).

According to Table 5 and Figure 13, the thermal conductivities of ED-based geopolymer foams produced in this study were higher than that of glass foam and lower than that of vertically perforated lightweight brick; similar results were obtained with pumice concrete, aerated autoclaved concrete, and foam concrete. Suppose protective layers can compensate for their lower compressive strength and higher water absorption ratio. In that case, this material may be used as a core layer of a laminated geopolymer composite, which behaves homogeneously regarding macro scale.

3.5. Comparison with Other Existing Studies in the Literature

The porosity, thermal conductivity, and compressive strength of ED-based geopolymer foams are com-

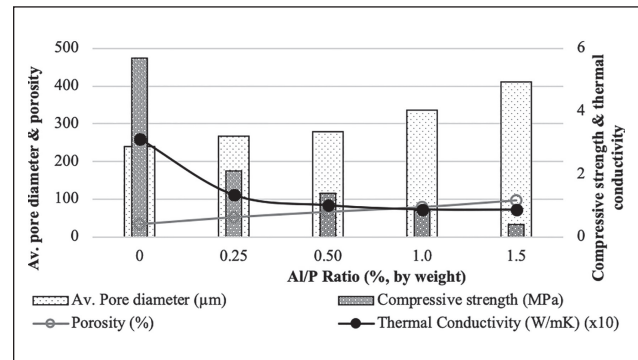


Figure 12. Effects of the Al/P ratio on porosity, average pore diameter, thermal conductivity, and compressive strength.

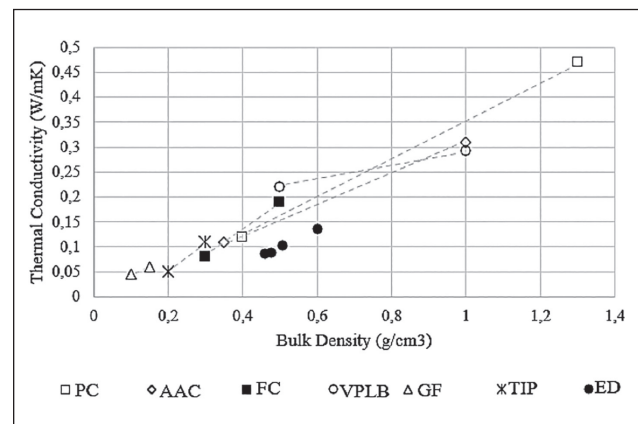


Figure 13. Comparison of the properties of ED-based geopolymer foam with inorganic ceramic wall and insulation materials (P.C.: Pumice concrete, A.A.C.: Aerated autoclaved concrete, F.C.: Foam concrete, VPLB: Vertically lightweight perforated brick, G.F.: Glass foam, T.I.P.: Thermal insulation plasters, ED: Earth of Datça-based geopolymer foam).

pared with those of geopolymer foams produced from various aluminosilicate sources and pore foaming agents (Table 6).

According to this comparison, the lowest thermal conductivity of ED-based geopolymer foam (0.087 W/mK) is higher than that of ultrafine perlite-based geopolymer foam [9]; similar to that of fly ash [3], bottom ash [20, 53], and a combination of metakaolin and fly ash [54] based foams; lower than that of fly ash [10, 38], calcined kaolin [55], natural soil of Pakistan [5], a combination of metakaolin and silica fume [6], metakaolin [13, 14, 16, 56], waste glass [19], and metakaolin waste, glass waste and steel-plant waste [21]-based geopolymer foams. It is seen that the porosity and compressive strength values of the produced foam like to those of the other materials in the table. Thus, ED-based geopolymer foam looks promising to be used as a rigid inorganic wall insulation material in the building industry.

Table 5. Compare ED-based geopolymer foam properties with other inorganic ceramic wall and insulation materials

Material	Bulk density (g/cm ³)	Thermal conductivity (W/mK)	Compressive strength (MPa)
Thermal insulation plasters [52]	≥0.2	0.05–0.10	–
Pumice concrete [52]	0.4–1.3	0.12–0.47	2.5–5.0
Aerated autoclaved concrete [52]	0.35–1.0	0.11–0.31	≥4
Foam concrete [10]	0.3–0.5	0.081–0.19	≥0.4
Vertically perforated lightweight brick [52]	0.5–1.0	0.22–0.29	2.5–7.5
Glass foam [52]	0.1–0.15	0.045–0.060	0.12–0.14
Earth of Datça-based geopolymer foam			
Al/P ratio (%)			
0	1.29	0.312	5.69
0.25	0.60	0.134	2.09
0.50	0.51	0.101	1.39
1.0	0.48	0.088	0.85
1.5	0.46	0.087	0.40

Table 6. Comparison of ED-based geopolymer foam properties with other geopolymer foams containing various aluminosilicate sources and pore-forming agents

Reference	Aluminosilicate source	Pore-forming agent	Porosity (%)	Thermal conductivity (W/mK)	Compressive strength (%)
[9]	Ultrafine perlite	H ₂ O ₂	74–89	0.03–0.06	0.2–0.8
[3]	Fly ash	H ₂ O ₂	74–81	0.07–0.09	0.4–1.4
[53]	Bottom ash	Sodium silicate	66–76	0.074–0.09	1.2–3.5
[20]	Bottom ash	Sodium silicate	42–73	0.075–0.091	3.0–6.2
[54]	Metakaolin+ fly ash	H ₂ O ₂	48–81	0.08–0.2	0.3–21
Current study	Earth of Datça	Al powder	72.3–82.6	0.087–0.134	0.40–2.09
[10]	Fly ash	H ₂ O ₂	41.5–72.5	0.10–0.40	1.2–6.6
[55]	Calcined kaolin	H ₂ O ₂	56–75	0.11–0.17	1.8–5.2
[14]	Metakaolin	H ₂ O ₂	60.2–83.1	0.11–0.17	0.3–11.6
[6]	Silica fume +metakaolin	Silica fume	78–85	0.12–0.17	–
[13]	Metakaolin	Silica fume	65–85	0.12–0.35	–
[56]	Metakaolin	Silica fume	65–85	0.12–0.35	–
[21]	Metakaolin waste, Glass waste, Steel-plant waste	Aluminum scrap recycling waste	83–86	0.14–0.15	1.1–2.0
[16]	Metakaolin	Al powder	30–70	0.15–0.60	–
[19]	Waste glass	H ₂ O ₂	55	0.21	7.3
[5]	Natural soil from Pakistan	H ₂ O ₂	54–63	0.27–0.35	1.57–2.41
[38]	Fly ash	SiC powder	32–52	0.42–0.67	1.2–4.1

4. CONCLUSIONS

In line with the results obtained throughout the study, the following remarks can be specified:

- Geopolymer mixture produced by mixing Al powder as a foaming agent and volcanic Tuff of Datça Peninsula in Turkey as aluminosilicate source gives promising results

in producing highly porous geopolymers with low thermal conductivity.

- The addition of finely ground silica sand ensures the volumetric stability of the geopolymer binder and prevents the collapse after swelling of the binder.
- The volume expansion ratio of the binder decreases with the increasing fine sand to pozzolan (FS/P) ratio.

The optimum FS/P ratio is determined as 20/100 since it enables the production of more homogeneous mortar without any collapse and surface deformation. The pores of sand-rich specimens show the non-homogeneous distribution of the larger pores with a higher degree of interconnectivity. Furthermore, because fine sand decreases the porosity and increases the density of the mortar, it leads to reduce thermal performance; the amount of fine sand should not be increased unnecessarily.

- The optimum Al powder to pozzolan (Al/P) ratio is determined as 0.5% because it gives better physical, mechanical, and thermal properties due to its more homogenous microstructure with finer pore size, regular (narrower) pore size distribution, and lower degree of interconnectivity (low amount of pore coalescence).
- The thermal conductivity is affected by the total volume of the macroscale pores (>10 µm), shape, and interconnectivity between pores. Smaller, more circular, and less interconnected pores increase the insulation capacity in porous structures.
- Thermal conductivities of ED-based geopolymer foams (0.087–0.134 W/mK) were found within a similar range with commonly used alternative inorganic ceramic wall materials.
- The high insulation capacity is considered the main key parameter. ED-based geopolymer foam provided promising data to be used as a rigid wall insulation material in the building industry. However, its comparatively lower mechanical properties and higher water absorption ratio could be compensated by protective layers, and it could be used as a core layer of a laminated geopolymer composite that behaves homogeneously with regard to macro scale.

ACKNOWLEDGMENTS

The authors express their gratitude to Prof. Dr. Emin Çiftçi, who provided the I.T.U. Department of Geological Engineering laboratory facilities for optical microscope analysis.

DATA AVAILABILITY STATEMENT

The authors confirm that the data that supports the findings of this study are available within the article. Raw data that support the finding of this study are available from the corresponding author, upon reasonable request.

CONFLICT OF INTEREST

The authors declare that they have no conflict of interest.

FINANCIAL DISCLOSURE

This research was financially supported by the Center for Scientific Research Projects of Istanbul Technical University [grant number MGA-2019-41837].

PEER-REVIEW

Externally peer-reviewed.

REFERENCES

- [1] Liu, M.Y.J., Alengaram, U.J., Jumaat, M.Z., & Mo, K.H. (2014). Evaluation of thermal conductivity, mechanical, and transport properties of lightweight aggregate foamed geopolymer concrete. *Energy and Buildings*, 72, 238–245. [CrossRef]
- [2] Allouhi, A., El Fouih, Y., Kousksou, T., Jamil, A., Zeraouli, Y., & Mourad, Y. (2015). Energy consumption and efficiency in buildings: current status and future trends. *Journal of Cleaner Production*, 109, 118–130. [CrossRef]
- [3] Feng, J., Zhang, R., Gong, L., Li, Y., Cao, W., & Cheng, X. (2015). Development of porous fly ash-based geopolymer with low thermal conductivity. *Materials Design*, 65, 529–533. [CrossRef]
- [4] Garcia-Lodeiro, I., Palomo, A., & Fernández-Jiménez, A. (2015). An overview of the chemistry of alkali-activated cement-based binders. In: Pacheco-Torgal F, Labrincha JA, Leonelli C, Palomo A, Chindapasirt P (Ed.). *Handbook of Alkali-Activated Cements, Mortars, and Concretes*, Woodhead Publishing, U.K., 19–47. [CrossRef]
- [5] Zaidi, S.F.A., Haq, E.U., Nur, K., Ejaz, N., Anis-Ur-Rehman, M., Zubair, M., & Naveed, M. (2017). Synthesis & characterization of natural soil based inorganic polymer foam for thermal insulations. *Construction and Building Materials*, 157, 994–1000. [CrossRef]
- [6] Papa, E., Medri, V., Kpogbemabou, D., Morinière, V., Laumonier, J., Vaccari, A., & Rossignol, S. (2016). Porosity and insulating properties of silica-fume based foams. *Energy and Buildings*, 131, 223–232. [CrossRef]
- [7] Duxson, P., Provis, J.L., Lukey, G.C., & van Deventer, J.S.J. (2007). The role of inorganic polymer technology in the development of 'green concrete'. *Cement and Concrete Research*, 37(12), 1590–1597. [CrossRef]
- [8] Bai, C., & Colombo, P. (2018). Processing, properties and applications of highly porous geopolymers: A review. *Ceramics International*, 44(14), 16103–16118. [CrossRef]
- [9] Vaou, V., & Paniais, D. (2010). Thermal insulating foamy geopolymers from perlite. *Minerals Engineering*, 23(14), 1146–1151. [CrossRef]
- [10] Novais, R.M., Buruberry, L.H., Ascensao, G., Seabra, M.P., & Labrincha, J.A. (2016a). Porous biomass fly ash-based geopolymers with tailored thermal conductivity. *Journal of Cleaner Production*, 119, 99–107. [CrossRef]
- [11] Łach, M., Pławecka, K., Bąk, A., Lichočka, K., Korniejewski, K., Cheng, A., & Lin, W.T. (2021). Determination of the influence of hydraulic additives on the foaming process and stability of the produced geopolymer foams. *Materials*, 14, Article 5090. [CrossRef]

- [12] Phavongkham, V., Wattanasiriwech, S., Cheng, T-W., & Wattanasiriwech, D. (2020). Effects of surfactant on thermo-mechanical behavior of geopolymer foam paste made with sodium perborate foaming agent. *Construction and Building Materials*, 243, Article 118282. [CrossRef]
- [13] Henon, J., Alzina, A., Absi, J., Smith, D.S., & Rossignol, S. (2013). Potassium geopolymer foams made with silica fume pore forming agent for thermal insulation. *Journal of Porous Materials*, 20, 37–46. [CrossRef]
- [14] Bai, C., Ni, T., Qiaoling, W., Hongqiang, L., & Colombo, P. (2018). Porosity, mechanical and insulating properties of geopolymer foams using vegetable oil as the stabilizing agent. *Journal of European Ceramic Society*, 38, 799–805. [CrossRef]
- [15] Qiao, Y., Li, X., Bai, C., Li, H., Yan, J., Wang, Y., Wang, X., Zhang, X., Zheng T., & Colombo, P. (2021). Effects of surfactants/stabilizing agents on the microstructure and properties of porous geopolymers by direct foaming. *Journal of Asian Ceramic Societies*, 9(1), 412–423. [CrossRef]
- [16] Kamseu, E., Nait-Ali, B., Bignozzi, M.C., Leonelli, C., Rossignol, S., & Smith, D.S. (2012). Bulk composition and microstructure dependence of effective thermal conductivity of porous inorganic polymer cements. *Journal of European Ceramic Society*, 32(8), 1593–1603. [CrossRef]
- [17] Peng, X., Li, H., Shuai, Q., & Wang L. (2020). Fire resistance of alkali activated geopolymer foams produced from metakaolin and Na_2O_2 . *Materials (Basel)*, 13(3), 535. [CrossRef]
- [18] Sornlar, W., Wannagon, A., & Supothina, S. (2021). Stabilized homogeneous porous structure and pore type effects on the properties of lightweight kaolinite-based geopolymers. *Journal of Building Engineering*, 44, Article 103273. [CrossRef]
- [19] Bai, C., Li, H., Bernardo, E., & Colombo, P. (2019). Waste-to-resource preparation of glass-containing foams from geopolymers. *Ceramics International*, 45(6), 7196–7202. [CrossRef]
- [20] Haq, E.U., Padmanabhan, S.K., & Licciulli, A. (2015). Microwave synthesis of thermal insulating foams from coal derived bottom ash. *Fuel Processing Technology*, 130, 263–267. [CrossRef]
- [21] Dembovska, L., Bajare, D., Ducman, V., Korat, L., & Bumanis, G. (2017). The use of different by-products in the production of lightweight alkali activated building materials. *Construction and Building Materials*, 135, 315–322. [CrossRef]
- [22] Akgül, E., & Tanaçan, L. (2011). Evaluation of the pozzolanic activity of the earth of Datça as a building material. *International Journal of Architectural Heritage*, 5, 1–26. [CrossRef]
- [23] Ercan, T., Günay, E., Baş, H., & Can, B. (1984). Petrology of quaternary volcanic rocks in the Datca Peninsula and comment on their origin. *Bulletin of the Mineral Research and Exploration*, 97/98, 21–23. [Turkish]
- [24] TS EN 196–6 (2010). Methods of testing cement – Part 6: Determination of fineness. *Turkish Standard Institution*, Ankara.
- [25] T.S. 25 (2008). *Tras*. Turkish Standard Institution.
- [26] Barış, K.E., & Tanaçan, L. (2021). Improving the geopolymeric reactivity of Earth of Datça as a Natural Pozzolan in developing green binder. *Journal of Building Engineering*, 41, Article 102760. [CrossRef]
- [27] Hajimohammadi, A., Ngo, T., & Kashani, A. (2018). Glass waste versus sand as aggregates: The characteristics of the evolving geopolymer binders. *Journal of Cleaner Production*, 193, 593–603. [CrossRef]
- [28] Wang, Y., Wang, Y., & Zhang, M. (2021). Effect of sand content on engineering properties of fly ash-slag based strain hardening geopolymer composites. *Journal of Building Engineering*, 34, Article 101951. [CrossRef]
- [29] Jones, M.R., Ozlutas, K., & Zheng, L. (2015). Stability and instability of foamed concrete. *Magazine of Concrete Research*, 68(11), 1–8. [CrossRef]
- [30] ASTM C1437–20 (2020). *Standard Test Method for Flow of Hydraulic Cement Mortar*. ASTM International, West Conshohocken.
- [31] TS EN 1015–10 (2001). *Methods of test for mortar for masonry – Part 10: Determination of dry bulk density of hardened mortar*. Turkish Standard Institution, Ankara.
- [32] TS EN 13755 (2009). *Natural stone test methods – Determination of water absorption at atmospheric pressure*. Turkish Standard Institution, Ankara.
- [33] TS EN 14579 (2006). *Natural stone test methods – Determination of sound speed propagation*. Turkish Standard Institution, Ankara.
- [34] TS EN 196–1 (2009). *Methods of testing cement – Part 1: Determination of strength*. Turkish Standard Institution, Ankara.
- [35] ASTM C518–17 (2017). *Standard test method for steady-state thermal transmission properties by means of the heat flow meter apparatus*. ASTM International, West Conshohocken.
- [36] Cui, Y., Wang, D., Zhao, J., Li, D., Ng, S., & Rui, Y. (2018). Effect of calcium stearate based foam stabilizer on pore characteristics and thermal conductivity of geopolymer foam material. *Journal of Building Engineering*, 20, 21–29. [CrossRef]
- [37] Zhang, Z., Provis, J.L., Reid, A., & Wang, H. (2014). Geopolymer foam concrete: An emerging material for sustainable construction. *Construction and Building Materials*, 56, 113–127. [CrossRef]

- [38] Gualtieri, M.L., Cavallini, A., & Romagnoli, M. (2016). Interactive powder mixture concept for the preparation of geopolymers with fine porosity. *Journal of European Ceramic Society*, 36(10), 2641–2646. [CrossRef]
- [39] Kamseu, E., Ngouloure, Z.N.M., Ali, B.N., Zekeng, S., & Melo, U.C., Rossignol, S., Leonelli, C. (2015). Cumulative pore volume, pore size distribution and phases percolation in porous inorganic polymer composites: Relation microstructure and effective thermal conductivity. *Energy and Buildings*, 88, 45–56. [CrossRef]
- [40] Lim, M.K., & Cao, H. (2013). Combining multiple NDT methods to improve testing effectiveness. *Construction and Building Materials*, 38, 1310–1315. [CrossRef]
- [41] Hajimohammadi, A., Ngo, T., Mendis, P., Kashani, A., & van Deventer, J.S.J. (2017). Alkali activated slag foams: The effect of the alkali reaction on foam characteristics. *Journal of Cleaner Production*, 147, 330–339. [CrossRef]
- [42] Hamad, A.J. (2014). Materials, production, properties and application of aerated lightweight concrete: Review. *International Journal of Materials Science and Engineering*, 2(2), 152–157. [CrossRef]
- [43] Huang, Y., Gong, L., Shi, L., Cao, W., Pan, Y., & Cheng, X. (2018). Experimental investigation on the influencing factors of preparing porous fly ash-based geopolymer for insulation material. *Energy and Buildings*, 168, 9–18. [CrossRef]
- [44] Zhang, Z., Provis, J.L., Reid, A., & Wang, H. (2015). Mechanical, thermal insulation, thermal resistance and acoustic absorption properties of geopolymer foam concrete. *Cement and Concrete Composites*, 62, 97–105. [CrossRef]
- [45] Xu, F., Gu, G., Zhang, W., Wang, H., Huang, X., & Zhu, J. (2018). Pore structure analysis and properties evaluations of fly ash-based geopolymer foams by chemical foaming method. *Ceramics International*, 44(16), 19989–19997. [CrossRef]
- [46] Zhang, Z., & Wang, H. (2016). The pore characteristics of geopolymer foam concrete and their impact on the compressive strength and modulus. *Frontiers in Materials*, 3, Article 38. [CrossRef]
- [47] Prud'homme, E., Joussein, E., & Rossignol, S. (2015). Alkali-activated concrete binders as inorganic thermal insulator materials, Chapter 26, In: Pacheco-Torgal F, Labrincha JA, Leonelli C, Palomo A, Chindaprasirt P (Ed.). *Handbook of Alkali Activated Cements, Mortars and Concretes*, Woodhead Publishing, U.K., 687–728. [CrossRef]
- [48] Gürdal, E. (1998). Isı iletkenlik katsayısının malzeme özellikleri ile ilişkileri. *Yapı*, 80, 44–46. [Turkish]
- [49] Schlegel, E., Häussler, K., Seifert, H., & Freiberg, K. (1999). Microporosity and its use in highly efficient thermal insulating materials. *Cfi-Ceramic Forum International*, 76, 7–10.
- [50] Dondi, M., Mazzanti, F., Principi, P., Raimondo, M., & Zanarini, G. (2004). Thermal conductivity of clay bricks. *Journal of Materials in Civil Engineering*, 16, 8–14. [CrossRef]
- [51] Hajimohammadi, A., Ngo, T., & Kashani, A. (2018). Sustainable one-part geopolymer foams with glass fines versus sand as aggregates. *Construction and Building Materials*, 171, 223–231. [CrossRef]
- [52] TS 825 (2013). Thermal insulation requirements for buildings. *Turkish Standard Institution*, Ankara.
- [53] Haq, E.U., Padmanabhan, S.K., Zubair, M., Ali, L., & Licciulli, A. (2016). Intumescence behaviour of bottom ash based geopolymer mortar through microwave irradiation – As affected by alkali activation. *Construction and Building Materials*, 126, 951–956. [CrossRef]
- [54] Novais, R.M., Ascensão, G., Buruberri, L.H., Senff, L., & Labrincha, J.A. (2016b). Influence of blowing agent on the fresh and hardened-state properties of lightweight geopolymers. *Materials Design*, 108, 551–559. [CrossRef]
- [55] Palmero, P., Formia, A., Antonaci, P., Brini, S., & Tulliani, J.M. (2015). Geopolymer technology for application-oriented dense and lightened materials. Elaboration and characterization. *Ceramics International*, 41(10), 12967–12979. [CrossRef]
- [56] Henon, J., Pennec, F., Alzina, A., Absi, J., Smith, D.S., & Rossignol, S. (2014). Analytical and numerical identification of the skeleton thermal conductivity of a geopolymer foam using a multi-scale analysis. *Computational Materials Science*, 82, 264–273. [CrossRef]



Research Article

Characterization of carbon fiber reinforced conductive mortars filled with recycled ferrochrome slag aggregates

Fatih DOĞAN¹, Heydar DEGHANPOUR^{*2}, Serkan SUBAŞI³, Muhammed MARAŞLI³

¹Munzur University, Rare Earth Elements Application & Research Center, Tunceli, Türkiye

²Fibrobeton Company, R&D Center, Düzce, Türkiye

³Department of Civil Engineering, Düzce University, Engineering Faculty, Düzce, Türkiye

ARTICLE INFO

Article history

Received: 05 August 2022

Accepted: 17 August 2022

Key words:

Carbon fiber, conductivity, dynamic resonance, ferrochrome slag aggregate, mortar

ABSTRACT

Recently, it has been known that carbon fiber, a conductive fiber, is used in different mixture designs and the development of electrically conductive cementitious materials. However, the evaluation of ferrochrome slag as a recycled aggregate in the mixture of these special concretes has still not been investigated. In this study, electrically conductive mortars were produced using 100% recycled ferrochrome slag aggregate with a particle size of less than 1 mm as filling material and using carbon fiber in 4 different ratios, 0%, 0.5%, 0.75%, and 1%. To investigate the electrical conductivity properties, the resistivity values of the samples were measured at five different times within 2–180 days. In addition, 28-day compressive strength, flexural strength, dynamic resonance, ultrasonic pulse velocity, Leeb hardness, scanning electron microscope, and X-Ray Diffraction tests were performed on all samples. The results were compared with the literature, proving that ferrochrome slag could be used as a reasonable aggregate in conductive mortars. The age effect was minimal in CF-added mixtures. With the addition of 1% CF, the resistivity values decreased approximately 40 times compared to the reference. Moreover, SEM analyses of the CF-0.75 sample showed that the CFs adhered to form a conductive network between the components in the ferrochrome-filled compact structure.

Cite this article as: Doğan, F., Dehghanpour, H., Subaşı, S., & Maraşlı, M. (2022). Characterization of carbon fiber reinforced conductive mortars filled with recycled ferrochrome slag aggregates. *J Sustain Const Mater Technol*, 7(3), 145–157.

1. INTRODUCTION

Cement and aggregate, used extensively in the construction sector, threaten the consumption of natural resources with each passing day. Therefore, different researches were carried out on industrial waste in concrete production [1]. Using industrial wastes as aggregates is im-

portant in reducing natural resource consumption and environmental impacts [2]. Industrial wastes, which are used instead of different components in concrete, improve concrete's mechanical and electrical properties. Research on alternative materials is continuing to minimize the greenhouse gases emerging from cement production, which is the main component material of concrete, and reduce en-

*Corresponding author.

*E-mail address: heydar.dehghanpour@fibrobeton.com.tr



ergy consumption. In addition, since the aggregates used in concrete production cause the consumption of natural resources, alternative material studies are carried out [3]. Since concrete, used as a basic material in structures such as buildings and bridges, exhibits brittle behavior under high pressure, various research has been carried out to improve the mechanical properties of concrete [4, 5]. Aggregate, which constitutes the largest volume of the composition in the concrete mix, plays a decisive role in terms of concrete strength and workability. Studies use industrial waste products such as copper, steel, and ferrochrome wastes instead of aggregates in the cement mixture [2]. Ferrochrome waste is one of the wastes preferred instead of aggregate in concrete production related to the reuse of industrial wastes [6]. Considering its adhesion and mechanical properties, it is seen as an alternative component that can be used instead of the aggregate used in the concrete mix [7]. It has been reported that ferrochrome waste particles have a higher density than aggregates [8]. If the ferrochrome waste released because of global ferrochrome production could be taken under control and reused, natural resources would be used more efficiently. In this context, it is foreseen that the use of ferrochrome waste in cement production will be beneficial in terms of both cost reduction and energy savings. In the study of Niemela and Kauppi [9], it was reported that ferrochrome waste is chemically stable and can be used safely. Also, Lind et al. [10] reported that ferrochrome waste is less likely to distribute harmful heavy metals to the environment. Acharya and Patro [11] reported that ferrochrome waste can be used with lime instead of Portland cement in concrete production. In addition, it was stated that lime and ferrochrome waste added to the concrete mixture improved the flexural and compressive strength of the concrete. Panda et al. [12] used ferrochrome waste as aggregate in the production of portland cement and reported that they obtained high-strength concrete. Kumar et al. [13] explained that they produced concrete with high compressive strength with the ferrochrome waste they used as aggregate. In addition, there are studies in which higher compressive and flexural strength results of ferrochrome aggregate concrete are obtained compared to conventional aggregate concrete [2, 14]. Since there are not many studies on the mechanical properties of ferrochrome waste, it is necessary to determine the mechanical properties of concrete by optimizing the amount of ferrochrome waste in the concrete mixture, which is likely to be used instead of sand as an aggregate in concrete production. Furthermore, in experimental studies, it is expected that concrete's structural and mechanical properties will be improved with the components used as additives in cement mortar production. Compared to conventional concrete, conductive concrete is superior in terms of mechanical properties and cost, and concretes produced with additives used in conductive concrete mix-

ture are used in application areas such as defrosting [15]. Studies are carried out to increase the mechanical properties of concrete with materials such as carbon nanotubes and carbon fiber (CF) included in cement-based mixtures [16]. It has been reported that CF concrete, which is one of the additives added to the concrete mix to give the concrete electrical properties, reduces the electrical resistance [17]. On the other hand, Chen and Liu [18] reported that the electrical resistance of the conductive concrete would increase in case of damage to the CF reinforced concrete. Roberts et al. [19] reported that CFs added to concrete improve the compressive and tensile strength of concrete. In addition, they explained that the damage to the conductive concrete can be determined by the relationship between the voltage applied to the concrete and its electrical resistance. Furthermore, CF incorporated into the concrete mix improves the mechanical properties of the concrete [20]. It has been confirmed by different studies that the electrical resistance of concrete is at high levels. While the electrical resistivity of outdoor dried concrete was determined as 6.54×10^5 – 11.4×10^5 Ω .cm, the electrical resistivity of saturated concrete and dry concrete were determined to be 10^6 Ω .cm and 10^9 Ω .cm, respectively [21]. There are various studies on the mechanical behavior of CF reinforced conductive concrete exposed to different loads such as pressure and bending [22]. In the literature, it has been reported that CF can inhibit microcrack growth in the study on the compressive strength of CF reinforced concrete [23]. Han et al. [24] stated that CF reinforced concrete has excellent compressive strength and high flexural strength compared to conventional concrete. Considering the use of industrial waste materials in concrete production and the studies on conductive concrete, research has been carried out to improve the strength properties of concrete by using recycled ferrochrome instead of aggregate. In addition, the CF additive in concrete was investigated in terms of both conductivity and mechanical properties. Studies on improving the mechanical properties of concrete by recycled ferrochrome, which is used as aggregate in concrete production, are limited. In addition, no studies have been conducted in which recycled ferrochrome and CF are used together in the concrete mix. In this paper, the effects of using recycled ferrochrome instead of aggregate used in the cement mixture and CF used as an additive on the microstructure, mechanical and electrical conductivity properties of the cement mortar were investigated. To understand the effect of recycled ferrochrome and CF on the performance of concrete, compressive strength, flexural strength, dynamic resonance, ultrasonic pulse velocity (UPV), Leeb hardness, and dry density tests were carried out. Considering that it will provide both low cost and energy savings, the use of recycled ferrochrome and CF mixture in the concrete mixture is research conducted to improve the mechanical and electrical properties of conductive concrete.

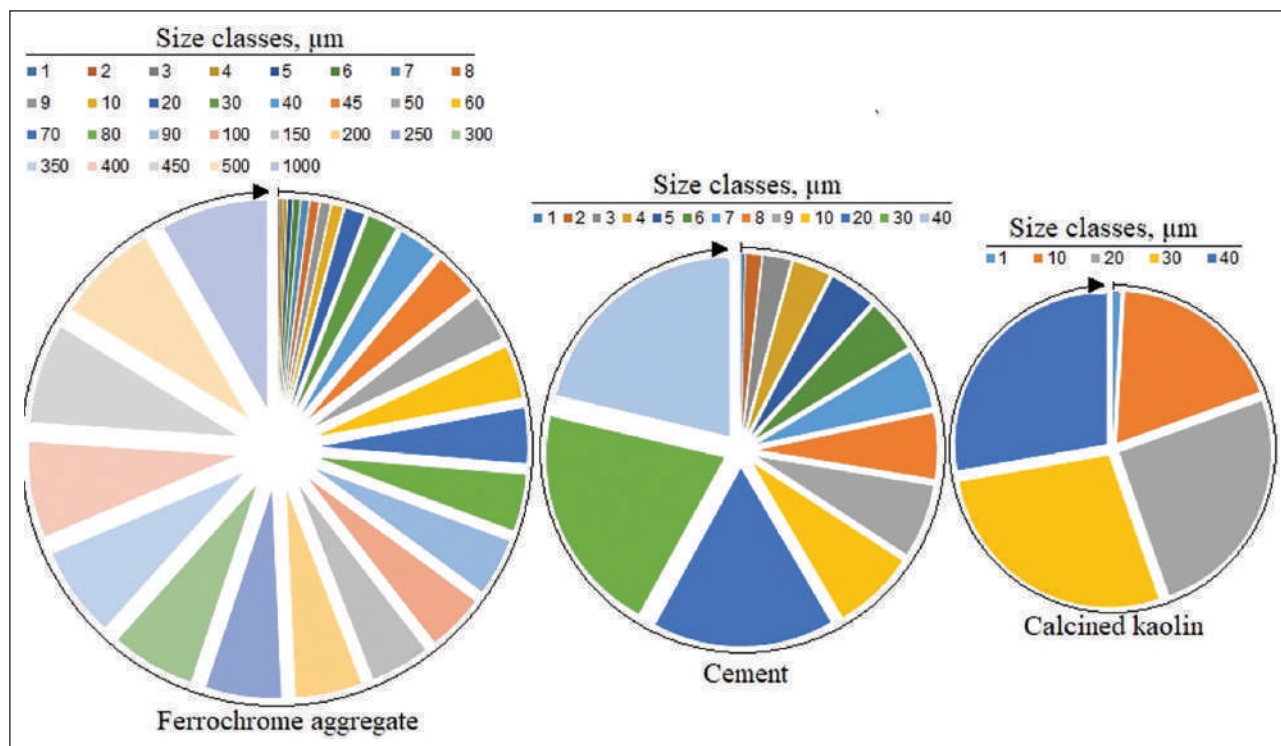


Figure 1. Grain size range of ferrochrome, cement, and calcined kaolin.

2. MATERIAL AND METHODS

2.1. Material Properties

100% ferrochrome aggregate was used as the filling material in all mixtures. The specific gravity of ferrochrome aggregate used was 3.33. CEM II-42.5 R white cement, preferred in facade cladding, was used as a binder. In all mixtures, 10% calcined kaolin by weight of cement was preferred. The particle size ranges of ferrochrome, cement, and calcined kaolin were compared in Figure 1. 12 mm long, 7.2 μm diameter, and 0.00155 Ω.cm electrical resistivity CF has been used as conductivity enhancing fiber. Carboxymethyl cellulose (0.2 wt%), which has been proven to have a positive effect in several previous studies [25–27], was used as a dispersing agent. Different ratios of polycarboxylate-based superplasticizers were used to ensure adequate workability in all mixtures.

The material content of the conductive mixtures produced within the scope of the study is summarized in Table 1. The mixture in the table's first row can be considered the matrix for all mixtures. All dry and liquid materials were weighed to form the matrix, and the dry materials were placed in the mixer for 90 seconds. 70% of the water was added and mixed for another 60 seconds. Finally, the required plasticizer was added to 30% of the water and added to the mixture, and the mixing process was continued for 60 seconds. After all the components came together in CF mixtures, when the matrix was ready, the fibers were added and mixed with a mixer for 90 seconds.

2.2. Test Methods

For all the planned tests, three 40x40x160 mm prismatic specimens were produced from each mixture, and all tests were performed on identical specimens, primarily non-destructive ones. The electrical resistivity of cementitious materials is measured for different purposes. For example, electrical resistivity values are measured, especially for corrosion detection in rebar reinforced structural elements. In these studies, the four-probe technique or other superficial test techniques are used as the measurement method. Since the resistivity measurement reason in the current study was to specify the bulk conductivity of the samples, the two-point uniaxial measurement method, which is also frequently used in the literature [21, 28], was preferred. A potential difference of 40 volts was applied to all samples for resistivity measurement. The frequency was kept constant at 50 Hz throughout the measurement. Longitudinal resonance frequency testing was performed for all mortar samples according to the ASTM C215 standard [29]. In this test method, the specimen is fixed midway between two supports, and a slight impact is applied from one end of the specimen, while the impact response from the other end is measured with an accelerometer. Resonance frequency diagrams are drawn for each sample using the data obtained with the accelerometer, and accordingly, the damping ratio of the mortars is determined.

Flexural and compressive strength tests were carried out following the TS EN 196-1 standard [30]. UPV tests were performed according to ASTM C597 [31]. The ASTM A956 standard [32] was used to determine the Leeb hardness of

Table 1. Component ratios in mixtures

No	Code	Ferrochrome slag aggregate (g)	Cement (g)	Calcined kaolin (g)	Water (g)	CF (g)	Superplasticizer (g)
1	Ref	1550	500	50	231	0.0	6.25
2	CF-0.50	1541	500	50	231	9.0	8.25
3	CF-0.75	1537	500	50	231	13.5	9.0
4	CF-1.0	1533	500	50	231	18.0	10.75

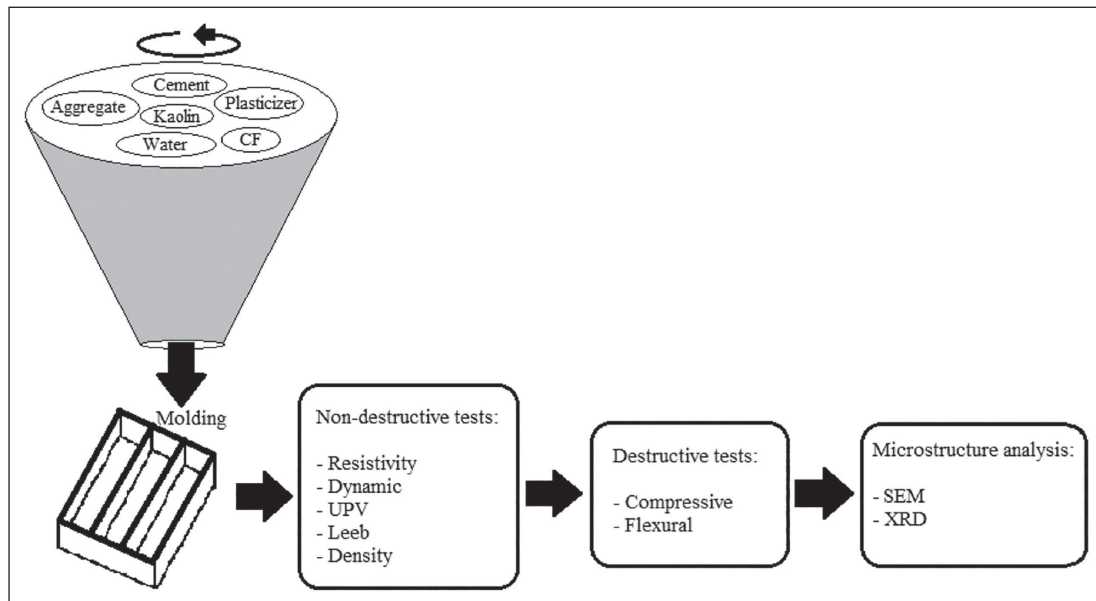


Figure 2. Experimental flow flowchart.

the produced samples. In addition, densities were calculated by measuring the dry weight and dimensions of all 28-day samples. The surface characterization of the mixture's ferrochrome aggregate used as aggregate was made by scanning electron microscopy (SEM) and elemental characterization by Energy Dispersive X-Ray Analysis (EDX). In addition, SEM and XRD analyses of FRC and FRC-0.75CF samples were performed. The experimental flow realized within the scope of the study is shown in Figure 2.

3. RESULTS AND DISCUSSION

3.1. Mechanical Test Results

The compressive and flexural strength test results of concrete samples are shown in Figure 3 comparatively. The CF additive component affected the mechanical properties of the conductive concrete. The compressive strength values of the samples vary between 66 MPa and 71 MPa. The highest compressive strength was determined in the 0.50 CF reinforced FRC-0.50CF sample. On the other hand, the compressive strength decreased with the increase of CF content in the cement mixture. Compared to the FRC-0.50CF sample, the compressive strength values in the FRC-0.75CF

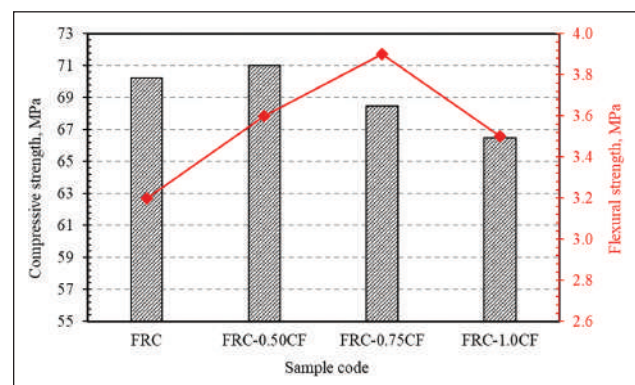


Figure 3. Compressive and flexural strength test results.

and FRC-1.0CF samples decreased by approximately 4% and 5%, respectively. It could be stated that the compressive strength value of the FRC-0.50CF sample is higher than the other samples, and the increased CF reinforcement element in the conductive concrete mixture causes a decrease in the compressive strength.

On the other hand, the flexural strength results of the samples are in the range of 63 to 72 MPa. The flexural strength test results increased with 0.50% CF added to the

concrete sample, as in the compressive strength test results. In the next test, the flexural strength value of the concrete of 0.75% CF reinforcement component in the cement mixture is 72 MPa. In the final test specimen, the flexural strength value decreased with increasing the CF content in the mixture to 1.0%. The flexural strength values of the FRC-0.50CF and FRC-1.0CF samples decreased approximately 5% and 8%, respectively, compared to the FRC-0.75CF sample with the highest flexural strength value. The flexural strength value of the ferrochrome-filled concrete sample without CF reinforcement is lower than that of the CF reinforced samples and could be associated with the improvement of the flexural strength of the concrete sample by the CF reinforcement component in the cement mixture. The flexural strength test results can be correlated with the load bearing capacity corresponding to the crack in the concrete material. Thus, the CF reinforcement increased the flexural strength by resisting crack propagation in the concrete material. Compressive strength in concrete materials containing CF reinforcement components was similar to flexural strength performance. While the highest compressive strength effect of the concrete material was achieved with 0.5% CF, the highest flexural strength increase was obtained with 0.75% CF. Al-Shamayleh et al. [33] associated the increase in compressive strength with high elasticity and reported that it contributed to the flexural strength. In addition, Chen et al. [23] pointed out that CF concrete increases compressive strength and prevents fractures in the concrete material. Therefore, it could be said that the ferrochrome-filled CF reinforced cement mixture provides compressive strength and flexural strength increase on the concrete material and prevents the spread of crack damage in the concrete structure.

3.2. Non-Destructive Test Results

3.2.1. Electrical Resistivity

Electrical resistivity values of 2, 14, 28, 90, and 180 days were measured and compared in Figure 4. Considering the time effect on the resistivity results, the resistivity values increased with the advancing age of the sample in all mixtures. This was more evident in the pure mixture without conductive fibers compared to the conductive mixtures. In FRC, FRC-CF0.5, FRC-CF0.75 and FRC-CF1.0 mixtures, 180-day resistivity values increased 6.07, 2.30, 1.16 and 1.23 times, respectively, compared to 2-day. This means that the conductivity of the materials decreases at these rates over time. When the resistivity values of 0.5%, 0.75%, and 1% CF added mixtures were compared with the pure sample, 56, 206, and 289 fold reductions were observed at 180-day values. The reason for the excessive conductivity loss of the pure mixture compared to the conductive mixtures is the presence of water in the matrix, the factor in which it conducts the current in this mixture. In cementitious materials, conductivity decreases with the evaporation of water

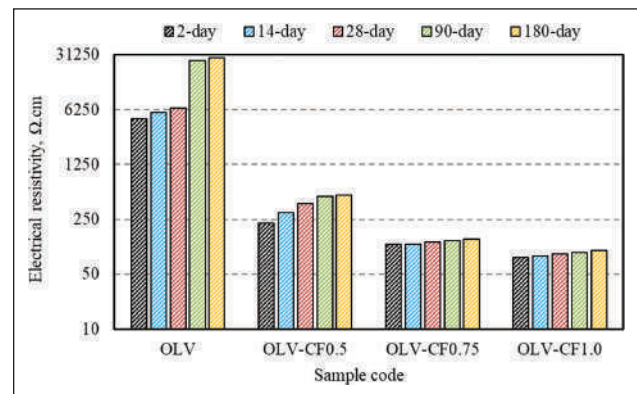


Figure 4. Electrical resistivity results from mortar specimens.

and the completion of hydration processes over time [34]. In conductive mortars, conductivity values were more stable since the current flow path was through the fibers. In the present study, 2-day resistivity values were obtained between 80–4762 and 180-day values between 100–28921 Ω.cm. Different studies have confirmed that the electrical resistance of concrete is at high levels.

While the electrical resistivity of outdoor dried concrete was determined as 6.54×10^5 – 11.4×10^5 Ω.cm, the electrical resistivity of saturated concrete and dry concrete were determined to be 10^6 Ω.cm and 10^9 Ω.cm, respectively [21]. The specification of a conductivity class for concretes may vary for different purposes. For example, in the study of Dehghanpour et al. [34], the maximum resistivity value of a heat-producing concrete is approximately 500 Ω.cm. This value may vary in self-perceiving concretes. D'Alessandro et al. [35] presented a systematic investigation of various procedures to fabricate self-sensing carbon-nanotube-containing cementitious materials. The dispersion quality, decomposition rate, and SEM images of nanotubes were investigated using the dispersion of nanotubes in water, chemical dispersants, and different mixing strategies. The resistivity values of different mixtures containing 0–1.6% multi-walled carbon nanotube (MWCNT) were obtained between about 10^3 – 10^7 Ω.cm according to different experimental procedures. According to the results of the study, it was found that the minimum MWCNT content was 1% by weight of cement in order to obtain self-sensing cementitious materials.

3.2.2. Dynamic Resonance Test Results

The defects of conventional concrete, such as low tensile strength, low ductility, and low damping, can be replaced and improved with additive phase materials. In addition to the mechanical, durability, and physical properties of cementitious materials, examining their dynamic behavior is important for the health of the building. Therefore, it is advantageous to investigate the effects of fibers and additives in cementitious materials on dynamic properties such as damping ratio. Different methods in materials can ob-

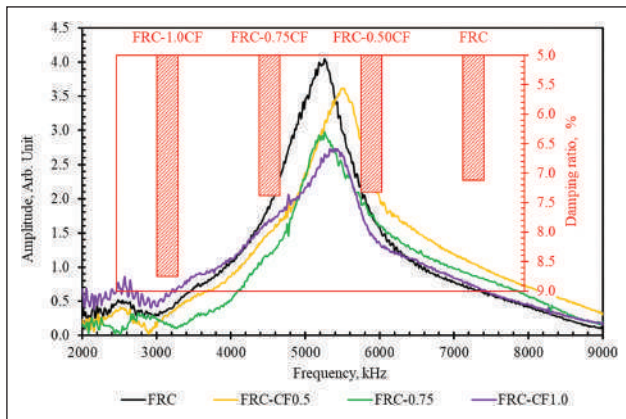


Figure 5. Damping ratio and amplitude-frequency curves.

tain the damping ratio. The half-Power method was used in this study. In the Half-Power method, the damping ratio is derived from the frequency spectrum of a structure's acceptance. For this, the upper and lower frequency values with an amplitude of 0.707 times the peak of the response signal are found. The damping ratio is calculated by dividing the difference between the upper and lower frequencies by twice the natural peak frequency. Amplitude-Frequency curves obtained by subjecting samples produced from four different mixtures to a dynamic resonance test and their damping ratios are summarized in Figure 5. When the curves in the Figure are considered, the amplitude values vary between 2.7-4 units. Also, the peaks were around 5500 kHz. When the damping ratios are considered, it is observed that the damping property increases with the addition of CF and the increase in its ratio. Damping ratios vary between 7.1% and 8.7%. The damping ratios of 0.5%, 0.75% and 1.0% CF added mixtures increased by 2.8%, 3.8% and 23% compared to the pure mixture. In a research paper [36], the damping ratios of conventional concrete samples filled with recycled aggregates at different rates were between 1 and 4. Nabavi et al. [37], polypropylene fibers and styrene butadiene rubber (latex) were selected for use in the concrete mix to obtain highly damped concrete. Four categories of laboratory concrete samples, including plain concrete, fiber reinforced concrete, polymer modified concrete, and fiber used in polymer modified concrete, were poured and tested to determine the damping rate of these concrete categories. Experiments have shown that polymer-concrete composites can absorb dynamic load energy much faster than conventional concrete. Therefore, the positive effects of synthetic fibers on the damping rate have been proven in the literature [38]. In Figure 5, when the curves and damping ratio results are compared, steeper peaks show lower damping and lower peak higher damping. This situation is explained in the literature as follows. It is known that narrow and steep Frequency-Amplitude curves have less damping properties of the relevant material, and wide and low curves have higher damping properties [39].

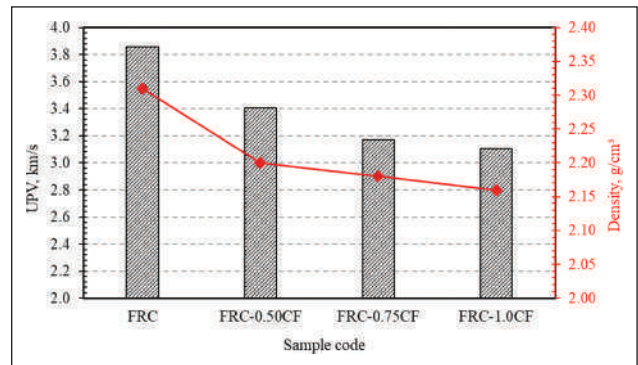


Figure 6. Ultrasonic pulse velocity test results.

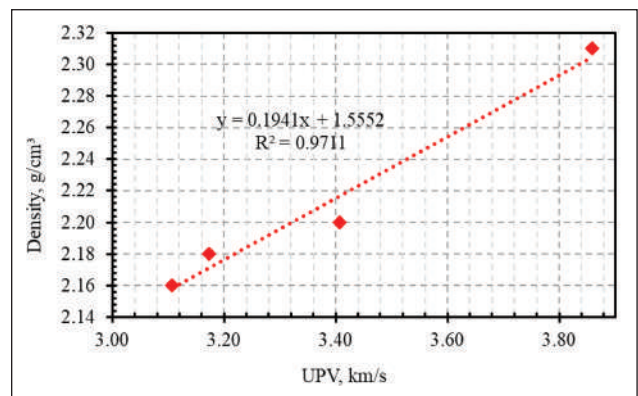


Figure 7. Relationship between UPV and density.

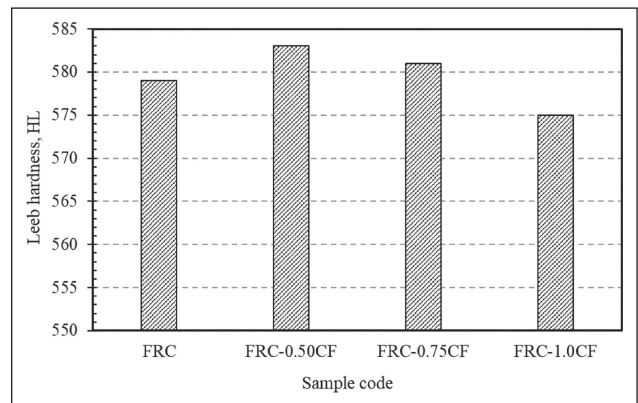


Figure 8. Leeb hardness test results.

3.2.3. Ultrasonic Pulse Velocity (UPV)

UPV and density measurement results of the prepared samples are shown in Figure 6. It is seen that the UPV and density values of the samples decrease with the CF additive added to the mixture. The highest UPV and density values are 3.9 km/s and 2.32 g/cm³ in the FRC sample, respectively. Vilaplana et al. [40] reported that the UPV and density values of high-strength materials showed linear similarity with the compressive strength. Also, Dabbaghi et al. [41] reported that interparticle voids occur in fiber-containing

concrete samples. They also explained a direct relationship between UPV and concrete density. It can be said that adding CF to the ferrochrome-filled cement mixture harms the compact structure of the matrix by reducing the UPV and density values.

On the other hand, it could be concluded that CF reinforcement, which provides the increase in compressive strength and flexural strength, is not effective on these parameters. When the UPV and density test results in Figure 7 are compared with the compressive strength test results in Figure 3, it is seen that the UPV and density values of the FRC-0.75CF sample with the highest compressive strength decreased. Thus, it is verified that the compact structure in the concrete material is obtained by ferrochrome filling. As stated by Dawood et al. [42], adding fiber to the mixture increased the porosity formation by decreasing the workability of the mixture. The CF in the cement mixture reduced the UPV velocity wave throughout the sample, decreasing the UPV value.

3.2.4. Leeb Hardness Results

Figure 8 shows the Leeb hardness test results of the samples. It is seen that there is a compatibility between the pressure values mentioned above and the Leeb hardness results. It is observed that the Leeb hardness value of the concrete sample increased with 0.5% CF added to the ferrochrome-filled cement mixture. On the contrary, the Leeb hardness value decreased with increasing CF content in the mixture. Gomez-Heras et al. [43] reported that the Leeb hardness value is related to porosity. It could be stated that the ferrochrome filler in the mixture fills the porous structures of the concrete material and thus contributes to the increase in strength of the concrete. In addition, adding CF to the mixture improved the Leeb hardness of the sample. It could be said that the CFs in the FRC-0.5CF sample with the highest Leeb hardness are evenly distributed in the mixture, and sufficient fiber reinforcement is made. The decrease in Leeb hardness value with the increase of CF in the mixture can be attributed to the fact that CFs begin to cluster in the mixture and form porosity in the structure. There are a few Leeb hardness studies on regular concretes, although limited. Song et al. [44] investigated the Leeb hardness of sodium silicate-based concrete and regular C30 concrete and concluded that the average hardness value of regular concrete was 362 HL, and that of sodium silicate-based concrete was 405 HL. In [38] studies, Leeb hardness values for UHPCs were measured between 620–640 HL. Leeb hardness values measured for samples vary between 575–583 HL.

3.2.5. Microstructure Analysis Results

SEM analysis of the ferrochrome aggregate, whose pictures are shown at three different resolutions, is given in Figures 9 a, b, and c. SEM images provide information about the pore structure of ferrochrome. Angular irregu-

lar distribution of ferrochrome particles is observed. The roughness of the particle surface shown in Figure 9 b can be attributed to the ferrochrome aggregate's strong adhesion with the cement mix's components. The microstructure of the high-magnification ferrochrome in Figure 9 c has seen a dense layer form. The fact that there are almost no voids in the ferrochrome structure could be attributed to the fact that crack formation can be prevented. In addition, it could be stated that when used instead of aggregate in ferrochrome cement mixture, it can increase concrete quality and contribute to compressive strength. The EDS results from the analysis of the selected area in Figure 9 c are shown in Figure 9 d. The presence of aluminum (Al), silica (Si), iron (Fe), and chromium (Cr) in the structure of ferrochrome aggregate from EDS peaks was determined. Also, the chemical composition is given in the table in Figure 9 d. It is seen that ferrochrome aggregate contains 52.85% Cr, 39.68% Fe, 6.29% Si, and 1.18% Al by weight. The very low carbon content can explain the absence of the C peak in the EDS analysis of the product. However, low levels of Al and Si contents confirm the high purity ferrochrome aggregate. The presence of elements such as Al and Si other than Fe and Cr elements in the ferrochrome structure is explained by the different spinel structures of ferrochrome [45].

The XRD analysis of the ferrochrome aggregate is shown in Figure 10. Also, the crystal phases analyzed from the x-ray diffraction of ferrochrome in Figure 10 are shown in the table. It can be noted that the seven minerals detected are stable products and intensify the microstructure mentioned above. Also, it can be stated that the crystal phase minerals contribute to the increase in strength in the ferrochrome-filled concrete sample [46]. In addition, The broadening peak between 2θ : 10 and 20 can be explained by the presence of the amorphous phase [7]. It is observed that crystalline phases of minerals mainly containing chromium and iron are formed.

On the other hand, the crystal phase formation of quartz, calcite, magnesium, and aluminum minerals is low. It is seen that the most intense peaks are seen in the crystal phase structures of the chromferide and fayalite minerals. The formation of calcite and quartz crystal phases can be associated with the mentioned C-S-H (Calcium Silicate Hydrate) formation in the microstructure of ferrochrome. Islam et al. [47] reported that the mineralogical properties of ferrochrome are complex due to the presence of chromium in different oxide states. On the other hand, in the crystal phase analysis of the ferrochrome aggregate characterized in this study, it was observed that only the chromferide mineral contained Cr.

Figure 11 shows the ferrochrome-filled pure FRC sample's SEM images at different magnifications. The surface morphology of the FRC sample gives information about the pore structure and crack formation. The rough surface morphology seen in Figure 11 a can be associat-

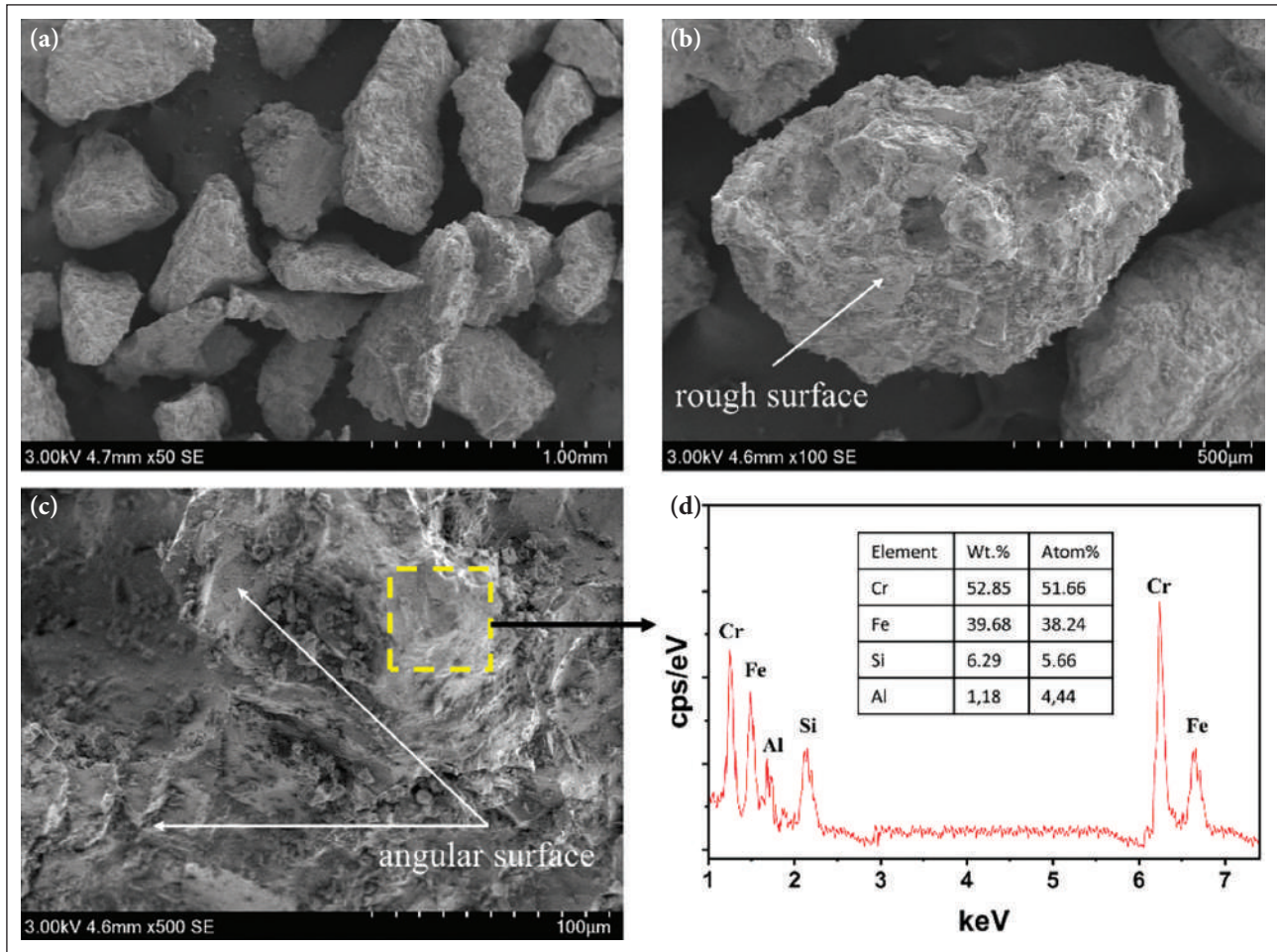


Figure 9. SEM images of ferrochrome aggregate (a–c), EDS analysis of ferrochrome aggregate (d).

ed with the rough surface of the ferrochrome mentioned above aggregate. In addition, the surface roughness of the ferrochrome aggregate significantly affected the bond strength in the cement mixture. However, at higher magnification microstructures (Fig. b and c), the aggregates appear to be irregularly dispersed angled particles. Moreover, the presence of C-S-H formations is related to the dense structure in the microstructure. The fact that the porous structure seen in Figure 11 c is not typical throughout the sample can be attributed to the inhibition of the increase in porosity by the dense structure of the ferrochrome aggregate.

The SEM image of the conductive concrete sample (FRC-0.75CF) in which CFs close to each other form a conductive network is given in Figure 12 a. Figure 12 b shows the high-magnification microphotograph of the SEM image with CF. SEM analyzes show that CF reinforcement reduces porosity in the microstructure. It could be stated that CFs in the cement matrix accelerate the formation of C-S-H, increasing the nucleation regions where stable growth occurs, filling the porous structure, and thus increasing the strength of the concrete sample [48]. In addition, it could

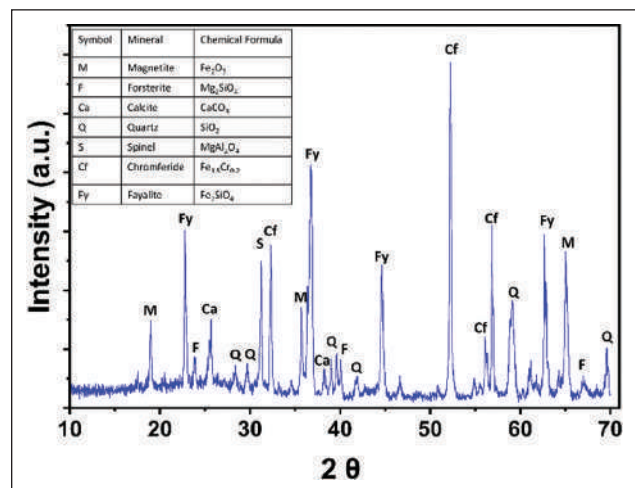


Figure 10. XRD patterns of ferrochrome aggregate.

be said that the fibers in the sample containing 0.75% CF do not agglomerate and do not adversely affect the strength properties mentioned above. Adding more than 0.75% CF to the cement mix causes the fibers to clump together,

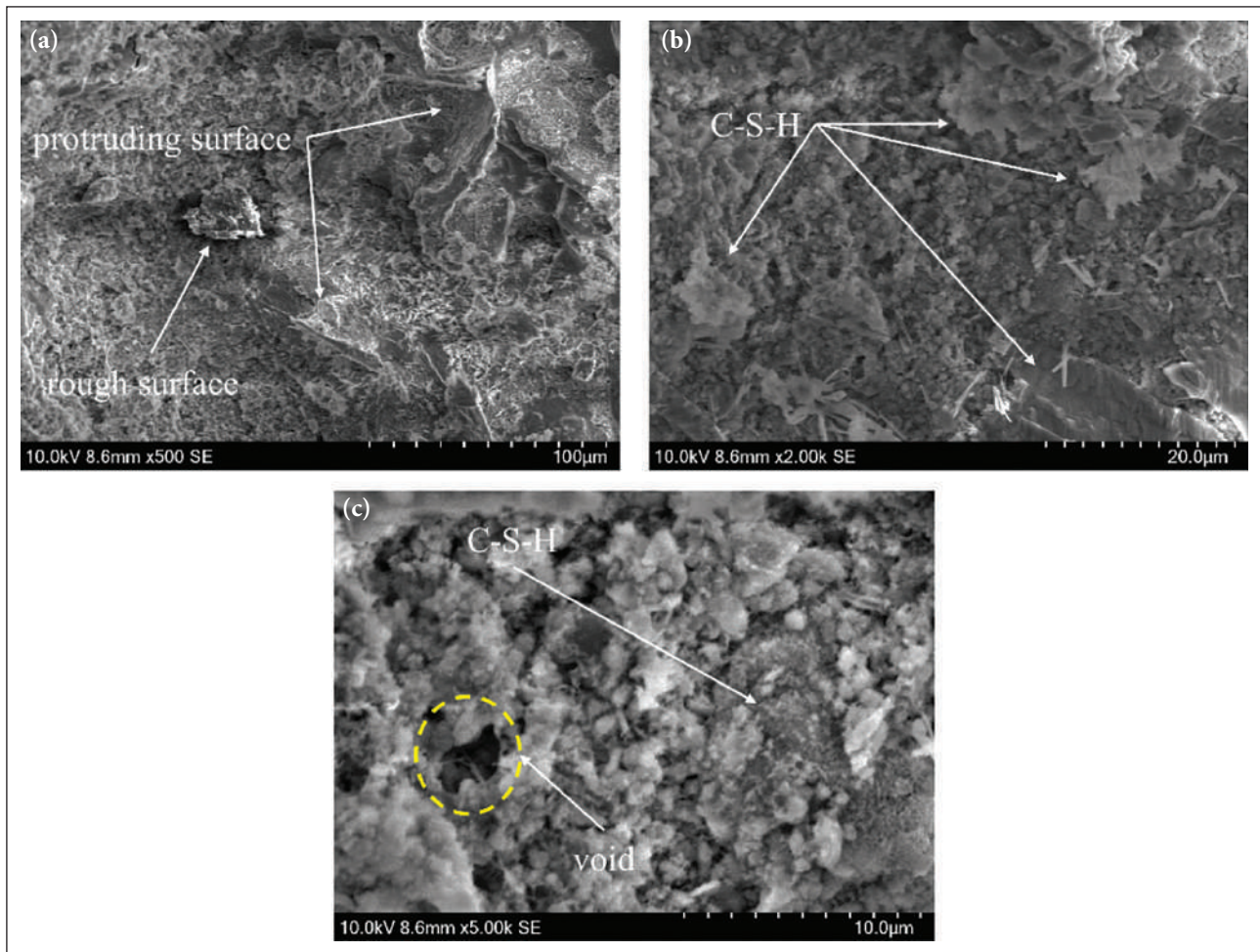


Figure 11. SEM microphotograph of FRC sample.

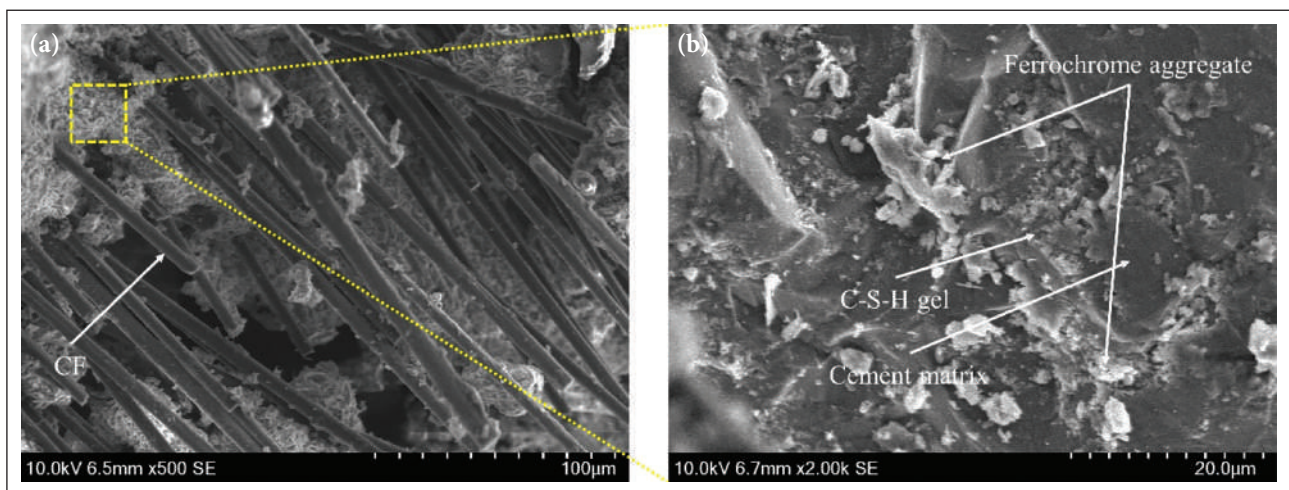


Figure 12. SEM images of conductive concrete FRC-0.75CF sample.

weakening the cement matrix, and crack propagation cannot be prevented. The compact microstructure formed by the ferrochrome aggregate particles settling in the cement matrix with CFs contributed to the increase mentioned

above in compressive strength. Also, the increased compressive and flexural strength of the CF mentioned above added concrete sample could be correlated with the dense microstructure shown in Figure 12 b.

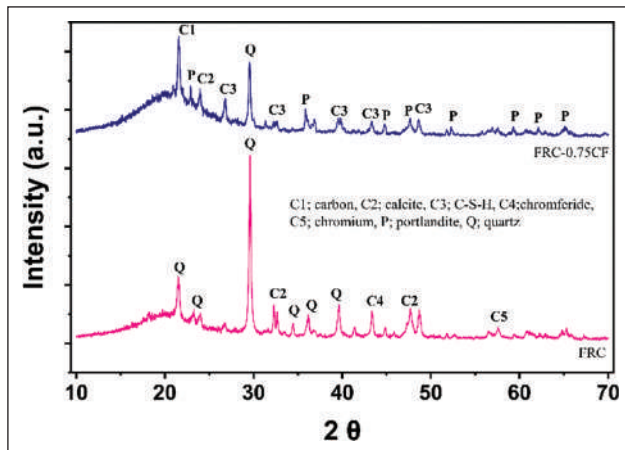


Figure 13. XRD patterns of ferrochrome filled (FRC) and carbon fiber reinforced cement (FRC-0.75CF).

Moreover, the increase in compressive strength in the 0.75% CF-added mortar sample was explained by the absence of ettringite formation, which causes internal stresses and cracks in the microstructure [49]. On the other hand, homogeneously distributed CFs formed a conductive network (Fig. 12 a). CF fibers in sample FRC-0.75CF increased the conductivity of the concrete by decreasing the electrical resistivity. The increase in conductivity can be explained by the CFs that form a conductive bridge between the aggregate and matrix in the cement mixture. It can be said that the cement hydration products seen in Figure 12 b adhere to the CF and increase the strength of the conductive concrete.

The crystal structures of the FRC and FRC-0.75CF samples and the minerals in the table are shown in Figure 13. In the XRD analysis of the FRC sample, the most quartz peaks are seen, and the chromiferide peak, which contains Cr and Fe elements in the ferrochrome aggregate structure, was found. Also, the chromium phase was formed although at low peak intensity. The quartz mineral with the highest peak intensity is explained by the availability of free silica [50]. Compared to the FRC-0.75CF sample, it is seen that the quartz peak density in the FRC sample is higher. In the XRD analysis of the ferrochrome mentioned above aggregate, the high densities of the mineral phases turned into low-intensity phases in the FRC sample. It can be attributed to the different reactions that take place in the cement mixture of the ferrochrome aggregate.

Moreover, compared to the FRC sample, the XRD analysis of the FRC-0.75CF sample shows carbon, portlandite, and C-S-H crystal phases. In the XRD patterns of the FRC-0.75CF sample, it is seen that the peak of the carbon crystal is intensity. Also, portlandite and C-S-H compositions contributed to the surface interaction between cement matrix and CF. The fact that the main crystalline phases are carbon and quartz can be attributed to the workability of the conductive network in the cement matrix [51]. The low peak densities of the C-S-H phases may be associated with the

reaction in the cement mixture. In addition, C-S-H characterized at different diffraction angles can be attributed to the compactness of the microstructure and the increase in strength in the concrete sample. C-S-H phase formation, which is compatible with the SEM images of the FRC-0.75CF sample, contributed to the compressive strength of the concrete sample. Also, the increase in compressive strength can be attributed to the collapse of the C-S-H gel around the CFs. In addition, according to Bai et al. [52], the high carbon peak intensity was attributed to the high specific surface area of the carbon and its association with other particles. It has also been reported that carbon particles in the cement mixture improve the hydration reaction. However, it is stated that the small gaps between the carbon particles cause the gaps in the cement mixture to increase, thus reducing the compressive strength of the concrete [53, 54]. It can be said that the effect of CFs on the strength increase is limited despite the increased matrix strength in the ferrochrome-filled cement mixture.

4. CONCLUSIONS

In this article, the effects of ferrochrome filler used instead of aggregate and CF added to the cement mixture as reinforcement in different proportions on the compressive strength, flexural strength, UPV, density, electrical resistivity, and Leeb hardness of the concrete sample were investigated. In addition, the effect of CF on the microstructure and phase formations in the cement matrix in the FRC-0.75CF sample, which has optimum values in mechanical and conductivity test results, was characterized. According to the resistivity test results, the age effect of ferrochrome slag aggregate-filled conductive mortars was more evident in the first ages, and the age effect decreased over time. Almost no age effect was observed in CF-added mixtures. With the addition of CF, the resistivity values decreased approximately 40 times compared to the reference. The lowest resistivity value was measured for the mixture containing 1% CF. According to the damping ratio values obtained from the dynamic resonance test results, adding CF improved the damping property, and the maximum increase was calculated for the mixture containing 1% CF as 23%.

CF's compressive and flexural strength effects on concrete materials were similar. In the above-mentioned compressive strength test results, the FRC-0.75CF sample with the highest value provided 2 MPa higher compressive strength than the unreinforced FRC sample. Also, among the CF reinforced samples, the compressive strength of the FRC-0.75CF sample was 5 MPa higher than that of the FRC-1.0CF sample. In the flexural strength test results, the use of CF in the cement mixture positively affected the concrete's mechanical properties. FRC-0.75CF sample with the highest flexural strength value has 9 MPa and 6 MPa more strength compared to unreinforced FRC and reinforced FRC-1.0CF samples, respectively.

On the contrary, increasing the CF content added to the mix did not improve the UPV and density results. While adding CF decreased the UPV value to 3.1 km/s, the increase in compressive strength confirmed the relationship between the ferrochrome filler in the mixture and the UPV. Ferrochrome filler reduced the porosity and increased the UPV value of the hardening concrete. UPV and density measurement results showed that the FRC-filled plain concrete sample had a compact structure with less damage than the CF-added concrete samples. Leeb hardness test results, which show parallelism with the compressive strength values, confirmed the effect of filler and additive material. While the ferrochrome filling in the mixture increased the density of the structure, the CF reinforcement increased the strength of the concrete sample up to a certain extent. In the SEM analysis of ferrochrome aggregate, almost no void structure and hydration product formation were observed. SEM analysis results contributed to the reduction of porosity in the matrix by densifying the cement matrix of 0.75% CF. In addition, C-S-H formations in the microstructure improved the compact structure, and the absence of ettringite structures facilitated increased mechanical strength. Moreover, SEM analyses of the FRC-0.75CF sample showed that the CFs adhered to form a conductive network between the components in the ferrochrome-filled compact structure.

As a result, ferrochrome-filled CF reinforced concrete, which is recommended instead of regular concrete, which is widely used in the construction industry, offers superior mechanical and electrical properties compared to regular concrete by providing low production cost and energy savings in production.

DATA AVAILABILITY STATEMENT

The authors confirm that the data that supports the findings of this study are available within the article. Raw data that support the finding of this study are available from the corresponding author, upon reasonable request.

CONFLICT OF INTEREST

The authors declare that they have no conflict of interest.

FINANCIAL DISCLOSURE

This study was carried out within the scope of the project coded STB-072161 of Fibrobeton R&D Center. Thank you to Fibrobeton Company for their support. We also thank Eti Krom Inc. for their support of ferrochrome slag materials.

PEER-REVIEW

Externally peer-reviewed.

REFERENCES

- [1] Islam, M. Z., Sohel, K. M. A., Al-Jabri, K., & Al Harthy, A. (2021). Properties of concrete with ferrochrome slag as a fine aggregate at elevated temperatures. *Case Studies in Construction Materials*, 15, e00599. [\[CrossRef\]](#)
- [2] Al-Jabri, K., & Shoukry, H. (2018). Influence of nano metakaolin on thermo-physical, mechanical and microstructural properties of high-volume ferrochrome slag mortar. *Construction and Building Materials*, 177, 210–221. [\[CrossRef\]](#)
- [3] Acharya, P. K., & Patro, S. K. (2016). Utilization of ferrochrome wastes such as ferrochrome ash and ferrochrome slag in concrete manufacturing. *Waste Management and Research*, 34(8), 764–774. [\[CrossRef\]](#)
- [4] Abbass, W., Khan, M. I., & Mourad, S. (2018). Evaluation of mechanical properties of steel fiber reinforced concrete with different strengths of concrete. *Construction and Building Materials*, 168, 556–569. [\[CrossRef\]](#)
- [5] de Alencar Monteiro, V. M., Lima, L. R., & de Andrade Silva, F. (2018). On the mechanical behavior of polypropylene, steel and hybrid fiber reinforced self-consolidating concrete. *Construction and Building Materials*, 188, 280–291. [\[CrossRef\]](#)
- [6] Fares, A. I., Sohel, K. M. A., & Al-mamun, A. (2021). Characteristics of ferrochrome slag aggregate and its uses as a green material in concrete – A review. *Construction and Building Materials*, 294, Article 123552. [\[CrossRef\]](#)
- [7] Al-Jabri, K., Shoukry, H., Khalil, I. S., Nasir, S., & Hassan, H. F. (2018). Reuse of Waste Ferrochrome Slag in the Production of Mortar with Improved Thermal and Mechanical Performance. *Journal of Materials in Civil Engineering*, 30(8), Article 0002345. [\[CrossRef\]](#)
- [8] Dash, M. K., & Patro, S. K. (2018). Effects of water cooled ferrochrome slag as fine aggregate on the properties of concrete. *Construction and Building Materials*, 177, 457–466. [\[CrossRef\]](#)
- [9] Niemelä, P., & Kauppi, M. (2007). Production, characteristics and use of ferrochromium slags. *Innovations In The Ferro Alloy Industry - Proceedings of the XI International Conference on Innovations in the Ferro Alloy Industry, Infacon XI*, 171–179.
- [10] Lind, B. B., Fällman, A.-M., & Larsson, L. B. (2001). Environmental impact of ferrochrome slag in road construction. *Waste Management*, 21(3), 255–264. [\[CrossRef\]](#)
- [11] Acharya, P. K., & Patro, S. K. (2015). Effect of lime and ferrochrome ash (FA) as partial replacement of cement on strength, ultrasonic pulse velocity and permeability of concrete. *Construction and Building Materials*, 94, 448–457. [\[CrossRef\]](#)
- [12] Panda, C. R., Mishra, K. K., Panda, K. C., Nayak, B. D., & Nayak, B. B. (2013). Environmental and technical assessment of ferrochrome slag as concrete aggregate material. *Construction and Building Materials*, 49, 262–271. [\[CrossRef\]](#)

- [13] Kumar, B. A. V. R., Keshav, L., Sivanantham, P. A., Arokiaraj, G. G. V., Rahman, D. R. Z., Kumar, P. M., & Somashekar, D. (2022). Comprehensive characterization of ferrochrome slag and ferrochrome ash as sustainable materials in construction. *Journal of Nanomaterials*, 2022, Article 8571055. [CrossRef]
- [14] Acharya, P. K., & Patro, S. K. (2018). Bond, permeability, and acid resistance characteristics of ferrochrome waste concrete. *ACI Materials Journal*, 115(3), 359–368. [CrossRef]
- [15] Kim, G. M., Yang, B. J., Ryu, G. U., & Lee, H. K. (2016). The electrically conductive carbon nanotube (CNT)/cement composites for accelerated curing and thermal cracking reduction. *Composite Structures*, 158, 20–29. [CrossRef]
- [16] Mokhtar, M. M., Abo-El-Enin, S. A., Hassaan, M. Y., Morsy, M. S., & Khalil, M. H. (2017). Mechanical performance, pore structure and micro-structural characteristics of graphene oxide nano platelets reinforced cement. *Construction and Building Materials*, 138, 333–339. [CrossRef]
- [17] Chiarello, M., & Zinno, R. (2005). Electrical conductivity of self-monitoring CFRC. *Cement and Concrete Composites*, 27(4), 463–469. [CrossRef]
- [18] Chen, B., & Liu, J. (2008). Damage in carbon fiber-reinforced concrete, monitored by both electrical resistance measurement and acoustic emission analysis. *Construction and Building Materials*, 22(11), 2196–2201. [CrossRef]
- [19] Roberts, R. H., & Mo, Y.-L. (2016). Development of carbon nanofiber aggregate for concrete strain monitoring. In *Innovative Developments of Advanced Multifunctional Nanocomposites in Civil and Structural Engineering* (pp. 9–45). Elsevier. [CrossRef]
- [20] Hou, Z., Li, Z., & Wang, J. (2007). Electrical conductivity of the carbon fiber conductive concrete. *Journal Wuhan University of Technology, Materials Science Edition*, 22(2), 346–349. [CrossRef]
- [21] Dehghanpour, H., & Yilmaz, K. (2020). Heat behavior of electrically conductive concretes with and without rebar reinforcement. *Medziagotyra*, 26(4), 471–476. [CrossRef]
- [22] Vaidya, S., & Allouche, E. N. (2011). Strain sensing of carbon fiber reinforced geopolymer concrete. *Materials and Structures*, 44(8), 1467–1475. [CrossRef]
- [23] Chen, M., Gao, P., Geng, F., Zhang, L., & Liu, H. (2017). Mechanical and smart properties of carbon fiber and graphite conductive concrete for internal damage monitoring of structure. *Construction and Building Materials*, 142, 320–327. [CrossRef]
- [24] Han, J., Wang, D., & Zhang, P. (2020). Effect of nano and micro conductive materials on conductive properties of carbon fiber reinforced concrete. *Nanotechnology Reviews*, 9(1), 445–454. [CrossRef]
- [25] Dehghanpour, H., Yilmaz, K., Afshari, F., & Ipek, M. (2020). Electrically conductive concrete: A laboratory-based investigation and numerical analysis approach. *Construction and Building Materials*, 260, Article 119948. [CrossRef]
- [26] Dehghanpour, H., & Yilmaz, K. (2020). Investigation of specimen size, geometry and temperature effects on resistivity of electrically conductive concretes. *Construction and Building Materials*, 250, Article 118864. [CrossRef]
- [27] Dehghanpour, H., & Yilmaz, K. (2021). A more sustainable approach for producing less expensive electrically conductive concrete mixtures: Experimental and FE study. *Cold Regions Science and Technology*, 184, Article 103231. [CrossRef]
- [28] El-Dieb, A. S., El-Ghareeb, M. A., Abdel-Rahman, M. A. H., & Nasr, E. S. A. (2018). Multifunctional electrically conductive concrete using different fillers. *Journal of Building Engineering*, 15, 61–69. [CrossRef]
- [29] ASTM C215. (2019). *Standard test method for fundamental transverse, longitudinal, and torsional resonant frequencies of concrete specimens*. American Society for Testing and Materials.
- [30] TS EN 196-1. (2005). *Methods of testing cement—Part 1: Determination of strength*. Turkish Standard.
- [31] ASTM C597. (2009). *Standard test method for pulse velocity through concrete*. American Society for Testing and Materials.
- [32] ASTM A956. (2006). *Standard test method for leeb hardness testing of steel products*. American Society for Testing and Materials.
- [33] Al-Shamayleh, R., Al-Saoud, H., Abdel-Jaber, M., & Alqam, M. (2022). Shear and flexural strengthening of reinforced concrete beams with variable compressive strength values using externally bonded carbon fiber plates. *Results in Engineering*, 14, Article 100427. [CrossRef]
- [34] Dehghanpour, H., Yilmaz, K., & Ipek, M. (2019). Evaluation of recycled nano carbon black and waste erosion wires in electrically conductive concretes. *Construction and Building Materials*, 221, 109–121. [CrossRef]
- [35] D'Alessandro, A., Rallini, M., Ubertini, F., Materazzi, A. L., & Kenny, J. M. (2016). Investigations on scalable fabrication procedures for self-sensing carbon nanotube cement-matrix composites for SHM applications. *Cement and Concrete Composites*, 65, 200–213. [CrossRef]
- [36] Liang, C., Liu, T., Xiao, J., Zou, D., & Yang, Q. (2016). The damping property of recycled aggregate concrete. *Construction and Building Materials*, 102, 834–842. [CrossRef]
- [37] Nabavi, F., Bhattacharjee, B., & Madan, A. (2011).

- Improving the damping properties of concrete. *21st Australasian Conference on the Mechanics of Structures and Materials*, 867–872. [\[CrossRef\]](#)
- [38] Dehghanpour, H., Subasi, S., Guntepe, S., Emiroglu, M., & Marasli, M. (2022). Investigation of fracture mechanics, physical and dynamic properties of UHPCs containing PVA, glass and steel fibers. *Construction and Building Materials*, 328, Article 127079. [\[CrossRef\]](#)
- [39] Tian, J., Fan, C., Zhang, T., & Zhou, Y. (2019). Rock breaking mechanism in percussive drilling with the effect of high-frequency torsional vibration. *Energy Sources, Part A: Recovery, Utilization and Environmental Effects*, 44(1), 2520–2534. [\[CrossRef\]](#)
- [40] Vilaplana, J. L., Baeza, F. J., Galao, O., Alcocel, E. G., Zornoza, E., & Garcés, P. (2016). Mechanical properties of alkali activated blast furnace slag pastes reinforced with carbon fibers. *Construction and Building Materials*, 116, 63–71. [\[CrossRef\]](#)
- [41] Dabbaghi, F., Sadeghi-Nik, A., Libre, N. A., & Nasrollahpour, S. (2021). Characterizing fiber reinforced concrete incorporating zeolite and metakaolin as natural pozzolans. *Structures*, 34, 2617–2627. [\[CrossRef\]](#)
- [42] Dawood, E. T., Mohammad, Y. Z., Abbas, W. A., & Mannan, M. A. (2018). Toughness, elasticity and physical properties for the evaluation of foamed concrete reinforced with hybrid fibers. *Heliyon*, 4(12), e011103. [\[CrossRef\]](#)
- [43] Gomez-Heras, M., Benavente, D., Pla, C., Martinez-Martinez, J., Fort, R., & Brotons, V. (2020). Ultrasonic pulse velocity as a way of improving uniaxial compressive strength estimations from Leeb hardness measurements. *Construction and Building Materials*, 261, Article 119996. [\[CrossRef\]](#)
- [44] Song, Z., Xue, X., Li, Y., Yang, J., He, Z., Shen, S., Jiang, L., Zhang, W., Xu, L., Zhang, H., Qu, J., Ji, W., Zhang, T., Huo, L., Wang, B., Lin, X., & Zhang, N. (2016). Experimental exploration of the waterproofing mechanism of inorganic sodium silicate-based concrete sealers. *Construction and Building Materials*, 104, 276–283. [\[CrossRef\]](#)
- [45] Mahamaya, M., & Das, S. K. (2020). Characterization of ferrochrome slag as a controlled low-strength structural fill material. *International Journal of Geotechnical Engineering*, 14(3), 312–321. [\[CrossRef\]](#)
- [46] Dash, M. K., Patro, S. K., Acharya, P. K., & Dash, M. (2022). Impact of elevated temperature on strength and micro-structural properties of concrete containing water-cooled ferrochrome slag as fine aggregate. *Construction and Building Materials*, 323, Article 126542. [\[CrossRef\]](#)
- [47] Islam, M. Z., Sohel, K. M. A., Al-Jabri, K., & Al Harthy, A. (2021). Properties of concrete with ferrochrome slag as a fine aggregate at elevated temperatures. *Case Studies in Construction Materials*, 15, e00599. [\[CrossRef\]](#)
- [48] Barbhuiya, S., & Chow, P. (2017). Nanoscaled mechanical properties of cement composites reinforced with carbon nanofibers. *Materials*, 10(6), 662. [\[CrossRef\]](#)
- [49] Nguyen, H.-A., Chang, T.-P., Shih, J.-Y., Chen, C.-T., & Nguyen, T.-D. (2016). Sulfate resistance of low energy SFC no-cement mortar. *Construction and Building Materials*, 102, 239–243. [\[CrossRef\]](#)
- [50] Jena, S., & Panigrahi, R. (2019). Performance assessment of geopolymer concrete with partial replacement of ferrochrome slag as coarse aggregate. *Construction and Building Materials*, 220, 525–537. [\[CrossRef\]](#)
- [51] Li, W., Pei, C., Zhu, Y., & Zhu, J.-H. (2021). Effect of chopped carbon fiber on interfacial behaviors of IC-CP-SS system. *Construction and Building Materials*, Article 275, 122117. [\[CrossRef\]](#)
- [52] Bai, Y., Xie, B., Li, H., Tian, R., & Zhang, Q. (2022). Mechanical properties and electromagnetic absorption characteristics of foam Cement-based absorbing materials. *Construction and Building Materials*, 330, Article 127221. [\[CrossRef\]](#)
- [53] Nambiar, E. K. K., & Ramamurthy, K. (2007). Air-void characterisation of foam concrete. *Cement and Concrete Research*, 37(2), 221–230. [\[CrossRef\]](#)
- [54] Dehghanpour, H., Doğan, F., & Yılmaz, K. (2022). Development of CNT–CF–Al₂O₃–CMC gel-based cementitious repair composite. *Journal of Building Engineering*, 45, Article 103474. [\[CrossRef\]](#)



Research Article

Effect of fiber type, shape and volume fraction on mechanical and flexural properties of concrete

Mahmut BAŞSÜRÜCÜ¹, Cenk FENERLİ², Ceren KINA^{*3}, Şadiye Defne AKBAŞ²

¹Department of Construction Technology, Malatya Turgut Özal University, Darende Vocational High School, Malatya, Türkiye

²Department of Construction, Malatya Turgut Özal University, Hekimhan Mehmet Emin Sungur Vocational High School, Malatya, Türkiye

³Department of Civil Engineering, Malatya Turgut Özal University, Faculty of Engineering and Natural Sciences, Malatya, Türkiye

ARTICLE INFO

Article history

Received: 28 June 2022

Accepted: 21 July 2022

Key words:

Fiber reinforced concrete, fiber volume fraction, flexural performance, polypropylene fiber, steel fiber, strength

ABSTRACT

An experimental work was herein presented focusing the effect of different type, shape and volume fraction of fibers on the hardened properties of concrete including compressive, splitting tensile and flexural strengths at 7 and 28 curing days. A control concrete mixture including no fiber was prepared and six fiber-reinforced concrete (FRC) mixtures were designed by using two different fiber types and volume fractions. Two types of steel fibers having different shapes (short straight and long hooked end) and polypropylene fiber were used with the volume fraction of 0.4% and 0.8%. The load-deflection curves and toughness of the specimens were analyzed based on ASTM C1609. The results showed that the utilization of short straight steel fibers with 0.8% volume fraction was most efficient at enhancing the compressive strength with 9.98% while the use of 0.8% long hooked end steel fibers provided better splitting tensile and flexural strengths with 33.33% and 30.35%, respectively, compared to specimen with no fiber at 28 curing day. Besides, the long hooked end steel fibers with the volume fraction of 0.8% contributed to an excellent deflection hardening behavior resulting in higher load deflection capacity and higher toughness values at peak load, L/600 and L/150. On the other hand, with incorporation of polypropylene fiber, all strength values decreased regardless of the volume fraction and curing days.

Cite this article as: Başsürücü, M., Fenerli, C., Kına, C., & Akbas, ŞD. (2022). Effect of fiber type, shape and volume fraction on mechanical and flexural properties of concrete. *J Sustain Const Mater Technol*, 7(3), 158–171.

1. INTRODUCTION

Traditional concrete is a brittle material that performs well in compression but can undergo brittle failure under tensile load. The increase in concrete strength enhances

the brittleness of concrete [1]. Therefore, concrete design should be optimized to achieve sufficient energy absorption capacity, ductility, and strength to withstand structural tensile, impact and fatigue loads. In order to improve the engineering properties of concrete in terms of brittle-

*Corresponding author.

*E-mail address: ceren.kina@ozal.edu.tr



Table 1. Chemical properties of PC

(%)	SiO ₂	Al ₂ O ₃	Fe ₂ O ₃	CaO	MgO	SO ₃	K ₂ O	Na ₂ O
PC	19.40	5.36	3.79	64.3	2.25	2.47	0.90	0.06

ness, post-cracking capability and burst failure, short and randomly distributed fibers can be gradually added into concrete [2, 3]. Adding fibers such as basalt, polypropylene (PP), glass, and steel fibers into cement-based composites is so common to upgrade the tensile performance and mechanical properties [4–10]. These advantageous properties of fibers cause an increase in the application of fiber-reinforced concrete throughout the world. For instance, it has been widely used in industrial and infrastructure applications such as overlays, channel lining, airport pavement, etc., due to its positive effect on the durability of concrete.

On the other hand, the influences of fiber types on the hardened properties of concrete differ according to their physical and geometrical properties. Besides, the fiber content of concrete has to be limited depending on the length, shape, and type of fiber because the demanded strength can be achieved by using an adequate amount of fiber. Therefore, their optimum usage of concrete should be determined in a manner that causes the maximum improvement in the mechanical and durability properties of concrete by the minimum decrease in workability [11, 12].

In recent years, many researchers have focused on the influences of adding fibers on the hardened properties of concrete. Most existing studies have been carried out about using fibers, but there are still contradictory results about their effects on concrete. Khaloo et al. [13] used hooked end steel fiber with the volume fraction of 0.5%, 1%, 1.5% and 2% and found that tensile strengths of self-compacting concrete increased by the increase in fiber content while the compressive strength was decreased. Zeyad et al. [14] explained compressive strength reduction due to the effect of the length and shape of hooked end fibers which affect compacting efficiency. On the other hand, Şahin and Köksal [15] used two different hooked end steel fibers with different lengths and a volume fraction of 0.33%, 0.67%, and 1%. They indicated that the steel fiber volume and length do not affect compressive strength, while the steel fiber with high tensile strength improved the tensile strengths of concrete.

Similarly, Olivito and Zuccarello [16] concluded that steel fiber length has little effect on compression behavior. In the study of Yoo et al. [17], 1%, 2%, 3% and 4% volume fractions of straight fiber were used and the specimen obtained the highest load carrying capacity and elastic modulus with fiber volume fraction of 3%. Altun et al. [18] utilized hooked end steel fiber at dosages of 0, 30 and 60 kg/m³ and found that the use of steel fiber at a dosage of 30 kg/m³ showed the highest enhancement in

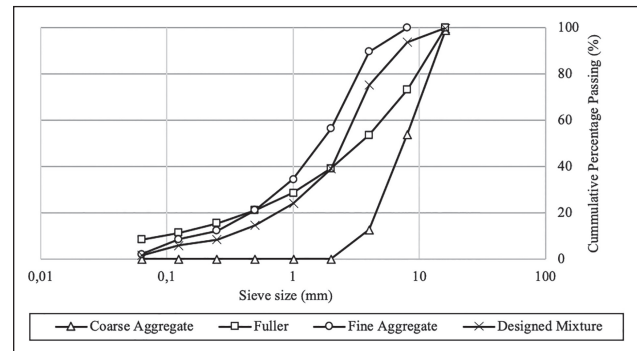





Figure 1. Grain size distribution of aggregates.

terms of flexural toughness and ultimate load. Özkılıç et al. [19] also used hooked end steel fiber with the volume fraction of 0.5%, 1%, 1.5% and 2% and concluded that 2% volume fraction of steel fiber was a limit value because the bending behavior began to dominate at that dosage. This finding was explained by the reduction in workability and bulking caused by high steel fiber content. In the study of Koroglu and Ashour [20] waste steel bead wires were added into concrete between 1% and 5% with an increment of 1%. They also found that the use of fiber ratio more than 2% caused a decrease in both compressive and splitting tensile strength, which was attributed to the reduction in workability.

Nonetheless, Cifuentes et al. [21] and Malek et al. [22] found that using PP fiber enhanced the ductility and flexural toughness compared to plain concrete in regardless of the fiber volume. Besides, some authors [23, 24] reported an increase of up to 10% in flexural strength with the addition of PP fiber. However, Ramesh et al. [25] concluded that the best flexural strength was observed by incorporating 0.6% PP fiber compared to those of 0.3%, 0.9% and 1.2% PP fiber. On the other hand, L. Bei-xing et al. [26] and Mazaheripour et al. [27] indicated that PP fiber changed the compressive strength hardly ever, while some other studies [28–30] found an increase up to 20%, which was attributed to the influence of fiber and aggregate interlocking mechanisms.

This study aimed to assess how different types, shapes and volume fractions of fibers influence the hardened properties, which were compressive, splitting and flexural tensile strengths of concrete. Within this scope, two types of fibers (PP and steel), two different shapes of steel fibers and two fiber volume fractions (0.4% and 0.8%) were considered. The flexural performance also included deflection capacity and toughness values based on ASTM C1609.

Table 2. Physical and geometrical properties for fibers

Name	Fiber type	Picture	d (mm)	l (mm)	Aspect ratio	E_f (GPa)	f_t (MPa)	Density (g/cm^3)
HL	Long hooked end steel fiber		0.90	60	66	210	Min 1150	7.8
SS	Short straight steel fiber		0.15	6	40	200	3000	7.2
PP	Polypropylene synthetic fiber		–	6	240	–	350	0.91

l=length of fiber, d=diameter of fiber, Aspect ratio=l/d, E_f =modulus of elasticity of fiber, f_t =tensile strength of fiber.

Table 3. Mixture proportions of fiber-reinforced concrete specimens

Mix code	Fiber content by volume (%)	Unit weight (kg/m^3)					Slump (mm)	
		Cement	Water	Fiber	Aggregates			SP
					0–5 mm	5–15 mm		
Control	–	350	200	0	1007.0	671.3	1.75	150
HL-0.4	0.4	350	200	31.4	1001.1	667.4	1.75	130
HL-0.8	0.8	350	200	62.8	995.2	663.5	1.75	120
SS-0.4	0.4	350	200	28.8	1000.8	667.4	2	150
SS-0.8	0.8	350	200	57.6	995.2	663.5	2	140
PP-0.4	0.4	350	200	3.64	1001.1	667.4	2	160
PP-0.8	0.8	350	200	7.28	995.2	663.5	2.5	170

HL=long hooked end steel fiber, SS=short straight steel fiber, PP=polypropylene fiber.

2. EXPERIMENTAL PROGRAM

2.1. Materials and Mixture Proportions

In this work, CEM I 42.5 Portland Cement (PC) with specific gravity of 3.15 was used as binder and its properties were as shown in Table 1. Fine and coarse aggregates with the maximum aggregate size of 5 mm and 16 mm, respectively, were used. The specific gravity and water absorption of sand was 2.39 and 2.30%, respectively. Gravel had the specific gravity of 2.68 and water absorption of 0.4%. Figure 1 shows the grain size distribution of the aggregates used in this study. Polycarboxylic polymer-based superplasticizer (SP) with a specific gravity of 1.06 was used in all mixtures.

Two different shapes of steel fibers, i.e., long hooked end and short straight fibers, and a polypropylene synthetic fiber were considered to investigate the influence of fiber shape and type on the mechanical and flexural performance of concrete as shown in Table 2. The long hooked end steel fiber, short straight steel fiber and polypropylene fiber were denoted as HL, SS and PP, respectively.

In this study, a control mixture including no fiber and six FRC mixtures were designed as shown in Table 3. In all mixtures, the ratio of water/PC was kept constant as 0.50 while fine and coarse aggregates were added into the mixtures in 60% and 40% of the total aggregate by weight, respectively. Besides, in order to adjust the similar slump val-

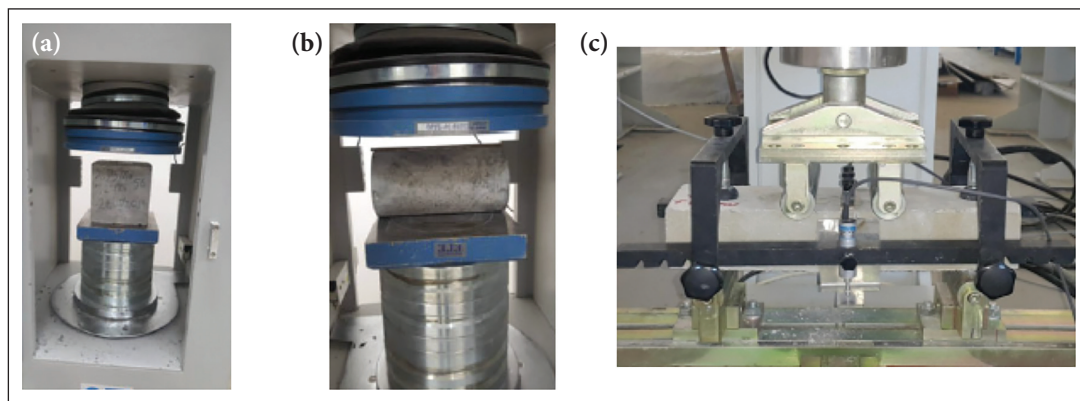


Figure 2. Mechanical tests: (a) compressive strength, (b) splitting tensile strength and (c) flexural tensile strength.

ues, SP were used as variable. Except control mixture, the fiber contents of 0.4% and 0.8% by the volume of concrete were used. In the Mix Code, the percentages of the fiber content of the mixtures were written next to the fiber types. That is, SS-0.4 represented the concrete mixture including 0.4% short straight steel fiber by volume.

2.2. Mix Procedure and Sample Preparation

For the mix procedure, all aggregates and steel fibers used in the designed mixture were mixed with 2/3 of the mixing water during 3 minutes. Then, PC and SP mixed with the rest of the water were mixed for additional 7 minutes. In the PP fiber-reinforced mixtures, at last, PP fiber was added and mixed into the mixture slowly to satisfy uniform distribution when the ingredients were dispersed effectively. To adjust the similar workability, slump flow test was carried out and the slump flow diameters of the fresh mixtures were measured. These values were found in the range of 120 mm–170 mm as shown in Table 3. Then, they were poured into moulds by two layers and vibrated for 60 times. After casting concrete, the specimens were covered with plastic sheets to inhibit the loss of moisture. They were kept in a room temperature and after 24 hours, the specimens were demolded and cured in saturated lime water until 7 and 28 curing days.

2.3. Test Procedure

In order to assess the effects of fiber type, shape and volume fraction on the mechanical and flexural properties of FRC, compressive, splitting tensile and flexural strength tests were conducted as shown in Figure 2. For each designed mixtures, three specimens were tested and mean value of them was reported as test results to obtain the hardened properties.

The compressive strength tests were carried out using 150x150x150 mm³ cube specimens according to ASTM C39 [31]. The loading rate was 6 kN/sec. The test was continued until it lost its all-load carrying capacity.

The splitting tensile strength test was carried out using cylindrical specimens with a diameter of 100 mm and a

height of 200 mm as per ASTM C496 [32]. The loading rate was arranged as 1.7 kN/sec. A thin plywood bearing strip was put along the length of the specimen to distribute the diametrical compressive force uniformly.

Four-point bending test through displacement control was carried out to measure the flexural strength based on ASTM C78 [33]. The beams with a cross-section of 100x100 mm² and a length of 400 mm were used and the mid-span deflection was measured using a Linear Variable Differential Transformer (LVDT) placed at the middle of the specimen. The loading rate was arranged as 0.003 mm/sec. The load-deflection curves determined the flexural behavior of the FRC specimens.

3. EXPERIMENTAL RESULTS AND DISCUSSIONS

3.1. Compressive Strength

3.1.1. Effects of Fiber Type and Shape on Compressive Strength

Figure 3 illustrates the effect of fiber type and shape on the compressive strength of concrete with/ without fiber at 7 and 28 days. For seven curing days, concrete specimens with no fiber had the highest compressive strength with 37.1 MPa compared to the FRC specimens, regardless of the fiber content. On the other hand, for 28 curing days, the highest compressive strengths were obtained in the short straight steel fiber-reinforced concrete specimens with 43.5 MPa and 45.2 MPa for 0.4% and 0.8% fiber content, respectively, representing increases of 5.84% and 9.98% compared to the control specimen. This may be because at early age, the fibers could not show their effects on the strength due to the immaturity of the matrices. However, by improving the matrix, the SS fibers could inhibit the crack initiation and propagation and contribute an effective bridging mechanism. The effectiveness of SS fiber was so sharp for all fiber contents at 28 days. This could be because the shortest fiber in length could bridge the micro cracks more effectively. In the other studies [10, 34–36], it was also found that short and straight micro fibers

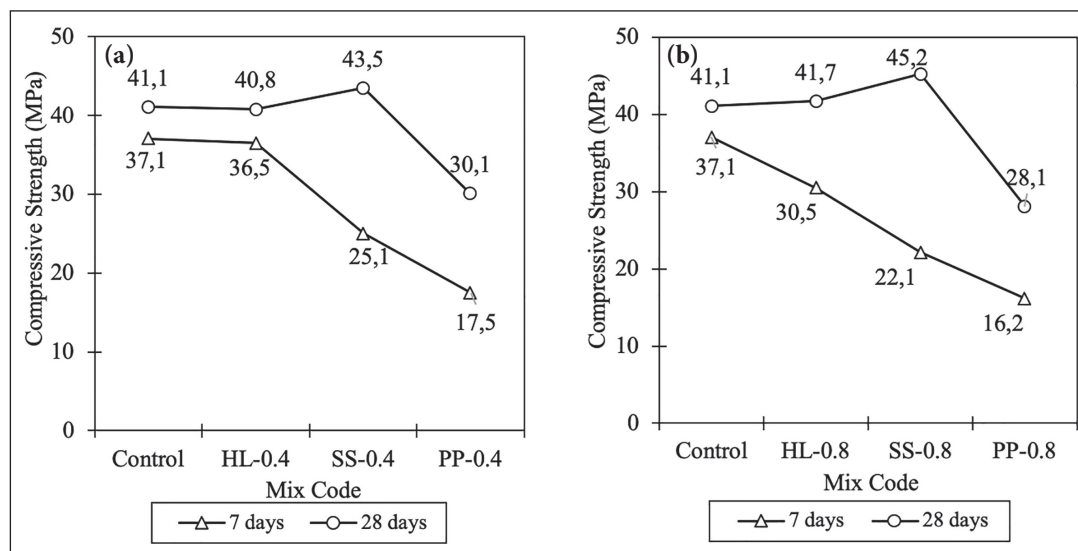


Figure 3. Effect of fiber type and shape on compressive strength for (a) 0.4% volume of fiber, (b) 0.8% volume of fiber.

played a vital role on the enhancement of the compressive strength of FRC because of inhibiting the micro-crack propagation. However, the compressive strength of PP fiber-reinforced concrete with the fiber volume of 0.4% and 0.8% were the lowest at 7 and 28 curing days. That is, the compressive strength of PP0.4 was lower than that of the control concrete by 52.83% and 26.76%, respectively, at 7 days while for PP0.8, it was 56.33% and 31.63% at the age of 28 days. Some researchers [37, 38] think that PP fiber plays an essential role in bridging cracks when distributed inside the concrete. Because the stress transferred between the crack tip and the concrete surface in the crack areas can be achieved by the great adhesion between the concrete and fiber. Therefore, the stress occurred in the concrete becomes uniform, resulting in alleviating the degree of stress concentration. However, the use of high amount of PP fiber in concrete cause poor dispersion of fibers resulting in weak interfacial transition areas in matrix. In this study, the high degradation in compressive strength of PP fiber-reinforced concrete specimens can be attributed to the inclusion of a high dosage of PP fibers because in the matrix, the average distances between the fibers can shorten by the high fiber content.

As a consequence, the fibers can overlap, thus worsening the bonding between the paste and fibers. According to the study of Zhang [39] about the compressive strength of PP fiber-reinforced concrete having fiber content of 0%, 0.089%, 0.13%, 0.17%, 0.22%, 0.56% volume fraction, it was found that the use of PP fiber at a certain percentage enhanced the compressive strength. However, the compressive strength of PP fiber-reinforced concrete with the fiber volume of 0.22% and 0.56% became lower than that of plain concrete. Moreover, in this study, referring to Table 3, the slump values of PP fiber-reinforced concrete mixtures also proved that PP fibers induced a de-

crease in flowability, leading to the use of a higher amount of SP. It was observed that PP fibers caused the formation of agglomerations during the mixing process due to their higher resistance to flowability. The decreased flowability of the new matrix could inhibit the dispersion of PP fibers resulting in a reduction in compressive strength. In the aspect of long hooked steel fiber-reinforced concrete, it was found that the inclusion of long hooked steel fiber with a volume fraction of 0.4% provided slightly lower compressive strength than that of control concrete for all curing ages while the specimen of HL0.8 exhibited slight improvement in compressive strength with 1.46% at 28 days. This increase can be due to the confining effect caused by long hooked end steel fibers to FRC.

3.1.2. Effects of Fiber Volume Fraction on Compressive Strength

The changes in compressive strength of FRC having different fiber volume fractions at 7 and 28 curing days were presented in Figure 4. As seen, at 7 days, compressive strength values were reduced with the increase in the fiber content for all fiber types and shapes. On the other hand, for 28 curing days, using short steel fiber with 0.4% and 0.8% volume content improved the compressive strength by 5.84% and 9.98% regarding control specimens, respectively. That could be because the stress between the matrix and fiber may reduce by the use of a higher dosage of short steel fiber content and thus, the crack initiation and propagation can be delayed resulting in an improvement of strength. This result is consistent with the other studies [40, 41]. However, it can be said that the quantity of HL did not have an essential influence on the compressive strength of concrete; that is, the specimen of HL0.4 and HL0.8 had the compressive strength of 40.8 MPa and 41.7 MPa, respectively, at 28 days.

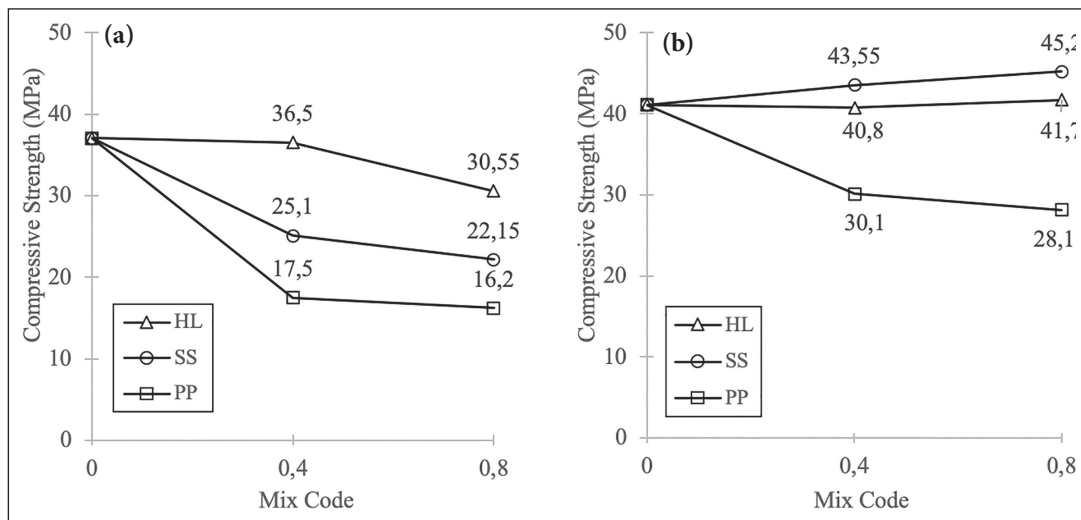


Figure 4. Effect of fiber volume fraction on compressive strength at (a) 7 days, (b) 28 days.

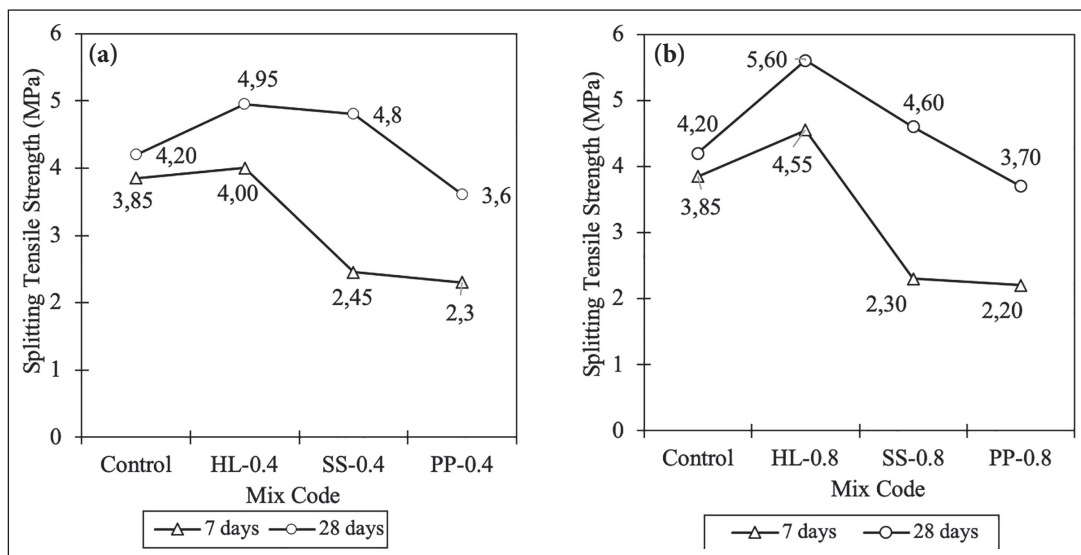


Figure 5. Effect of fiber type and shape on splitting tensile strength for (a) 0.4% volume of fiber, (b) 0.8% volume of fiber.

In contrast, an increase in PP fiber volume content resulted in a significant reduction in the compressive strength at all curing ages. Using PP with 0.4% and 0.8% by volume fraction decreased the compressive strength by 52.83% and 56.33%, respectively, for seven days and 26.75% and 31.63%, respectively, for 28 days. In general, especially for higher fiber content, a decreasing trend can be observed due to the poor dispersion of fibers and the formation of clumps of fibers during the mixing process, as in the case of this study. According to the research carried out by Ahmed et al. [42], the use of PP fibers at the percentage of 0.18% to 0.40% increased the compressive strength by about 5%, but at high PP fiber volume contents i.e., 0.55% to 0.60%, it decreased nearly 3–5% compared to plain concrete at 28 days. Wang et al. [43] also found that 0.5% PP fiber volume content negatively affected the compressive strength and the

reason of this result was explained by the reduction in the elastic modulus of the entire concrete matrix [44]. Besides, the reduction in compressive strength may be explained by having a high water/cement ratio of mixtures. As already known, the lower water/cement ratio affects the microstructure of paste-aggregate interfacial transition zone by reducing the capillary porosity of the hardened paste [45]. The adhesion between aggregates and paste can be influenced by the increase in water content in the bulk paste resulting in a reduction of concrete performance. Therefore, the high w/c ratio could weaken the reinforcement effect of PP fibers. Zhang et al. [39] used the PP fiber contents of 0.8, 1.2, 1.6, 2.0, and 5.0 kg/m³ for 0.4, 0.5 and 0.6 water/cement ratios and they concluded that the increase in water/cement ratio reduced the compressive strengths of the specimens for all PP fiber content.

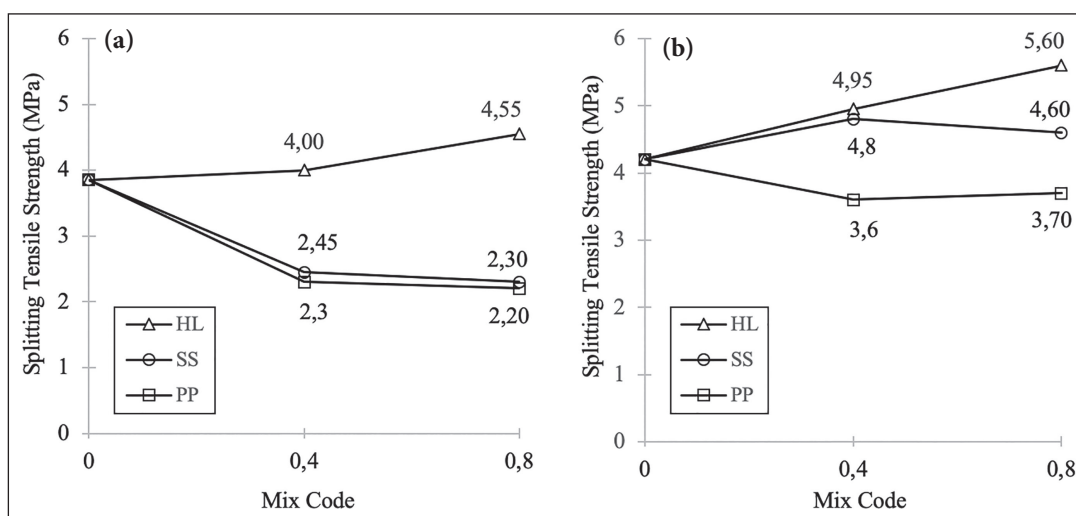


Figure 6. Effect of fiber content on splitting tensile strength at (a) 7 days, (b) 28 days.

3.2. Splitting Tensile Strength

3.2.1. Effects of Fiber Type and Shape on Splitting Tensile Strength

The effect of fiber type and shape on the splitting tensile strength of concrete with and without fiber at 7 and 28 days was presented in Figure 5. Unlike the compressive strength test results, more pronounced enhancement in the splitting tensile strength values were found for HL reinforced concrete specimens compared to plain concrete. That is, the improvement in splitting tensile strength of HL-0.4 and HL-0.8 were about 3.90% and 17.86% at 7 days and 18.18% and 33.33% at 28 days, respectively. It can be explained by the prevention of macro cracks caused by the presence of HL. This is because, long steel fibers with hooked end were more effective in the transfer of tensile stress and they had higher elastic modulus with regards to short steel fibers. Tabatabaeian et al. [46] and Haddadou et al. [47] also proved the effectiveness of HL on the bridging of cracks. On the other hand, adding SS into concrete led to a reduction in splitting tensile strength values for all fiber volume fractions for 7 curing days while for 28 curing days, the splitting tensile strength of SS-0.4 and SS-0.8 increased with 14.28% and 9.52%, respectively, with regards to that of control specimen. At 7 days, the reduction could be due to the immaturity of matrix. However, it was found that, the increase rate of splitting tensile strength of concrete with SS with regards to plain concrete was less than those of the concrete with HL. This result also prove that short fibers can control the opening of the cracks at a certain level but long fibers play a vital role to prevent the propagation of localized cracks and macrocracks. As for PP fibers, the lowest splitting tensile strength values were obtained among all concrete specimens regardless of the fiber content and curing days. This may be because, in this study, the use of PP fibers decreased the workability of concrete resulting in the

formation of agglomerations during mixing process. The insufficient dispersion of PP fiber could cause the reduction in splitting tensile strength.

3.2.2. Effects of Fiber Volume Fraction on Splitting Tensile Strength

The effects of fiber volume fraction on splitting tensile strength of concrete at 7 and 28 curing days were shown in Figure 6. It was clear that the use of 0.4% SS and 0.4% PP caused a sharp decrease in splitting strength while a slight improvement in splitting strength was observed as HL volume fraction increased at the curing age of 7. On the other hand, with the incorporation of 0.4% and 0.8% HL and SS fiber, the improvements in the splitting tensile strength were more pronounced at 28 days. The reason is that the steel fiber is tightly gripped by the concrete matrix along the crack resulting in a solid binding capacity between the matrix and steel fiber [48]. However, the increase in splitting tensile strength with increased steel fiber content was more evident for HL reinforced concrete specimens at 28 days. That is, the splitting tensile strength of HL-0.4 and HL-0.8 increased by 17.88% and 33.33%, respectively. It may be attributed to the fact that the stress caused by the external load could be transferred more effectively between the concrete matrix and steel fiber due to the addition of a higher amount of HL, resulting in the use of full tensile strength of steel fiber. In the study of Turk et al. [49], the short steel fiber content was changed as 0%, 0.25%, 0.50%, 0.75% and 1% instead of long, double hooked end steel fiber. They found that concrete specimens with 1% long, double hooked end steel fiber had the highest splitting tensile strength and it reduced as the content of long, double hooked end steel fiber decreased.

Splitting tensile strength is reduced with increased PP fiber volume fraction at all curing ages. It decreased by 40.26% and 42.86% for 7 days and 14.29% and 11.90% for 28 days when 0.4% and 0.8% PP by volume fraction was

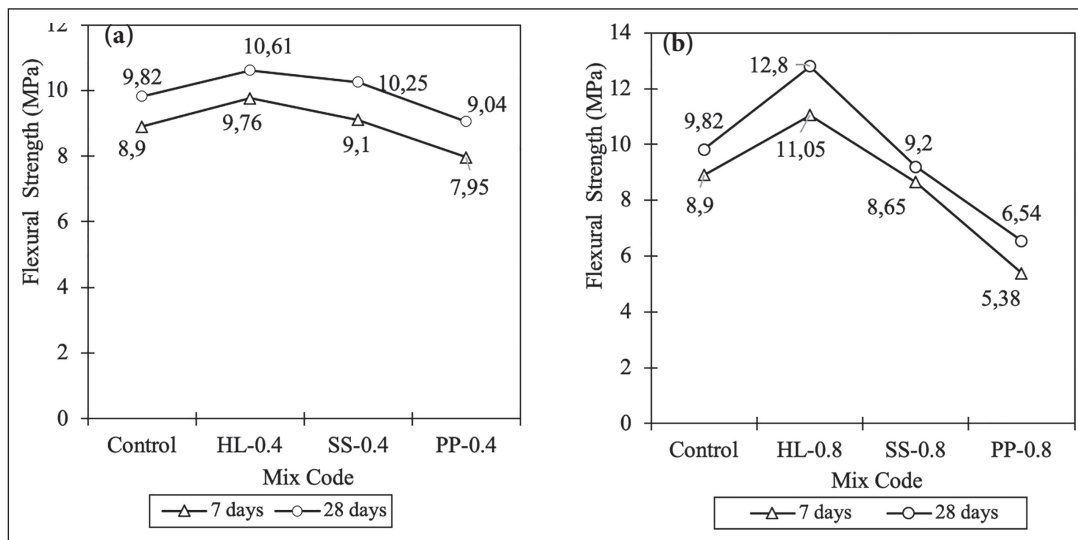


Figure 7. Effect of fiber type and shape on flexural strength for (a) 0.4% volume of fiber, (b) 0.8% volume of fiber.

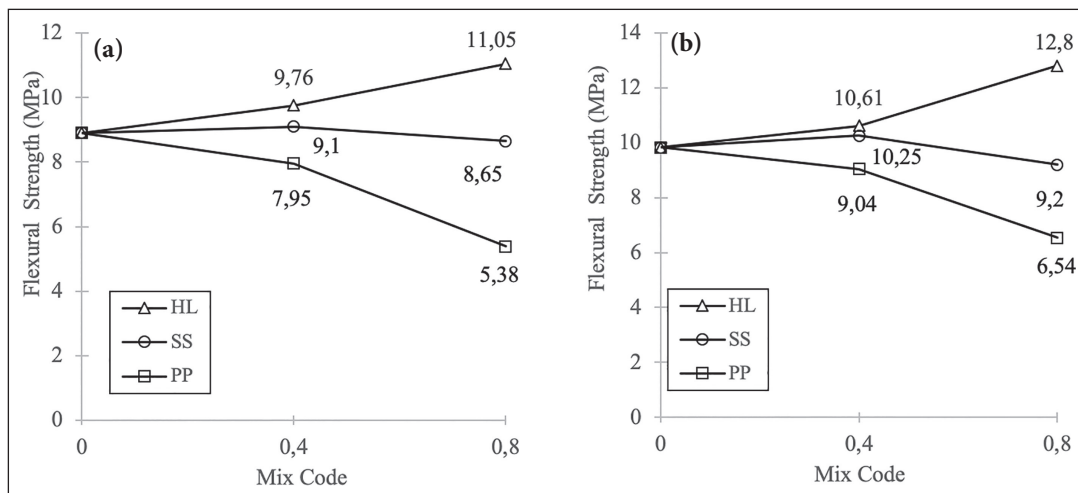


Figure 8. Effect of fiber content on flexural strength at (a) 7 days, (b) 28 days.

added, respectively. It could be due to having a higher aspect ratio of PP with regards to steel fibers which causes a reduction in workability of the fresh mixture resulting in lower tensile strength [50]. The higher PP fiber volume fraction can worsen the dispersion of fibers during the mixing process, as in the case of this study.

3.3. Flexural Performance

3.3.1. Flexural Strength

3.3.1.1. Effects of Fiber Type and Shape on Flexural Strength

Figure 7 shows the effect of fiber type and shape on the flexural strength of concrete with and without fiber at 7 and 28 days. The concrete reinforced with HL fiber had the highest flexural strength, that is, the use of 0.4% and 0.8% long hooked steel fiber by volume enhanced the flexural strength by 9.66% and 24.16%, respectively, at 7 days while

these values were 8.04% and 30.35% at 28 days. It may be attributed to the fact that HL can hold more stress than SS due to its fiber-end, which provides a better mechanical interlock and anchoring effect. Researchers also proved similar findings [49, 51–53]. On the other hand, 0.8% volume of SS caused a reduction in flexural strength by 2.81% and 6.31% at 7 and 28 days, respectively, while 0.4% volume of SS increased the flexural strength by 2.25% and 4.38% at 7 and 28 days, respectively. As for PP fiber-reinforced concrete, PP fiber caused the lowest flexural strength regardless of the fiber content and curing days. This result could be due to the poor bonding between the cement paste and PP because PP fiber has a hydrophobic nature with a relatively smooth surface [54]. Besides, the reduction in fresh properties caused by PP and its lower elastic modulus could lead to limited flexural strength values. Therefore, as seen in the load-deflection curve (Fig. 9 and 10) of PP fiber-reinforced

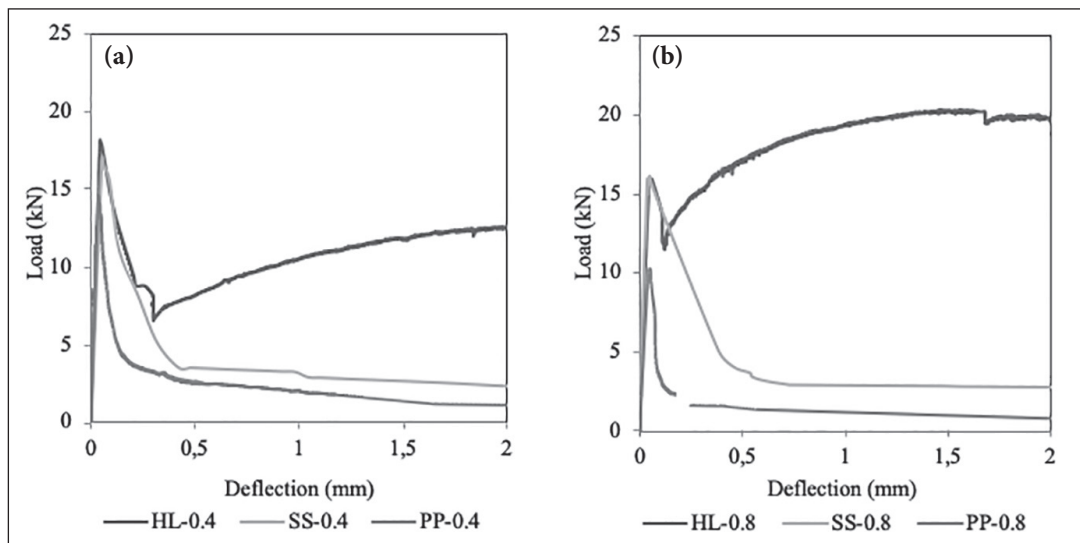


Figure 9. Effect of fiber type and shape on load-deflection curves for (a) 0.4% volume of fiber, (b) 0.8% volume of fiber at 7 days.

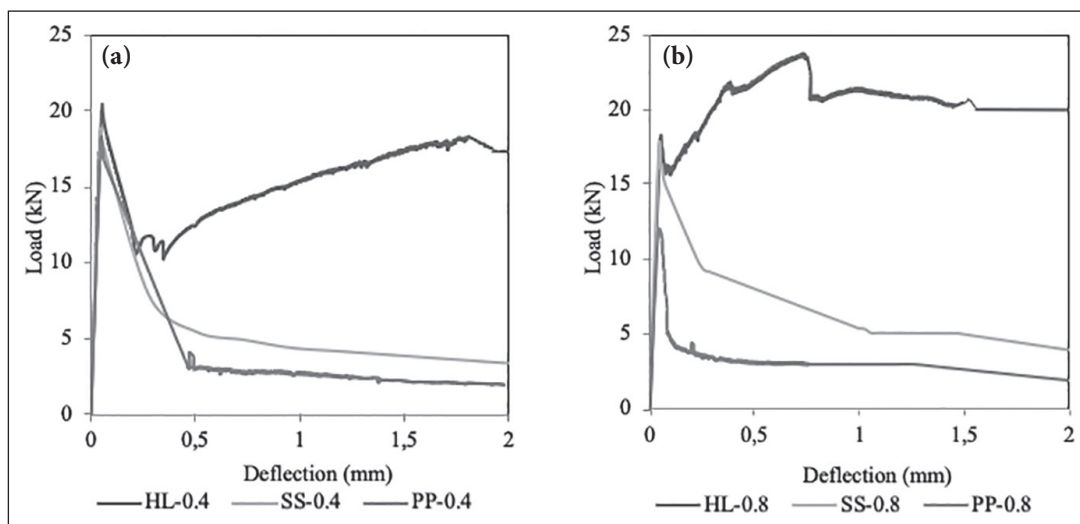


Figure 10. Effect of fiber type and shape on load-deflection curves for (a) 0.4% volume of fiber, (b) 0.8% volume of fiber at 28 days.

concrete, the peak load was taken as the ultimate failure force and after that point, the specimens lost all load carrying capacity regardless of the curing day and fiber content.

3.3.1.2. Effects of Fiber Volume Fraction on Flexural Strength

Figure 8 shows the effects of fiber volume fraction on flexural strength of concrete at 7 and 28 curing days. As observed, the flexural strength increased gradually with HL fiber dosage at 7 and 28 curing days. 0.4% and 0.8% volume of HL improved the flexural strengths by 9.66% and 24.16%, respectively, at 7 days, while these values were 8.04% and 30.35%, respectively, at 28 days. Besides, the use of 0.4% SS caused a slight improvement in flexural strength but 0.8% SS fiber significantly decreased the flexural strength

of specimens, especially at 28 days. As mentioned before, long hooked steel fiber positively affected flexural strength due to having a better anchoring effect. The increased long hooked steel fiber volume fraction could reduce the average space between the fibers and thus, more amounts of fibers could sustain the load resulting in a decrease in the stress between the matrix and fiber. Therefore, the initiation and propagation of cracks could be delayed and it could cause an improvement in flexural strength [40].

On the other hand, the increase in PP fiber volume fraction reduced the flexural strength for both 7 and 28 curing days. It decreased by 10.61% and 39.50% for seven days and 7.94% and 33.40% for 28 days when 0.4% and 0.8% PP by volume fraction were added, respectively. It could be

Table 4. Flexural performance of concrete specimens at (a) 7 curing day and (b) 28 curing day based on ASTM C1609

	a					
	HL0.4	HL0.8	SS0.4	SS0.8	PP0.4	PP0.8
δ_M (mm)	0.056	1.280	0.045	0.048	0.037	0.049
f_M (MPa)	9.76	11.05	9.10	8.65	7.95	5.38
T_M (N.mm)	0.50	1.03	0.46	0.68	0.29	0.31
$\delta_{L/600}$ (mm)	0.50	0.50	0.50	0.50	0.50	0.50
$f_{L/600}$ (MPa)	4.37	9.10	1.88	1.96	1.41	0.78
$T_{L/600}$ (N.mm)	4.93	7.33	4.03	4.73	2.31	1.38
$\delta_{L/150}$ (mm)	2.00	2.00	2.00	2.00	2.00	2.00
$f_{L/150}$ (MPa)	6.68	10.57	1.24	1.48	0.61	0.42
$T_{L/150}$ (N.mm)	24.25	36.50	8.35	9.03	4.93	3.03
	b					
	HL0.4	HL0.8	SS0.4	SS0.8	PP0.4	PP0.8
δ_M (mm)	0.053	0.606	0.046	0.048	0.050	0.045
f_M (MPa)	10.61	12.80	10.25	9.20	9.04	6.50
T_M (N.mm)	0.59	11.55	0.44	0.50	0.50	0.32
$\delta_{L/600}$ (mm)	0.50	0.50	0.50	0.50	0.50	0.50
$f_{L/600}$ (MPa)	6.67	11.73	0.63	0.13	1.66	1.69
$T_{L/600}$ (N.mm)	6.37	9.17	6.16	5.39	4.86	2.20
$\delta_{L/150}$ (mm)	2.00	2.00	2.00	2.00	2.00	2.00
$f_{L/150}$ (MPa)	9.24	10.67	1.75	2.14	1.04	0.98
$T_{L/150}$ (N.mm)	31.13	41.78	15.03	13.37	8.54	8.33

because adding a higher dosage of PP fiber led to further harm and defects in terms of mechanical strengths.

3.3.2. Load Deflection Curves and Flexural Toughness Based on ASTM C1609

ASTM C1609 [55] ensures flexural strength and toughness values corresponding to L/600 and L/150 in load-deflection curves. L symbolizes the length of span of the specimen and due to the reason that L is 300 mm in this study, $\delta_{L/150}$ and $\delta_{L/600}$ are the deflection points at 0.5 mm and 2 mm, respectively. $f_{L/600}$ and $f_{L/150}$ are the flexural strength of concrete specimen at the small flexural deformation (L/600) and at the large flexural deformation (L/150), respectively. $T_{L/150}$ and $T_{L/600}$ are the toughness values at L/150 and L/600, respectively, i.e., the area under the load-deflection curve until L/150 and L/600. Besides, δ_m , f_m and T_m are the deflection, flexural strength and toughness values corresponding to peak load.

3.3.2.1. Effects of Fiber Type and Shape on Load-Deflection Curves and Toughness

The effects of fiber type and shape on load-deflection curves of FRC specimens at 7 and 28 days were shown in Figure 9 and 10, respectively. As seen in figures, the linear elastic region of all load-deflection curves were similar, but the FRC specimens' flexural behavior was observed as

deflection hardening and deflection softening according to the type and shape of the fibers. For example, concrete with HL exhibited deflection hardening behavior, resulting in higher load bearing capacity after matrix cracking. HL eliminated sudden failure through crack bridging and thus, increased the energy absorption capacity and the post-crack resistance. In other words, including long hooked steel fiber to concrete caused more ductile behavior instead of brittle. Besides, HL reinforced concrete specimens had the highest peak load for all curing days and fiber content. As seen in Table 4, the peak deflections were also obviously enhanced, especially by the use of 0.8% volume of HK fiber, i.e., the peak deflections were found as 1.28 mm and 0.606 mm at 7 and 28 curing days, respectively. It can be due to the strong anchoring influence of long hooked steel fiber associated with fiber geometry. Besides, it could be because longer fibers could handle the greater load in cracks which could delay the crack formation and propagation [56]. On the other hand, referring Figure 8 and 9, deflection softening behavior was observed for both SS and PP fiber-reinforced concrete specimens, i.e., after reaching the peak load, they exhibited a sudden drop and lost their load carrying capacity, regardless of the curing age and fiber content. Abu-Lebdeh [57] also found that hooked end fibers caused 95% and 115% increase in pull-out energy and peak load regarding straight fiber.

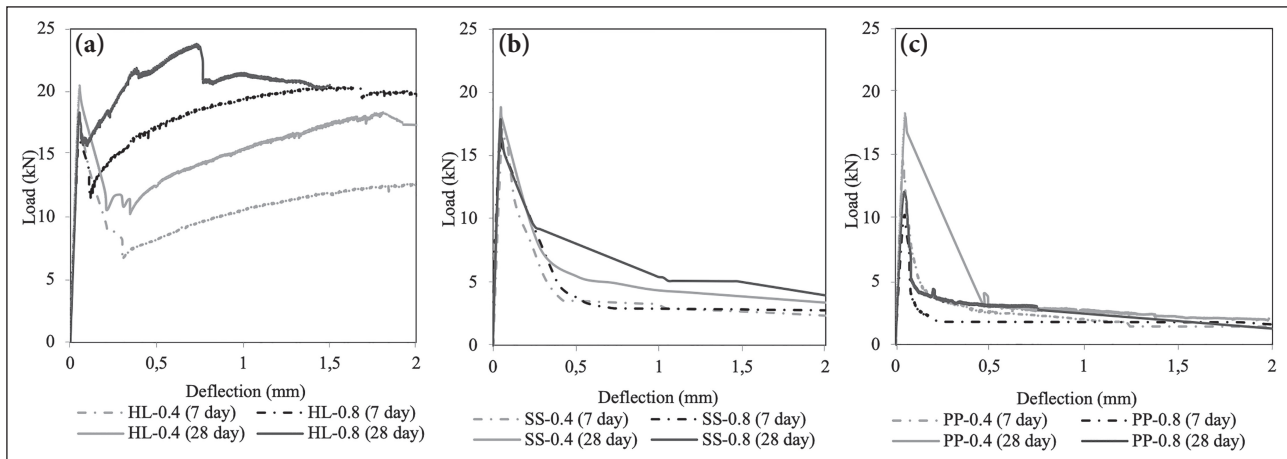


Figure 11. Effect of fiber content of (a) HL, (b) SS, and (c) PP on load-deflection curves.

At deflection point $L/600$, HL fiber-reinforced concrete specimens were in the strain hardening region regardless of the curing age and fiber content while SS and PP fiber-reinforced concrete specimens were in the softening range. This situation provided higher toughness at deflection $L/600$, that is 0.4% HL increased $TL/600$ by 3.34% and 31.19% with regards to 0.4%SS and 0.4%PP, respectively, at 28 days and these values were 70.18% and 316.28% when 0.8% fiber volumes were incorporated.

As expected, the flexural strength and toughness of HL reinforced concrete specimens at $L/150$ were higher than the others for all curing ages and fiber contents. However, the outcomes of the load-deflection curves also showed that SS and PP fiber-reinforced concrete specimens lost almost all load carrying capacity at deflection $L/150$. For example, $fL/150$ of SS fiber-reinforced concrete specimens were 1.36 MPa and 1.94 MPa, in average, at 7 and 28 days, respectively, while these values were 0.51 MPa and 1.0 MPa in average for PP fiber-reinforced concrete specimens.

3.3.2.2. Effects of Fiber Volume Fraction on Load-Deflection Curves and Toughness

The effects of fiber volume fraction on load-deflection curves of FRC specimens at 7 and 28 days were shown in Figure 11. The load-deflection curves became voluminous with higher peak load as HL content increased for all curing days. This deflection hardening behavior demonstrates the more effective reinforcing effect of HL. The deflection capacity and flexural strength at the peak were also increased with the increased HL volume fraction. The quantity of HL had an important influence on the pre-peak portion of the curve, which improved the flexural performance. Namely, FRC specimens having 0.8% volume of HL were in the range of pre-peak response at the deflection point $L/600$ at 7 and 28 days, while the concrete specimens with 0.4% HL were in the post-peak portion of the curve. Besides, the use of 0.8% volume of HL caused the highest toughness at peak load, $L/600$ and $L/150$ for all curing ages, and it shows that they absorbed

more energy, which indicates higher ductility in the hardening portion. This may be due to providing effective crack bridging caused by the higher content of HL. This finding is consistent with the studies of Turk et al. [10] and [8].

On the other hand, because of the insufficiency of SS in the bridging of crack and having a lower aspect ratio than HL, SS reinforced concrete specimens exhibited less post-peak load carrying capacity and showed similar flexural performance for all fiber volume fractions. However, using a higher volume fraction of PP fiber in concrete caused a slightly negative effect on deflection capacity and toughness at 7 and 28 days. For example, 0.8% volume of PP decreased the toughness at peak load and $L/600$ by 35.74% and 54.62%, respectively, compared to the concrete specimens with 0.4% PP at 28 days. As mentioned before, PP fiber decreased the efficiency of the fresh mixture and using a higher volume of PP fiber could increase this negative effect more apparent, resulting in a reduction in flexural performance.

4. CONCLUSION AND SUMMARY

This study designed seven concrete mixtures with a constant water/cement ratio. A control mixture had no fiber and the other six mixtures included fibers with different types, shapes and volume fractions. Within this scope, two types of steel fibers having different shapes and PP fiber were used with the volume fraction of 0.4% and 0.8%. The following conclusions can be listed according to the test results;

1. The highest compressive strength was achieved at the control specimen with no fiber at 7 curing day while for 28-day, the use of short straight steel fibers enhanced the compressive strength. The increase in fiber volume fraction led to a decrease in the compressive strength at 7 days, possibly due to the cement matrix's immaturity. On the other hand, adding 0.8% volume fraction of short straight steel fiber enhanced the compressive strength while long hooked end steel fiber did not show any effect at 28 curing days. Besides, as the PP fiber vol-

ume fraction increased, the compressive strength reduced significantly at all curing ages.

2. The long hooked end steel fiber was the most effective fiber at improving splitting tensile and flexural strength of concrete at all volume fractions and curing days. The highest enhancement was observed at the volume fraction of 0.8% long hooked end steel fiber at 28 curing days. The splitting tensile strength was reduced by adding short straight steel fiber for all fiber volume fractions at 7 days, while for 28 curing days, the use of 0.4% short straight steel fiber enhanced the splitting tensile and flexural strengths more. PP fibers reduced the splitting tensile and flexural strength values regardless of the fiber volume fractions and curing days.
3. Load-deflection curves showed that adding long hooked end steel fiber caused deflection hardening behavior, resulting in higher load bearing capacity after matrix cracking, while the reinforced concrete specimens with short straight steel fibers and PP exhibited deflection softening. The highest enhancement in flexural performance in terms of toughness, peak load and pre-peak response at the deflection point $L/600$ was observed by the utilization of 0.8% volume fraction of long hooked end steel fiber.

In summary, 0.8% volume fraction of short straight steel fibers showed the best compressive strength reinforcement while long hooked steel fiber did not cause a significant effect regardless of fiber volume. On the other hand, the highest enhancement in splitting tensile and flexural strengths were achieved by utilizing 0.8% volume fraction of long hooked end steel fiber and using 0.4% volume fraction of short straight steel fibers also enhanced the splitting tensile and flexural strength compared to plain concrete. However, PP fibers reduced the compressive, splitting tensile and flexural strength values regardless of the fiber content and curing days. In addition to these, as future work, the effect of hybrid use of different volume fractions of long hooked end steel fiber, short straight steel fibers and PP fiber on mechanical properties of concrete specimens can be investigated to reveal the interaction of these fibers into the matrix.

DATA AVAILABILITY STATEMENT

The authors confirm that the data that supports the findings of this study are available within the article. Raw data that support the finding of this study are available from the corresponding author, upon reasonable request.

CONFLICT OF INTEREST

The authors declare that they have no conflict of interest.

FINANCIAL DISCLOSURE

The authors declared that this study has received no financial support.

PEER-REVIEW

Externally peer-reviewed.

REFERENCES

- [1] Rong, Z., Sun, W., & Zhang, Y. (2010). Dynamic compression behavior of ultra-high performance cement based composites. *International Journal of Impact Engineering*, 37, 515–520. [CrossRef]
- [2] Park, S. H., Kim, D. J., Ryu, G. S., & Koh, K. T. (2012). Tensile behavior of ultra high performance hybrid fiber reinforced concrete. *Cement and Concrete Composites*, 34, 172–184. [CrossRef]
- [3] Kang, S. T., Lee, Y., Park, Y. D., & Kim, J. K. (2010). Tensile fracture properties of an Ultra High Performance Fiber Reinforced Concrete (UHPFRC) with steel fiber. *Composite Structures*, 92, 61–71. [CrossRef]
- [4] Xie J, Li J, Lu Z, Li, Z., Fang, C., Huang, L., & Li, L. (2019). Combination effects of rubber and silica fume on the fracture behaviour of steel-fibre recycled aggregate concrete. *Construction and Building Materials*, 203, 164–173. [CrossRef]
- [5] Ali, B., Qureshi, L.A., Raza, A., Nawaz, M. A., & Rehman, S. U., & Rashid, M. U. (2019). Influence of glass fibers on mechanical properties of concrete with recycled coarse aggregates. *Civil Engineering Journal*, 5, 1007–1019. [CrossRef]
- [6] Kina C, Turk K, Tanyildizi H (2022) Estimation of strengths of hybrid FR-SCC by using deep-learning and support vector regression models. *Structural Concrete*. [Epub ahead of print]. doi: 10.1002/suco.202100622 [CrossRef]
- [7] Kina C, Turk K, Tanyildizi H (2022) Deep learning and machine learning-based prediction of capillary water absorption of hybrid fiber reinforced self-compacting concrete. *Structural Concrete*. [Epub ahead of print]. doi: 10.1002/suco.202100756. [CrossRef]
- [8] Turk, K., Kina, C., & Oztekin, E. (2020). Effect of macro and micro fiber volume on the flexural performance of hybrid fiber reinforced SCC. *Advances in Concrete Construction*, 10, 257–269. [CrossRef]
- [9] Bassurucu, M., & Turk, K. (2022). An experimental and statistical investigation on the fresh and hardened properties of HFR-SCC: the effect of micro fibre type and fibre hybridization. *European Journal of Environmental and Civil Engineering*. [Epub ahead of print]. doi: 10.1080/19648189.2022.2042396 [CrossRef]
- [10] Turk, K., Bassurucu, M., & Bitkin, R. E. (2021). Workability, strength and flexural toughness properties of hybrid steel fiber reinforced SCC with high-volume fiber. *Construction and Building Materials*, 266, Article 120944. [CrossRef]
- [11] Deeb, R., Ghanbari, A., & Karihaloo, B. L. (2012). Development of self-compacting high and ultra high performance concretes with and without steel fibres. *Cement and Concrete Composites*, 34, 185–190. [CrossRef]

- [12] Kulasegaram, S., Karihaloo, B. L., & Ghanbari, A. (2011). Modelling the flow of self-compacting concrete. *International Journal for Numerical and Analytical Methods in Geomechanics*, 35, 713–723. [CrossRef]
- [13] Khaloo, A., Raisi, E. M., Hosseini, P., & Tahsiri, H. (2014). Mechanical performance of self-compacting concrete reinforced with steel fibers. *Construction and Building Materials*, 51, 179–186. [CrossRef]
- [14] Zeyad, A. M. (2020). Effect of fibers types on fresh properties and flexural toughness of self-compacting concrete. *Journal of Materials Research and Technology*, 9, 4147–4158. [CrossRef]
- [15] Şahin, Y., & Köksal, F. (2011). The influences of matrix and steel fibre tensile strengths on the fracture energy of high-strength concrete. *Construction and Building Materials*, 25, 1801–1806. [CrossRef]
- [16] Olivito, R. S., & Zuccarello, F. A. (2010). An experimental study on the tensile strength of steel fiber reinforced concrete. *Composites Part B: Engineering*, 41, 246–255. [CrossRef]
- [17] Yoo, D. Y., Lee, J. H., & Yoon, Y. S. (2013). Effect of fiber content on mechanical and fracture properties of ultra high performance fiber reinforced cementitious composites. *Composite Structures*, 106, 742–753. [CrossRef]
- [18] Altun, F., Haktanir, T., Ari, K. (2007). Effects of steel fiber addition on mechanical properties of concrete and RC beams. *Construction and Building Materials*, 21, 654–661. [CrossRef]
- [19] Ozkılıc, Y. O., Aksoylu, C., & Arslan, M. H. (2021). Experimental and numerical investigations of steel fiber reinforced concrete dapped-end purlins. *Journal of Building Engineering*, 36, Article 102119. [CrossRef]
- [20] Koroglu, M. A., & Ashour, A. (2019). Mechanical properties of self-compacting concrete with recycled bead wires. *Revista de la Construcción*, 18(3), 501–512. [CrossRef]
- [21] Cifuentes, H., García, F., Maeso, O., & Medina, F. (2013). Influence of the properties of polypropylene fibres on the fracture behaviour of low-, normal- and high-strength FRC. *Construction and Building Materials*, 45, 130–137. [CrossRef]
- [22] Małek, M., Łasica, W., Kadela M., Kluczyński, J., & Dudek, D. (2021). Physical and mechanical properties of polypropylene fibre-reinforced cement-glass composite. *Materials*, 14, 1–19. [CrossRef]
- [23] de Souza Castoldi, R., de Souza, LMS., & de Andrade Silva, F. (2019). Comparative study on the mechanical behavior and durability of polypropylene and sisal fiber reinforced concretes. *Construction and Building Materials*, 211, 617–628. [CrossRef]
- [24] Szeląg, M. (2019). Evaluation of cracking patterns of cement paste containing polypropylene fibers. *Composite Structures*, 220, 402–411. [CrossRef]
- [25] Ramesh, B., Gokulnath, V., & Ranjith Kumar, M. (2020). Detailed study on flexural strength of polypropylene fiber reinforced self-compacting concrete. *Materials Today: Proceedings*, 22, 1054–1058. [CrossRef]
- [26] Li, B. X., Chen, M. X., Cheng, F., & Liu, L. P. (2004). The mechanical properties of polypropylene fiber reinforced concrete. *Journal Wuhan University of Technology, Materials Science Edition*, 19, 68–71. [CrossRef]
- [27] Mazaheripour, H., Ghanbarpour, S., Mirmoradi, S. H., & Hosseinpour, I. (2011). The effect of polypropylene fibers on the properties of fresh and hardened lightweight self-compacting concrete. *Construction and Building Materials*, 25, 351–358. [CrossRef]
- [28] Fu Q, Xu W, Bu M, Guo, B., & Niua, D. (2021) Effect and action mechanism of fibers on mechanical behavior of hybrid basalt-polypropylene fiber-reinforced concrete. *Structures*, 34, 3596–3610. [CrossRef]
- [29] Rostami, R., Zarrebini, M., Mandegari, M., Sanginabadi, K., Mostofinejad, D., & Abtahib, S. M. (2019) The effect of concrete alkalinity on behavior of reinforcing polyester and polypropylene fibers with similar properties. *Cement and Concrete Composites*, 97, 118–124. [CrossRef]
- [30] Afroughsabet, V., & Ozbakkaloglu, T. (2015). Mechanical and durability properties of high-strength concrete containing steel and polypropylene fibers. *Construction and Building Materials*, 94, 73–82. [CrossRef]
- [31] ASTM C39 / C39M-20. (2020). Standard Test Method for Compressive Strength of Cylindrical Concrete Specimens. ASTM International.
- [32] ASTM C496 / C496M-17. (2017). Standard Test Method for Splitting Tensile Strength of Cylindrical Concrete Specimens. ASTM International.
- [33] ASTM C78 / C78M-18. (2018). Standard Test Method for Flexural Strength of Concrete (Using Simple Beam with Third-Point Loading). ASTM International.
- [34] Bozkurt, N., & Yazicioğlu, S. (2017). The strength properties of fibre reinforced self compacting concrete. *Acta Physica Polonica A*, 132, 775–778. [CrossRef]
- [35] Ahmad, S., & Umar, A. (2018). Fibre-reinforced self-compacting concrete: A review. *IOP Conference Series: Materials Science and Engineering*, 377, Article 012117. [CrossRef]
- [36] Shi, X., Park, P., Rew, Y., Huang, K., & Sim, C. (2020). Constitutive behaviors of steel fiber reinforced concrete under uniaxial compression and tension. *Construction and Building Materials*, 233, Article 117316. [CrossRef]

- [37] Bicer, K., Yalciner, H., Pekrioglu Balkis, A., & Kumbaroglu, A. (2018). Effect of corrosion on flexural strength of reinforced concrete beams with polypropylene fibers. *Construction and Building Materials*, 185, 574–588. [CrossRef]
- [38] Caggiano A, Gambarelli S, Martinelli E, Nisticò, N., & Pepe, M. (2016). Experimental characterization of the post-cracking response in Hybrid Steel/Polypropylene Fiber-Reinforced Concrete. *Construction and Building Materials*, 125, 1035–1043. [CrossRef]
- [39] Zhang, H., Wang, L., Zheng, K., Tijjani Jibrin B, Totakhil, & P. G. (2018). Research on compressive impact dynamic behavior and constitutive model of polypropylene fiber reinforced concrete. *Construction and Building Materials*, 187, 584–595. [CrossRef]
- [40] Sahmaran, M., Yaman, I. O. (2007). Hybrid fiber reinforced self-compacting concrete with a high-volume coarse fly ash. *Construction and Building Materials*, 21, 150–156. [CrossRef]
- [41] Pourbaba, M., Asefi, E., Sadaghian, H., Mirmiran, A. (2018). Effect of age on the compressive strength of ultra-high-performance fiber-reinforced concrete. *Construction and Building Materials*, 175, 402–410. [CrossRef]
- [42] Ahmed, S., Bukhari, I., Siddique, J. I., & Qureshi, S. A. (2006). A study on properties of polypropylene fiber reinforced concrete, 31th Conference on our world in concrete, 31st Conference on Our World in Concrete & Structures: 16 – 17 August 2006, Singapore.
- [43] Wang, J., Dai, Q., Si, R., Guo, S. (2019). Mechanical, durability, and microstructural properties of macro synthetic polypropylene (PP) fiber-reinforced rubber concrete. *Journal of Cleaner Production*, 234, 1351–1364. [CrossRef]
- [44] Bayasi, Z., Zeng, J. (1993). Properties of Polypropylene Fiber Reinforced Concrete. *ACI Materials Journal*, 90(6), 605–610. [CrossRef]
- [45] Gao, Y., De Schutter, G., Ye, G., Tan, Z., & Wu, K. (2014). The ITZ microstructure, thickness and porosity in blended cementitious composite: Effects of curing age, water to binder ratio and aggregate content. *Composites Part B: Engineering*, 60, 1–13. [CrossRef]
- [46] Tabatabaeian, M., Khaloo, A., Joshaghani, A., Hajibandeh, E. (2017). Experimental investigation on effects of hybrid fibers on rheological, mechanical, and durability properties of high-strength SCC. *Construction and Building Materials*, 147, 497–509. [CrossRef]
- [47] Haddadou, N., Chaid, R., Ghernouti, Y., & Adjou, N. (2014). The effect of hybrid steel fiber on the properties of fresh and hardened self-compacting concrete. *Journal of Building Materials and Structures*, 1, 65–76. [CrossRef]
- [48] Yu, R., Spiesz, P., & Brouwers, H. J. H. (2014) Static properties and impact resistance of a green Ultra-High Performance Hybrid Fibre Reinforced Concrete (UHPHFRC): Experiments and modeling. *Construction and Building Materials*, 68, 158–171. [CrossRef]
- [49] Turk, K., Oztekin, E., & Kina, C. (2022). Self-compacting concrete with blended short and long fibres: experimental investigation on the role of fibre blend proportion. *European Journal of Environmental and Civil Engineering*, 26, 905–918. [CrossRef]
- [50] Park, J. J., Yoo, D. Y., Kim, S., & Kim, S. W. (2019). Benefits of synthetic fibers on the residual mechanical performance of UHPFRC after exposure to ISO standard fire. *Cement and Concrete Composites*, 104, Article 103401. [CrossRef]
- [51] Ponikiewski, T., & Golaszewski, J. (2013). Properties of steel fibre reinforced self-compacting concrete for optimal rheological and mechanical properties in precast beams. *Procedia Engineering*, 65, 290–295.
- [52] Mastali, M., Ghasemi Naghibdehi, M., Naghipour, M., & Rabiee, SM. (2015). Experimental assessment of functionally graded reinforced concrete (FGRC) slabs under drop weight and projectile impacts. *Construction and Building Materials*, 95, 296–311. [CrossRef]
- [53] Alrawashdeh, A., & Eren, O. (2022). Mechanical and physical characterisation of steel fibre reinforced self-compacting concrete: Different aspect ratios and volume fractions of fibres. *Results in Engineering*, 13, Article 100335. [CrossRef]
- [54] Niu, D., Huang, D., & Fu, Q. (2019). Experimental investigation on compressive strength and chloride permeability of fiber-reinforced concrete with basalt-polypropylene fibers. *Advances in Structural Engineering*, 22, 2278–2288. [CrossRef]
- [55] ASTM C1609/C1609M. (2019). Standard Test Method for Flexural Performance of Fiber-Reinforced Concrete (Using Beam With Third-Point Loading). ASTM International. [CrossRef]
- [56] Han, J., Zhao, M., Chen, J., & Lan, X. (2019). Effects of steel fiber length and coarse aggregate maximum size on mechanical properties of steel fiber reinforced concrete. *Construction and Building Materials*, 209, 577–591. [CrossRef]
- [57] Abu-Lebdeh, T., Hamoush, S., Heard, W., & Zornig, B. (2011). Effect of matrix strength on pullout behavior of steel fiber reinforced very-high strength concrete composites. *Construction and Building Materials*, 25, 39–46. [CrossRef]



Research Article

An evaluation of vertical dynamic stress attenuation for compacted coarse-grained soils

Kuangbiao SUN¹, Mingjing FANG^{*,2}, Donglin SHU³, Yang PU⁴, Wenbing WANG³

¹Anhui Provincial Communications Holding Group Co., LTD, Anhui, China

²Wuhan University of Technology, School of Civil Engineering and Architecture, Wuhan, China

³Anhui Expressway Test and Inspection Research Center Co. LTD., Anhui, China

⁴China Construction Fifth Engineering Bureau Investment Management Company, Changsha, China

ARTICLE INFO

Article history

Received: 08 July 2022

Accepted: 21 August 2022

Key words:

Coarse-grained soil, dynamic stress attenuation, numerical simulation, particle composition, test and evaluation

ABSTRACT

Coarse-grained soil (CGS), as a filler with the characteristics of high bearing capacity but difficult compaction for embankment construction, requires an appropriate thickness of a single compaction layer according to the influence depth of vertical dynamic stress. This paper used a numerical analysis using PFC2D following a scale model test with different particle gradations of compacted CGS fillers by adopting a modified PFWD. The results show that the influence depth is about 50 cm under the maximum impact stress of 0.066 MPa if defined the depth as the maximum stress attenuation to 20%. The compacted CGS filler with dense particle gradation and high strength has a rapid attenuation on vertical dynamic stress. Meanwhile, with the increase of stone content (P₅, particle size ≥ 5 mm), the vertical dynamic stress of compacted CGS is attenuated exponentially. The maximum particle size also affects the attenuation of vertical dynamic stress, which needs further research. The findings support the development of non-destructive devices to inspect the compactness of subgrade construction rapidly.

Cite this article as: Sun, K., Fang, M., Shu, D., Pu, Y., & Wang, W. (2022). An evaluation of vertical dynamic stress attenuation for compacted coarse-grained soils. *J Sustain Const Mater Technol*, 7(3), 172–183.

1. INTRODUCTION

With the rapid development of highway engineering and increasing environmental protection requirements, the coarse-grained soil (CGS) with a mixture of soil and gravel particles has enormous potential for being widely used in highway subgrade construction due to the high bearing capacity. However, the compaction of CGS fillers is quite tricky, which needs to confirm an appropriate thickness of

the compacted layer [1]. As the soil fillers, the particle composition of CGS is essentially a vital factor in influencing the mechanical properties of compacted soil layers. Generally, the methods to study the influence mechanism of coarse-grained particle content on macroscopic and mesoscopic properties of CGS fillers are usually using the discrete element method (DEM) and large-scale direct shear test (DST) or both. The previous research compared physical tests, and numerical simulation indicated that the gra-

*Corresponding author.

*E-mail address: mingjingfang@whut.edu.cn





Figure 1. Three classifications of the CGS sample.

gradation characteristics of CGS filler, such as controlling the optimal coarse-grained content, significantly influence the compaction behaviors [2, 3]. Therefore, several related research findings, including the gradation equation, were put forward to quantitatively express the influence of gradation on the mechanical behaviors of CGS fillers [4–6].

Meanwhile, the fine particles are the factors to influence the soil type, which further affects the mechanical performances of CGS [7, 8]. Moreover, the influence of particle

gradation on volume deformation is related to dilatancy. The critical reason is that the particle composition of CGS fillers is the main factor determining the shear strength [9, 10]. Additionally, the test study on controlling the seepage failure gradient of CGS with different particle gradations indicated that the failure gradient of CGS with more coarse-grained components usually occurred later than that of the gradation with more fine-grained components. Meanwhile, the type of infiltration failure of CGS fillers reflects the in-

ternal structural stability of soil particles under specific particle composition and compactness degree [11]. Furthermore, the methods to estimate the deformation modulus of compacted CGS fillers were also developed [12, 13]. For the influence of the stiffness modulus, both the maximum dry density (MDD) and the optimum moisture content (OMC) were proved as the main factors by the portable falling weight deflectometer (PFWD), which is also currently and widely used in rapidly estimating the modulus of the structure intergradation of pavement or roadbed [14–18].

However, the current research for CGS fillers mainly refers to the conventional static features such as the MDD, compressive shear strength, and impermeability, while rarely from the perspective of dynamic response. For the soil subgrade, the previous research on the dynamic stress attenuation with different resilience modulus of compacted fillers under axial loads showed that the greater the modulus, the faster the dynamic stress attenuates [19]. The mechanical properties of CGS fillers, as a complex mesostructure, are essentially influenced by various factors. Under dynamic loads, the particles of CGS filler often occur microscopic behaviors such as straight movement, rotation, and even breakage. In practice, however, it is difficult to study its mesoscopic mechanical properties directly due to various restrictions of different conditions. Hence, using DEM, typically the program known as the particle flow code (PFC), is convenient to simulate the mechanical behavior of CGS fillers in terms of different particle interactions [20].

Therefore, the first objective for subgrade construction applying CGS fillers is to confirm an appropriate thickness of a single compaction layer by considering soil particle interaction behavior. From the application of PFWD, it is adequate to test the integration of pavement compaction. The thickness of a single CGS soil compacting layer also strongly correlates with the vertical attenuation of dynamic stress induced by non-destructive devices while not more significant efforts by compactor roller. Accordingly, this paper presents a test and numerical evaluation of dynamic stress attenuation for the compacted CGS fillers with different particle gradations using a modified PFWD tester.

2. MATERIALS AND METHODS

2.1. Test Materials

The CGS filler is an inhomogeneous mixture of earth and stone in the natural state. The soil sample of disintegrated granite in this research was from Chizhou City of Anhui Province in China. The CBR values of all samples meet the required values according to the highway earthwork specification (>14.3%). Meanwhile, the MDD and the optimal moisture content of CGS are 2.119 g/cm³ and 7.6%, respectively. During the geotechnical sampling, the compaction work is between 2677.2 and 2687.0 kJ/m³, according to the specification. Specifically, in this research, the CGS soil samples were divided into three categories

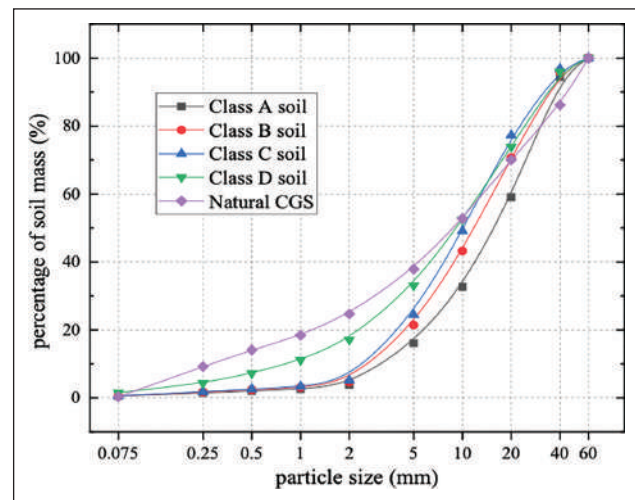


Figure 2. Gradation curves of test soil samples.

Table 1. Particle composition parameters

Soil types	Class A	Class B	Class C	Class D	Natural CGS
d10/mm	3.63	2.955	2.752	0.918	0.291
d30/mm	9.86	6.971	6.125	4.925	3.211
d60/mm	20.53	19.545	16.812	13.540	14.201
C _u	5.65	6.615	6.109	14.748	48.849
C _c	1.31	0.841	0.811	1.951	2.498

in terms of particle size, fine particles (0–2 mm), medium particles (2–20 mm), and coarse particles (20–60 mm). The soil sample classification is processed in Figure 1a–c.

According to the particle filling theory, the sample soil materials are blended based on the proportion of the test soil samples and filled step by step until the original soil composition is recovered. Finally, we obtain five types of CGS with different particle gradations. Based on the soil classifications above, the original proportion of CGS particles with three ranges is *Fine* (0–2): *Medium* (2–20 mm): *Coarse* (20–60 mm) = 1:3.84:1.87 in the mass ratio by using sieve analysis. From this proportion, five test samples with different particle gradations are designed as, Class A = 1/3 *Medium*+3/3 *Coarse*, Class B = 2/3 *Medium*+ 2/3 *Coarse*, Class C = 3/3 *Medium*+3/3 *Coarse*, Class D = 1/2 *Fine*+3/3 *Medium*+3/3 *Coarse*, Natural CGS = 2/2 *Fine*+3/3 *Medium*+3/3 *Coarse*. The gradations of the test CGS sample are shown in Figure 2. The parameters, including C_c and C_u of five particle compositions, are listed in Table 1.

2.2. Test Device and Principles

The test device used in this research, named dynamic, resilient modulus tester (DEM450) and shown in Figure 3, is modified based on the portable falling weight deflectometer (PFWD) [21]. The significant difference compared with PFWD is that the diameter of the loading plate base enlarged to 450 mm from 300 mm, and the mass of the

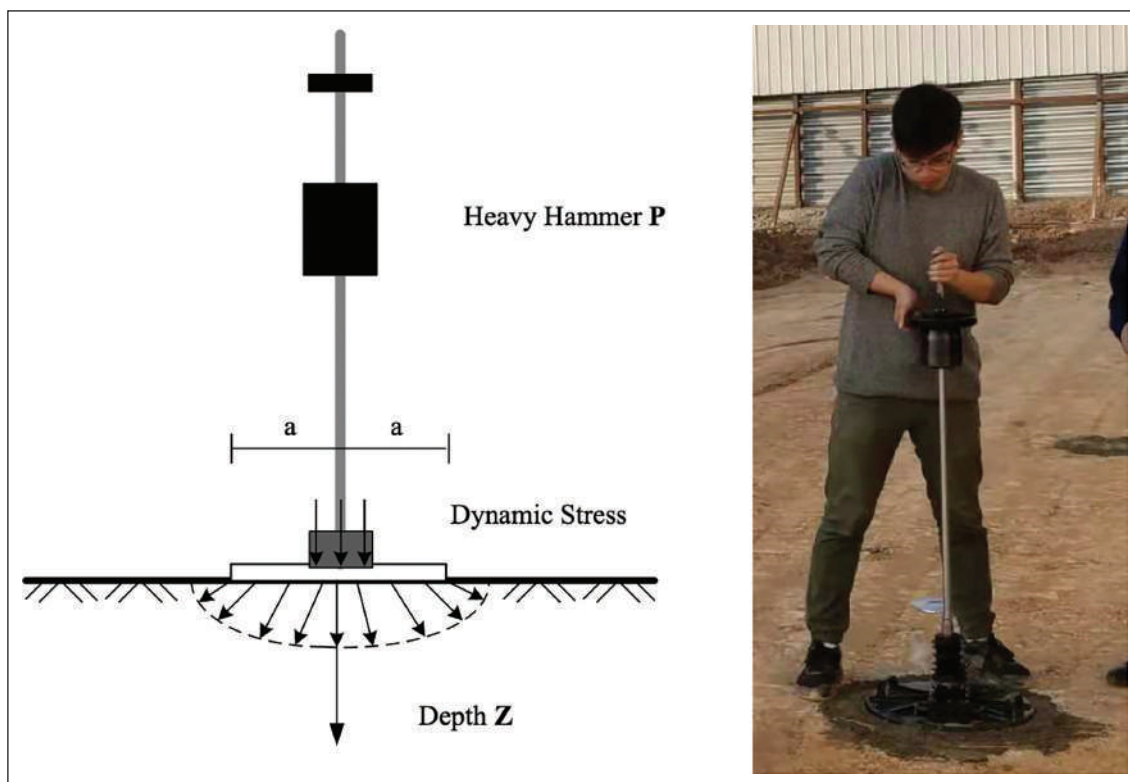


Figure 3. Dynamic, resilient modulus tester (DEM450).

drop hammer increased to 12 kg from 10 kg, which makes the acceptable size of the filler particle increased to 150 mm from 75 mm. Besides, the maximum stress is decreased to 0.066MPa from 0.1MPa due to the consistency of the initial tri-axle loading and the lightweight design. All modifications in DEM450 are for testing the soil filler with big size particles such as CGS.

The testing principle of DEM450 is the same as that of PFWD. Specifically, using a certain mass of the hammer, from a certain height with free fall, through the spring damping element and a particular area of the carrier plate to apply a specific size and time of action of the dynamic stress on the surface of compacted fillers, and then cause the surface to produce dynamic bending. By collecting the maximum impact force (N) and the corresponding resilient deformation (mm), then calculate the dynamic, resilient modulus (E_d) of the compacted soil layer. According to the correspondence between E_d and the degree of compaction (K), it is possible to use this modified device to check the compaction status of soil fillers. Especially this device is convenient for particular soils such as CGS fillers compared with the traditional sand cone method or others.

2.3. Test Methods

2.3.1 General Method

Using PFC2D, a DEM model was established to study the influence of three crucial factors of CGS fillers, name-

ly, different particle gradation, the maximum particle size, and the stone content (P5, particle size ≥ 5 mm), on the dynamic stress attenuation of compacted CGS soil filler. After that, the numerical analysis results were verified by physical model tests in the laboratory. However, the scale model test needs to carry out firstly, using the impact loading on the top of compacted fillers in the layered stacked mold. In the test, an earth pressure cell is embedded at the bottom of the first compacted layer. The impact load is applied to the top to collect the dynamic strain values at locations with different depths of the structural layer. The dynamic stress values in the layer are obtained by converting the calibration coefficient and the formula of the applied strain sensor. The actual influence depth can be obtained by assuming 20% of the maximum stress value, as defined by the dynamic stress attenuation depth, which is consistent with the subgrade work zone under the standard axial load. The dynamic stress attenuation law of compacted CGS fillers with different particle compositions under impact stress (0.066MPa) was studied using the scale model test in the laboratory. The test results can directly reflect the strength and mechanical properties of compacted CGS fillers from the dynamic response, providing a significant reference for the gradation selection of CGS filler in road subgrade construction. The objective of this research is to provide support for the research and development of rapid compaction quality control. Significantly, this research is also a theoretical basis for

Table 2. Mesoscopic parameters for DEM modeling

Project	Mesoscopic parameters	Symbol/unit	Values
Ball	Density	$\rho/\text{kg}\cdot\text{m}^3$	2500
	friction coefficient	f	0.7
	initial elastic modulus	E_c/Pa	2.5×10^7
	stiffness ratio	κ_n/κ_s	2.5
	Porosity	n	0.1
Ball-wall	normal stiffness	κ_n/Pa	2.5×10^6
	tangential stiffness	κ_s/Pa	2.5×10^6
Clump-ball	Density	$\rho/\text{kg}\cdot\text{m}^3$	3167
	contact stiffness	$\kappa_n, \kappa_s/\text{Pa}$	1×10^7

the feasibility of rapid inspection of CGS filler compactness and verifying whether the stress influencing depth meets the inspection requirements of highway construction.

2.3.2 Numerical Calculation

According to the rules of PFC, the number of particles generated in particle generation can reach hundreds of thousands if the actual gradation determines the value. For better efficiency, a reasonable simplification is essential in normal. Particles below 2 mm are replaced by related particles between 2 mm and 60 mm in equal amounts using a weighted average according to their mass proportion. After running the PFC program, according to the basic principles of dynamics, the initially generated overlapping particles repel each other and fill the whole space, finally forming the specified particle accumulation model. To simplify the analysis and improve the calculation efficiency, the size of the specimen model is 0.9 m long and 0.9 m wide.

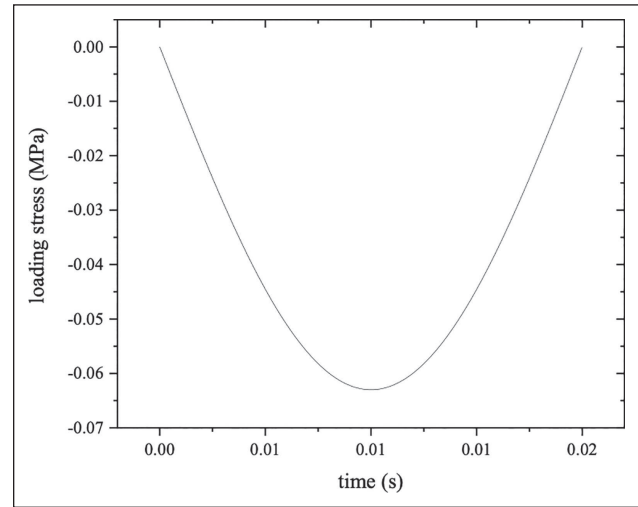
In PFC2D, the voids in two-dimensional space differ from the actual voids in three-dimensional space and are slightly smaller than the latter numerically. Therefore, the voids in two and three dimensions need to transform quantitatively. Based on the assumption of particles with equal particle size and the principle of compactness modification, the formula for converting three-dimensional voids of particles to two-dimensional voids was proposed as follows [22].

$$\varepsilon_{3d} = 1 - \xi(1 - \varepsilon_{2d})^2 \quad (1)$$

$$\text{Where } \xi = \frac{\sqrt{2}}{\sqrt{\pi\sqrt{3}}} + D_r \left(\frac{2}{\sqrt{\pi\sqrt{3}}} - \frac{\sqrt{2}}{\sqrt{\pi\sqrt{3}}} \right);$$

D_r is the relative compactness of the soil.

In this test, the relative compactness of CGS is 0.79, and the two-dimensional voids are 0.1. According to formula (1), the voids under three-dimensional condition is 0.31, which meets the compaction quality standard of this kind of filler. As there is no direct correspondence between pa-

**Figure 4.** The time-history curve of semi-sinusoidal load.

rameters of the mesoscopic and the macroscopic scale of the actual soil particles, they have co-relation under natural conditions. Combined with relevant laboratory test data and repeated numerical simulation tests, the corresponding mesoscopic parameters affecting the macroscopic parameters and their relationship were determined. Accordingly, the mesoscopic parameters matching the macroscopic parameters of soil mass were listed in Table 2.

The dynamic impact loading is in the form of semi-sinusoidal loads, and the maximum impact load and the bearing area determine the transient impact stress. According to the axial load in the standard test method of dynamic resilience modulus of subgrade soil specified in the highway subgrade design code [23], to study the dynamic properties and strength properties of compacted CGS filler subgrade, the semi-sinusoidal pulse load of 0.066MPa as the maximum axial preload in the dynamic triaxial test is selected for the transient impact stress on the bearing plate, with the standard action time of 18–20 ms. The time-history curve of the impact load stress is shown in Figure 5.

2.3.3. Scale Model Test

A physical model test was conducted in the laboratory to verify the reliability of the numerical modeling and the calculation results. Firstly, a specific size of layered and stacked mold was applied, and the categorized filler was added and compacted to the mold for the dynamic impact stress test. An earth pressure cell was pre-installed at the bottom of the first compacted soil layer to monitor the vertical dynamic stress transferred from the top of the model, as shown in Figure 5a. Three of the five fillers with different gradations mentioned above were selected for the test to verify the accuracy of the numerical simulation results. The loading model with and without molds and the loading process of the laboratory test are shown in Figures 5b and 4c, and 4d, respectively.



Figure 5. Dynamic, resilient test for compacted CGS fillers in laboratory. (a) Installation of earth pressure cell. (b) Parallel tests with molds. (c) Stacked models without mold. (d) Dynamic impact loading.

3. RESULTS AND DISCUSSION

3.1. Calculation Results

Since the PFC program cannot apply force directly to the wall, it must use particle loading conditions and fix the angular velocity of the clump in the horizontal direction to avoid horizontal displacement and rotation. The loading force of the clump is set for the loading of the numerical model. Taking CGS particles as an example, the force chain diagrams of its loading force diffusion process are shown in Figure 6 (left). The particle velocity vector diagrams under the corresponding loading force are shown in Figure 6 (right). The loading stress diffusion diagram and the corresponding particle velocity vector diagram show that the clump can load the DEM model effectively.

3.2. Effect of Stress Attenuation

3.2.1 Gradation Effect

Using the generation method and calibrated mesoscopic parameters model above, the PFC program gen-

erated the numerical model of particle flow of CGS with five different particle gradations and carried out the impact dynamic stress loading simulation test. The generated particle flow models are shown in Figure 7 (left). The stress distributions among the corresponding model particles are shown in Figure 7 (right). In Figure 7 (right), the dark part represents the compressive stress, distributed in chains on the geometric plane called the force chain. The force chain can intuitively show particles' properties, strength, and stress distribution. It was noticed that under the same conditions, as the particle gradation of soil samples is gradually better, the pressure chain is gradually increased, and the intercalation effect between particles is significant. Meanwhile, the distribution of the force chain is gradually uniform, and the transmission and distribution of forces also tend to be uniform.

The above numerical model loading method is used to load the test CGS filler. For example, the time-history curve of vertical dynamic stress response of the CGS filler embankment at different depths is shown in Figure 8. The time-history curve shows that the transfer of dynamic

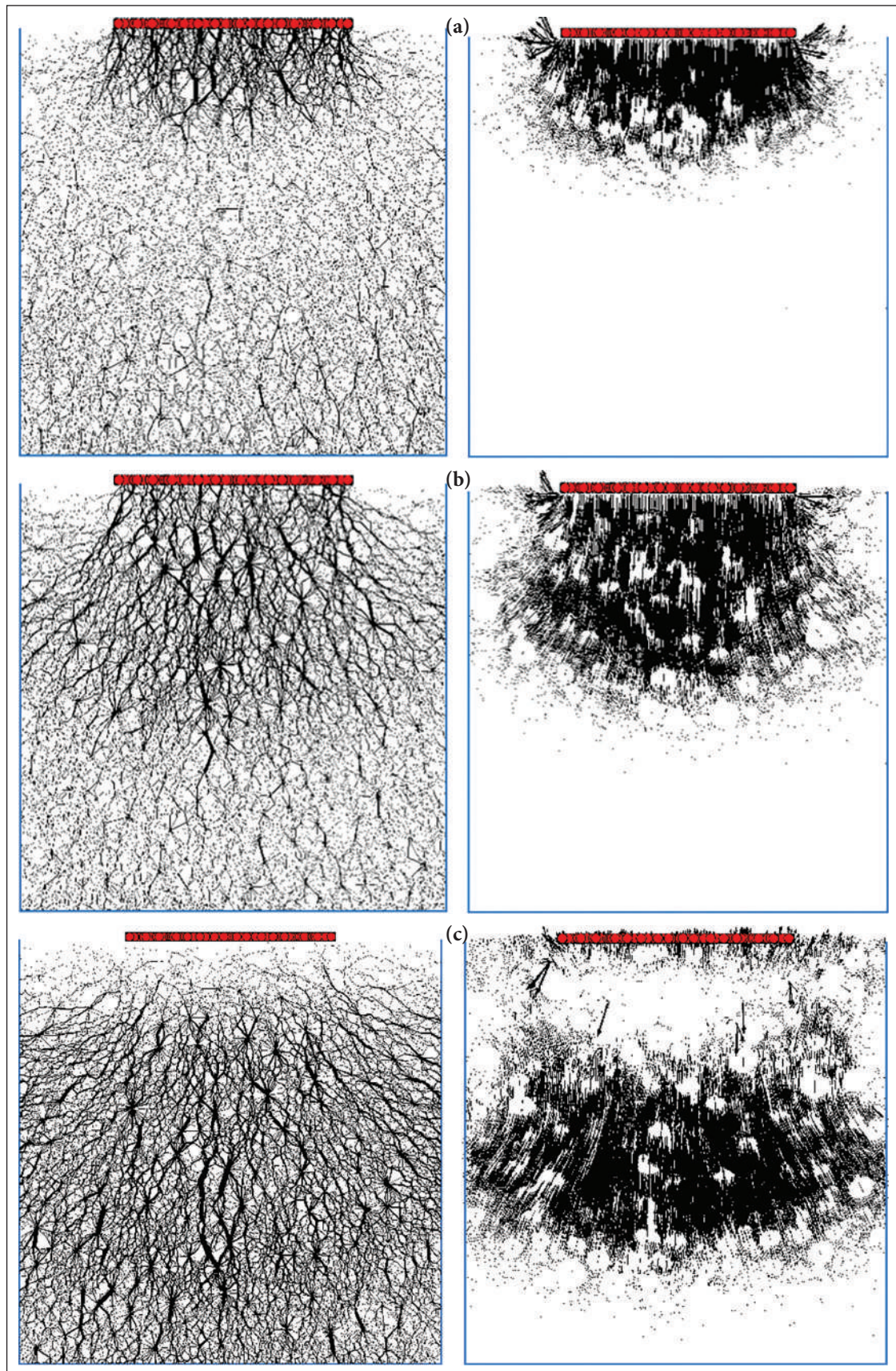


Figure 6. Dynamic loads and diffusion processing in three stages. (a) Initial loading. (b) During loading. (c) After loading.

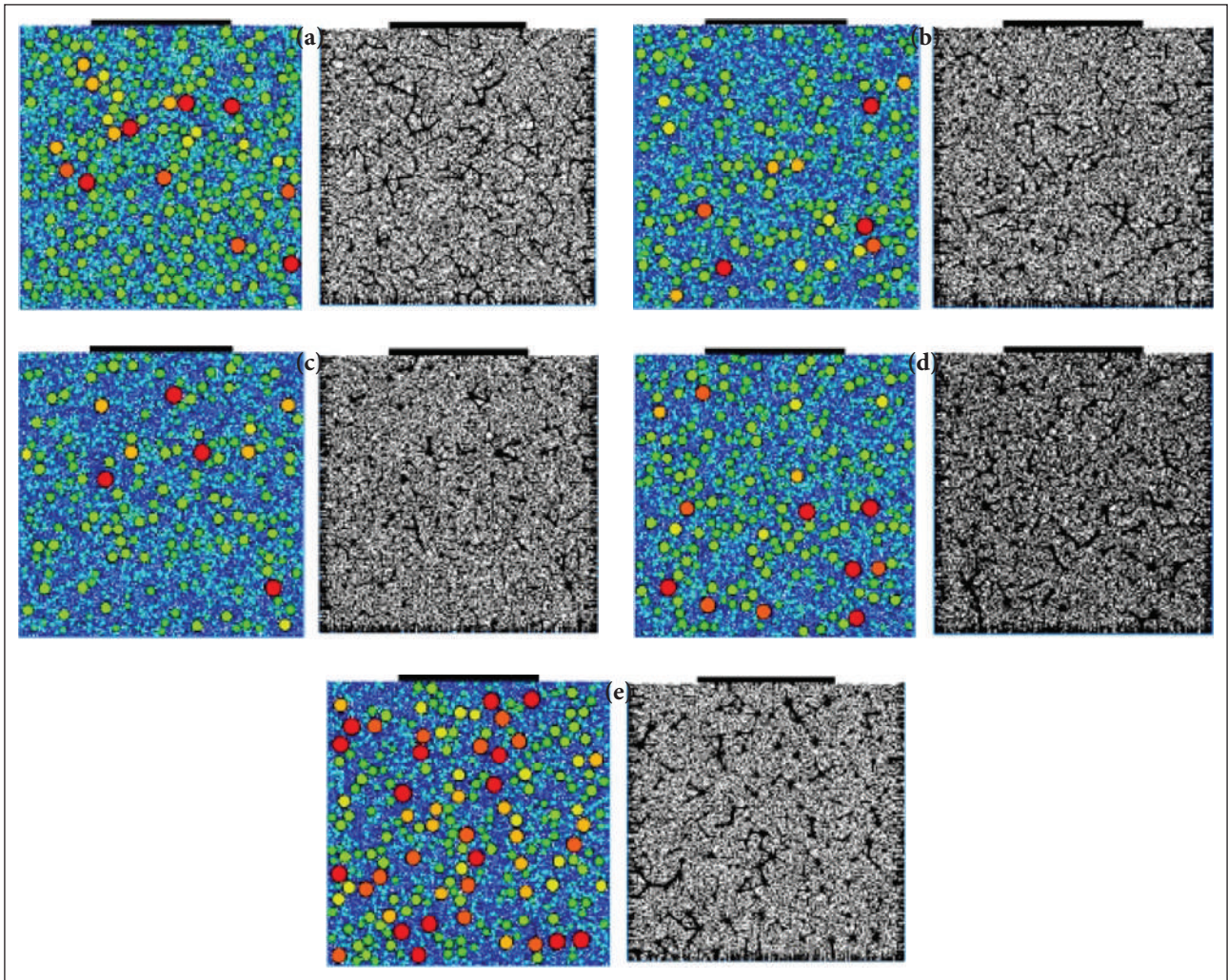


Figure 7. Different gradation models and force chains distribution among particles. (a) Class A. (b) Class B. (c) Class C. (d) Class D. (e) Natural CGS.

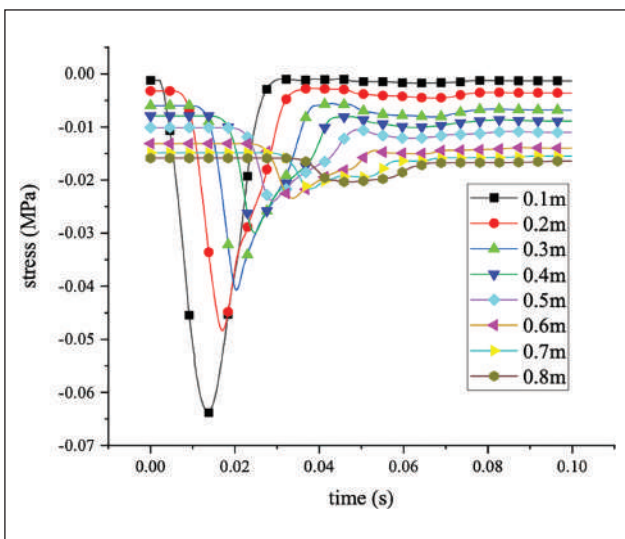


Figure 8. Time-history curves of dynamic stress at different depths.

stress delays along the depth direction. Under the action of semi-sinusoidal load, the emergence of stress peak is gradually delayed with the increase of depth. In addition, the dynamic stress of different depths under the loading of other groups of filler samples has similar regularity.

According to the numerical calculation results, the five test fillers' corresponding vertical dynamic stress curves are shown in Figure 9. The test results showed that the CGS filler gradation directly affected the transfer of dynamic stress in soil. The better the particle gradation of the filler, the greater the non-uniformity coefficient, the faster the attenuation of its vertical dynamic stress, and the more uniform the transmission of its stress. From Figure 9, the Natural CGS and Class D soil have a more significant attenuation rate of dynamic stress than the three others, which is caused by fine particles. For Natural CGS with complete gradation, the attenuated depth of vertical dynamic stress is about 50 cm. In other words, the single compaction thickness for CGS fillers is

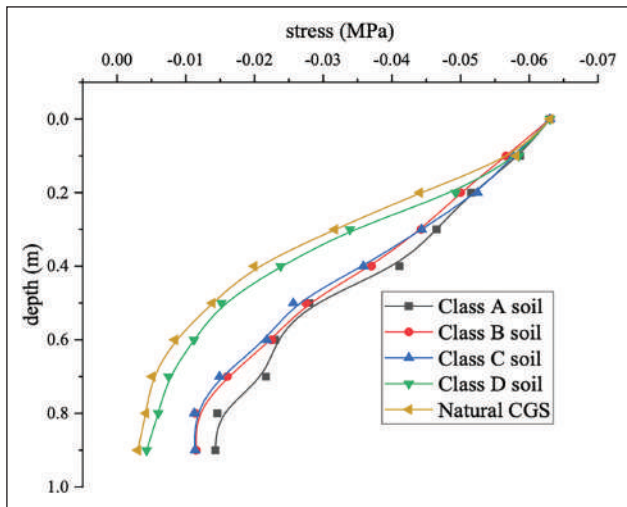


Figure 9. Vertical dynamic stress attenuation curves under different soil gradations.

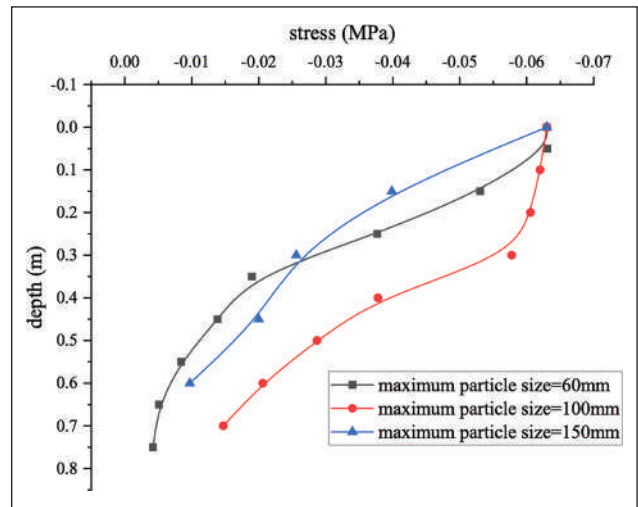


Figure 11. Dynamic stress attenuation curves with different maximum particle sizes.

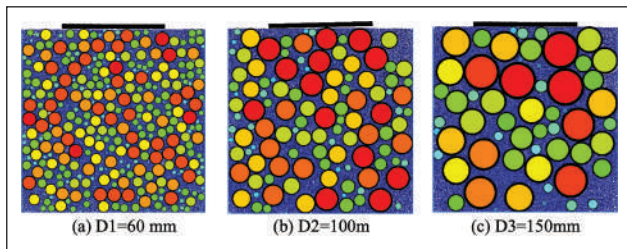


Figure 10. Models with different maximum particle size.

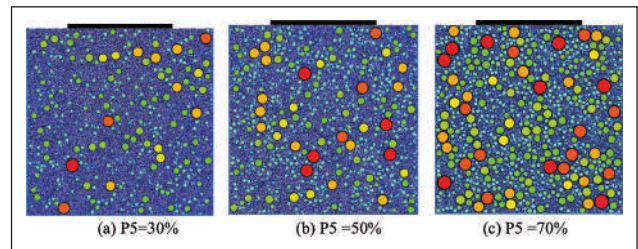


Figure 12. DEM models with different stone contents.

recommended to be less than 50 cm, which can match the influence depth of modified PFWD for quick compactness inspection.

3.2.2. Effect of the Maximum Particle Size

Taking the maximum particle size as a variable and considering the requirement of the maximum particle size of subgrade fillers for highway subgrade construction [24], set the two more maximum particle size variables of 100 mm and 150 mm to study the change of subgrade dynamic stress. The fillers to be simulated include two groups of particle size ranges and three gradations of soil samples with different maximum particle sizes, (2–5) mm+(5–60) mm, (2–5) mm+(5–100) mm, and (2–5) mm+(5–150) mm. The numerical simulation randomly generated related particles in two groups of gradations, and the generated model is shown in Figure 10. The calculation results show the curve of vertical dynamic stress changing with depth in Figure 11. The results show that the maximum particle size of filler affects stress transmission and attenuation. However, with the increase in the maximum particle size of soil particles, the relationship between the stress attenuation and the maximum particle size is not apparent. Overall, the influence depth of vertical stress is above 48 cm under three maximum particle sizes.

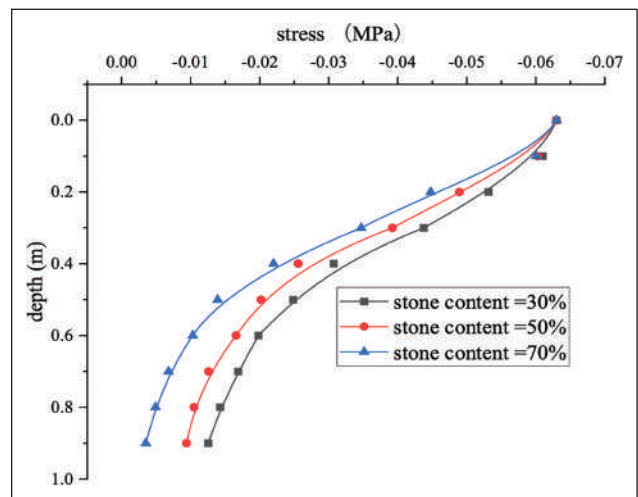


Figure 13. Stress attenuation with different stone contents.

3.2.3. Effect of Stone Content on Dynamic Stress Attenuation

In previous studies, they often took the particle size of 5 mm as the limit, and the particle size above 5 mm was defined as stone components, while the particle size below 5 mm as soil components. Therefore, P5 is a short expression for the stone content of the subgrade filler. With the

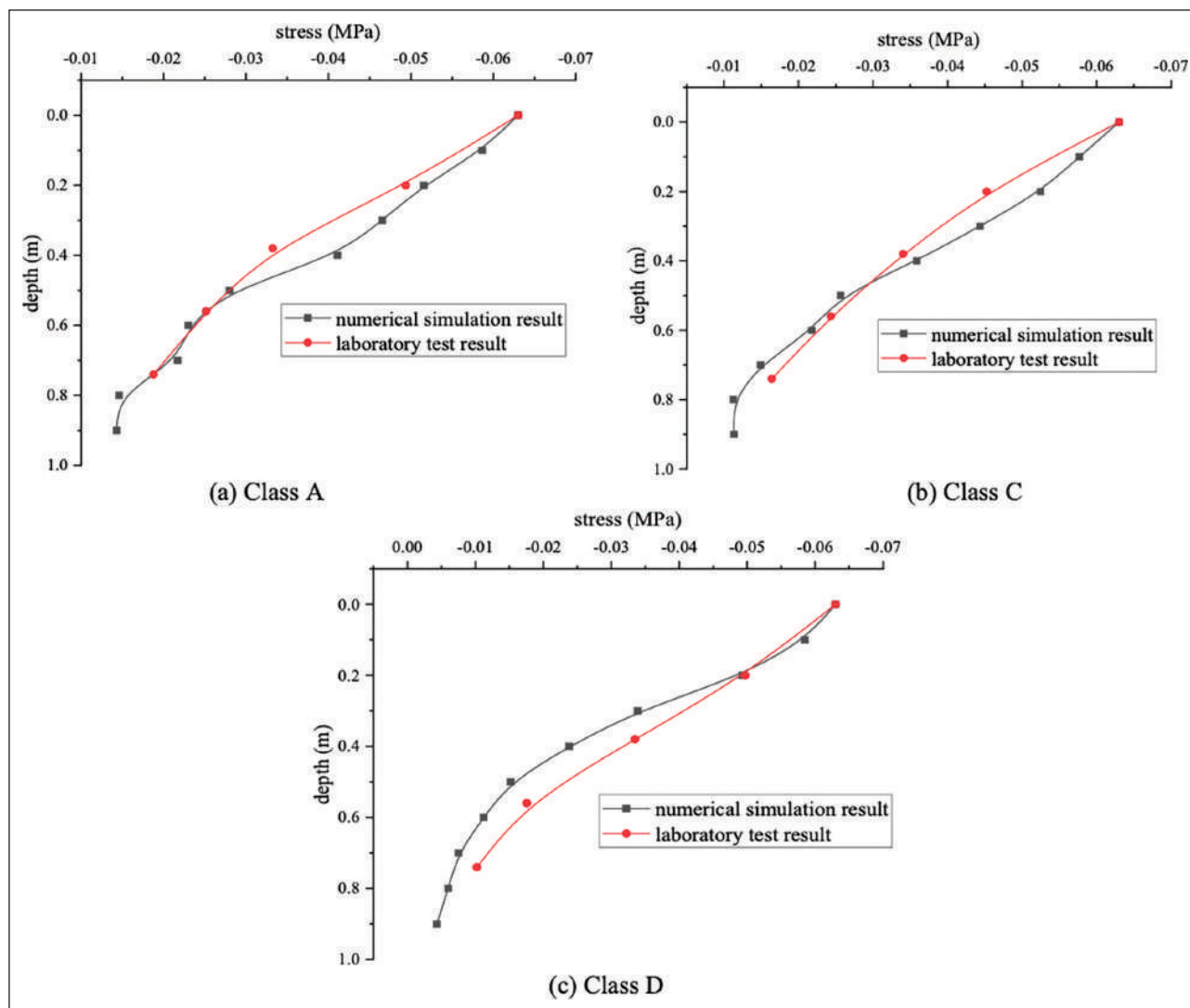


Figure 14. Comparison of results between laboratory tests and numerical simulations.

increase of P5, the structure of CGS is gradually changed from a dense-suspended structure ($P5 < 30\%$) to a skeleton-dense structure ($30\% < P5 < 70\%$), and finally to a skeleton-void structure ($P5 > 70\%$) [25]. Taking P5 as the limit stone content of 30% and 70%, it generally showed that the CGS filler could not show the best mechanical properties when P5 is less than 30% or more than 70%. When the P5 is between them, its mechanical properties gradually increase with P5 increasing, and when the P5 is about 70%, the filler can achieve the best compaction characteristics in an excellent dense structure [26]. Based on this, this paper intends to take the limit stone content as the research variable, change the stone content in the PFC model, and analyze the change of subgrade dynamic stress under this condition. The simulated packing includes two particle size ranges, namely (2–5) mm+(5–60) mm. PFC program randomly generates related particles within the particle size range in two groups, and the generated model is shown in Figure 12.

The calculation results show the variation curve of vertical dynamic stress with the subgrade depth in Figure 13. The results show that P5 significantly influences the vertical dynamic stress attenuation. Accordingly, with the increase of P5, the overall trend of the transfer of dynamic stress in soil mass is that the stress attenuation accelerates with the increase of depth. Then the attenuation rate is sharp down, showing an exponential attenuation. Meanwhile, the rate of stress attenuation also increases with the increase of the P5. The minimum influence depth of dynamic stress is about 54 cm for the CGS filler with $P5=70\%$, which means the attenuation effect is best.

3.3. Comparison between Laboratory tests and Numerical Analysis

According to the above laboratory tests, select the fillers with the same properties as the Class A, C, and D soils mentioned above for the impact dynamic stress loading test. Then,

compare the numerical simulation results to verify the accuracy of the numerical simulation data. The corresponding vertical dynamic stress variation data is shown in Figure 14.

The test data shows that the numerical simulation results under the same conditions fit the scale model test results well. The vertical dynamic stress attenuates with the increase of depth. Therefore, using PFC to simulate the attenuation law and the influence depth of dynamic stress for CGS fillers is reasonable. However, according to the data curve, there is still a particular deviation between the data simulation and the model test. The possible reason for this difference is that particle gradation dramatically affects dynamic stress distribution. When generating the particles numerically, the simulation and the calculation efficiency must take into account, and the fine particles in the actual gradation are replaced, resulting in errors between the calculated gradation and the actual gradation, thus making the attenuation law of actual dynamic stress deviation.

4. CONCLUSIONS

- (1) Particle gradation of coarse-grained soil (CGS) filler affects vertical dynamic stress attenuation of compacted subgrade. Under the same conditions, the better the filler gradation, the denser the filler, the higher its overall strength, the faster the vertical dynamic stress attenuation, and the more uniform the stress transfers will be. The minimum depth of dynamic stress under different gradations is about 50 cm.
- (2) The maximum particle size of CGS filler affects the vertical dynamic stress transfer of the compacted subgrade. However, with the increase of the maximum particle size, the relationship between the vertical stress attenuation and the effect of the maximum particle size is insignificant. The influence depth of dynamic stress under the three maximum particle sizes is above 48 cm.
- (3) The stone content (P5) of CGS filler significantly influences the dynamic stress attenuation of the compacted subgrade. In a specific range, with the increase of P5, the denser the soil structure, the faster the attenuation of vertical dynamic stress will be. The minimum influence depth of dynamic stress under three conditions of the P5 ranges is about 54 cm.
- (4) The recommended thickness of a single compaction layer for CGS fillers is 50 cm when modified PFWD to inspect the compactness status rapidly. In this depth, it is reliable to build the relationship between the dynamic, resilient modulus from the modified PFWD and compactness degree from the conventional test method during subgrade fillers construction.
- (5) The attenuation influenced by the comprehensive interaction of particle gradations, morphology, and crushing status needs further research. This research majorly focused on the gradation of CGS particles. However, the particles have random irregular shapes, and there is an

“interlock” force besides friction between the particles. Besides, their size and shape affect the contact stress between particles. When the stress is significant, the particles will be crushed by extrusion, which will inevitably affect the attenuation of actual dynamic stress.

ACKNOWLEDGEMENTS

The Transport Science and Technology Progress Program of Anhui Province (2018-029) and the Research Programs of Anhui Communications Holding Group (JKKJ-2018-13 and JKKJ-2021-15) jointly supported this research. The authors especially appreciated Ting Hu, Yun Dang, and Xiao Wang for their patient checking.

DATA AVAILABILITY STATEMENT

The authors confirm that the data that supports the findings of this study are available within the article. Raw data that support the finding of this study are available from the corresponding author, upon reasonable request.

CONFLICT OF INTEREST

The authors declare that they have no conflict of interest.

PEER-REVIEW

Externally peer-reviewed.

REFERENCES

- [1] Feng, Z. & Zhang, Y. (2004). Compaction test of coarse-grained soil subgrade. *Journal of Chang'an University (Natural Science Edition)*, 24(3), 9–12.
- [2] Bagherzadeh-Khalkhali, A. & Mirghasemi, A. A. (2009). Numerical and experimental direct shear tests for coarse-grained soils. *Particuology*, 7, 83–91. [\[CrossRef\]](#)
- [3] Huang, S., Wang, S., Xu, C., Shi, Y. & Ye, F. (2019). Effect of grain gradation on the permeability characteristics of coarse-grained soil conditioned with foam for EPB shield tunneling. *KSCE Journal of Civil Engineering*, 23(11), 4662–4674. [\[CrossRef\]](#)
- [4] Wu, E. L., Zhu, J.G., Chen, G., Bao, M. D. & Guo, W. L. (2020a). Gradation Equation of Coarse-Grained Soil and its Applicability. *Journal of Central South University*, 27, 911–919. [\[CrossRef\]](#)
- [5] Wu, E., Zhu, J., Guo, W. & Zhang, Z. (2020b). Effect of Gradation on the compactability of coarse-grained soils. *KSCE Journal of Civil Engineering*, 24(2), 356–364. [\[CrossRef\]](#)
- [6] Zhu, J. G., Guo, W. L., Wen, Y. F., Yin, J. H. & Zhou, C. (2018). New gradation equation and applicability for particle-size distributions of various soils. *International Journal of Geomechanics*, 18(2), Article 04017155. [\[CrossRef\]](#)
- [7] Ling, H., Fu, H. & Han, H. Q. (2017). Experimental Study on Effects of Gradation on Strength and Deformation of Coarse-Grained Soil. *Chinese Journal*

- of *Geotechnical Engineering*, 39(Supp 1), 12–16.
- [8] Jiang, M., Zhu, J. & He, S. (2019). Experimental study on influence of initial relative density on K0 of coarse grained soil. *Advanced Engineering Sciences*, 51(4), 69–74.
- [9] Kouakou, N. M., Cuisinier, O. & Masrouri, F. (2020). Estimation of the Shear Strength of Coarse-Grained Soils with Fine Particles. *Transportation Geotechnics*, 25(100407), 1–10. [CrossRef]
- [10] Meng, F., Zhang, J. S., Chen, X. B. & Wang, Q. Y. (2014). Deformation Characteristics of Coarse-Grained Soil with Various Gradations. *Journal of Central South University*, 21, 2469–2476. [CrossRef]
- [11] Liu, M., Luo, Q., Guo, J. & Lian, J. (2017). Experiment on seepage deformation of the transitional coarse-grained soil and criterion of failure type. *Chinese Journal of Rock Mechanics and Engineering*, 36(12), 3102–3110.
- [12] Shahien, M. M. & Farouk, A. (2013). Estimation of deformation modulus of gravelly soils using dynamic cone penetration tests. *Ain Shams Engineering Journal*, 4, 633–640. [CrossRef]
- [13] Meng, F., Zhang, J., Chen, X., & Wang, Q. (2014) Deformation characteristics of coarse-grained soil with various gradations. *Journal of Central South University*, 21, 2469–2476. [CrossRef]
- [14] El-Raof, H. S. A., El-Hakim, R. T. A., El-Badawy, S. M., & Afify, H. A. (2018) Simplified closed-form procedure for network-level determination of pavement layer moduli from falling weight deflectometer data. *Journal of Transportation Engineering*, 144(4), Article 04018052. [CrossRef]
- [15] George, V., & Kumar, A. (2017). Effect of soil parameters on modulus of resilience based on portable falling weight deflectometer tests on lateritic subgrade soils. *International Journal of Geotechnical Engineering*, 14, 55–61. [CrossRef]
- [16] Elbagalati, O., Elseifi, M., Gaspard, K. & Zhang, Z. (2018). Development of the pavement structural health index based on falling weight deflectometer testing. *International Journal of Pavement Engineering*, 19(1), 1–8. [CrossRef]
- [17] Li, C., Ashlock, J. C., Lin, S. & Vennapusa, P. K. R. (2018). In situ modulus reduction characteristics of stabilized pavement foundations by multichannel analysis of surface waves and falling weight deflectometer tests. *Construction and Building Materials*, 188, 809–819. [CrossRef]
- [18] Fu, G., Zhao, Y., Zhou, C., & Liu, W. (2020). Determination of effective frequency range excited by falling weight deflectometer loading history for asphalt pavement. *Construction and Building Materials*, 235(117792), 1–9. [CrossRef]
- [19] Dong, C., Yue, Z., Li, Z. & Leng, W. (2012). Design of subgrade resilient modulus based on coordinate deformation of subgrade and pavement. *Journal of Highway and Transportation Research and Development*, 29(1), 38–42/69.
- [20] Kotrocz, K., Mouazen, A. M., & Kerényi, G. (2016). Numerical simulation of soil–cone penetrometer interaction using discrete element method. *Computers and Electronics in Agriculture*, 125, 63–73. [CrossRef]
- [21] ASTM. (1996). D4965-96 General Pavements Deflection Measurements. ASTM International.
- [22] Zhang, G., Zhou, J. & Yao, Z. (2007) Study on mesomechanical simulation of piping with model test and PFC2D. *Hydrogeology Engineering Geology*, 34(6), 83–86.
- [23] ASTM (1993). D4602-93 Nondestructive Testing of Pavements Using Cyclic-Loading Dynamic Deflection Equipment. ASTM International.
- [24] ASTM (1990). D422-63 Particle-Size Analysis of Soils. ASTM International.
- [25] Qin, Y. (2013). Laboratory full-scale experimental study on construction technology of soil-rock mixed filling subgrade. *Journal of China & Foreign Highway*, 33(3), 39–43.
- [26] Dong, Y. & Chai, H. (2006). Study on engineering classification of soil-rock mixture. *Subgrade Engineering*, (3), 38–41.



Research Article

Assessment of the adoption of 3D printing technology for construction delivery: A case study of Lagos State, Nigeria

Akintayo OPAWOLE¹, Betty Oluwafunso OLOJEDE², Kahilu KAJİMO-SHAKANTU¹

¹Department of Quantity Surveying & Construction Management, Faculty of Natural & Agricultural Science, University of the Free State, Bloemfontein, South Africa

²Department of Quantity Surveying, Faculty of Environmental Design & Management, Obafemi Awolowo University, Ile-Ife, Nigeria

ARTICLE INFO

Article history

Received: 21 June 2022

Accepted: 30 July 2022

Key words:

Construction automation, construction firms, technology, innovation, 3D printing

ABSTRACT

The innovative solutions offered by integrating 3D printing technology in construction over the conventional practices have established its globally rising adoption in the construction industry. This study assessed the awareness, application, drivers, and barriers to adopting enhanced 3D printing technology for construction to enhance faster and more sustainable construction processes. The study adopted a quantitative descriptive analysis which was based on primary data. The primary data were obtained using structured questionnaires self-administered to construction firms/contractors in Lagos State, Nigeria. Data collected were analyzed using descriptive and inferential statistics. The study established that the awareness and application levels of the technology are still deficient, as the vast majority (80.8%) of the firms who had an awareness of the technology in the study area acquired it through personal research and professional dialogue, rather than through the practical application of the technology. This finding showed that 3DP technology is a new construction option in the study area. The findings showed statistically significant differences among the drivers ($0.039 \leq p \leq 0.017$) for the adoption of 3D printing technology, which is influenced by the client's demand and desire. The study further established that inadequate power source is a significant limiting factor to adopting 3D printing in the study area. Implications are indicated by the findings on the technology drivers and barriers that could help the construction industry in developing countries towards capability improvement for better adoption of 3D printing innovation and enhanced sustainable construction process.

Cite this article as: Opawole, A., Olojede, B. O. & Kajimo-Shakantu, K. (2022). Assessment of the adoption of 3D printing technology for construction delivery: A case study of Lagos State, Nigeria. *J Sustain Const Mater Technol*, 7(3), 184–197.

*Corresponding author.

*E-mail address: tayoappmail@gmail.com



1. INTRODUCTION

The technological revolution in building construction dates to the 19th century, when semi-automated equipment was introduced to allay the rigor of construction activities, enhance easier and faster construction tasks and improve environmental sustainability [1, 2]. For instance, hydraulic excavators and bulldozers were introduced to replace the cable-operated shovels for earthworks, while the conveyors and pumps replaced cranes for concrete placement. This optimized concrete works from 12 m³/hour to 50 m³/hour speed of placing fresh concrete. Studies have established the enhanced performance and efficiency of building automated technologies for complex structures over conventional construction [3, 4].

The current trend of the fourth industrial revolution (Industry 4.0) launched a variety of innovative technologies to improve product quality and increase industry performance through the digitization of complex industrial tasks, viz—3D printing (3DP) technology, robotic arms, drones, etc. [5]. The invention of 3DP for building construction is a dynamic technological panacea for some uncontrollable changes induced by the conventional procurement process that cause cost over-run, time over-run, etc. Unabated innovative studies by 3DP proponents and advocates have therefore been persuasive towards adapting 3DP technology to the construction industry to improve, complement, and eventually replace conventional building construction methods [6, 7]. However, the full potentials of the technology are yet to be explored through its high practical applications in the construction industry like the automotive and manufacturing industry [1, 5].

3DP was established to solve the growing housing demands from rapid urbanization in developed and developing countries, where conventional construction methods err to meet the rising demands [8–10]. For example, the rising application of the technology in China and the Netherlands is practically indicative of having met these countries' housing demands [5, 7, 9]. Technologically developing countries, especially Nigeria, are yet to experience the prominent implementation of 3DP technology for construction activities like the developed countries [1]. Whereas 3DP technology has the innovative potential to solve the housing deficit in Nigeria, this is put at 18 million units and 24.4 million units between the low-income earners and the homeless, respectively [11]. Nigeria creates a high market potential for 3DP technology in its construction industry to enhance housing provision while deriving benefits of faster construction, reduced material use and cost, improved safety on site, labor requirement savings, and durable and sustainable construction [7, 12, 13].

Empirical evidence on 3D printing of building construction in Africa is generally scanty. This study, therefore, investigated the awareness level of 3DP in Nigeria; examined the drivers and barriers to its adoption; and the level of its use for construction in the country. This is to inform

policy development and implementation for the application of 3DP in the Nigerian construction industry to boost housing provisions and enhance the country's economy.

2. LITERATURE REVIEW

2.1. 3DP Technology in Construction and its Awareness

Innovative solutions to enhancing the performance of construction concerning cost, time, and the environment by implementing 3D printing have gained popularity in the construction industry in recent decades [7, 14]. 3DP is also known as additive manufacturing (AM) by its layer-upon-layer process of fabricating 3D solid objects. 3DP technology produces objects from a digital 3D CAD model by slicing the model into a series of 2D building layers before printing. The processed sliced 2D building layers (a set of 2D contour lines) generate control commands to position the printing head for printing by depositing materials using nozzle and print head/laser beams [15].

The United States of America, Russia, China, Germany, and the Netherlands have used 3DP in construction industries for buildings and bridges with satisfactory results [16]. It is believed that 3DP addresses the problem of low labor productivity and labor shortage in the USA, UAE, Qatar, and Singapore, where migrant workers account for about 90% of the construction workforce [1]. The potential opportunities and benefits of 3DP have influenced future construction plans, policies, and countries' targets in the global construction markets. For instance, Dubai planned 25% of its construction targets to be 3D printed by 2030. The 3D construction printing (3DCP) market forecast is expected to reach USD 314 million from USD 130 million between 2017 and 2023. Over 7000 construction robots are forecast to be deployed between 2018–2025 [1, 17].

The level of awareness of 3DP technology in developing countries is low, particularly in Africa [18]. South Africa, which has embraced additive manufacturing with up to 450 AM machines installed in the industry, has relatively limited use of the 3D printer for building construction. Lack of awareness of the benefits and understanding of the technical know-how of 3DP by professionals in the construction industry were proven as barriers to adopting the technology for housing delivery in South Africa [19]. Farabiye & Abioye [18] revealed that the awareness of automation techniques in the Nigerian construction industry is limited to CAD, crane, and BIM. This implied that the awareness level of 3DP is low in the country.

2.1.1. 3D Printing Software

The design of the 3D CAD model is generated by open source packages like the Autodesk Inventor and Blender [20, 21]. Other software packages include SolidWorks, Google SketchUp, and Autodesk Revit (the construction industry BIM software) [5]. The model is exported to an STL

Table 1. 3D printing techniques

3D printing techniques	Machine	Production process	Material	Structure	Source
Contour crafting (printing dimension is mega-scale)	Gantry system, (with gantry-driven nozzle); i.e 150mx10mx6.6m gigantic 3D printer (by WinSun); RepRap 3D print	Extrusion process: Cementitious concreting layer by layer (no formwork) Filling process	Cementitious material: Cement and sand	Concrete buildings, houses	[30, 32]
D-shape/Binder jetting (printing dimension is limited by frame)	D-shape 3D printer (2007, Italy)) 6mx6mx6m printing dimension	Binder jetting Powder-based/selective binding	Powder bases; selective binder; sand	Architectural artifacts (for example, 1.6m freeform sculpture); a whole house; landscape house design	[7, 30, 32]
	Robotic 3D printer (2012, Spain)			Architectural structures	[30]
Concrete printing (printing dimension is limited by frame)	Concrete 3D printer, i.e., four-axis gantry robot with a print bed of 9.0mx4.5mx3m	Extrusion & deposition (no formwork)	High-performance concrete; cement mixture		[30, 32]

(Stereolithography) format to interpret and decompose the model into building layers or slices [15]. The slices are sets of 2D contour lines that generate control commands to activate the printing processes by the printer. The production/fabrication of 3D structures is in layers. This technology requires little or no external human (skilled or unskilled) assistance, unlike the labor-intensive requirements in conventional construction, except for the computerized building design experts, digitally savvy, and machine operators [1, 22]. The 3D CAD models of different structures have been successfully printed into physical edifices by some companies, institutes, and universities. Some of them are Winsun company (China), 3D Printhuset (Denmark), CyBe (Netherlands), ApisCor (Russia), COBOD (Germany), and Tsinghua University School of Architecture (China) [23, 24].

2.1.2. Techniques of 3DP in Construction

The evolution of 3DP technology in construction has applied two main techniques for large-scale 3D concrete printing: binder jetting and material deposition method (MDM). The basic principle of the techniques is to build up complex structures layers upon layers [7]. Binder jetting creates 3D objects in a repeated cycle by depositing binder in droplets on a thin layer of powder material over a powder bed in a build tray [25]. This is called powder bed-based printing. The technique eliminates waste generation because unbound raw materials in the build tray are removed with a vacuum cleaner and used to support subsequent layers [26]. There is a minimal distance between layers with a relatively high resolution which gives a good surface finish [27]. The principle of binder jetting is commonly employed in D-shape 3DP process.

The MDM is similar to fused deposition modeling (FDM, used in the manufacturing industry), which prints 3D objects in successive layers of extruded materials in line with the CAD model [28]. It is commonly adopted in contour crafting (CC), concrete printing, stick dispensers, digital construction platforms, flow-based fabrication, mini-builder, and mesh-mould [7].

D-shape, contour crafting/concrete crafting, and concrete printing are the prominent 3DP technologies in construction [29, 30]. The disparities between these three technologies are shown by the limits of the scale of their printing dimensions (large or small scale printing ability), the configuration of their printer design, the printing process, and their printing materials (Table 1). D-shape is a 3DP technology that binds sand with a selective binder like magnesium (inorganic binding agent) to make the stone-like 3D structure. The D-shape printer has a set of spreading nozzles (hundreds of spraying nozzles) equipped with its print head, which deposits liquid binder on powdery sand at desired thickness layer upon layer in a repeated manner to form the digital prototypes. D-shape effectively prints large-scale structures [27, 31].

The CC operates on a computer-controlled gantry system that supports a concrete nozzle's movements with an attached trowel [28]. The installed trowel(s) enables the CC to create very smooth and accurate free-forms and planar surfaces at a higher build speed using a wide range of selective printing materials [30]. The CC technology combines extrusion and filling processes to print large-scale/industrial scale structures without the use of formwork. The process of CC can create openings and voids while printing for the insertion of reinforcement, installation of electrical fittings, and mechanical fittings using a robotic arm [32].

Table 2. Some existing 3D printing projects

3D projects	Project description	Year	Location	Method/Material	Source
Concrete Bridge	86ft long bridge	2019	Shanghai	Concrete printing	[5]
YHNOVA™	95m ² house	2017	France	Concrete printing	[30]
Landscape House	1100m ² landscape house based on a Mobius strip	2017		Concrete paste, bio-plastic (80% vegetable oil)	
Gemert bicycle bridge	8m x 3.5m bridge	2017	Gemert, Netherlands	Concrete printing	[14]
Winsun offices	Office	2016	Dubai	Cement, sand, reinforcing glass fiber, proprietary additive mix, 150x10x6.6m machine	[14]
Castilla-La Mancha 3D bridge	12m x 1.75m pedestrian bridge	2016	Madrid, Spain	Concrete printing: fused concrete, polypropylene reinforcement	[14]
Urban temple project	1.6m freeform sculpture	2008	Pisa, Italy	Sand/mineral dust; inorganic binder,	[30]
Winsun houses	1,100m ² two-story house	2013	China	Concrete printing	[14]
	200m ² houses (10 nr)	2014	Shanghai, China	High-grade cement and glass fiber	[30]
	1100m ² five-story apartment	2015	China	Cement combinations, glass fiber, construction waste	[30]
3D print canal house	6m hose	2014	Amsterdam, Netherlands	Polymer printing: 2.2x2.2x3.5m polypropylene blocks	[14]
The MX3D bridge	10m x 2.5 metal bridge		Amsterdam, Netherlands	Metallic printing: Wire and Arc AM; directed energy deposition (DED); 6-axis robotic welding arm	[14]

Concrete printing, on the other hand, prints large-scale 3D structures by combining the principles of extrusion and deposition. It is similar to CC because its print head is mounted on a crane but operates without a trowel [28, 30, 32]. Therefore, the printed works do not have a very smooth surface like those printed by CC because the use of a trowel in the printing technique is absent.

The innovative D-shape, CC, and concrete printing technologies have been explored on-site and off-site to build concrete, metallic, and plastic structures ranging from houses to offices to bridges and connection nodes [14] (Table 2). The components of building work printed off-site are often transported to the site and assembled to form the designed shapes. For example, the Winsun office in Dubai was printed in China and shipped to Dubai for assemblage with estimated reductions in construction cost by 80%, labor costs by 60%, and waste management costs by 60%; when compared to the conventional office building construction [23].

The patronage of the 3DP technologies in the global construction market is recorded to be low. This is despite the attempts by extensive research activities to increase customizations at reduced construction time and improved affordability, as other benefits and opportunities of the technologies are considered [28, 29]. Perkins and Skitmore [25] attributed the low and slow paradigm shift to the adoption of innovative technology in the construction industry to the fear of outright replacement of conventional construction methods by the disruptive nature of 3DP. The disruptive nature of 3DP describes the propensity of

the technology to replace a broad range of activities performed by skilled, semi-skilled, and unskilled labor in the construction industry, thereby causing human resources downsizing, increased unemployment rate, and a cut in the Gross Domestic Product (GDP) of a country.

2.1.3. Printable 3D Printing Materials

The printable 3DP materials in construction are cementitious, polymer, and metallic, but cementitious materials are the most commonly used [5, 14]. Research interests in addressing the compatibility of cementitious materials for a large-scale 3D printer in industrial-scale construction have generated the consideration of different components of concrete-related material in experimental studies [33]. Ascertaining the right constituents and mix ratio of the viscous cementitious materials, which are easy to extrude, workable within proper setting time/open time, and the challenges of material buildability have been the research focus for 3D printable materials [5, 30]. Since the conventionally placed load-bearing walls are reinforced concretes, the exploratory research efforts on printable reinforcement alternatives for the 3D print concrete wall without compromising on sufficient strength (pa) of concrete are on the increase [30].

Selective printable materials for 3DP in construction have addressed material and labor resource scarcity [14]. The 3D print walls of self-compacting concrete have self-supporting strength to hold individual layers in place from subsequent depositions without deformation [1]. This reveals the effectiveness of the 3DP materials for construction purposes and dismisses the skepticisms on the

production of large-scale construction structures in recent past years, by the innovations of printable cementitious (cement-based) materials and industrial scale printers that have printed up to and over 1,100 m² building structures of houses and offices in China and Dubai [14, 22].

The printable 3DP cementitious materials that were applied for exploratory construction included rapid-hardening Portland cement (RHPC) used in the binder jetting 3DP system, calcium aluminate types of cement (CAC), slag-based geopolymers (comprising slag, fine sand, and silicate-based activator), plaster and clay-like materials, and reactive powder concrete (RPC) mixture (comprising high-efficiency superplasticizer, fly ash, silica fume, quartz powder, cement, and fine sand) [34–36]. These are self-compacting concrete compositions considered applicable for 3DP of large-scale construction. Fiber-reinforced concrete using steel fibers constitution, rather than manually placed reinforcement, has shown its printability strength of high flexural strength research works by [5] and [37].

In general, 3DP materials are in three forms viz. liquid (i.e., thermoformable epoxy, photopolymer, photocurable acrylic resin), powders (i.e., plastic, metal, ceramic), and solid (metal alloy, thermoplastic, rubber) [38]. These materials include ceramics, composites, chemicals, concrete, metallic materials (i.e., aluminum, gold, alloys, magnesium), sand, river sand, limestone, sandstones, wax, silicone, resin, wood, plastics, water, paper, and foodstuff [14, 39].

2.2. Drivers of 3DP Technology in Construction

A quest to overcome the challenges of time cost overrun and declining labor productivity in building construction has compelled construction companies to consistently seek resolvable construction methods [5]. Bricklaying automation, intelligent, dynamic casting, and robot-winding have been explored to address those challenges and innovatively complement the conventional construction of some building components [7, 40, 41]. Several other technologies have been invented with the advent of Industry 4.0, which have boosted the performance of the automotive and manufacturing industry. The 3DP is one of the latest technologies of Industry 4.0 [7], with increased attention to construction automation [1]. Tay et al. [7] opined that the numerous benefits of 3DP, which meet the targeted demands in building and construction, are the drivers for its adoption for construction.

El-Sayegh et al. [5] reviewed 3DP in construction and categorized the benefits of 3DP into two groups: constructability and sustainability. The constructability benefits are lower construction cost, faster construction, more geometry freedom, shorter supply chain, and better productivity. It is established that the speed of construction is faster with 3DP than the traditional method by 42%, enabling clients to generate revenue early and release resources for subsequent projects [42]. Thus, the use of the technology of 3DP is stressed as a new way of satisfying client's needs

in the construction market [35]. Hager et al. [15] emphasized the possible realization of architectural geometry in construction irrespective of its geometric complexity as a driver for the adoption of 3DP.

The sustainability benefits of 3DP are reduced formwork, less construction waste generation, safer sites, eco-friendly structure, and social good. Printing concrete by the 3D printer is done without the need for formwork, eliminating 40% of the total cost associated with concrete work [43]. 3DP creates mass production of customized construction products at a reduced cost, minimal material waste through recycling and reuse of unused materials, increased design flexibility, and less human intervention in building construction [7, 14, 23]. The reduced human intervention improves safety on construction sites through reduced construction-related falls, injuries, and fatalities [25]. It has also been established that 3DP reduces CO₂ emission through its innovative technology in construction [7]. Therefore, 3DP offers much-needed innovative solutions for performance improvement in construction toward solving sustainability problems in the global society [15].

Buchanan & Gardner [14] revealed the opportunities inherent in 3DP from a review of the methods of metal 3DP in construction. The opportunities of 3DP are geometric flexibility and optimization of material properties; customization of building elements; reduced construction time; hybridization and structural strengthening of damaged or corroded elements to update the structural design of elements; environmental advantages of reduction in consumption of total energy, raw materials, and portable water; reduction in labor cost (15–50% of total construction project cost), elimination of risk of human error from the compulsion to work in adverse weather conditions and at night. These opportunities were founded as the drivers for adopting 3DP in building construction.

Kotchman & Faber [43] underscored the high rate of advancement in technology coupled with the need to realize a better eco-performing society as the driver for 3DP adoption in construction. The study further explained the benefit of 3DP in shortening the construction supply chain by merging the roles of consumers/client and producer/contractor to prosumers through integrating different steps and functions in construction into a digitized production chain. This creates the direct fabrication of building components using digital design and a 3D printer by the prosumer. Integrating roles implies a shorter supply chain, less professional and unskilled labor requirements, less complicated design, and virtual design change evaluation through CAD and direct printing simulation techniques. These benefits give a hedge against resource scarcity in the construction industry.

2.3. Barriers to 3DP Technology in Construction

Despite the numerous benefits of 3DP in construction, several challenging limitations have inhibited and discouraged its wide acceptance and high utilization in the global

construction market. Wu et al. [29] identified the barriers to the broader acceptance and adoption of 3DP as low technological readiness, weak organizational support, and lacking policy and regulatory standards. The technological readiness of 3DP in construction is low because of the very high initial cost of incurring the 3DP printer, its running and maintenance costs, and unascertained compatibility standards for the right mix design of 3DP materials.

Hayes [44] stressed that skepticisms and cynicism about the potential of 3DP by top managements of construction companies and limited availability of resources discourage their commitments to adopting the technology. On the other hand, the fear of job insecurity by low-skilled labor, whose tasks are replaced by printers, and the need for up-skilling labor with equipment and software technical know-how are challenged to 3DP adoption [1]. Arora et al. [45] opined that the lack of developed policy standards on building codes and regulations that address 3DP materials and processes facilitated the unwillingness of stakeholders to change from the conventional method of construction to the new technology. Lacking regulatory controls on contracts, especially the legal backing, for the party(ies) that is/are liable for the defects of the 3D printed building components and structures also limits the broader acceptability and application of 3DP in the construction industry.

El-Sayegh et al. [5] asserted that clients' expectations are yet to be achieved by applying 3DP technology, owing to the rigid design requirements of 3D printers and materials limitations, and some other limiting factors. The factors are related to 3D printers, software, architecture and design, construction management, regulations and liability, and stakeholders' issues. According to Zhang et al. [46], the fixed scale design of a 3D printer limits the printing of construction works with sizes that range outside the scale of the printer's design. This implies that printing of building plans with sizes (floor surface area) more significant than that of the printer's scale and printing of the height of building plans that are higher than the range of reach of the robotic arm of the printer are not feasible. The opponents of 3DP hold this limitation of printing scale as the main reason for the unsuitability of 3DP for automated construction of large-scale production [5]. The printer's capacity to print only straight edge corners is also a limitation to the benefit of freedom of geometric architecture for 3DP.

Another critical barrier to the adoption of 3DP in the construction industry is the uncontrolled nature of the construction site, which does not support a controlled environment needed for the printing process of a 3DP printer on-site. In addition, the inherent risk of transportation of equipment on-site, equipment set up, site equipment, and adaptability of software applications for different geometric designs are identified barriers to the adoption of 3DP in building construction. The programmed system of the continuous printing process of 3DP printers for construction is

averred as incompatible with the conventional scheduling of construction activities, which makes the adaptability of 3DP in construction a challenge [47].

3. RESEARCH METHODOLOGY

The study examined the level of awareness of 3DP technology, the level of use, and the drivers and barriers to the adoption of the technology in construction among professionals in small-sized and medium-sized construction firms (the SMEs) in Lagos State, Nigeria. Large-sized construction firms were excluded because the present capacity of 3D printers is yet beyond large-scale mass customization and production of building and construction works [25]. The target population was construction firms registered with the Nigerian Institute of Builders (NIOB) in Lagos State. Lagos State is Nigeria's hub of active construction activities [48].

The study employed a quantitative research methodology using a well-structured questionnaire to obtain information from a sample of respondents to generalize findings for a population [49]. The similar questions in the questionnaire design for the survey facilitated the researchers to compare the data obtained from different professionals in the study area.

Statistics from the Nigerian Institute of Building site showed that a total of 103 construction firms were registered and certified to practice building construction by the Institute in Lagos State. Only 39% of the registered firms that were financially active members of the Institute were considered for the survey exercise during this study. Trochim [50] indicated that a percentage range from 10–30% is deemed adequate for a survey on a small population, while a 5% representation for a large population is deemed adequate. The 39% representation of the construction firms built up to 40 registered construction firms in the study area, constituting the study's sample size.

The target respondents were registered professionals at the top management level and project and senior managers. The professionals were architects, builders, engineers, and quantity surveyors. At least one of these professionals was sampled to represent the general position of each construction firm (as a contractor) on 3DP technology awareness and use. The professionals were sampled based on their availability and readiness to supply resource information on 3DP practices and the agreed choice of representation by the professionals for the firm. These steps were taken to avoid the possibility of duplicating information from a firm/contractor for the study. A total number of 35 questionnaires were retrieved from the survey exercise. This represented a total retrieval rate of 89.74%.

The questionnaire was structured by information extracted from experimental studies and reviews in the existing literature on 3DP technology to form the primary data source for this study. A structured questionnaire is an effective data

Table 3. The profile of respondents

Characteristics	Parameters	N	%
Specialization of firm	Building works (architecture design & contractor)	7	20.0
	Civil works (contractor)	3	8.6
	Building and civil works (consultants, architecture designs & contractors)	25	71.4
Size of firm	Medium	25	71.4
	Small	10	28.6
Annual revenue	₦20,000,000 - ₦30,000,000	11	31.4
	≥₦40,000,000	24	68.6
Professions	Architect	8	22.9
	Builder	11	31.4
	Engineer	10	28.6
	Quantity Surveyor	6	17.1
Year of work experience	≤ 9	9	25.7
	10-19	19	54.3
	≥20	7	20.0
3D printing awareness	Aware	26	74.3
	Unaware	9	25.7
	Direct personal experience	5	19.2
Awareness medium	Personal research	12	38.5
	Professional dialogue	13	42.3

N= Number.

collection method for measuring respondents' beliefs, attitudes, and opinions [51]. The questionnaire was designed as close-ended for easy answering by respondents and analysis by researchers as established by [52]. The construct of the 3DP technology in reviewed literature formed the basis for the questionnaire design, which was divided into two sections. Section A and section B. section A of the questionnaire comprised the profile information about the respondents. Section B of the questionnaire addressed the objectives of the study. The questionnaires were self-administered.

The data obtained were analyzed based on descriptive and inferential statistics. The descriptive statistical tools employed were frequency tables and mean score rating. Name [53] stressed that descriptive statistics are practical tools to present the characteristics of the respondents for a quick understanding of the underlying details in a data set. The inferential statistical tool adopted by the study was the Mann-Whitney u-test. The tool looked at the differences in the ranked positions of scores (for variables on the application of 3DP in construction, drivers, and barriers of 3DP) in different groups. The test makes inferences from respondents from unequal independent groups in an observed population [54]. These groups were the SMEs (medium-sized firms=25numbers; small-sized firms=10 numbers).

Using Cronbach's alpha test, a validity and reliability test were conducted on the research data. The values of Cronbach's Alpha extracted from the test were used to determine the internal consistency of variables generated from the respondents' responses on 3DP technology questions [55]. An acceptable range of reliability is established at 0.70–0.95 values of Cronbach's Alpha [56].

4. RESULTS AND DISCUSSION

4.1. The Respondents' Profile

Table 3 shows the background information about the respondents on the specialization of the firm, size of the firm, educational qualifications, and professional affiliations of respondents. Each of the captured respondents represented an individual firm. About 71.4% of the construction firms were specialized building/ civil works contractors, architects, and consultants. Up to 71.4% of the firms were medium-sized with over 40,000,000 annual revenue, while 28.6% were small-sized firms. The respondents were registered professionals with percentage representations of 31.4% (builders), 28.6% (engineers), 22.9% (architect), and 17.1% (quantity surveyors). The average work experience of the respondents was estimated at approximately 12 years, indicating that about 49% of the firms have been in the business of construction works for 12 years. Up to 74.3% of the firms had awareness about 3D printing through professional dialogue (42.3%), personal research (38.5%), and direct personal experience (19.2%). These results underscored the adequacy of the respondents' information obtained for the study.

4.2. Application of 3DP Technology for Construction

The results of the validity and reliability test on the research instrument and the analysis of data obtained from the respondents' perception of the application of 3D printing are shown in Tables 4 and 5, respectively. A Cronbach's alpha value (Table 4) greater than 0.70 implied that the scale is reliable and valid to measure the underlying con-

Table 4. Reliability statistics

Cronbach's Alpha	Cronbach's Alpha is based on standardized items	N of items
0.885	0.898	25

Table 5. Application of 3D printing technology

Variables	Medium			Small			Overall			Mann-Whitney U test		
	MS	SD	R	MS	SD	r	MS	SD	r	z-score	Sig.	R
Constructing a structure at a low price	3.400	0.577	3	4.100	0.994	1	3.600	0.774	1	-2.031	0.042	*
Creating scale mockups for building components	3.400	0.916	1	4.000	0.942	3	3.600	0.945	1	-1.517	0.129	**
Printing pedestrian bridge	3.400	0.957	3	4.000	0.942	3	3.571	0.978	3	-1.669	0.095	**
Construction midsize homes	3.400	0.500	3	4.000	0.942	3	3.571	0.698	3	-1.838	0.066	**
Creating metal surface for a solid structure	3.320	1.029	9	4.100	0.875	1	3.542	1.038	5	-2.063	0.039	*
Constructing structures in a quick manner	3.320	0.476	9	3.900	0.875	6	3.485	0.658	6	-1.978	0.048	*
Habitable concrete 3D printed house	3.360	0.637	6	3.700	0.674	8	3.457	0.657	7	-1.377	0.169	**
Construction of columns	3.440	0.583	1	3.300	0.674	13	3.400	0.603	9	-0.554	0.579	**
Complete scale building components fabrication i.e., interior wall	3.320	0.476	9	3.400	0.516	11	3.342	0.481	10	-0.444	0.657	**
Constructing partitions	3.360	0.489	6	3.300	0.823	13	3.342	0.591	10	-0.473	0.636	**
Road curbs	3.240	0.778	15	3.500	0.527	9	3.314	0.718	12	-1.000	0.317	**
Using plastic as materials for construction	3.280	0.541	12	3.400	0.843	11	3.314	0.631	12	-0.358	0.721	**
Prefabrication of full-scale building exterior wall	3.360	0.489	6	3.200	0.421	16	3.314	0.471	12	-0.908	0.364	**
In-situ 3D printing house	3.160	0.472	17	3.500	0.707	9	3.257	0.560	15	-1.410	0.159	**
Construction of slab	3.280	0.613	12	3.200	0.421	16	3.257	0.560	15	-0.516	0.606	**
Construction of beams	3.280	0.541	12	3.100	0.316	18	3.228	0.490	17	-1.067	0.286	**
Construction of foundation	3.120	0.665	19	3.300	0.483	13	3.171	0.617	18	0.651	0.515	**
Prefabrication of roof	3.120	0.832	19	3.000	0.666	21	3.085	0.781	19	-0.594	0.552	**
Prefabrication of doors	3.040	0.675	23	3.100	0.737	18	3.057	0.683	20	-0.243	0.808	**
Prefabrication of windows	3.040	0.675	23	3.100	0.737	18	3.057	0.683	20	-0.243	0.808	**
Construction of parapet	3.080	0.812	22	3.000	0.666	21	3.057	0.764	20	-0.439	0.660	**
Construction of stairs	3.160	0.687	17	2.800	0.632	23	3.057	0.683	20	-1.415	0.157	**
Construction of finished floor	3.120	0.665	19	2.600	0.699	26	2.971	0.706	24	-1.829	0.067	**
Painting	3.040	0.789	23	2.700	0.823	25	2.942	0.802	25	-1.127	0.260	**
Construction of median strip	2.960	0.789	26	2.800	0.632	23	2.914	0.742	26	-0.531	0.595	**

MS: Mean score; SD: Standard deviation; r: Rank; Sig.: Significance; R: Remark; *: Significant difference; **: No difference.

struct of its design for the analysis. In Table 5, the creation of scale mockups for building components and construction of columns ranked highest (MS=3.440, SD=0.577; MS=3.440, SD=0.583 respectively) by the respondents in the medium firm category. Construction of structure at a low price and creating a metal surface for solid structure ranked highest (MS=4.100, SD=0.994; MS=4.100, SD=0.875 respectively) by the respondents in the small-sized firm. Overall, the application of 3D printing for the construction of finished floors, painting, and construction of median strips ranked lowest with mean score values of 2.971, 2.942, and 2.914, respectively.

There were no significant differences in the ranking of the three least variables by the respondents from the two groups of the firm, $z=-1.829$, -1.127 , and -0.531 , respectively; $p=0.067$, 0.260 , and 0.595 , respectively. This implies that the differences in the revenue base of the firms' sizes may not be contributory factors to the application of 3DP technology on the least ranked variables. On the other hand, there is a significant difference in the respondents' perception of the three items' application of 3DP technology. These were construction of structure at a low price ($z=-2.031$, $p=0.042$), creating metal surface for solid structure ($z=-2.063$, $p=0.039$), and

Table 6. Reliability statistics

Cronbach's Alpha	Cronbach's Alpha is based on standardized items	N of items
0.885	0.878	28

Table 7. Driver for the adoption of 3DP technology in Nigeria

Variables	Medium			Small			Overall			Mann-Whitney U test		
	Mean	SD	r	Mean	SD	r	Mean	SD	r	z-score	Sig.	R
Reduced paper-based delivery methods	4.200	0.645	2	4.500	0.707	4	4.280	0.667	1	-1.310	0.190	**
Architecture geometry freedom	4.280	0.678	1	4.300	0.823	9	4.285	0.710	1	-0.199	0.842	**
Improved contractors and client relationships	4.080	0.571	4	4.600	0.699	2	4.228	0.645	3	-2.329	0.020	*
Enabling fast project completion	4.160	0.687	3	4.400	0.699	7	4.228	0.689	3	-0.961	0.337	**
Technological advancement	3.960	0.840	13	4.700	0.483	1	4.171	0.821	5	-2.383	0.017	*
Improved client satisfaction	4.000	0.707	10	4.600	0.699	2	4.171	0.746	5	-2.241	0.025	*
Enhances cost efficiency	4.040	0.454	7	4.400	0.516	7	4.142	0.493	7	-1.962	0.050	*
Enhance sustainability	3.960	0.675	13	4.500	0.707	4	4.114	0.718	8	-2.063	0.039	*
Increased employee productivity	4.040	0.611	7	4.300	0.823	9	4.114	0.676	8	-1.114	0.265	**
A reduced error by better coordination of work	4.040	0.351	7	4.200	0.623	11	4.085	0.445	10	-1.022	0.307	**
Speed up the construction process	4.080	0.640	4	4.100	0.567	15	4.085	0.612	10	-0.064	0.949	**
Reduction in technology and material cost	4.000	0.577	10	4.200	0.632	11	4.057	0.591	12	-0.913	0.361	**
Client desire	3.840	0.850	21	4.500	0.707	4	4.028	0.857	13	-2.088	0.037	*
Operational efficiency	3.880	0.665	19	4.200	0.788	11	3.971	0.706	14	-1.198	0.231	**
Shorter supply chain	3.920	0.493	15	4.100	0.737	15	3.971	0.568	14	-0.825	0.409	**
Improves visualization	3.920	0.702	15	4.100	0.737	15	3.971	0.706	14	-0.679	0.497	**
Improves construction skills of users	4.000	0.408	10	3.900	0.994	22	3.971	0.617	14	-0.046	0.963	**
Increases emergency response	4.080	0.640	4	3.700	1.059	25	3.971	0.785	14	-1.104	0.269	**
Value management skill	3.920	0.640	15	4.000	0.666	18	3.942	0.639	19	-0.223	0.824	**
Automation of quantities	3.880	0.665	19	4.000	0.942	18	3.914	0.742	20	-0.354	0.723	**
Companies management	3.920	0.702	15	3.900	0.994	22	3.914	0.781	20	-0.156	0.876	**
Decreased construction costs	3.760	0.597	26	4.200	0.632	11	3.885	0.631	22	-1.837	0.066	**
Change in market	3.800	0.816	23	4.000	1.333	18	3.857	0.974	23	-1.018	0.308	**
Convenience	3.800	0.763	23	3.800	1.135	24	3.800	0.867	24	0.000	1.000	**
High level of competition	3.840	0.687	21	3.700	1.337	25	3.800	0.900	24	-0.236	0.813	**
Management of carbon consumption	3.680	0.690	27	4.000	0.666	18	3.771	0.689	26	-1.152	0.249	**
Unified ways of service delivery	3.800	0.500	23	3.700	0.674	25	3.771	0.546	26	-0.096	0.924	**
Professional competence of users	3.680	0.476	27	3.600	0.516	28	3.657	0.481	28	-0.444	0.657	**

MS: Mean score; SD: Standard deviation; r: Rank; Sig.: Significance; R: Remark; *: Significant difference; **: No difference.

constructing structures in a quick manner ($z=-1.978$, $p=0.48$). This established that the sizes of firms influence the level of application of 3DP technology in the three high-ranked construction activities. That is, the larger the size and capacity of the contractor, the higher the responsiveness of the firms to adopting the application of 3DP technology to deliver construction services. The findings on the low application of 3DP technology support the existing studies on the technology's infancy in developing countries [17, 18].

4.3. Drivers of 3DP Technology in Nigerian Construction Industry

The results of the factors that influence the acceptance, adoption, and application of 3D printing technology by the firms in construction are shown in Tables 6 and 7. Table 6 shows Cronbach's alpha value of 0.885, which is within the acceptable range of reliability (0.70–0.95) for the scale used for the analysis [57]. Table 7 shows the ranking of scores on the drivers of 3DP in construction from respondents' assessments between the two groups of the firms. All the examined drivers (28) of 3DP technology ranked high with

Table 8. Reliability statistics

Cronbach's Alpha	Cronbach's Alpha is based on standardized items		N of items
0.803	0.783		23

Table 9. Barriers to the adoption of 3DP technology in Nigeria

Variables	Medium			Small			Overall			Mann-Whitney U test		
	Mean	SD	r	Mean	SD	r	Mean	SD	r	z-score	Sig.	R
Technical challenges	4.120	0.600	1	4.100	0.737	2	4.114	0.631	1	-0.042	0.967	**
Unwillingness to change from the traditional method	3.960	0.611	2	4.000	0.942	3	3.971	0.706	2	-0.120	0.905	**
High purchasing power	3.960	0.789	2	3.800	0.918	4	3.914	0.817	3	-0.437	0.662	**
Inadequate power supply	3.920	0.571	4	3.700	0.674	5	3.857	0.601	4	-1.023	0.306	**
Lack of information on 3D printing technology	3.840	0.472	5	3.700	0.674	5	3.800	0.531	5	-0.808	0.419	**
The unfamiliarity of workers with 3D printing technology	3.541	0.931	15	4.200	0.632	1	3.735	0.898	6	-1.976	0.048	*
Structure of organization	3.760	0.522	8	3.600	0.516	7	3.714	0.518	7	-0.794	0.427	**
Social and habitual resistance to change	3.720	0.458	10	3.600	0.843	7	3.685	0.582	8	-0.417	0.677	**
High cost of training	3.760	0.435	8	3.500	0.527	9	3.685	0.471	8	-1.475	0.140	**
Maintenance cost	3.840	0.943	5	2.900	1.3270	20	3.571	1.144	10	-1.957	0.050	*
Fear of job security	3.840	0.800	5	2.900	1.370	20	3.571	1.065	10	-2.171	0.030	*
Fear of incorporating 3DP technology into existing practice by the organization manager	3.720	0.890	10	3.100	0.994	16	3.542	0.950	12	-1.624	0.104	**
Trained professional to handle tools	3.560	0.506	14	3.400	0.699	12	3.514	0.562	13	-1.062	0.288	**
Proper legislative support	3.480	0.714	18	3.500	0.849	9	3.485	0.742	14	-0.247	0.805	**
Complex 3D printing technology	3.600	0.645	13	3.200	0.421	14	3.485	0.612	14	-1.756	0.079	**
High cost of incorporating 3D printing technology	3.640	0.810	12	3.000	0.816	19	3.457	0.852	16	-2.069	0.039	*
Lack of critical knowledge	3.520	0.714	17	3.200	0.632	14	3.428	0.698	17	-1.518	0.129	**
Complicated modeling process	3.541	0.779	15	3.100	0.737	16	3.411	0.783	18	-1.361	0.174	**
Investment in 3DP technology	3.291	0.624	20	3.500	0.707	9	3.352	0.645	19	-0.784	0.433	**
High cost of 3DP technology adoption	3.458	0.588	19	3.100	0.737	16	3.352	0.645	19	-1.261	0.207	**
Client demand	3.083	0.583	21	3.300	0.823	13	3.147	0.657	21	-0.995	0.320	**
Customers' expectations	3.083	0.775	21	2.600	1.074	23	2.941	0.885	22	-1.355	0.175	**
Cost of project	2.875	0.612	23	2.700	0.948	22	2.823	0.716	23	-0.862	0.388	**

MS: Mean score; SD: Standard deviation; r: Rank; Sig.: Significance; R: Remark; *: Significant difference; **: No difference.

4.280 ≤ MS ≤ 3.680 by the medium-sized construction firms and 4.500 ≤ MS ≤ 3.600 by the small-sized construction firms. The firms' overall high-ranked drivers of 3DP technology have a range of 4.280 ≤ MS ≤ 3.657. This established that all the examined drivers of 3DP technology are critical success factors that encourage the application of 3DP technology in construction. The implication of these findings underscores the existing scholarly findings that the technology offers tremendously high benefits to the clients, contractors, projects, and environmental sustainability [30]. In support of the existing studies, this study establishes that the benefits of 3DP technology in construction are the driv-

ers that have influenced the increased exploratory research to improve the technology's applicability for construction automation. The study established that the drivers of 3DP technology in construction in developed countries [5, 7, 14, 28] are likewise relevant for increased technology adoption by contractors, consultants, and clients in developing countries, particularly Nigeria.

Among all the high-ranked drivers of 3DP technology by firms, up to 6 drivers significantly differ in their ranked scores by the two independent groups of respondents. The drivers were improved contractors and client relationship (z=-2.329, p=0.020), technological advancement (z=-2.383,

$p=0.017$), improved client satisfaction ($z=-2.241$, $p=0.025$), enhanced cost efficiency ($z=-1.962$, $p=0.05$), enhanced sustainability ($z=-2.063$, $p=0.039$), and client desire ($z=-2.088$, $p=0.037$). This established that despite the high rankings of the six drivers, there exist differences in the acceptability and adoption of the technology in construction by the firms, which are majorly influenced by the size, demand, and taste of their respective construction clients. It is included that the sizes of the firms attract different sizes and types of clients who influence the choice of 3DP technology by the firms in their respective demands.

4.4. Barriers to 3DP Technology in Nigeria Construction Industry

The examined barriers to the adoption of 3DP technology in construction have the valid and reliable scale of Cronbach's alpha value of 0.803, within the acceptable range of values established for ascertaining reliability statistics test. The Cronbach's alpha value is shown in Table 8. This indicates that the scale can measure the underlying construct for barriers assessed in this study. The ranked scores of the barriers limiting the adoption of 3DP technology in construction as assessed by the independent groups are shown in Table 9. Technical challenges of 3DP technology concerning the operation of 3D printers ranked highest ($MS=4.120$) by medium-sized construction firms. The challenges are attributed to the specificity of materials limited to the printer and the fixed design scale of the 3D printer, which restrict the printing size of objects within the printer's dimension. The unfamiliarity of workers with 3D printing technology ranked highest ($MS=4.200$) among the barriers limiting small-sized construction firms' adoption of the technology.

Overall, technical challenges ($MS=4.114$), unwillingness to change from the traditional method ($MS=3.971$), the high purchasing power of 3D printers ($MS=3.914$), and inadequate power supply ($MS=3.857$) were high-ranked barriers of 3DP technology adoption by construction firms in Nigeria. This established that the construction industries in the global view are change-averse as regards the transition from conventional construction methods to automation. This corroborates the low technological readiness of the industry for construction automation, as opined by [29]. The issue of poor power supply as a high-ranked barrier to adopting 3DP technology in construction in developing countries is mainly relative to the Nigerian construction industry. The continuous printing process by a 3D printer requires an uninterrupted power supply to create 3D objects effectively.

Notwithstanding, the inadequate power supply is a severe challenge in Nigeria, where approximately 21% of the electricity supply for the national peak demand is met. As of January 13, 2022, only 4,187 megawatts (MW) of electricity was supplied against the national demand forecast of 19,798MW [57]. This power supply challenge in Nigeria

indicates that the level of adoption of 3DP technology in construction in the country will be shallow and slow until an adequate supply of electricity is achieved and sustained.

Overall, the customers' expectations ($MS=2.941$) and project cost ($MS=2.823$) ranked lowest among the firms' barriers to the adoption of 3DP technology. The finding established that significant differences exist in four high-ranked barriers to 3DP technology adoption by the firms. These were unfamiliarity of workers with 3D printing technology ($z=-1.976$, $p=0.048$), maintenance cost ($z=-1.957$, $p=0.050$), fear of job security ($z=-2.171$, $p=0.030$) and high cost of incorporating 3D printing technology ($z=-2.069$, $p=0.039$). This result indicates that the four significant barriers equally affect and limit the adoption of 3DP technology by contractors regardless of the contractor size.

5. CONCLUSIONS AND RECOMMENDATIONS

The study assessed the awareness, application, drivers, and barriers to adopting 3D printing technology for building construction in Nigeria. The study established that the current adoption of 3D printing technology in construction is low in Nigeria because only 19.2% of the firms have had direct personal experience and involvement in using the technology to deliver construction services. Based on the results obtained, the vast majority (80.8%) of the firms who had an awareness of the technology in construction acquired it only through personal research and professional dialogue rather than through practical involvement in the application of the technology. This finding showed that 3DP technology is a new option for construction method alternatives in the Nigerian construction industry.

All the drivers of 3DP technology adoption indicated were rated as highly important (average weighted score=4.01, 93.6%) factors influencing the acceptance and application of the technology in construction. The study established no statistically significant difference in the highly rated scores of the 22 drivers of the technology by the SMEs with $-0.046 \leq z \leq -1.837$, $0.963 \leq p \leq 0.066$. However, the respective demands of the different sizes and types of clients that the firms attract, which are influenced by the technical strength and financial integrity of the firms, are significant determinants that establish significant differences in the six highly rated drivers of 3DP technology in Nigeria. These drivers were client desire, satisfaction, contractor and client relationships, cost efficiency, sustainability, and technological advancement.

Most (95.7%) of the barriers to adopting 3DP technology in construction were rated high. The inadequate power supply is a relative barrier to the application of technology in the Nigerian construction industry. The Nigerian Electricity Supply Industry (NESI) currently meets just 21% of national energy demand in the country, which is reasonably low to support the continuous printing process of 3D printers that are highly dependent on the stable power supply for effec-

tive construction automation delivery. It is recommended that the government restructure the country's power sector and diversify energy sources to improve its capacity to meet energy demands and sustain the power supply for better adoption of 3DP innovative technology in Nigeria. The study provided implications for the construction industry in developing countries on areas of improvement for better adoption of 3D printing innovation, which could enhance faster and more sustainable construction processes.

DATA AVAILABILITY STATEMENT

The authors confirm that the data that supports the findings of this study are available within the article. Raw data that support the finding of this study are available from the corresponding author, upon reasonable request.

CONFLICT OF INTEREST

The authors declare that they have no conflict of interest.

FINANCIAL DISCLOSURE

The authors declared that this study has received no financial support.

PEER-REVIEW

Externally peer-reviewed.

REFERENCES

- [1] Hossain, M.A., Zhumabekova, A., Paul, S.C. & Kim, J.R. (2020). A review of 3D printing in construction and its impact on the labour market. *Sustainability*, 12, 84–92. [CrossRef]
- [2] Masia, T., Kajimo-Shakantu, K., & Opawole, A. (2020). A case study on the implementation of green building construction in Gauteng Province, South Africa, *Management of Environmental Quality*, 31(3), 602–623. [CrossRef]
- [3] Grigoryan, E.A., & Semenova, M.D. (2020). Automation of the construction process by using a hinged robot with interchangeable nozzles. *Materials Today Proceeding*, 30, 380–387. [CrossRef]
- [4] Brehm, E. (2019). Robots for masonry construction-Status quo and thoughts for the German market. *Mauerwerk*, 23, 87–94. [CrossRef]
- [5] El-Sayegh, S., Romdhane, L. & Manjikian, S. (2020). A critical review of 3D printing in construction: benefits, challenges and risks. *Archives of Civil and Mechanical Engineering*, 20, 34. [CrossRef]
- [6] Lee, D., Kim, H., Sim, J., Lee, D., Cho, H. & Hong, D. (2019). Trends in 3D printing technology for construction automation using text mining. *International Journal of Precision Engineering and Manufacturing*, 20, 871–882. [CrossRef]
- [7] Tay, Y.W.D., Panda, B., Paul, S.C., Mohamed, N.A., Tan, M.J., & Leong, K.F. (2017). 3D printing trends in building and construction industry: A review. *Virtual and Physical Prototyping*, 12, 261–276. [CrossRef]
- [8] Elistratkin, M.Y., Lesovik, V.S., Alfimova, N.I., & Shurakov, I.M. (2019). On the question of mix composition selection for construction 3D printing. *Materials Science Forum*, 95, 218–225. [CrossRef]
- [9] Lilis, G., Conus, G., Asadi, N. & Kayal, M. (2017). Towards the next generation of intelligent buildings: An assessment study of current automation and future IoT based systems with a proposal for transitional design. *Sustainable Cities and Society*, 28, 473–481. [CrossRef]
- [10] Weinstein, D. and Nawara, P. (2015). Determining the applicability of 3D concrete construction (contour crafting) of low income houses in select countries. *Cornell Real Estate Review*, 13, 94–111.
- [11] Afolabi, A. O., Ojelabi, R. A., Omuh, I. O. & Tunji-Olayeni, P. F. (2019). 3D house printing: a sustainable housing solution for Nigeria's housing needs. *IOP Conf. Series: Journal of Physics: Conference Series*, 1299, Article 012012. [CrossRef]
- [12] Saleem, F. (2020). *World's largest 3D-printed building in Dubai*. <https://www.engineering.com/BIM/ArticleID/19863/Worlds-Largest-3D-Printed-Building-in-Dubai.aspx>. Accessed on 14 July, 2021.
- [13] Delgado Camacho, D., Clayton, P., O'Brien, W.J., Seepersad, C., Juenger, M., Ferron, R., & Salamone, S. (2018). Applications of additive manufacturing in the construction industry—A forward-looking review. *Automation in Construction*, 89, 110–119. [CrossRef]
- [14] Buchanan, C. & Gardner, L. (2019). Metal 3D printing in construction: a review of methods, research, applications, opportunities and challenges. *Engineering Structures*, 180, 332–348. [CrossRef]
- [15] Hager I, Golonka A, & Putanowicz R. (2016). 3D printing of buildings and building components as the future of sustainable construction? *Procedia Engineering*, 151, 292–299. [CrossRef]
- [16] Molitch-Hou, M. (July 1, 2020). *World's Largest. 3D Printed Building Unveiled in Dubai*. Available online: <https://3dprint.com/261978/worlds-largest-3d-printed-building-unveiled-in-dubai-d/>
- [17] Tractica. (July 1, 2020). *Construction Robotics Market to Reach \$226 Million Worldwide by 2025*. 2019. Available online: <https://tractica.omdia.com/newsroom/press-releases/construction-robotics-market-to-reach-226-million-worldwide-by-2025/> (accessed on 1 July 2020).
- [18] Farabiyi, P. K. & Abioye, T. E., (2017). A study on the awareness level of additive manufacturing technology in south-western Nigeria. *African Journal of Science, Technology, Innovation and Development*, 9(2), 157–162. [CrossRef]
- [19] Aghimien, D., Aigbavboa, C., Aghimien, L., Thwala, W. D., & Ndlovu, L. (2020). Making a case for 3D

- printing for housing delivery in South Africa. *International Journal of Housing Markets and Analysis*, 2020, 13(4), 565–581. [CrossRef]
- [20] Blender Foundation. (June 12, 2020). *Blender*. www.blender.org
- [21] TEKLA. (June 13, 2006). Trimble statement on Ukraine. www.tekla.com)
- [22] Fish, E. (2011). Rapid prototyping how it's done at GM: Additive manufacturing technology is helping the automaker reduce product development times and costs. *Automotive Design and Production*, 123(5), 46–48.
- [23] World Economic Forum. (December 15, 2019). Winsun: Demonstrating the viability of 3D printing at the construction scale, 2016. <https://futureofconstruction.org/case/winsun>
- [24] CNN Style. (Feb 2, 2019). *The world's longest 3D-printed concrete bridge is finished*. <https://edition.cnn.com/style/article/shanghai-3dprinted-bridge-scli-intl/index.html> (Feb 2, 2019).
- [25] Perkins, I., & Skitmore, M. (2015). Three-dimensional printing in the construction industry: a review. *International Journal of Construction Management*, 15(1), 1–9. [CrossRef]
- [26] Khoshnevis, B., Hwang, D., Yao, K-T., & Yeh, Z. (2006). Mega-scale fabrication by contour crafting. *International Journal of Industrial and Systems Engineering*, 1(3), 301–320. [CrossRef]
- [27] Cesaretti, G., Dini, E., De Kestelier, X., Colla, V., & Pambaguian, L. (2014). Building components for an outpost on the lunar soil by means of a novel 3D printing technology. *Acta Astronautica*, 93, 430–450. [CrossRef]
- [28] Wu, P., Wang, J., & Wang, X. (2016). A critical review of the use of 3D printing in the construction industry. *Automation in Construction*, 68, 21–31. [CrossRef]
- [29] Wu, P., Zhao, X., Baller, J. H., & Wang, X. (2018). Developing a conceptual framework to improve the implementation of 3D printing technology in the construction industry. *Architectural Science Review*, 61(3), 133–142. [CrossRef]
- [30] Ma, G., Wang, L., & Ju, Y. (2018). State-of-the-art of 3D printing technology of cementitious material – An emerging technique for construction. *Science China Technological Sciences*, 60, 475–495. [CrossRef]
- [31] Lim, S., Buswell, R. A., Le, T. T., Austin, S.A., Gibb, A. G. F., & Thorpe, T. (2012). Developments in construction scale additive manufacturing processes. *Automation in Construction*, 21, 262–268. [CrossRef]
- [32] Lediga, R., & Kruger, D. (2017). Optimizing concrete mix design for application in 3D printing technology for the construction industry. *Solid State Phenomena*, 263, 24–29. [CrossRef]
- [33] Kazemian, A., Yuan, X., Cochran, E., & Khoshnevis, B. (2017). Cementitious materials for construction-scale 3D printing: laboratory testing of fresh printing mixture. *Construction and Building Materials*, 145, 639–647. [CrossRef]
- [34] Ju, Y., Wang, L., Liu, H., & Tian, K. (2015). An experimental investigation of the thermal spalling of polypropylene-fibered reactive powder concrete exposed to elevated temperatures. *Science Bulletin*, 60, 2022–2040. [CrossRef]
- [35] Maier, A. K., Dezmirean, L., Will, J., & Grell, P. (2011). Three-dimensional printing of flash-setting calcium aluminate cement. *Journal of Material Science*, 46, 2947–2954. [CrossRef]
- [36] Gibbons, G. J., Williams, R., Purnell, P., & Farahi, E. (2010). 3D Printing of cement composites. *Advances in Applied Ceramics*, 109(5), 287–290. [CrossRef]
- [37] Doo-Yeol, Y., Young-Soo, Y. (2016). A review on structural behavior, design, and application of ultra-high-performance fiber-reinforced concrete. *International Journal of Concrete Structures and Materials*, 10(2), 125–142. [CrossRef]
- [38] Griffini, G., Invernizzi, M., Levi, M., Natale, G., Postiglione, G., & Turri, S. (2016). 3D-printable CFR polymer composites with dual-cure sequential IPNs. *Polymer*, 91, 174–179. [CrossRef]
- [39] Lowke, D., Dini, E., Perrot, A., Weger, D., Gehlen, C., & Dillenburger, B. (2018). Particle-bed 3D printing in concrete construction: Possibilities and challenges. *Cement and Concrete Research*, 112, 50–65. [CrossRef]
- [40] Lloret, E., Shahab, A.R., Linus, M., Flatt, R.J., Gramazio, F., Kohler, M., & Langenberg, S. (2015). Complex concrete structures: Merging existing casting techniques with digital fabrication. *CAD Computer Aided Design*, 60, 40–49. [CrossRef]
- [41] Aejmelaeus-Lindström, P., Willmann, J., Tibbits, S., Gramazio, F., & Kohler, M. (2016). Jammed architectural structures: towards large-scale reversible construction. *Granular Matter*, 18(2), 2–12. [CrossRef]
- [42] Maskuriy, R., Selamat, A., Maresova, P., Krejcar, A., & Olalekan, D. O. (2019). Industry 4.0 for the construction industry: review of management perspective. *Economies*, 68(7), 1–14. [CrossRef]
- [43] Kothman, I., & Faber, N. (2016). How 3D printing technology changes the rules of the game insights from the construction sector. *Journal of Manufacturing Technology Management*, 27(7), 932–943. [CrossRef]
- [44] Hayes, J. (2007). *The Theory and Practice of Change Management*. (2nd ed.), Palgrave Macmillan.
- [45] Arora, S. K., Foley, R. W., Youtie, J., Shapira, P., & Wiek, A. (2014). Drivers of technology adoption—the case of nanomaterials in building construction. *Technological Forecasting and Social Change*, 87,

- 232–244. [CrossRef]
- [46] Zhang, X., Li, M., Lim, J., Weng, Y., Tay, Y., Pham, H., Pham, Q. (2018). Large-scale 3D printing by a team of mobile robots. *Automation in Construction*, 95, 98–106. [CrossRef]
- [47] Bos, F. Wolfs, R., Ahmed, Z., & Salet, T. (2016). Additive manufacturing of concrete in construction: Potentials and challenges of 3D concrete printing. *Virtual and Physical Prototyping*, 11, 209–225. [CrossRef]
- [48] Ameh, O. J., & Osegbo, E. E. (2011). Study of relationship between time overrun and productivity on construction sites. *International Journal of Construction Supply Chain Management*, 1(1), 56–67. [CrossRef]
- [49] Nasila, M., & Cloete, C. (2018). Adoption of building information modeling in the construction industry in Kenya. *Acta Structilia*, 25(2), 1–38. [CrossRef]
- [50] Trochim, W. M. K. (2008). *The research method knowledge based*. (3rd ed.), Atomic Dog Publisher.
- [51] Van Laerhoven, H., Van der Zaag-Loonen, H. J., & Derkx, B.H.F. (2009). A comparison of Likert scale and visual dialogue scales as response options in children's questionnaire. *Acta Paediatric*, 93(1), 830–835. [CrossRef]
- [52] Kothari C. R. (2004). *Research Methodology Methods and Technique*. (2nd revised ed.), New Age International (P) Limited Publishers.
- [53] Naoum, S. (2007.) *Dissertation research and writing for construction students*. Routledge, Taylor & Francis.
- [54] Field, A. (2009). *Discovering Statistics Using SPSS, 3rd Edition (Introducing Statistical Methods)*. (3rd ed.), Sage Publications.
- [55] Wahab, O. M., Ayodele, A. E., & Moody, J. O. (2010) TLC phytochemical screening in some Nigerian Loranthaceae. *Journal of Pharmacognosy and Phytotherapy*, 2(5), 64–70.
- [56] Garson, G.D. (2013). *Scales and Measures (Statistical Associates Blue Book Series 31)*. Statistical Associates Publishers.
- [57] Ofikhenua, J. (February 18, 2022). *TCN: Nigeria needs 15,611MW more to meet demands*. The Nation. <https://thenationonline.net/tcn-nigeria-needs-15611mw-more-to-meet-demands/>



Review Article

Bibliographic analysis on 3D printing in the building and construction industry: Printing systems, material properties, challenges, and future trends

Qamar SHAHZAD¹, Muhammad UMAIR², Saad WAQAR³

¹College of Civil Engineering and Architecture, Zhejiang University, Hangzhou, China

²State Key Laboratory of Automotive Safety and Energy, Tsinghua University, Beijing, China

³School of Mechanical Engineering, Shandong University, Jinan, China

ARTICLE INFO

Article history

Received: 12 July 2022

Accepted: 20 August 2022

Key words:

Additive manufacturing, construction automation, construction systems, digital construction, material properties, 3D concrete printing

ABSTRACT

In recent years, significant advancements in developing large-scale 3D printers and construction materials have been made to meet industrial-scale 3D printing construction demand. Constructing the buildings and structural components using 3D concrete printing is significant. The main benefits of additive manufacturing (AM) are freedom of design, construction waste reduction, mass customization, and the ability to manufacture complex structures. The major issues include optimizing the printing material with suitable properties for 3D concrete printing. However, this technology for green building construction seems to improve conventional methods by reducing human resource requirements, high investment costs, and formworks. The research community's interest in 3D printing for architecture and construction has grown significantly over the last few years. As a result, there is a need to combine existing and ongoing research in this area to understand better current problems and their potential solutions based on future research work. This paper reviews the latest trend of research and state-of-the-art technologies in 3D printing in building and construction by analyzing the publications from 2002 to 2022. Based on the above-mentioned analysis of publications, printing methods, concrete printing systems, and the influence of constituent materials and chemical admixtures on concrete material properties are briefly discussed. The challenges and recommendations of 3DCP, including reinforcement, development of new materials, multi-nozzle combinations, life cycle assessment of 3DCP, and development of hybrid systems, are then examined. This paper concluded with a discussion of the limitations of existing systems and potential future initiatives to enhance their capability and print quality.

Cite this article as: Shahzad, Q., Umair, M., & Waqar, S. (2022). Bibliographic analysis on 3D printing in the building and construction industry: Printing systems, material properties, challenges, and future trends. *J Sustain Const Mater Technol*, 7(3), 198–220.

1. INTRODUCTION

Additive manufacturing (AM), also referred to as 3D printing, is a process that creates a three-dimensional ob-

ject from a computer-aided design (CAD) model by layering on the material to achieve the object's final shape [1, 2]. In 1998, at the University of Southern California, Behrokh Khoshnevis invented a large-scale 3D printing process

*Corresponding author.

*E-mail address: 12012147@zju.edu.cn



called "Contour Crafting," which later became the standard method for real-world constructions [3]. In 2007, Italian engineer Enrico Dini invented the D-Shape, a large-scale powder-based 3D printer [4]. In 2014, a Chinese company named Win Sun built ten houses in Shanghai using a gigantic 3D printer with dimensions of (150 m×10 m×6.6 m) within 24 hours [5]. High-grade cement and glass fiber was used to build these ten houses by Win Sun. They also built the world's first 3D printed Villa and a five-story apartment. In 2015, Andy used a large-scale 3D Printer to build a Castle using sand and cement. The castle was built in parts and then assembled [6]. In 2015, a huge 3D printer named Big Delta was introduced by Worlds advanced saving project (WASP), which measures 12 m tall, 6m wide, and surprisingly uses less than 100 watts of power. It was constructed outdoors using eco-friendly materials such as clay, straw, water, and dirt. An elevator was connected to deliver the solid material [7]. The construction engineering industry has much potential for large-scale 3D printing.

As 3D printing becomes more prevalent in construction, the design and preparation of concrete materials compatible with 3D printers have been identified as a significant issue. Some cementitious materials were explored for 3D printing construction applications. Gibbons investigated the feasibility of using rapid hardening Portland cement (RHPC) in a powder-binding 3D printing system to create structures [8]. Maier explained that calcium aluminates types of cement (CAC) have a high potential to be used for 3D printing structures because of suitable fresh and hardening properties [9]. A slag-based geopolymer ecofriendly material introduced by Xia and Sanjayan, composed of slag, fine sand, and a silicate-based activator [10]. The proposed geopolymer demonstrated sufficient deposit ability to replace the currently available material in powder-based 3D printers and excellent and distinct accuracy during structure construction. The method was later scaled up and used in large-scale 3D construction. A cementitious composite material composed of plaster and clay-like materials can be smoothly extruded using the Khoshnevis contour crafting system [11]. Physical properties and performance of 3D printing concrete materials, such as fluidity, extrudability, and buildability, are entirely dependent on the composition and characteristics of their constituents in both hardened and fresh states [12].

A material prepared by Nerella using limestone, brick, light concrete, and aerated concrete to replace already used material for concrete 3D printing. Printed objects have a strength 9.85% higher than before [13]. A high-performance cementitious material developed by Lim for concrete 3D printing. It consists of sand, water, and reactive cementitious compounds. The water-to-binder ratio used was 0.28 [14]. Feng worked on the mechanical properties of 3D printing structures by using cementitious powder but was unsuccessful in maintaining an excellent mechanical strength of structures [15]. Gosselin made another effort

to prepare the concrete printing material using Portland cement, crystalline silica, silica fume, and limestone filler, but the material's performance was far away from replacing 3D printing material. There is currently no widely accepted standard for material selection and design procedures for 3D printing [16].

Generally, 3D printing is primarily concerned with designing and preparing concrete compatibility with the printer. The printable concrete should have suitable properties like flowability, buildability, extrudability, good setting time, enough strength, low shrinkage, etc. To meet these requirements, partially replace cement with mineral powders to enhance the physical and mechanical properties of the concrete printing material [17, 18]. Fresh and hardened concrete properties are improved by adding mineral admixtures such as limestone, fly ash, silica fume, and Nano-silica [19, 20]. 3D printing of concrete materials' mechanical and physical properties depend on the dosage and type of chemical additives and mineral admixtures in fresh and hardened states [21]. Another way to improve the 3D concrete material is by adding superplasticizer, retarder, and accelerator additives. This is a hot topic and ongoing research these days. Concrete fluidity increases without affecting mechanical strength as the addition of superplasticizer increases [22, 23]. To stabilize the rheological properties and consistency of concrete and enhance the dimensional stability of concrete, viscosity modifying agents are very effective [24].

In addition, raw material and chemical additives make the material suitable for the requirement of 3D printing construction to work optimally as designed. The most critical factor in 3D printing concrete is the setting time. The Vicat needle test is frequently used to determine the setting time of materials, but it cannot continuously record the setting time of materials [25]. In recent years, many efforts have been made to measure concrete's setting time and hardening properties effectively with the help of ultrasonic methods such as ultrasonic wave transmission and ultrasonic wave reflection methods [26, 27]. Later, Voigt, Sharma, and Liu modified the setting time measuring methods mentioned above to use them more accurately and effectively [28–31].

With global demand for CO₂ emission reductions, it is critical to introduce innovative construction technologies to pave the way for a sustainable construction future. It will help to reduce the construction cost, material waste, and time waste while providing a competitive edge. It can save up to 40% of the cost of the total budget of a concrete work building project. This is possible with the 3D printing construction technology [32].

This paper introduces the diverse range of concrete printing processes currently being developed worldwide and discusses the latest research trends by conducting a comprehensive review of the published literature over the

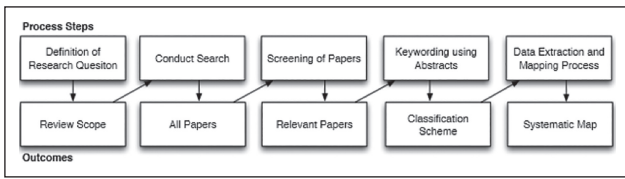


Figure 1. Petersen’s Well-ordered mapping system [33].

last two decades. It is organized as follows. Publications screening methodology and state-of-the-art technologies for 3D printing by showing the significance of BIM incorporation discussed in section 2. Subsequently, the paper will highlight the ongoing research on 3D concrete printing systems and printing material properties along with additive selection given in section 3—moreover, the Challenges, limitations, and future work recommendations discussed in section 4, and finally, the concluding remarks in section 5.

2. BIBLIOGRAPHIC ANALYSIS

The interest in 3D printing building and construction has increased in recent years. While the increase in interest enhances the quality of literature in this discipline, it causes to make challenges for the researchers to express an overview of the research development. Mapping the number of publications can be an effective way to comprehend the research trend. Peterson suggested a well-ordered mapping study shown in Figure 1. It provides quality and type of research results with an overview of the research area [33]. To understand the research development in a specific discipline, it is essential to capture the literature review systematically. It will be helpful to understand the trend of research development in the field of 3D printing for building and construction.

2.1. Data Source Analysis and Methodology

Two multi-disciplinary scientific research databases were examined for this review analysis, including Science Direct, Web of Science, and Scopus. Almost 12000 journals

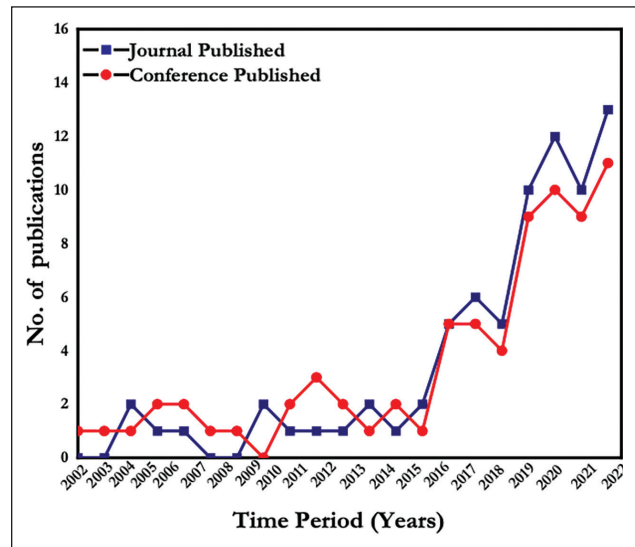


Figure 2. Represents the journal and conference publications trend from 2002 to 2022.

and 160,000 conference proceedings are covered by these databases mentioned above. Only the journal papers and conference papers were selected, directly related to 3D printing for B&C industry applications. The Boolean operator, quotations, and parentheses were used to refine the research content, while other publications such as book reviews and other irrelevant content were excluded.

During the Web of Science search, 1767 publications were discovered that matched the initial search's keywords, and 374 were screened out. For Scopus, 2124 publications were found, and 308 were considerable of the total. In the case of Science Direct, 326 publications were screened out from a total of 1445 because of the limit criteria of Science Direct. Thus, these publications were screened for duplicates and categorized according to their title and abstract for relevance. The screening system for publications used during the search of various databases and keywords used in titles are shown in Tables 1 and 2, respectively.

Table 1. Frequently used keywords in the title of publications

Keywords	2002	2004	2006	2008	2010	2012	2014	2016	2018	2020	2022	Total
	to 2003	to 2005	to 2007	to 2009	to 2011	to 2013	to 2015	to 2017	to 2019	to 2021		
Printing	0	0	0	0	1	3	4	3	2	5	3	21
Additive manufacturing	0	0	1	2	2	1	0	2	1	5	2	16
Rapid prototyping	1	0	0	2	1	2	1	2	2	1	2	14
Concrete construction	0	0	0	0	0	2	1	1	3	3	0	10
Contour crafting	1	1	3	1	0	0	1	1	0	2	1	11
Large scale	0	1	0	2	1	1	3	1	1	4	7	23
Construction material	0	0	0	0	1	3	1	5	3	1	0	14
Mega scale	0	0	0	0	0	1	1	1	0	1	1	5
Digital construction	0	0	1	0	0	0	2	2	0	1	2	8
Green buildings	0	0	0	0	3	1	2	1	1	1	3	12

Table 2. Data-based keyword search performed on 07 January 2022

No	Same words searched	At least with one of these words searched	Web of Science		Scopus Search		Science-Direct	
			Doc. founds	Doc. screened	Doc. founds	Doc. screened	Doc. founds	Doc. screened
1.	3D printing	Construction	200	45	389	25	300	67
2.	Rapid prototyping	Engineering	75	23	120	34	290	45
3.	Additive manufacturing		320	54	201	12	123	23
4.	Digital fabrication	Green buildings	480	90	257	56	66	67
5.	Contour crafting		54	20	34	10	75	31
6.	Additive construction	Automation construction	76	12	90	25	87	20
7.	Digital construction		120	35	290	12	128	15
8.	Concrete printing	Carbon dioxide reduction	80	20	259	78	234	39
9.	3D concrete construction		93	31	104	20	90	12
10.	Construction 3D printing	Large scale construction	269	44	380	36	52	7
	Total documents		1767	374	2124	308	1445	326

Doc.: Documents.

2.2. Screened Data Results and Discussions

From the screening process, 132 publications were selected and classified based on the work represented. At the same time, innovative research studies found during the screening process, such as dynamic casting by smart way technique [34], automation method of brick laying techniques [35], and one about jammed structures, were considered mentioned in the latest [36]. Although these studies had a significant impact on recent research, they did not fit the purpose of this paper and were therefore excluded.

2.3. Publications Output Characteristics From 2002 to 2022

Figure 2 illustrates the information about the published papers in journals and conferences related to 3D printing for B&C from 2002 to 2022.

In the first 15 years of 3D printing for B&C studies, there were 43 publications from 2002 to 2016. From 2017 to 2022, there were a total of 89 publications found related to 3D printing in B&C. Those were slightly over double the of published in the first 15 years. That research shows the significant rise in interest in 3D printing for B&C applications, especially in the past six years.

From the statistics and search, it is noticeable that from 2002 to 2012, the conference proceedings are higher in numbers than the journal publications. Furthermore, from 2013 onwards, it can be seen that the number of journal publications started at a good pace and a higher rate as compared to conference proceedings. As a result, journal publications overtook the conference proceedings till the present. This significant change depicts the start of comprehensive and exciting research in that innovative discipline.

2.4. 3D printing for B&C Publications Origin

Only first-author publications were considered to represent the contribution of different countries in the research of 3D printing for B&C applications. Figure 3 shows the

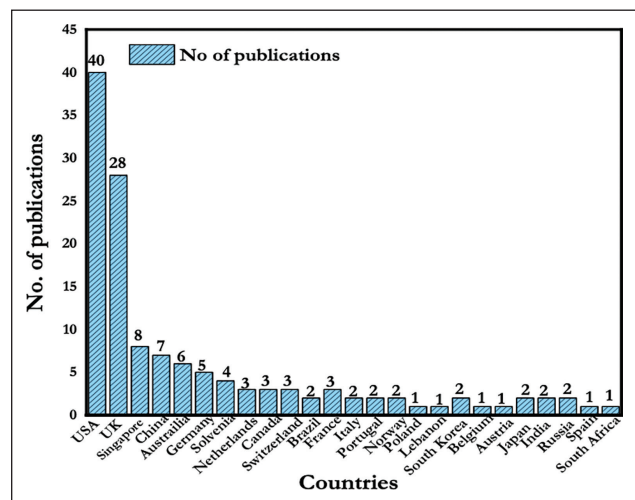


Figure 3. Research publications origin countries trend.

origin countries of publications found related after the examination. Selected papers show that the USA and the UK contribute the most in the discipline research of 3D printing for B&C. About 51% of the total publications were identified from these two countries on the list, followed by Singapore and China with about 15% of the total publications jointly. Moreover, the remaining contributions of different countries are shown in Figure 3.

Most publications from the United States and the United Kingdom come from the University of Southern California, the Massachusetts Institute of Technology, and a few other renowned universities in this field, accounting for more than 33% of the publications selected for this study. According to Figure 3, the United States of America ranks first in the publication of 3D printing for B&C research.

Moreover, Figure 4 illustrates that the USA's contribution toward publications remains constant over time while the publications from all over the world have dif-

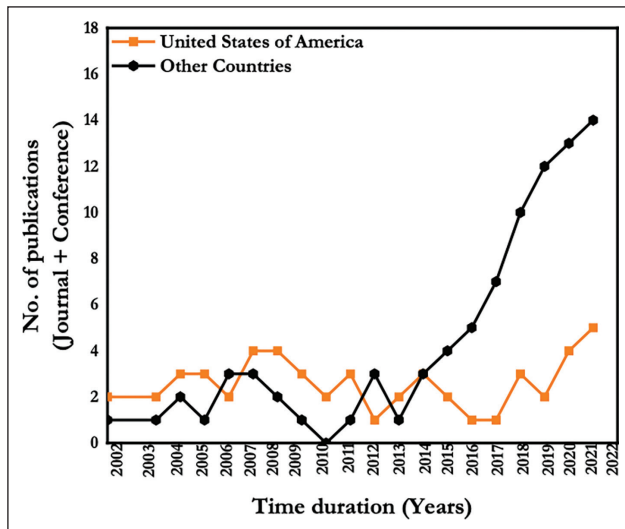


Figure 4. Comparison of the growing trend of the publications between the USA and other countries.

ferent fluctuating trends from 2002 to 2022, especially in the last six years. The global trend of 3D printing in B&C research is moving toward globalization of scientific research, with the remaining countries gradually closing the gap with the USA.

2.5. Major Research Findings

To check the development trend of 3D printing for B&C, selected publications were classified to get information deeply. The results depict that most of the authors focused on almost six categories of research in the identified publications as each paper contained more than one research interest, so publications were grouped on the bases of interests separately. It is entirely unpredictable which research interests will define the scope of each paper. As the same group of researchers took the research, other research interests were eliminated due to irrelevant context according to this paper's review aims. The purpose of conducting this study is just comparison, and it looks appropriate to mention these six focused categories of research. Detailed descriptions are mentioned ahead.

(1) Printing technique analysis included new methods to deliver the material for printing purposes, such as the

innovative idea of using a nozzle for the material extrusion and a suitable material delivery method for a smooth flow. This kind of research is mainly observed in the selected publications and differs from conventional printing techniques [37]. These printers included printing and the extrusion method category, as Yoshida described [38]. His work is mainly based on material analysis, architectural design, and construction.

- (2) Some material analysis publications generally analyzed the material and improved its properties. After this data analysis was done to check how many layers can be constructed using the 3D printing technique, this research contributes to data analysis and material analysis [39].
- (3) Another category worth mentioning is the control system observed. There is a concept about controlling a device or machine by the given command to perform a required task that could be useful for the 3D printing operating system for B&C, so it is selected from the publication and mentioned [40].
- (4) Data analysis depends on the computer system and the software being used. It also depends on the way how they exchange the data with each other. It helps to create a physical object by processing the given information or command.
- (5) Architectural design is discussed in many of the selected publications. The thing appropriate to mention here is that sometimes the architectural design is impossible to construct using a 3D printing layer mechanism or procedure. It is best if use curvature demonstration of an object otherwise impossible with simple techniques to build it [37].
- (6) The other observing thing was the literature review which included the work done by the previous persons and review articles in plenty and many examples demonstrated by the authors [41].

Due to the limited amount of selected papers and focused research areas, results have been divided into Table 3 and grouped in every two years of research. Printing technique analysis deals with the gantry or robotic system to control the printing process and other technical features as some excellent research has been found related to this [42, 43]. The material analysis focuses on product surface finish

Table 3. Research Interests Found from selected publications from 2002 to 2022

Research interest	2002 to 2003	2004 to 2005	2006 to 2007	2008 to 2009	2010 to 2011	2012 to 2013	2014 to 2015	2016 to 2017	2018 to 2019	2020 to 2021	2022	Total
Printing technology	2	1	4	3	2	1	2	3	2	2	2	24
Material inspection	1	0	0	3	1	1	2	2	3	4	4	21
Construction design	0	0	3	1	1	1	4	3	1	2	2	18
Literature review	2	0	2	2	2	1	1	2	2	7	3	24
Controlling mechanism	1	3	1	1	2	3	2	4	2	0	6	25
Data inspection	0	2	1	1	3	2	2	2	1	1	5	20

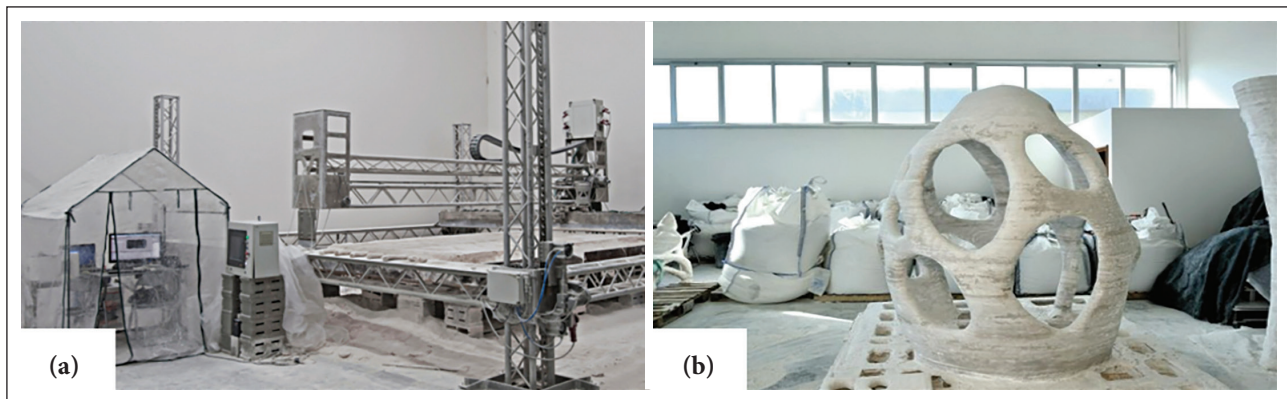


Figure 5. (a) D-shape second generation 3D-Printer (b) final printed structure after removal of extra sand-based materials [41, 51, 52].

and other functionally graded components production [44, 45]. Printing construction material properties and characteristics adjustment attempts were also carried out, which is the primary reason for developing an interest in material analysis [46, 47]. Large-scale printing rose in the last couple of years, as shown in Table 3, and as the printing technique and material properties will improve, the construction of complex structures will also improve, as some previous research proved [48, 49].

2.6. Selected Publication Titles Review

Analysis of publication title results illustrates that authors frequently use some words in the publication titles selected during the screening process. Repeated words such as 3D printing, concrete, additive manufacturing, and large-scale manufacturing are mentioned in Table 3 briefly, with the growing trend of each famous term used in the titles. The word "concrete" is not much noticed in the far past publications. It just started a couple of years before as the material options for 3D printing increased.

Alternatively, some words used went down over the last decade, such as large scale and free form construction, and there is a possible reason for that may be the authors do not like to use this word or may sometimes be these words did not fulfill the actual proper meaning. For example, and as observed in one of the studies, free-form structures utilizing material extrusion are impossible due to the inability of large cantilevers and angles to be printed [16].

3. 3D PRINTING STATE OF THE ART TECHNOLOGIES IN B&C

Selected publications represent the rapid development of large-scale 3D printing, and most authors categorized it into two primary techniques named as (1) binder jetting technique and (2) material deposition and extrusion techniques. The basic principle of these techniques is to build a physical object by depositing material layers one by one over each other. It started with the help of a CAD model,

which shows the 2D shape, and after processing the model and operating the command, it created a 3D prototype shape. Only 10 percent of the total number of selected publications focused on the binder jetting technique, which will discuss in this section.

3.1. Binder Jetting

Binder jetting is a 3D printing process in which objects are created by layering a binder over a powder bed. Binder is ejected in tiny droplets spread across the powder material's thin layer on the build tray. This method connects the two parts of 2D cross-section components over each layer of the powder [41]. The process continues until the final object is completed. Using a vacuum cleaner, unbound material can be removed and suitable to use further again for another 3D printing task after recycling the material [50]. This method can work on complex geometries with voids and overhanging features. Because of the narrow distance between the layers, this method's resulting surface finish is excellent. Layer thickness matters a lot. It depends and measures on the penetration of the binder between the two components or cross sections; if the layer is too thick, it is difficult for the binder to penetrate completely between the layers [51]. Figure 5 illustrates the D-shape printer and the final printed component after removing additional sand-based materials.

3.2. Method of Material Deposition

Material deposition method (MDM) is a 3D printing process in which material follows and comes out as the CAD model, similar to fused deposition modeling (FDM) [52]. The extruded material must be able to bear its weight and the coming layers over layers without any collapse or deformation [53]. Many automated systems use MDM for fabrication, which will be discussed in this section.

3.3. Stick Dispenser

A stick dispenser is a device developed by Yoshida, and it is a kind of hand-help printing device that allows a con-

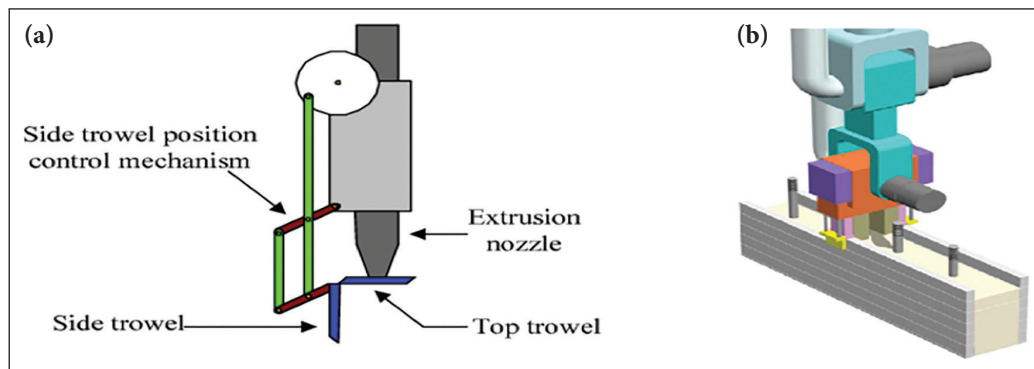


Figure 6. (a) Single nozzle (b) multiple nozzle assemblies [55, 56].

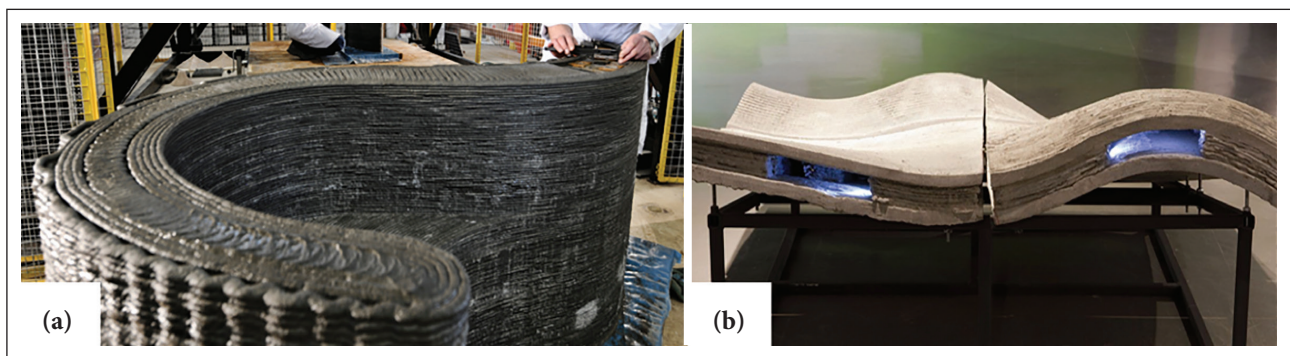


Figure 7. 3D concrete printing progress at Loughborough University [57].

stant feed of chopstick material composites [38]. Chopsticks coated in wood glue are randomly dropped during this process, forming a porous structure that is later evaluated using volume-based analyses. The device is guided by basically two main tools one is a depth camera, and the second one is the real-time projector. Using a simple color code and these two tools help inform the place where the chopsticks are deposited. There is a condition of low light while using the projector. There was some mechanical properties test carried out by applying the different load conditions, and the results show that the load bearing capabilities are not good enough, but this method is innovative for the use of aesthetic purpose by making the complex architectural design [38, 53].

3.4. Contour Crafting (CC)

Contour crafting is a process that utilizes a gantry-based system to extrude material layer by layer in a systematic manner. The uniqueness of this technique is the use of trowels with the nozzle, as shown in Figure 6. The benefit of the trowels is that they guide the printer about the smoothness and surface accuracy. The trowels can be adjusted at different angles according to the object's shape, which gives an extra benefit of surface finish even during the higher thickness of the layers of the material [54]. Some authors describe explicit material and compositions in the selected publications [55, 56]. It is also noted that CC technique

conduits for electricity, plumbing, and structural reinforcement can be used [54].

3.5. Flow-Based Fabrication

MIT researchers designed a single pneumatic system connecting with the end effector of six robotic arms, which enables the extrusion of water-based polysaccharide gels and natural composites. The design and fabrication of the printed parts are two-dimensional (2D). High stiffness, light weight, and high wear and resistance will be the characteristics of the advanced manufacturing materials structures [57]. This work has many applications, such as temporary lightweight shading structures to highly complex automated structures for architectural purposes, as shown in Figure 7.

3.6. Digital Construction

A system developed by the researchers working at MIT can be used for the analyses and fabrication with a feature of on-site sensing [58]. The system is intended to achieve high speeds, accuracy, and ease of access through a small robotic arm, as illustrated in Figure 8. The whole system is designed around a large boom used for gross positioning. An accelerometer and ground reference sensor accurately positioned the end effector for the closed-loop system. There was a need to use a material with rapid cure time and high insulating value, so polyurethane foam was selected as

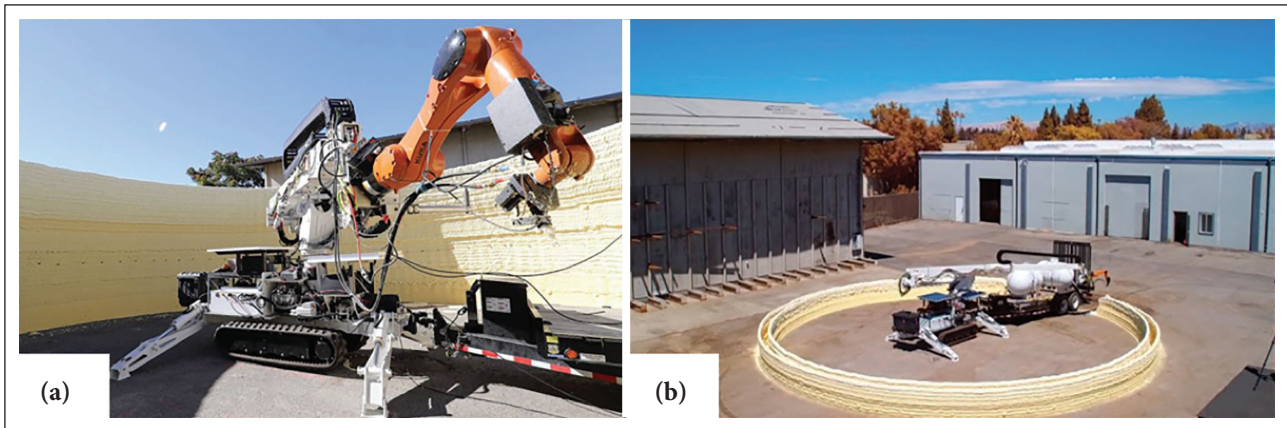


Figure 8. 3D concrete printing progress at Loughborough University [58].

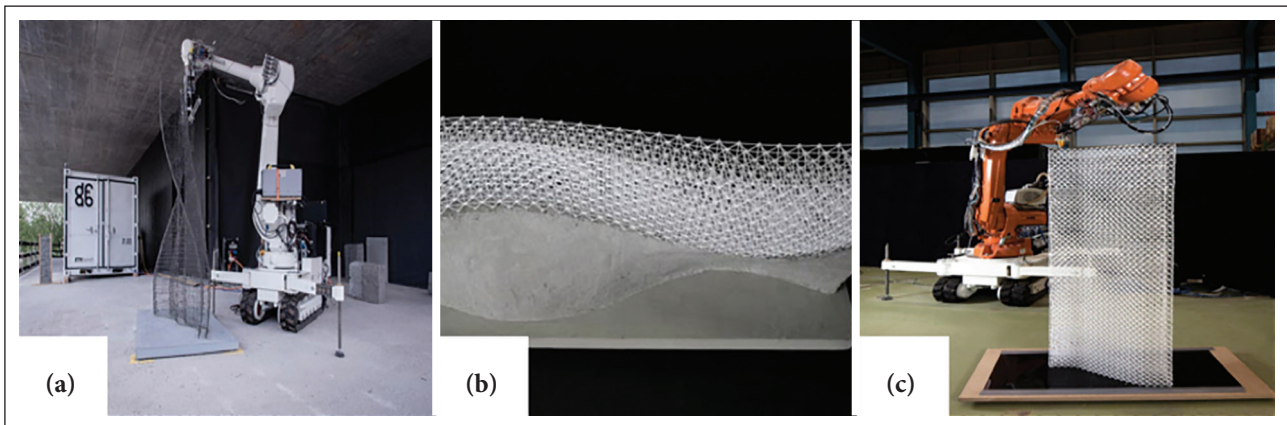


Figure 9. Mesh-mould technique-based formwork and reinforcement setup for concrete materials [60].

a printing material. A 12-foot-long wall will take five minutes the completion. To get a final surface finish, the end effector can be changed as a mill head for subtractive manufacturing and suitable for the desired surface finish [58].

3.7. Small Constructor

A coordinated system build consists of three small robots for the fabrication of in situ construction. They are lightweight, compact in size, and quickly available for mobility. During the printing process, each small robot has its unique feature to perform, described by Nan in detail [59]. Extrusion rate determines by the movement and speed of the robots, so a binary component resin material was prepared for these robots. Curing time must be compatible with flow rate and robot movement speed to avoid material clogging in the hose. To meet the required curing time property, an external heat source can be applied according to the environmental conditions, which will help adjust the material curing time by using the heat source's chemical effect.

3.8. Mesh-Mould Construction Technique

This technique is capable of printing in situ structures freely in three-dimensional space. For this purpose, a giant

six-axis robot was used to extrude the thermoplastic polymer material to print structures. For a high level of control of the printing process, pressurized air has been used at the nozzle during printing, facilitating the weaving of structures freely in space. A relevant research application found that structures act as reinforcement for the concrete, as shown in Figure 9. Then concrete is poured over the formwork and later on troweled manually to get the smoothness of the surface [60]. This technique enables the fabrication of complex structures by reducing time consumption and making it feasible for large-scale applications. At the same time, the different densities of mesh can be printed. The most exciting thing is that the tensile force of concrete increases with the presence of mesh, ultimately a possible way to replace conventional steel reinforcement.

3.9. Building Information Modelling (BIM)

Building construction management covers the complete life cycle of a construction process, and the best way to deal with it is BIM [61]. For example, planning, scheduling, facility management, and estimation. BIM has the potential to provide the solution to problems that the construction industry has always faced, such as lack of innovation and

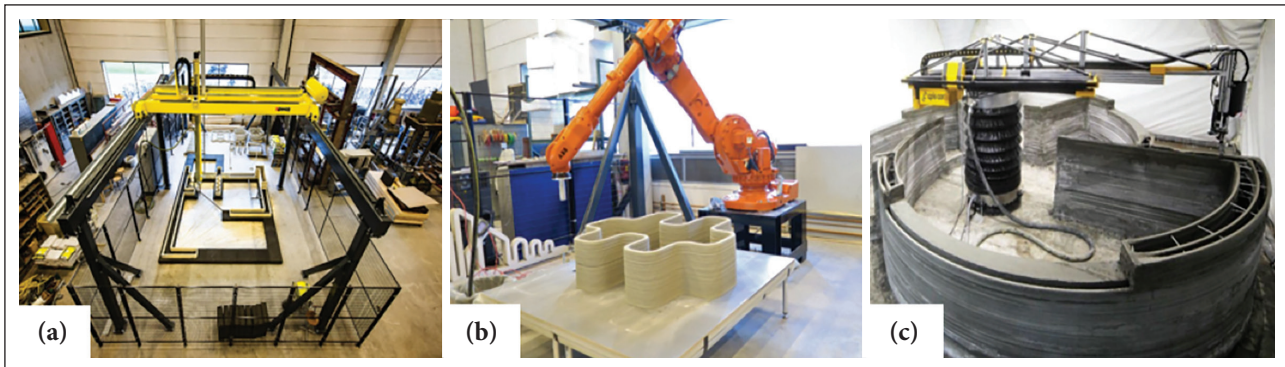


Figure 10. Currently used main 3D concrete printer (a) gantry printer [77] (b) robotic printer [82] (c) crane printer [83].

low productivity in its ongoing process [62, 63]. BIM also deals with equipment, material, available sources, and manufacturing data to deal with geometrical data [64]. This technique helps to overcome the lack of collaboration between the different teams during execution stages and provides an essential platform for automation applications such as mechanical construction and 3D printing.

A 3D printing construction based on BIM can quickly reduce the time required for the process completion in each step just by using a single software or interface. A common issue in the construction industry is that design is constantly changing, and BIM also deals with that issue effectively. As 3D printing needs no formwork, quickly abrupt changes can be done with little effect on the design compared to the conventional construction methods. It can effectively automate the printing process by storing and synthesizing the control data of the printer, delivery of material, and later on, process performance.

BIM is observed as a primary language in the construction industry and is a standardized method followed by the construction industries as 3D printing have a game changer effect in the construction industry, the same as BIM can bring many benefits in terms of labor and cost savings. Unfortunately, there is not enough research done in collaboration between 3D printing and BIM, while there is a potential opportunity for the researchers to fill the research gap between 3D printing and BIM.

4. CONCRETE 3D PRINTING IN B&C

A group of researchers at Loughborough University, England, built a system of concrete printing similar to a contour crafting system that extrudes concrete as a material layer by layer to build a physical object according to the CAD model [65, 66]. Concrete is used globally as one of the primary construction materials. It has several benefits as a construction material, such as high thermal resistance, low cost, good durability, high strength, good flow gaining ability, and molding into different shapes. There could be three reinforced concrete (RC) construction components: concrete, reinforcement, and formwork. Research shows that

formwork waste a lot of cost and time of the total cost and time accounted for 35–54% and 50–75%, respectively [67]. However, as a new technique of Concrete 3D printing, construction companies can easily save a lot of time and cost compared to traditional construction methods. According to the UK's statistics, the UK construction industry produces about 54 Mt of construction and demolition (C&D) waste annually, from which only 9% goes for reuse after crushing [68]. It is welcomed that the adoption of 3D Concrete printing construction would be able to control the construction waste because the material's mixing and using will be in a systematic way as compared to the traditional ones. Ultimately, it will be economical, time-saving, good productivity, and help towards good environmental impact by reducing global warming because of this construction wastage.

4.1. 3D Printing Construction Systems

The most important advantage of 3D printing construction is that it rapidly manufactures complex structures and objects with non-standard geometries [69–71]. The 3D printing construction processes could be divided into three main categories by names given by their founder Contour Crafting, D-Shape, and concrete printing. These processes are discussed in detail and accessible in [72–74]. To utilize these processes for construction purposes, two kinds of approaches are extrusion and pumping approaches. In both approaches, the first step is slicing the 3D CAD model into 2D layers of the model. Then all the basic requirements to print an object are given to the printer in a readable language, such as printing speed, extrusion rate of the material, and other coordinate info of the object to get the final desired shape of the product [75, 76]. 3D concrete printers, nozzles, pumps and control systems, and feed mechanisms will be discussed in this section. These system parts must be in an excellent combination to achieve high-quality 3D printed products.

4.2. 3D Concrete Printers in B&C

Currently, according to the latest research review in universities and construction industries, three kinds of 3D concrete printers are successfully used: Robotic, Crane, and Gantry, as shown in Figure 10 [77–83]. Gantry belongs to

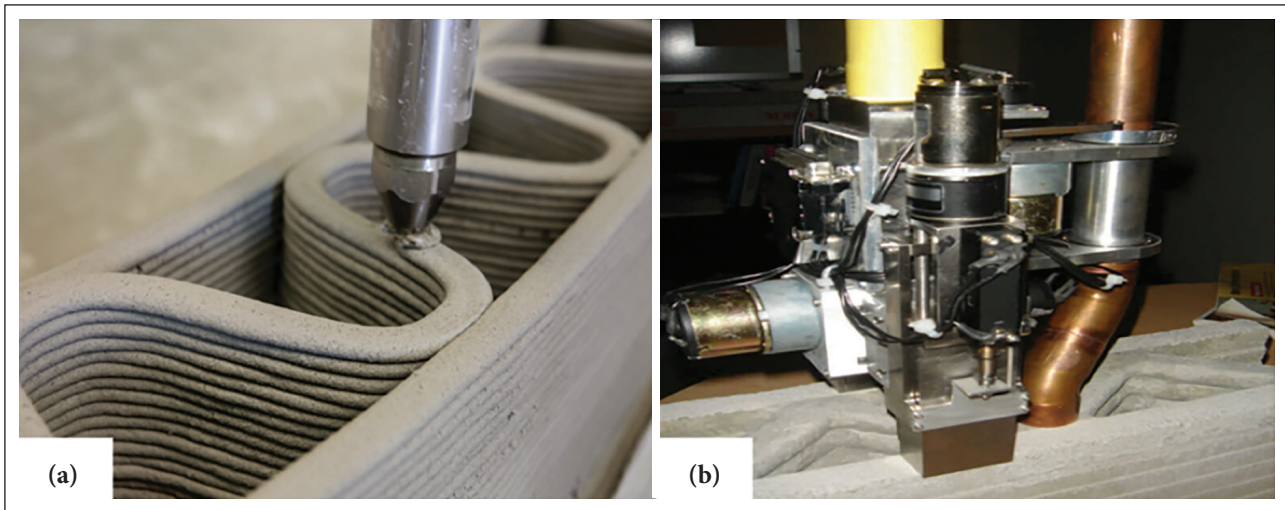


Figure 11. Concrete extruder nozzles main types (a) single orifice nozzle [86] (b) multiple orifice nozzle [91].

the crane type, but the main difference between these two is that gantry is a kind of fixed design regarding height, whereas Crane type printer's height can be adjustable in the vertical direction. The main benefit of these two printers is that they can get easily scalable concerning the size. While the robots are typically fixed in size, making it difficult to scale up according to the requirements. However, the degrees of freedom are more suitable in robotics six arms and enable them to perform many valuable operations compared to the 4-arms gantry printer.

Furthermore, using gantry printers is suitable where the printing object has little complexity instead of using the robotic printers. Robotics, like gantry printers, require high cost and less weight on the arms. The size of gantry printers varies from small-scale laboratory printers to large building construction scale printers, depending on the site and usage [77, 78]. Win sun Construction Company in china also used the same gantry printer technique to build multiple houses, including a five-story building apartment and a mansion. The material used for that construction consists of glass fiber, cement, hardening agents, sand, and some recycled waste of construction materials [77]. All the houses built were not wholly 3D printed. They prepared the parts at the company and then assembled them on the site [77].

Another Netherlands company, CyBe additives, used the CC technique to print a mortar capable of gaining bearable strength within 5 minutes. They used a print head with a six-axis robotic arm to perform the experiments with high speed and good strategy [82]. The additional rotational axis of a robotic over a gantry printer allows the designer to print more complex geometries easily. A Russian Company has built a crane-type printer that enables a printing area of 58 m² [83].

In 3D concrete, printing observed that print head speed affects the bead dimensions. For example, when the print head speed is higher, material layer deposition will not be

enough, and the bead dimension will be short. On the other hand, if the print head speeds too slow, then the layer of deposition material will be higher than the nozzle orifice, increasing the bead dimensions and wasting the material too [76]. One of the previous research has noticed that the time gap between the two layers was a range of 11 to 60s, which enables the build of a 3D column at a rate of 1.1 to 6 m/h [84]. The extrusion rate generally varies in concrete construction processes ranging between 15 to 125 mm/s. It appears that the quality of the surface limits the extrusion speed to about 200 mm/s depending on the extrusion plate size, which was 15 x 70 mm [85]. Ultimately, it can vary from material to material for 3D construction printing.

4.3. Concrete Extrusion Nozzles

The shape and size of the material layer depend on the nozzle, which is the end part of the print head [86]. An appropriate nozzle at the end of the print head is essential to achieve the desired shape and quality of the material layers over the bedding layers. To obtain this nozzle, the printer should be tangent to the path [86] to avoid the collapse of the layers. Various kinds of orifice shapes of the nozzle are used, such as circular, rectangular, square, and elliptical. Furthermore, side trowels can be used for a better surface finish. Results of the research show that the circular shape orifice nozzle has more advantages than other orifice shapes, such as freedom in printing angle or vertices during the printing of an object [86]. Some studies show that a square orifice is far better than the elliptical one in terms of surface finishing and ease of manufacturing [87, 88]. Nozzle orifice sizes vary according to the shape and size of the object to be printed. Circular orifices vary in size from about 4–24 mm in use, while the other orifice shapes, such as rectangular, vary from 9x6 mm to 38x15 mm [76, 89].

Existing nozzles deliver material of about 0.05–0.1 L/s [90]. However, for 3D printing construction, the rate of ex-

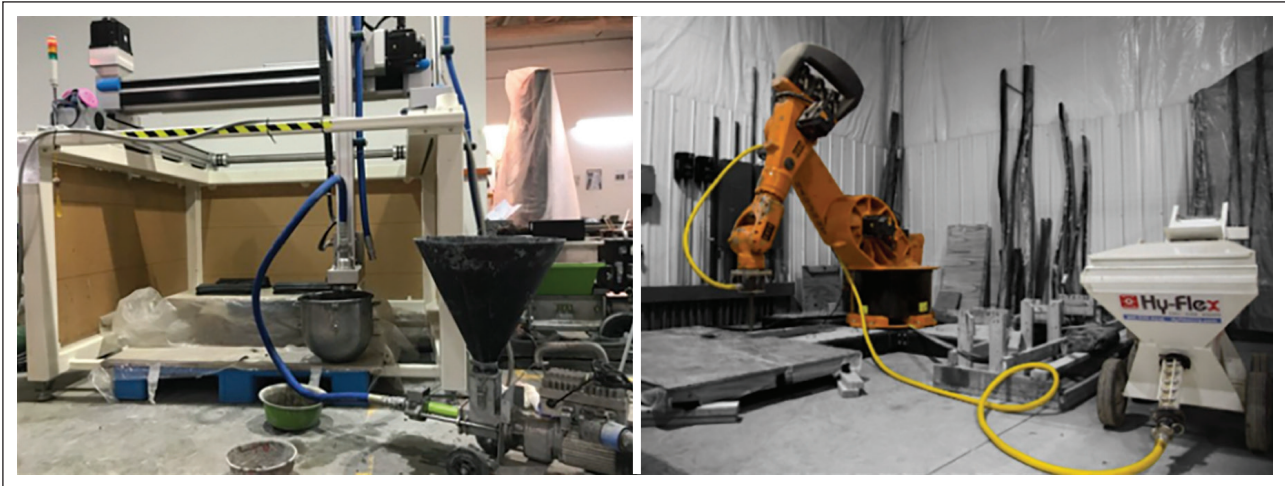


Figure 12. Concrete pumping and feeding systems for 3D concrete printing [76, 92].

trusion from the nozzle is about 1L/s, and a roughly estimated speed up to 2L/s is considered a realistic target rate, and multiple nozzle orifices can be used according to the shape and design of the object to be printed [91].

4.4. Pumping, Feeding, and Control System

One of the essential parts of the 3D printing construction system is pumping the material at a reasonable delivery speed without separating the particles. The pump feeds the material from the mixer through a pipe or hose to the nozzle from where the material is extruded to print the required object. The pump should be able to transport the material from the mixing unit to the nozzle by overcoming the challenge of large particle size aggregate and range of water to cement (w/c) ratio. Maintaining the high viscosity of the fresh material demands relatively higher pumping pressure ranging from about 1 to 5 MPa [92]. Blockage of material in the pipe may occur during pumping at high pressure, which can be caused to the loss of the smearing layer. The balance between the feeding system, Nozzle, and material properties is essential to obtain a smooth printing process and product. Pumping speed can be managed concerning the object size and shape, especially at the angles, to avoid the extra deposition of material.

It is essential to adjust the pumping speed to follow the shape discontinuities and movement of nozzle extrusion. Therefore, a complete single-unit control system is better for simultaneous control of nozzle movement, printer speed, and material pumping. One effective way to avoid collapse is to put chemical additives in the material at a stage when the material is in the nozzle instead of mixing additives in the mixer to boost the setting of the material [76].

4.5. 3D Printable Materials Properties

Viscosity, available time, shear stress, and strength are the essential properties of freshly prepared material and are directly related to pump ability, extrudability, and build-

ability. Flowability changes depending on available time, which enables the material to be printed without affecting the material properties like hardening etc. Generally, the Vicat apparatus is used to measure the initial and final setting time. The time between mixing and initial setting time is named open time. At the same time, pump ability and extrudability could be affected directly by shear stress and viscosity which Rheometers can measure.

Furthermore, the Slump test can indirectly measure fresh material's shear stress [93, 94]. The green strength of the material should be enough to bear the subsequent layers' load on the bed layers without any collapse or shape damaged [84]. Table 4 presents the mechanical performance of fiber-reinforced 3D-printable concrete materials.

4.5.1. Pumpability

Pumpability means the mobility of the material along with its initial properties under pressure conditions [95]. The material state needed at the nozzle and pump both are contrary, such as the material at the pump should be soft, which will be easy to move. On the other hand material at the nozzle should be stiff enough to maintain the shape. Concrete is a heterogeneous material consisting of different sizes and particles, so a pumpability system must be optimized and good enough to pump the material [96]. Acceptable paste content and consistency of grout of grains are necessary to improve pumpability [97]. Studies proposed that sliding pipe Rheometers are suitable for measuring permeability [95, 98].

4.5.2. Extrudability

The commonly concrete extrusion process for instance, the manufacturing of pre-cast hollow core slab elements, involves a plastic-like mixture forced through the nozzle, and for this kind of production, high shear force and compressive force are required [85, 99, 100]. In 3D printing construction, it depends on the type of printer (gantry,

Table 4. The mechanical performance and parameters used for fiber reinforced 3D-printed concrete [8–22]

References	Fiber parameter				Strength (MPa)		
	Length	Shape	Content	Type	Compressive	Flexural	Tensile
[8]	3 mm	Straight	–	Carbon	83.7–87.4	20.3–119.6	–
[9]	3/6/8 mm	Straight	0.25–1.00%	Glass	20–27	2.6–7.0	0.9–1.5
[10]	18 mm	Straight	0–0.7%	Basalt	29.8–39.6	3.34–6.51	3.0–5.2
[11]	6/12 mm	Straight	0–1.4%	PE	–	2.13–15.09	–
[12]	6 mm	Straight	0.25–1.00%	PP	13.5–35.8	6.1–8.1	–
[13, 14]	12 mm	Straight	2%	PVA	23–30	–	3.4–5.0
[15]	8 mm	Straight	2%	PVA	24.2	10.8	4.7
[16]	12 mm	Straight	2%	PVA	16.45–19.23	–	1.6–3.5
[17]	8 mm	Straight	2%	PVA	34.98–44.09	1.64–2.41	4–8
[18]	6 mm	Straight	0.3–1.5%	PE	–	0.88–8.31	5.3–8.3
[19]	12 mm	Straight	1–2%	PE	–	3.2–19.4	4.6–5.8
[20]	12 mm	Straight	1–2%	PE	36.7–53.4	14.4–22.0	4.5–4.7
[21]	3/6/13 mm	Straight	0.25–2%	Steel	70–156	6–16	–
[22]	3/6/13 mm	Straight	0.25–2%	Steel	70–156	6–16	–

Fiber content in this table refers to volume fraction unless stated.

robotic, crane) size and the working volume, e.g., length, width, and height. These two parameters give information about fresh material pumping over the required distance. For the pumping, thixotropic concrete is desired, and fresh concrete material at the nozzle stage is less dense than the traditional ones. Stiffness is essential to maintain the object's shape and quick building of the object's layers. Segregation must be avoided at the nozzle because, at that point, the size of the nozzle becomes smaller compared to the delivery pipe, which may cause pressure at the nozzle end [78]. Material contents and proportions should be chosen carefully to achieve the properties of good thixotropic and permeability of the concrete material. On the other hand, failure at this stage may lead to the blockage of the material delivery pipe or nozzle.

4.5.3. Buildability

Properties of layers to maintain the shape of the object, being self-supportive, and enabling the bedding layers to bear the weight of subsequent layers without collapse and deformation of the shape; these all properties refer to the buildability of the material. Imperfection in layers may lead to an unbalanced shape during successive layers of material added [101]. Traditional work has formwork, so there was no worry about it, but 3D concrete printing is a formwork-free technique, so concrete must be self-supportive to achieve good results. There are several ways to achieve the buildability of the printed material instead of improving the properties of the material. The simplest way to change the structural buildability is the change of nozzle shape. For example, the contact area between the two beads is less in a circular orifice nozzle than in the rectangular one, and the contact area would help improve the structure's buildability [78, 101]. Another way to improve

the buildability is by increasing the number of adjacent layers and cellular structure of layers by using a single nozzle or multiple nozzle head. However, a single nozzle's starting and ending point should be the same but not necessary for multiple nozzle heads [73].

4.5.4. Flowability Control

Flowability is a crucial parameter of 3D printable material, enabling the performance of fresh concrete material. Flowability control ensures that material is good enough to pump through the delivery system toward the nozzle without any blockage [102]. It depends on the grain size, and the wider particle size helps to gain a good flowability of a fresh state material mixer [102, 103]. Fine powder admixtures help the material to get a fluid shape which attains good flowability of cement mortar instead of getting bonds and getting higher in size [104, 105]. Incorporating an excess amount of fine powders may lead to an increase in viscosity and inter-particle friction forces. As a result, an adverse effect will be on the fluidity [106–109]. Studies proved that adding a superplasticizer can improve the flowability and the higher ratio of water to binding material also leads to improved flowability [110–113].

4.5.5. Setting Time Control

For a continuous flow and deposition of material layers, correctly printing material requires a long time to maintain. However, the material also needs a short setting time for early strength after extruding from the nozzle [114, 115]. Setting time property mostly depends on the retarder and accelerator admixtures, and studies show that by altering the amount of retarder or accelerator, every material can achieve the required initial and final setting time [116, 117]. The recommendation observed during the research

shows the addition of accelerator should be in dry mixing instead of dilute with water mixing, and mixing speed and time should be 52 rpm in 20 seconds, respectively [118]. Studies proved the effect of retarder on the setting time; for instance, sodium tetra borate, and the mixing ratio varies from 0.1% to 0.3% could increase the jelling time about up to 29 minutes to 110 minutes and the final setting time slightly up to 50 to 148 minutes [119].

4.5.6. Compressive Strength

The stiffness and strength of concrete can be increased by using fine powder admixtures of small size compared to the Portland cement will be helpful to fill the voids and increase the packing density, resulting in good compressive strength. Silica fume and fly ash are usually rich in SiO_2 and affect the material's mechanical strength and help enhance the strength. These two ingredients affect the hydration process of the system and make the material denser and more compact by improving the mechanical strength of the concrete material or cement mortars [120]. It is reported that 10% use of silica fume by mass can increase the strength of concrete by up to 8–20% [120]. The effect of silica fume is not prominent at the starting stage of addition. It shows the effect after three days [121]. Concrete strength ration 1 day/28 day decreases as the silica fume addition amount increases and it ranges about 6% to 30% [122]. It does not work at the early stages to gain enough strength as needed [120]. Concrete 3days strength has been increased up to 81% by adding four wt.% of nano- SiO_2 [123, 124]. Studies showed that seven days and 28 days samples compared with the addition of silica fume and SiO_2 , results revealed that the strength of samples containing SiO_2 is higher than all others [125]. Dispersing agents must disperse the particles effectively to get good strength [126]. It is noted that a large amount of fly ash into the material will lead to a decrease in the strength of concrete [127]. Fly ash works slowly to increase the strength but rises at the later stages [128]. One research also proposed that the high amount of limestone powder will decrease compressive strength at the early stages [129].

4.5.7. Shrinkage Control

Whenever disturbed, the dimensional accuracy and stability of the printed object are responsible for shrinkage, which usually affects the printing performance. To ensure good flowability and extrudability, high water content is necessary beyond the volume needed for the hydration process. The excess water evaporation leads the printed object toward shrinkage during the setting time and hardening stages [130]. As in 3D printed objects, most of the area is open and freely in contact with the environmental condition compared to the conventional methods, so it causes to evaporate the water easily from the object, and shrinkage occurs [131]. The possible solutions to control the shrinkage are increasing the mineral admixtures content and using the fine aggregates to avoid shrinking

the composites [132]. The addition of fly ash to reduce shrinkage has been shown to have significant effects, as replacing cement with 80% fly ash can reduce shrinkage by approximately 67% [133, 134]. Shrinkage reduces up to 80% in dry conditions if combined use of fly ash and sulfoaluminate cement [135, 136]. Adding 10% to 15% of the silica fume can increase concrete's autogenous shrinkage, ranging from 33% to 50% [137–140].

4.6. Selection of Chemical Additives

4.6.1. Superplasticizer

To maintain the workability and strength of the concrete during preparation, using less water is possible by adding a chemical known as a superplasticizer. Negatively charged superplasticizer repels the cement particles to release the entrapped water, enabling the material to gain good flow ability [141, 142]. Research shows that superplasticizer addition did not change the hydration process but improved the process by improving the crystal structure [143]. Superplasticizer is divided into four primary groups and is readily available in the markets [144]. However, even from the same group, their effect on strength, setting time, and flow is different because of the different chemical structures of molecules [145–148].

4.6.2. Accelerator

3D concrete printing usually needs a quick setting of the material after coming out from the nozzle to bear the weight of the coming layer. Therefore accelerator is an additive that enables concrete to get enough early strength. Accelerator compositions work on a quick hydration process by reducing the setting time and quickly enhancing the material's setting. Accelerators can be an alkali or alkali-free group [149].

4.6.3. Retarder

Retarder is used to delay the hydration process of the cement by building an insoluble layer on the surface of the cement particles. Researchers recommend using Tartaric acid, citric acid, and sodium gluconate to achieve a favorable retarding effect [119, 150, 151].

4.6.4. Viscosity Modifying Agents (VMA)

Viscosity modifying agents are soluble in water and are frequently used to modify concrete flow and rheological properties. Even small dosages of viscosity modifying agents significantly affect the cement mortars and improve flowability and dimensional stability. The VMA decrease down the powder requirement still has the required dimension stability and flow properties [152]. The VMA connected the molecules through Van der Waals interaction and stopped the extra water movement, leading to increased plastic viscosity. The point to be noted is that if 3D printing material viscosity increases, higher pumping pressure is needed.

5. CURRENT LIMITATIONS, CHALLENGES, AND FUTURE WORK

Besides the benefits of 3D printing in the construction industry, such as the ability to build complex geometry and structures, freedom of design, and customization, there are a few limitations, challenges, and drawbacks observed from the previous research. These limitations and drawbacks required some further research and development of technology to overcome. In this section, limitations and future work will be discussed to provide a new direction for the reader and the researchers to explore so that the traditional construction industry can take full advantage of 3D Construction printing.

5.1. Limitations of 3D Construction Printing

Every production domain almost makes progress in automation and technology since the early decades of the 20th Century except the Construction industry, which is still facing a lack in automation and technology because of several factors [53–54, 153] most common ones:

- Automated fabrication technologies for large-scale production are not suitable.
- Automation technology is not according to the conventional design approaches.
- As compared to other production industries, its production ratio is significantly small.
- Expensive automated equipment reduces interest and attractiveness.
- Limitations of the materials.
- Management issues to deal with the process effectively.

Furthermore, the building industry's production rate cannot easily match other industries' production rates [154]. Because of different sites, materials, and client requirements, each building is different from others and reflects its prototype. Despite the differences, most designers believe that eventually, 3D printing will significantly contribute to the construction industry. They agreed that the 3D construction printing process is slow initially and becomes quicker in the later stages compared to the traditional methods [155]. The Figure 13 shows the time consumption by both the 3D construction process by a continuous line and the traditional process taking time by fluctuating dash lines.

The components for 3D construction printing are significantly heavy and oversized, and avoid moving and lifting these parts of the system as much as possible. The other major problem is material sensitivity, which makes it challenging to perform at ambient conditions compared to UV or heated conventional systems; it is less controllable. Other limitations that need to be considered during the process are enlisted [156, 157].

- The concrete material will solidify and block the machinery if the idling time of the nozzle is too long.
- The time interval cannot be shorter than the minimum curing time, so the first layer must be able to bear a load

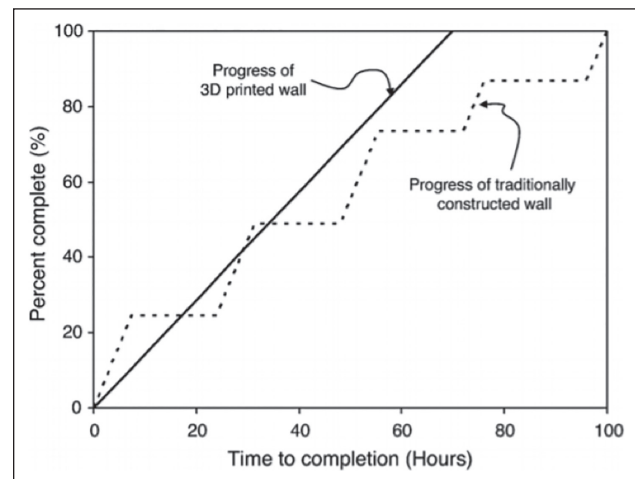


Figure 13. Time consumed by the 3D printing process and traditional construction method to complete a wall [64].

- of subsequent layers without any collapse or deformation.
- Subsequent layers of the material should be able to stick quickly because the time interval should not exceed a specific limit between the subsequent layers.
- The nozzles cannot be allowed to collide with deposited layers. If this happens, the nozzle cannot move in a straight line to avoid the hurdles.

The results come from these factors and the material limitations together recommends that at the moment, traditional construction methods should be continued for heavy construction and multi-story buildings, and small, lightweight construction should be done with the help of 3D Construction printing. There is a need to improve the technology to support 3D construction printing without any limitations and wait until success achieves, and 3D construction printing will enable building heavy construction [155, 156].

5.2. Challenges of 3D Construction Printing

5.2.1. Balance of Stability & Flow

There is a need for a material having two states for 3D concrete printing, and both states have opposite properties. Such as, before the extrusion of the material, it should be easy to pump and have a consistent flow. After extrusion from the nozzle, the material should be stable and robust enough to bear loads of the upcoming layers. This is a challenge faced many times during the experiments.

5.2.2. Maintain Workability

To achieve good printing results workability of the material is one of the critical factors. However, the material takes time to harden but loses its workability quickly as soon as it is mixed. Here is a need to add additives such as water reducing agents to maintain the material's workability and achieve good printing product results. Often, this challenge has been faced during working on the printing material.

5.2.3. After Extrusion, no Deformation

The 3D printing process proceeds by depositing material layers one by one. Each layer should be strong enough to bear the load of the next layer and each coming layer loaded by the previous layer. A material problem often occurs when the load of the layer is put onto the previous layer; it shows a slump problem. An effort for this challenge by using no slump material but no slump material has a problem while pumping the material, so it is a challenge faced during the experiments.

5.2.4. Avoid Cracking Around the Corners

Another common problem faced while working on 3D construction is cracking around the corners of the object to be printed. Cracking around the corner comes because of the fast nozzle speed around the corners. So this is a challenge to the product's strength that has been faced generally. These are some challenges observed during the review of previous studies. The following section will suggest future work and highlight the research gap for the researchers.

5.3. Future Work Recommendations

5.3.1. Multi-Nozzle Combination

A multi-nozzle combination could make possible high achievements and problem solutions in 3D construction printing. It can be done by using multiple nozzles at a single printer, and construction work can be done quicker than before by using a printer at different parts of the object simultaneously, which leads to fast production within a short period. Although, the system will become complex and need proper planning for handling the whole process. Moreover, one benefit is to use different materials from different nozzles simultaneously as per the hybrid construction requirement of the part to be printed.

5.3.2. 3D Construction Printing Hybrid Systems

Hybrid systems for 3D construction printing could be developed. Different materials and various components for structures can be used. For structural and non-structural applications, different grade types of material can be used for 3D printing in B&C in future work projects. For continuous monitoring of constructed buildings, using sensors and actuators in the material will be significantly worth full. These will provide real-time monitoring even during the phase of construction [158]. However, using sensors to get load-bearing properties and improved structural design reinforcement can be used with concrete.

5.3.3. New Material Development

Several friendly efforts were carried out to develop the material for 3D Construction printing using different combinations of cement, sand, flash, and fibers, which is still a challenging task for the researcher [13–14, 46, 159]. The success of 3D printing is majorly dependent on the development of new materials having properties according to

each application. The material should contain functionality added values of light weight, thermal insulation, low cost, good setting time, enough mechanical strength, and good flow ability to be effective for future complex and large-scale construction [160–162]. However, the future of 3D printing is bright and has the potential to print complex and large-scale structures, as most researchers believe.

5.3.4. Property of Reinforcement

The low tensile strength and ductility of concrete is another major challenge for 3D printing in B&C. Adding steel reinforcement can solve this problem, but in the case of the 3D printing process, reinforcement of steel automatically is not straightforward compared to conventional one. Imbedding and post-tensioning reinforcements can be inserted manually instead of automatically [50, 56]. Vertical direction tensile strength could be increased using a steel extrusion gun similar to the staple gun at the back of the nozzle. Although to control the force of steel staple penetrating the filament would be a challenge. There could be two possibilities of force: fresh concrete will be destroyed if the force is too large, while there will be no penetration if there is a too small force. Using fibers in steel reinforcement will improve the ductility of concrete material.

5.3.5. Optimization of Printing Parameters

3D Concrete printing is significantly affected by printing parameters such as printing speed, the flow rate of the material, and the thickness of printing material layers because these properties play an essential role during the construction process [86]. Precautions are necessary to adjust these parameters. If something goes wrong, it will lead to severe failure and lousy printing quality. The major limitation in the printing process is void formation, which causes uneven material layers. Studies showed that this layering effect could be controlled by the proper selection of the layer thickness, but the time required would be more to complete the product if the layer thickness is too small. So printing time, layer thickness, and surface finish of the output product should be considered to print an object [163]. Finally, the overall surface quality can be improved by using post-processing such as grinding or plastering.

5.3.6. Life Cycle Assessment (LCA) for 3D Concrete Printing

In the construction industry, while the more significant impact of industries on the environment, Concrete 3D printing delivered a green and clean construction process without waste of material during construction compared to conventional methods. Researchers highlighted the environmental benefits of using material-efficient design in digitally fabricated architecture [164]. In these studies, the main focus was digital fabrication instead of 3D printing, which is related to some extent and necessary. There is a research gap in this study, and LCA must be used to assess

the environmental impacts of all stages of the product life & process and the impact of 3D printing improvement on the environment.

5.3.7. Life Cycle Cost Analysis (LCCA) for Concrete 3D Printing

There is a lack of fundamental understanding of economics found in the past studies, and it should be included in future research as it can be helpful in 3D concrete printing. This way, an early analysis of the relationship between cost and design parameters could be proposed. The primary objective of LCCA is to achieve the lowest possible total cost of design, production rate, part disposal, product use, and product development [165]. Incorporating the LCCA system with a 3D concrete printing process will save all the process stages. The process will improve production rate, total cost, and product design.

5.3.8. Requirement of Safety and Skills

Safety on the construction site is one of the biggest challenges observed and proved by the studies. During designing preventive security systems, collisions, falling on the machine, and machines running over should be considered [166]. A physical barrier is necessary during the printing process to prevent the workers from a collision with the moving parts of the machinery. A safety video camera should be installed on the work site to avoid accidents and continuously monitor by safety management staff during construction [165, 166].

Another major challenge is the requirement for workers to have experience in both robotic and civil site work. Knowledge of printing parameters and material properties significantly impacts the design's quality and limitations. The 3D printing industry expects to grow significantly by 2022, as recent research shows the quickness in this field. Hence, existing workers need new skills for 3D concrete printing instead of conventional methods, and much research is needed to understand and overcome all challenges.

6. CONCLUSIONS

In conclusion, Concrete 3D printing in B&C is an emerging method that has the potential to revolutionize the traditional building and construction methods by providing the benefits in terms of low cost, high efficiency in automatic construction, freedom of design, and reduction of labor cost and risk of injury during the construction at working site. The main challenge is the development of appropriate material for continuous extrusion from the nozzle and stacking of depositing material layers over one another and should be able to bear a load of subsequent layers without destruction or deformation and collapse. For this purpose, some simulation work can be done to check the behavior of different materials under loaded conditions, which will be helpful for future work.

Concrete 3D printing use in large-scale buildings construction needs some requirements such as the development of building information modeling (BIM), degree of requirements at mass customization scale, and the essential requirement is the life cycle cost analysis of 3D printed projects/ products. The life cycle performance of the printed projects remains unclear as 3D printing construction is still growing. However, BIM can examine printed objects based on shape, performance, and assembly levels. Furthermore, the construction industry partially examined the degree of customization and categorization based on projects.

There is no need to abolish traditional construction methods altogether because the construction industry's future will most likely be a hybrid process that will simultaneously take advantage of both conventional and 3D printing technologies. By overcoming these obstacles, it is expected that 3D printing construction will reach its full potential in the building and construction industry.

ACKNOWLEDGEMENTS

The authors are grateful for the financial support from the Chinese Government Scholarship Council to fulfill the research requirements in the field of additive manufacturing-concrete 3D printing.

DATA AVAILABILITY STATEMENT

The authors confirm that the data that supports the findings of this study are available within the article. Raw data that support the finding of this study are available from the corresponding author, upon reasonable request.

CONFLICT OF INTEREST

The authors declare that they have no conflict of interest.

FINANCIAL DISCLOSURE

The authors declared that this study has received no financial support.

PEER-REVIEW

Externally peer-reviewed.

REFERENCES

- [1] Janis, R., Nerella, V. N., Mechtcherine, V., & Meschke, G. (2022). Extrusion process simulation and layer shape prediction during 3D-concrete-printing using the Particle Finite Element Method. *Automation in Construction*, 136, Article 104173. [CrossRef]
- [2] Mustafa, B., Jotangia, R., Baaj, M. Y., & Mousleh, I. (2022). 3D concrete printing for sustainable and economical construction: A comparative study. *Automation in Construction*, 134, Article 104087. [CrossRef]
- [3] Clément, G., Duballet, R., Roux, P., Gaudillière, N., Dirrenberger, J., & Morel, P. (2016). Large-scale 3D printing of ultra-high performance concrete—a new

- processing route for architects and builders. *Materials & Design*, 100, 102–109. [CrossRef]
- [4] Behrokh, K., & Dutton, R. (1998). Innovative rapid prototyping process makes large sized, smooth surfaced complex shapes in a wide variety of materials. *Materials Technology*, 13(2), 53–56. [CrossRef]
- [5] Ruper, S., & Andreen, D. (2012). The role of additive manufacturing and physiometric computational design for digital construction. *Architectural Design*, 82(2), 126–135. [CrossRef]
- [6] Starr, M. J. C. (2015). World's first 3D-printed apartment building constructed in China. www.cnet.com/news/worlds-first-3d-printed-apartment-building-constructed-in-china
- [7] Shahzad, Q., Wang, X., Wang, W., Wan, Y., Li, G., Ren, C., & Mao, Y. (2020). Coordinated adjustment and optimization of setting time, flowability, and mechanical strength for construction 3D printing material derived from solid waste. *Construction and Building Materials*, 259, Article 119854. [CrossRef]
- [8] Guowei, M., & Wang, L. (2018). A critical review of preparation design and workability measurement of concrete material for largescale 3D printing. *Frontiers of Structural and Civil Engineering*, 12(3), 382–400. [CrossRef]
- [9] John, G. G., Williams, R., Purnell, P., & Farahi E. (2010). 3D Printing of cement composites. *Advances in Applied Ceramics*, 109(5), 287–290. [CrossRef]
- [10] Anne-Kathrin, M., Dezmierean, L., Will, J., & Greil, P. (2011). Three-dimensional printing of flash-setting calcium aluminate cement. *Journal of Materials Science*, 46(9), 2947–2954. [CrossRef]
- [11] Behrokh, K., Bukkapatnam, S., Kwon, H., & Saito J. (2001). Experimental investigation of contour crafting using ceramics materials. *Rapid Prototyping Journal*, 7(1), 32–42. [CrossRef]
- [12] Perrot, A., Rangeard, D., Pierre, A. J. M. (2016). Structures, Structural built-up of cement-based materials used for 3D-printing extrusion techniques. *Materials and Structures*, 49(4), 1213–1220. [CrossRef]
- [13] Lim, S., Buswell, R. A., Le T. T., Austin, S. A., Gibb, A. G., & Thorpe, T. J. A. (2012). Developments in construction-scale additive manufacturing processes. *Automation in Construction*, 21, 262–268. [CrossRef]
- [14] Feng, P., Meng, X., Chen, J.-F., & Ye L. (2015). Materials, Mechanical properties of structures 3D printed with cementitious powders. *Construction and Building Materials*, 93, 486–497. [CrossRef]
- [15] Gosselin, C., Duballet, R., Roux, P., Gaudillière, N., Dirrenberger, J., & Morel P. (2016). Design, Large-scale 3D printing of ultra-high performance concrete—a new processing route for architects and builders. *Materials & Design*, 100, 102–109. [CrossRef]
- [16] Mazloom, M., Ramezani-pour, A., & Brooks, J. (2004). Effect of silica fume on mechanical properties of high-strength concrete. *Cement and Concrete Composites*, 26(4), 347–357. [CrossRef]
- [17] Aqel, M., & Panesar D. K. (2016). Materials, hydration kinetics and compressive strength of steam-cured cement pastes and mortars containing limestone filler. *Construction and Building Materials*, 113, 359–368. [CrossRef]
- [18] Brooks, J. J., Johari, M. A. M., & Mazloom, M. (2000). Effect of admixtures on the setting times of high-strength concrete. *Cement and Concrete Composites*, 22(4), 293–301. [CrossRef]
- [19] Bouzoubaa, N., & Lachemi, M. (2001). Self-compacting concrete incorporating high volumes of class F fly ash: Preliminary results. *Cement and Concrete Research*, 31(3), 413–420. [CrossRef]
- [20] Plank, J., & Winter, C. (2008). Competitive adsorption between superplasticizer and retarder molecules on mineral binder surface. *Cement and Concrete Research*, 38(5), 599–605. [CrossRef]
- [21] Agarwal, S. K., Masood, I., & Malhotra, S. K. (2000). Compatibility of superplasticizers with different cements. *Construction and Building Materials*, 14(5), 253–259. [CrossRef]
- [22] Nkinamubanzi, P.-C., & Aïtcin, P.-C. (2004). Cement and superplasticizer combinations: compatibility and robustness. *Cement, Concrete and Aggregate*, 26(2), 1–8. [CrossRef]
- [23] Lachemi, M., Hossain, K., Lambros, V., Nkinamubanzi, P.-C., & Bouzoubaa, C. (2004). Performance of new viscosity modifying admixtures in enhancing the rheological properties of cement paste. *Cement and Concrete Composites*, 34(2), 185–193. [CrossRef]
- [24] Soroka, I. (1984). The determination of setting time of portland cement by the vicat test. *Cement and Concrete Research*, 14(6), 884–886. [CrossRef]
- [25] Valič, M. I. (2000). Hydration of cementitious materials by pulse echo USWR: method, apparatus and application examples. *Cement and Concrete Research*, 30(10), 1633–1640. [CrossRef]
- [26] Kamada, T., Uchida, S., & Rokugo, K. (2005). Non-destructive evaluation of setting and hardening of cement paste based on ultrasonic propagation characteristics. *Journal of Advanced Concrete*, 3(3), 343–353. [CrossRef]
- [27] Voigt, T., Grosse, C. U., Sun, Z., Shah, S.P., & Reinhardt, H. (2005). Comparison of ultrasonic wave transmission and reflection measurements with P- and S-waves on early age mortar and concrete. *Materials and Structures*, 38(8), 729–738. [CrossRef]
- [28] Sharma, S., & Mukherjee A. (2015). Monitoring

- freshly poured concrete using ultrasonic waves guided through reinforcing bars. *Cement and Concrete Composites*, 55, 337–347. [CrossRef]
- [29] Sharma, S., & Mukherjee, A. (2014). Ultrasonic guided waves for monitoring the setting process of concretes with varying workabilities. *Construction and Building Materials*, 72, 358–366. [CrossRef]
- [30] Liu, S., Zhu, J., Seraj, S., Cano, R., & Juenger, M. (2014). Monitoring setting and hardening process of mortar and concrete using ultrasonic shear waves. *Construction and Building Materials*, 72, 248–255. [CrossRef]
- [31] Kothman, I., & Faber, N. (2016). How 3D printing technology changes the rules of the game: Insights from the construction sector. *Journal of Manufacturing Technology*, 27(7), 932–943. [CrossRef]
- [32] Shahzad, Q., Shen, J., Naseem, R., Yao, Y., Waqar, S., & Liu, W. (2021). Influence of phase change material on concrete behavior for construction 3D printing. *Construction and Building Materials*, 309, Article 125121. [CrossRef]
- [33] Lloret, E., Shahab, A. R., Linus, M., Flatt, R. J., Gramazio, F., Kohler, M., & Langenberg, S. (2015). Complex concrete structures: merging existing casting techniques with digital fabrication. *Computer-Aided Design*, 60, 40–49. [CrossRef]
- [34] Aejmelaeus-Lindström, P., Willmann, J., Tibbits, S., Gramazio, F., & Kohler, M. (2016). Jammed architectural structures: towards large-scale reversible construction. *Granular Matters*, 18(2), 28. [CrossRef]
- [35] Shahzad, Q., Wang, X., Wang, W., Wan, Y., Li, G., Ren, C., & Mao, Y. (2020). Coordinated adjustment and optimization of setting time, flowability, and mechanical strength for construction 3D printing material derived from solid waste. *Construction and Building Materials*, 259, Article 119854. [CrossRef]
- [36] Lim, S., Buswell, R. A., Valentine, P. J., Piker, D., Austin, S.A., & De Kestelier X. (2016). Modelling curved-layered printing paths for fabricating large-scale construction components. *Additive Manufacturing*, 12, 216–230. [CrossRef]
- [37] Yoshida, H., Igarashi, T., Obuchi, Y., Takami, Y., Sato, J., Araki, M., Miki, M., Nagata, K., Sakai, K., & Igarashi, S. (2015). Architecture-scale human-assisted additive manufacturing. *ACM Journals*, 34(4), 88. [CrossRef]
- [38] Le, T. T., Austin, S. A., Lim, S., Buswell R. A., Gibb, A. G. F., & Thorpe, T. (2012). Mix design and fresh properties for high-performance printing concrete. *Materials and Design*, 45(8), 1221–1232. [CrossRef]
- [39] Williams, R. L. II, Albus, J. S., & Bostelman R. V. (2004). Self-contained automated construction deposition system. *Automation in Construction*, 13(3), 393–407. [CrossRef]
- [40] Perkins, I., & Skitmore, M. (2015). Three-dimensional printing in the construction industry: A review. *International Journal of Construction*, 15(1), 1–9. [CrossRef]
- [41] Capua A., Shapiro A., & Shoal S. (2014). Theory, SpiderBot: a cable-suspended walking robot. *Mechanism and Machine Theory*, 82, 56–70. [CrossRef]
- [42] Oxman, N. Duro-Royo, J., Keating S., Peters, B., & Tsai, E. (2014). Towards robotic swarm printing. *Architectural Design*, 84(3), 108–115. [CrossRef]
- [43] Kwon, H., Bukkapatnam, S., Khoshnevis, B., & Saito, J. (2002). Effects of orifice shape in contour crafting of ceramic materials. *Rapid Prototyping*, 8(3) 147–160. [CrossRef]
- [44] Craveiro, F., Bártolo, H., & Bártolo, P. J. (2013). Functionally graded structures through building manufacturing. *Advanced Materials Research*, 683, 775–778. [CrossRef]
- [45] Le, T. T., Austin, S. A., Lim, S., Buswell, R. A., Law, R., Gibb, A. G., & Thorpe, T. (2012). Hardened properties of high-performance printing concrete. *Cement and Concrete Research*, 42(3), 558–566. [CrossRef]
- [46] Weger, D., Lowke, D., & Gehlen, C. (2016). 3D printing of concrete structures using the selective binding method—Effect of concrete technology on contour precision and compressive strength. Proceedings of 11th fib international PhD symposium in civil engineering, The University of Tokyo, Tokyo, 403–410.
- [47] Rictor, A., & Riley, B. (2016). Optimization of a heated platform based on statistical annealing of critical design parameters in a 3D printing application. *Procedia Computer Science*, 83, 712–716. [CrossRef]
- [48] Biljecki, F., Stoter, J., Ledoux, H., Zlatanova, S., & Çöltekin, A. (2015). Applications of 3D city models: State of the art review. *International Journal of Geo-information*, 4(4), 2842–2889. [CrossRef]
- [49] Khoshnevis, B., Hwang, D., Yao, K.-T., & Yeh, Z. (2006). Mega-scale fabrication by contour crafting. *Systems Engineering*, 1(3), 301–320. [CrossRef]
- [50] Cesaretti G., Dini E., De Kestelier, X., Colla, V., & Pambaguian L. (2014). Building components for an outpost on the Lunar soil by means of a novel 3D printing technology. *Acta Astronautica*, 93, 430–450. [CrossRef]
- [51] Panda B.N., Bahubalendruni R. M., Biswal B. B., & Leite M. (2017). A CAD-based approach for measuring volumetric error in layered manufacturing. *Proceedings of the Institution of Mechanical Engineers Part C: Journal of Mechanical Engineering Science*, 231(13), 2398–2406. [CrossRef]
- [52] Hwang, D., Khoshnevis B., Daniel E. (2004). Concrete wall fabrication by contour crafting, 21st International Symposium on Automation and Robotics in Construction (ISARC 2004), Jeju, South Korea,

- Robotics in Construction*, 301–307. [CrossRef]
- [53] Khoshnevis, B. (2004). Automated construction by contour crafting—related robotics and information technologies. *Automation in Construction*, 13(1), 5–19. [CrossRef]
- [54] Hwang, D., Khoshnevis, B. (2005). *An innovative construction process-contour crafting (CC)*. 22nd International Symposium on Automation and Robotics in Construction [CrossRef].
- [55] Lim, S., Buswell, R. A., Le, T. T., Wackrow, R., Austin, S. A., Gibb, A. G., & Thorpe, T. (2011). *Development of a viable concrete printing process*. 28th International Symposium on Automation and Robotics in Construction (ISARC2011), 29 Jun - 2 Jul 2011, Seoul, South Korea, pp. 665–670. [CrossRef]
- [56] Bos, F., Wolfs, R., Ahmed, Z., Salet, T. (2016). Additive manufacturing of concrete in construction: potentials and challenges of 3D concrete printing. *Virtual and Physical Prototyping*, 11(3), 209–225. [CrossRef]
- [57] Keating, S.J., Leland, J. C., Cai, L., & Oxman, N. (2017). Toward site-specific and self-sufficient robotic fabrication on architectural scales. *Science Robotics*, 2(5), eaam8986. [CrossRef]
- [58] Nan, C. (2015). *A new machinecraft*. International Conference on Computer-Aided Architectural Design Futures, (pp. 422–438). Springer. [CrossRef]
- [59] Hack, N., & Lauer W. V. (2014). Mesh-mould: Robotically fabricated spatial meshes as reinforced concrete formwork. *Architectural Design*, 84(3), 44–53. [CrossRef]
- [60] Eastman, C., Teicholz, P., Sacks, R., Liston, K. (2011). *BIM handbook: A guide to building information modeling for owners, managers, designers, engineers and contractors*. John Wiley & Sons.
- [61] Arayici, Y., Egbu, C., & Coates, P. (2012). Building information modelling (BIM) implementation and remote construction projects: issues, challenges, and critiques. *Journal of Information Technology in Civil Engineering*, 17, 75–92.
- [62] Elmualim A., & Gilder J. (2014). BIM: innovation in design management, influence and challenges of implementation. *Architectural Engineering and Design*, 10(3–4), 183–199. [CrossRef]
- [63] Wu, P., Wang, J., & Wang, X. (2016). A critical review of the use of 3-D printing in the construction industry. *Automation in Construction*, 68, 21–31. [CrossRef]
- [64] Buswell, R. A., Soar, R. C., Gibb, A.G., Thorpe, A. (2007). Freeform construction: mega-scale rapid manufacturing for construction. *Automation in Construction*, 16(2), 224–231. [CrossRef]
- [65] Kazemian, A., Yuan, X., Cochran, E., & Khoshnevis, B. (2017). Cementitious materials for construction-scale 3D printing: Laboratory testing of fresh printing mixture. *Construction and Building Materials*, 145, 639–647. [CrossRef]
- [66] Singh, M. M., Sawhney, A., & Sharma, V. (2017). Utilising building component data from BIM for formwork planning. *Economics and Building*, 17(4), 20–36. [CrossRef]
- [67] Lawson, N., Douglas, I., Garvin, S. McGrath, C., Manning, D., & Vetterlein, J. (2001). Health, Recycling construction and demolition wastes—a UK perspective. *Environmental Management and Health*, 12(2), 146–157. [CrossRef]
- [68] Chua, C. K., & Leong, K.F. (2014). *3D Printing and Additive Manufacturing: Principles and Applications (with Companion Media Pack) of Rapid Prototyping*. (Fourth ed). World Scientific Publishing Company. [CrossRef]
- [69] Gardiner, J. (2011). *Exploring the emerging design territory of construction 3D printing-project led architectural research* [Unpublished Doctorial Thesis]. School of Architecture and Design, Design and Social Context Portfolio RMIT University.
- [70] Edgar J., & Tint, S. (2015). Additive manufacturing technologies: 3D printing, rapid prototyping, and direct digital manufacturing. *Technology Review*, 59(3), 193–198. [CrossRef]
- [71] Kwon, H. K. (2007). *Initial investigation of 3D free form fabrication Using Contour Crafting*. Proceedings of the Safety Management and Science Conference, 27–37.
- [72] Pegna, J. J. (1997). Exploratory investigation of solid freeform construction. *Automation in Construction*, 5(5), 427–437. [CrossRef]
- [73] Dos Reis, A. F. (2017). *Antunes, BIM-based parametric optimisation of structural systems* [Unpublished Master Thesis]. Tecnico Lisboa.
- [74] Wolfs, R. R. (2015). *3D printing of concrete structures* (Publication No. A-2015.85) [Master dissertation, Eindhoven University of Technology]. ProQuest Dissertations & Theses Global.
- [75] Nerella, V., Krause, M., & Näther, V. (2016). Mechtcherine, 3D printing technology for on-site construction. *Concrete in Australia*, 42(3), 36–39.
- [76] Ma, G., Wang, L. & Ju, Y. (2018). State-of-the-art of 3D printing technology of cementitious material—An emerging technique for construction. *Technological Sciences*, 61(4), 475–495. [CrossRef]
- [77] Paul, S. C., van Zijl, G. P. Tan, M. J., Gibson, I. (2018). A review of 3D concrete printing systems and materials properties: Current status and future research prospects. *Rapid Prototyping Journal*, 24(4), 784–798. [CrossRef]
- [78] Silva, R., Sereno, P., Mateus, A., Mitchell, G. R., Carreira, P., Santos, C., Vitorino, J., & Domingues,

- J. (2019). Adaptive platforms and flexible deposition system for big area additive manufacturing (BAAM). *Applied Mechanics and Materials*, 890, 3–20. [CrossRef]
- [79] Nerella, V.N., Krause, M., & Mechtcherine, V. (2019). Practice-oriented buildability criteria for developing 3d-printable concretes in the context of digital construction. *Automation in Construction*, 109. Preprint doi: 10.1016/j.autcon.2019.102986. [CrossRef]
- [80] Furet, B., Poullain, P., & Garnier, S. (2019). 3D printing for construction based on a complex wall of polymer-foam and concrete. *Additive Manufacturing*, 28, 58–64. [CrossRef]
- [81] Klaudius, H., Talke, D., & Bau, F. Z. (2016). *Additive fertigung frei geformter bauelemente durch numerisch gesteuerte extrusion von holzleichtbeton* [Unpublished Master Thesis]. Technische Universität München. [Deutsch]
- [82] Liu, Z., Li, M., Weng, Y., Wong, T.N., & Tan, M. J. (2019). Mixture Design Approach to optimize the rheological properties of the material used in 3D cementitious material printing. *Construction and Building Materials*, 198, 245–255. [CrossRef]
- [83] Wolfs, R., Bos, F., & Salet, T. J. C. (2018). Early age mechanical behaviour of 3D printed concrete: Numerical modelling and experimental testing. *Cement and Concrete Research*, 106 103–116. [CrossRef]
- [84] Visser, C. R. (2007). *Mechanical and structural characterisation of extrusion moulded* [Unpublished Master Thesis]. Stellenbosch University.
- [85] Labonnote, N., Rønquist, A., Manum, B., Rührter, P. (2016). Additive construction: State-of-the-art, challenges and opportunities. *Automation in Construction*, 72, 347–366. [CrossRef]
- [86] Kwon, H. (2002). *Experimentation and analysis of contour crafting (CC) process using uncured ceramic materials* [Unpublished Master Thesis]. University of Southern California.
- [87] Kaszyńska, M., Hoffmann, M., Skibicki, S., Zieliński, A., Techman, M., Olczyk, N., & Wróblewski, T. (2018). Evaluation of suitability for 3D printing of high performance concretes, MATEC Web of Conferences. EDP Sciences, Article 01002. [CrossRef]
- [88] Ma G., Li Z., & Wang L. (2018). Printable properties of cementitious material containing copper tailings for extrusion based 3D printing. *Construction and Building Materials*, 162, 613–627. [CrossRef]
- [89] Malaeb, Z., Hachem, H., Tourbah, A., Maalouf, T., El Zarwi, N., & Hamzeh, F. (2015). 3D concrete printing: machine and mix design. *Materials Science*, 6(6), 14–22.
- [90] Haymond, L. (2008). *Full scale contour crafting applications* (Publication No. 1454117) [Master dissertation, Faculty of the School of Architecture University of Southern California]. ProQuest Dissertations & Theses Global.
- [91] Secrieru, E., Mechtcherine, V., Schröfl, C., Borin, D. (2016). Rheological characterisation and prediction of pumpability of strain-hardening cement-based-composites (SHCC) with and without addition of superabsorbent polymers (SAP) at various temperatures. *Construction and Building Materials*, 112, 581–594. [CrossRef]
- [92] Pierre, A., Lanos, C., & Estellé P. (2013). Extension of spread-slump formulae for yield stress evaluation. *Applied Rheology*, 23(6), 36–44.
- [93] Roussel, N., & Coussot, P. (2005). “Fifty-cent rheometer” for yield stress measurements: from slump to spreading flow. *Journal of Rheology*, 49(3), 705–718. [CrossRef]
- [94] Jolin, M., Burns, D., Bissonnette, B., Gagnon, F., & Bolduc, L.-S. (2009). *Understanding the pumpability of concrete*. Proceedings Shotcrete for Underground Support XI Engineering Conferences International.
- [95] Mechtcherine, V., Nerella, V.N., Kasten, K. (2014). Testing pumpability of concrete using Sliding Pipe Rheometer. *Construction and Building Materials*, 53, 312–323. [CrossRef]
- [96] Vasić, M. (2016). *Vpliv vrste veziva na lastnosti sanacijskih ometov* [Unpublished Master Thesis]. Univerza v Ljubljani.
- [97] Taylor, M., & Sanjayan, J. (2020). Mesh reinforcing method for 3D Concrete Printing. *Automation in Construction*, 109, Article 102992. [CrossRef]
- [98] Shao, Y. & Shah S. P. (1997). Mechanical properties of PVA fiber reinforced cement composites fabricated by extrusion processing. *Materials Journal*, 94(6), 555–564. [CrossRef]
- [99] Akkaya, Y., Peled, A., & Shah, S.P. (2020). Parameters related to fiber length and processing in cementitious composites. *Materials and Structures*, 33(8), 515–524. [CrossRef]
- [100] Hambach, M., Rutzen, M., & Volkmer, D. (2019). Properties of 3D-printed fiber-reinforced Portland cement paste, 3D Concrete Printing Technology. (pp. 73–113). Elsevier. [CrossRef]
- [101] Claisse, P. A., Lorimer, P., & Al Omari, M. (2001). Workability of cement pastes. *American Concrete*, 98(6), 476–482. [CrossRef]
- [102] Lee, S. H., Kim, H. J., Sakai, E., & Daimon, M. (2003). Effect of particle size distribution of fly ash–cement system on the fluidity of cement pastes. *Cement and Concrete Research*, 33(5), 763–768. [CrossRef]
- [103] Park, C. K., Noh, M., & Park, T. H. (2005). Rheological properties of cementitious materials containing mineral admixtures. *Cement and Concrete Research*, 35(5), 842–849. [CrossRef]
- [104] Burgos-Montes, O., Palacios, M., Rivilla, P., & Puer-

- tas, F. (2012). Compatibility between superplasticizer admixtures and cements with mineral additions. *Construction and Building Materials*, 31, 300–309. [CrossRef]
- [105] Grzeszczyk, S., & Lipowski, G. Effect of content and particle size distribution of high-calcium fly ash on the rheological properties of cement pastes. *Cement and Concrete Research*, 27(6), 907–916. [CrossRef]
- [106] Kwan, A., & Wong, H. H. C. (2008). Effects of packing density, excess water and solid surface area on flowability of cement paste. *Advances in Cement Research*, 20(1), 1–11. [CrossRef]
- [107] Mastali, M., & Dalvand, A. J. C. (2016). Use of silica fume and recycled steel fibers in self-compacting concrete (SCC). *Construction and Building Materials*, 125, 196–209. [CrossRef]
- [108] Güneşli, E., Gesoğlu, M., Al-Goody, A., & İpek, S. (2015). Fresh and rheological behavior of nano-silica and fly ash blended self-compacting concrete. *Construction and Building Materials*, 95, 29–44. [CrossRef]
- [109] Kong, H.-J., Bike, S.G., & Li, V. C. (2003). Composites, Development of a self-consolidating engineered cementitious composite employing electrosteric dispersion/stabilization. *Cement and Concrete Composites*, 25(3), 301–309. [CrossRef]
- [110] Mardani-Aghabaglou, A., Tuyan, M., Yılmaz, G., Arıöz, Ö., Ramyar, K. (2013). Effect of different types of superplasticizer on fresh, rheological and strength properties of self-consolidating concrete. *Construction and Building Materials*, 47 1020–1025. [CrossRef]
- [111] Singh, S., Munjal, P., & Thammishetti, N. (2015). Role of water/cement ratio on strength development of cement mortar. *Journal of Building Engineering*, 4, 94–100. [CrossRef]
- [112] Leemann, A., Winnefeld, F. (2007). The effect of viscosity modifying agents on mortar and concrete. *Cement and Concrete Composite*, 29(5), 341–349. [CrossRef]
- [113] Robeyst, N., Gruyaert, E., Grosse, C. U., & De Belie, N. (2008). Monitoring the setting of concrete containing blast-furnace slag by measuring the ultrasonic p-wave velocity, *Cement and Concrete Research*, 38(10), 1169–1176. [CrossRef]
- [114] Gesoğlu, M., & Özbay, E. (2007). Effects of mineral admixtures on fresh and hardened properties of self-compacting concretes: binary, ternary and quaternary systems. *Materials and Structures*, 40(9), 923–937. [CrossRef]
- [115] Kim, J., Ryu, J., & Hooton, R. D. (2008). Evaluation of strength and set behavior of mortar containing shotcrete set accelerators. *Canadian Journal of Civil Engineering*, 35(4), 400–407. [CrossRef]
- [116] Maltese, C., Pistolesi, C., Bravo, A., Cella, F., Cerulli, T., & Salvioni, D. (2007). A case history: Effect of moisture on the setting behaviour of a Portland cement reacting with an alkali-free accelerator. *Cement and Concrete Research*, 37(6), 856–865. [CrossRef]
- [117] Galobardes, I., Salvador, R. P., Cavalaro, S. H., de Figueiredo, A. D., & Goodier, C. I. (2016). Adaptation of the standard EN 196-1 for mortar with accelerator. *Construction and Building Materials*, 127, 125–136. [CrossRef]
- [118] Li, Z., Wang, L., & Ma, G. (2018). Method for the enhancement of buildability and bending resistance of 3D printable tailing mortar. *International Journal of Concrete*, 12(1), 37. [CrossRef]
- [119] Gesoğlu, M., & Güneşli, E. (2007). Strength development and chloride penetration in rubberized concretes with and without silica fume. *Materials and Structures*, 40(9), 953–964. [CrossRef]
- [120] Klobes, P., Rübner, K., Hempel, S., & Prinz, C. (2008). *Investigation on the microstructure of ultra high performance concrete*. Characterisation of Porous Solids VIII. Proceedings of the 8th International Symposium on the Characterisation of Porous Solids.
- [121] Benaicha, M., Roguiez, X., Jalbaud, O., Burtschell, Y., & Alaoui, A.H. (2015). Influence of silica fume and viscosity modifying agent on the mechanical and rheological behavior of self compacting concrete. *Construction and Building Materials*, 84, 103–110. [CrossRef]
- [122] Panda, B., Unluer, C., Tan, M. (2018)., Investigation of the rheology and strength of geopolymer mixtures for extrusion-based 3D printing. *Cement and Concrete Composites*, 94, 307–314. [CrossRef]
- [123] Sobolev, K., Flores, I., Torres-Martinez, L. M., Valdez, P., Zarazua, E., & Cuellar E. (2009). Engineering of SiO₂ nanoparticles for optimal performance in nano cement-based materials. *Nanotechnology in Construction*, 3, 139–148. [CrossRef]
- [124] Jo, B.-W., Kim, C.-H., Tae, G.-H., & Park, J.-B. (2007). Characteristics of cement mortar with nano-SiO₂ particles. *Construction and Building Materials*, 21(6), 1351–1355. [CrossRef]
- [125] Sanchez, F., & Sobolev, K. (2010). Nanotechnology in concrete—a review. *Construction and Building Materials*, 24(11), 2060–2071. [CrossRef]
- [126] Malhotra, V. M., Zhang, M.-H., Read, P. H., & Ryell, J. (2000). Long-term mechanical properties and durability characteristics of high-strength/high-performance concrete incorporating supplementary cementing materials under outdoor exposure conditions. *Materials Journal*, 97(5), 518–525. [CrossRef]
- [127] Liu, B., Xie, Y., Zhou, S., & Yuan, Q. (2000). Influ-

- ence of ultrafine fly ash composite on the fluidity and compressive strength of concrete. *Cement and Concrete Research*, 30(9), 1489–1493. [CrossRef]
- [128] Ghezal, A., & Khayat, K. H. (2002). Optimizing self-consolidating concrete with limestone filler by using statistical factorial design methods. *Materials Journal*, 99(3), 264–272. [CrossRef]
- [129] Lee, S.-J., & Won J.-P. (2016). Shrinkage characteristics of structural nano-synthetic fibre-reinforced cementitious composites. *Composite Structures*, 157 236–243. [CrossRef]
- [130] Bissonnette, B., Attiogbe, E. K., Miltenberger, M. A., & Fortin, C. (2007). Drying shrinkage, curling, and joint opening of slabs-on-ground. *ACI Materials*, 104(3), 259. [CrossRef]
- [131] Zhang, J., Gong, C., Guo, Z., & Zhang, M. (2009). Engineered cementitious composite with characteristic of low drying shrinkage. *Cement and Concrete Research*, 39(4), 303–312. [CrossRef]
- [132] Khatib, J. M. (2008). Performance of self-compacting concrete containing fly ash. *Construction and Building Materials*, 22(9), 1963–1971. [CrossRef]
- [133] Rongbing, B., & Jian, S. (2005). Synthesis and evaluation of shrinkage-reducing admixture for cementitious materials. *Cement and Concrete Research*, 35(3), 445–448. [CrossRef]
- [134] Güneş, E., Gesoğlu, M., Karaoğlu, S., & Mermerdaş, K. (2012). Strength, permeability and shrinkage cracking of silica fume and metakaolin concretes. *Construction and Building Materials*, 34, 120–130. [CrossRef]
- [135] Al-Khaja, W. A. (1994). Strength and time-dependent deformations of silica fume concrete for use in Bahrain. *Construction and Building Materials*, 8(3), 169–172. [CrossRef]
- [136] Li, J., & Yao, Y. (2001). Research, A study on creep and drying shrinkage of high performance concrete. *Cement and Concrete Research*, 31(8), 1203–1206. [CrossRef]
- [137] Bhanja, S., & Sengupta, B. (2005). Influence of silica fume on the tensile strength of concrete. *Cement and Concrete Research*, 35(4), 743–747. [CrossRef]
- [138] Sellevold, E.J. (1987). *The function of condensed silica fume in high strength concrete*. Symposium on Utilization of HSC, Trondheim, Norway, 39–50.
- [139] Shah, S., Karaguller, M. E., & Sarigaphuti, M. (1992). Effects of shrinkage-reducing admixtures on restrained shrinkage cracking of concrete. *Materials Journals*, 89(3), 289–295. [CrossRef]
- [140] Wongkornchaowalit, N., & Lertchirakarn, V. (2011). Setting time and flowability of accelerated Portland cement mixed with polycarboxylate superplasticizer. *Journal of Endodontics*, 37(3), 387–389. [CrossRef]
- [141] Zhang, D.-F., Ju, B.-Z., Zhang, S.-F., He, L., & Yang, J.-Z. (2007). The study on the dispersing mechanism of starch sulfonate as a water-reducing agent for cement. *Carbohydrate Polymers*, 70(4), 363–368. [CrossRef]
- [142] El-Gamal, S. M., Al-Nowaiser, F. M., & Al-Baity, A. O. (2012). Effect of superplasticizers on the hydration kinetic and mechanical properties of Portland cement pastes. *Journal of Advanced Research*, 3(2), 119–124. [CrossRef]
- [143] Chandra, S., & Björnström, J. (2002). Influence of cement and superplasticizers type and dosage on the fluidity of cement mortars—Part I. *Cement and Concrete Research*, 32(10), 1605–1611. [CrossRef]
- [144] Zingg, A., Winnefeld, F., Holzer, L., Pakusch, J., Becker, S., Figi, R., & Gauckler, L. (2009). Composites, Interaction of polycarboxylate-based superplasticizers with cements containing different C3A amounts. *Cement and Concrete Research*, 31(3), 153–162. [CrossRef]
- [145] Gołaszewski, J., & Szwabowski, J. (2004). Influence of superplasticizers on rheological behaviour of fresh cement mortars. *Cement and Concrete Research*, 34(2), 235–248. [CrossRef]
- [146] Zhang, M.-H., Sisomphon, K., Ng, T. S., & Sun, D. J. (2010). Effect of superplasticizers on workability retention and initial setting time of cement pastes. *Construction and Building Materials*, 24(9), 1700–1707. [CrossRef]
- [147] Chandra, S., & Björnström, J. (2002). Influence of superplasticizer type and dosage on the slump loss of Portland cement mortars—Part II. *Cement and Concrete Research*, 32(10), 1613–1619. [CrossRef]
- [148] Salvador, R. P., Cavalaro, S. H., Segura, I., Figueiredo, A. D., & Pérez, J. (2016). Early age hydration of cement pastes with alkaline and alkali-free accelerators for sprayed concrete. *Construction and Building Materials*, 111, 386–398. [CrossRef]
- [149] Zhang, G., Li, G., & Li, Y. (2016). Effects of superplasticizers and retarders on the fluidity and strength of sulphoaluminate cement. *Construction and Building Materials*, 126, 44–54. [CrossRef]
- [150] Khayat, K. H. (1998). Viscosity-enhancing admixtures for cement-based materials—an overview. *Cement and Concrete Composites*, 20(2-3), 171–188. [CrossRef]
- [151] Vinodh, S., Sundararaj, G., Devadasan, S., Kuttalingam, D., & Rajanayagam, D. (2009). Agility through rapid prototyping technology in a manufacturing environment using a 3D printer. *Journal of Manufacturing Technology*, 20(7), 1023–1041. [CrossRef]
- [152] Ren, C., Wang, W., & Li, G. (2017). Preparation of high-performance cementitious materials from industrial solid waste. *Construction and Building Materials*, 152, 39–47. [CrossRef]

- [153] Hodson, H. (April 17, 2013). Robo-builders deliver architects' dreams. <https://www.newscientist.com/article/mg21829135-600-robot-builders-deliver-architects-dreams/>
- [154] Smith, D. (2012). Printed buildings: an international race for the ultimate in automation. *Construction Research and Innovations*, 3(2), 26–31. [CrossRef]
- [155] Duballet, R., Baverel, O., & Dirrenberger, J. (2017). Classification of building systems for concrete 3D printing. *Automation in Construction*, 83, 247–258. [CrossRef]
- [156] Zhang, J., & Khoshnevis, B. (2013). Optimal machine operation planning for construction by Contour Crafting. *Automation in Construction*, 29, 50–67. [CrossRef]
- [157] Jiang, X., & Adeli, H. (2007). Pseudospectra, MUSIC, and dynamic wavelet neural network for damage detection of highrise buildings. *International Journal for Numerical Methods*, 71(5), 606–629. [CrossRef]
- [158] Van Zijl, G. P., Paul, S. C., Tan, M. J. (2016). *Properties of 3D printable concrete*. Conference: 2nd International Conference on Progress in Additive Manufacturing (Pro-AM 2016) At: Nanyang, Singapore.
- [159] Bekas, D., Tsirka, K., Baltzis, D., & Paipeti, A. S. (2016). Self-healing materials: A review of advances in materials, evaluation, characterization and monitoring techniques. *Composites Part B*, 87, 92–119. [CrossRef]
- [160] Mahamood, R. M., Akinlabi E. T., Shukla M., & Pityana S. (2014). Revolutionary additive manufacturing: an overview. *Lasers in Engineering*, 27(3), 161–178.
- [161] Park, J.-M., Kwon, D.-J., Wang, Z.-J., & DeVries, K. (2015). Review of self-sensing of damage and interfacial evaluation using electrical resistance measurements in nano/micro carbon materials-reinforced composites. *Advanced Composite*, 24(3), 197–219. [CrossRef]
- [162] Jin, Y.-A., He, Y., Fu J.-Z., Gan, W.-F., & Lin, Z.-W. (2014). Optimization of tool-path generation for material extrusion-based additive manufacturing technology. *Additive Manufacturing*, 1, 32–47. [Cross-Ref]
- [163] Agustí-Juan, I., & Habert G. (2016). *An environmental perspective on digital fabrication in architecture and construction*. Proceedings of the 21st International Conference on Computer-Aided Architectural Design Research in Aaia (CAADRIA 2016), CAADRIA, 797–806. [CrossRef]
- [164] Ahuja, J., Panda, T. K., Luthra, S., Kumar, A., Choudhary, S., & Garza-Reyes, J. A. (2019). Do human critical success factors matter in adoption of sustainable manufacturing practices? An influential mapping analysis of multi-company perspective. *Journal of Cleaner Production*, 239, Article 117981. [CrossRef]
- [165] Shin, H.-W., Kim, G.-H., Kim, T.-H., Kim, T.-H., & Choi, E.-K. (2010). The effectiveness of emotional safety using PIR sensors in building construction site. *Journal of Korean Institute of Building Construction*, 10(4), 59–65. [CrossRef]
- [166] Zhou, Z., Irizarry J., & Li, Q. (2013). Applying advanced technology to improve safety management in the construction industry: A literature review. *Construction Management and Economics*, 31(6), 606–622. [CrossRef]



Review Article

Effect of thermal variances on flexible pavements

Michael Toryila TIZA¹, Kavnen JIRGBA², Habibu Abubakar SANI³, Terlumun SESUGH³

¹Directorate of Works and Services, Joseph Sarwuan Tarka University, Makurdi, Nigeria

²Department of Civil Engineering, Joseph Sarwuan Tarka University, Makurdi, Nigeria

³Department of Civil and Environmental Engineering, Air Force Institute of Technology, Kaduna State, Nigeria

ARTICLE INFO

Article history

Received: 28 June 2022

Accepted: 11 August 2022

Key words:

Asphalt, bitumen, pavements, thermal, temperature

ABSTRACT

This article presents recent findings on the effect of thermal variances on pavements. It covers temperature measurement in asphalt pavement; the history of asphalt pavement temperature prediction models, determination of asphalt layer depth temperature; main factors contributing to temperature variations in the asphaltic pavement; energy balance in flexible pavements; asphalt pavement design incorporating the temperature factor; the effect of temperature on the structural performance of asphalt pavement; and environmental factors. The study concluded that temperature substantially affects the asphalt pavement layer's mechanical and physical material characteristics. This study has taken a close look at how pavement temperatures are measured and the models used to predict future temperatures. The research shows that temperature significantly affects the mechanical and physical properties of asphalt pavement layers.

Cite this article as: Tiza, MT., Jirgba, K., Sani, H. A., & Sesugh, T. (2022). Effect of thermal variances on flexible pavements. *J Sustain Const Mater Technol*, 7(3), 221–230.

1. INTRODUCTION

When a mechanistic-empirical method is used to design a flexible pavement, the temperature is the factor that has the most effect on the process. While studies have looked into how climate affects pavement designs, not many have looked into whether or if specific temperature indices connect with distress on the flexible pavement.

Seasonal and daily changes substantially influence the stability of flexible pavements, especially the design process's long-term success in terms of ambient air temperatures, solar radiation, pavement materials and shape, convective surface, and precipitation. The precise forecast of the temperature and their variances is essential for pave-

ment deflection evaluation, pavement modulus back-calculations, frost action estimates, and diurnal and seasonal thermal and cooling impacts assessments.

In selecting the level of asphalt used in various works, it is essential to correctly evaluate the thermal stresses between asphalt layers to precisely forecast asphalt pavement temperatures at various depths and horizontal positions based on thermal conditions. This is particularly important when the asphalt pavement is exposed to severe extremes of freeze and thaw [1]. A precise understanding of the pavement temperature combined with the thermal stress distribution enables a more intelligent choice of asphalt binding grades for different pavements. Lower-grade lower-cost binders may thus be specified for lower lifts where more

*Corresponding author.

*E-mail address: tizamichael@gmail.com



minor temperature changes are usually encountered, and lower-grade lower-cost binders are available for lifts with substantial temperature variations. This difference will be a cost-effective answer to increased pavement expenses [1, 2]. A typical Pavement Structure is presented in Figure 1.

2. TEMPERATURE MEASUREMENT IN ASPHALT PAVEMENT

One significant element for road quality is the asphalt temperature at which the road is constructed but experiences over the past several years indicate a connection between certain other critical variables in road construction, such as compaction, segregation, and temperature [3, 4]. Authorities and construction firms are beginning to think about finding a method to analyze the quality of work and the material by measuring the temperature of the material being supplied and analyzing the thermal variances at different stages from construction to the usage of the pavements [5]. Doing so would better understand a lot, and the process would lead to a better pavement and create new opportunities to improve its quality. Temperature measurement in pavement engineering is fundamental and must not be trivialized. There are many methods and solutions to accomplish it, depending on what and why the pavement temperature needs to be checked or assessed. The temperature is sometimes measured using a sensor in contact with the pavement in question. However, the heat radiation of a substance may also be measured contact-free. This radiation is its infrared surface emission. Both techniques have benefits and are reliable [6, 7].

The binder bitumen is an essential component of asphalt. Bitumen itself is a very temperature-dependent substance. One of the significant reasons why it is essential to pay attention to the temperature of the asphalt material is, On the one hand, asphalt at too low temperatures is not desirable as it leads to many distresses, while on the other hand, excessively high temperatures may have a poor effect on the pavement as it leads to melting of the pavement as is seen in many countries with high temperatures. It is thus essential to operate with asphalt in a specific temperature range [8].

3. CLIMATE AND ENVIRONMENTAL FACTORS

A comprehensive literature analysis was carried out to examine previous studies that captured the impacts of climatic variables on thermal stresses in pavements, particularly concerning ambient air temperature variations. Research indicates that the climate and the environment significantly impact moisture damage and increase distress in flexible pavements [9, 10]. In addition to the quantity of rainfall, sub-surface water in the pavement and other environmental variables may influence the degree of moisture damage to flexible pavements [11].

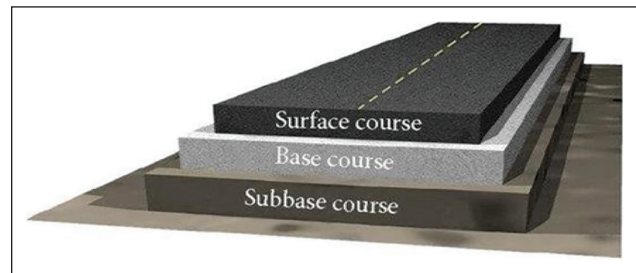


Figure 1. Typical pavement structure [2].

Below are some climatic and environmental variables contributing to Hot Mix Asphalt (HMA) pavement deterioration.

- Heat after the rainfall may generate blisters on the pavement surface, which can form a depression if ruptured [12].
- High precipitation impacts the water in the pavement [12].
- Freezing and thawing pressure and water motions may break up asphalt and encourage deterioration [12].
- Fatigue or low-temperature cracks may encourage peeling because they enable water to enter [11–13].
- Temperature may also influence moisture damage.

Field experience has shown that pavements installed in cold seasons may be more difficult to compact, thus having a higher air vacuum and a more excellent permeability than pavements placed in warm weather. This may enhance the moisture susceptibility of the pavement [13]. In addition to the above, some other essential points responsible for distresses in pavements to be considered are;

- Aging improves asphalt stiffness, thus reducing the vulnerability to moisture damage [13].
- Research has found that low water pH (i.e., acidic) supports acidic asphalt retention, while high pH (i.e., primary) supports acidic asphalt retention on essential aggregates [14].
- High water table frequently allows moisture/humidity vapor to migrate to a pavement, increasing moisture damage [14–16].
- Microorganisms may also be present in the binder and the surrounding soil [16, 17]. These asphalted bacteria are fed on the hydrocarbons found in the asphalt, thus, allowing the water to reach the binder interface by establishing voids in the structure this water availability in the voids and the pumping action of repeated wheel loads may trigger stripping problems.

The performance of bituminous materials is primarily influenced by the maximum and lowest temperatures and may vary considerably in their mechanical characteristics [18]. The impact may be seen through changes in the bitumen or asphalt mixture stiffness and the life span of the materials. In addition, temperature variations that could negatively affect a pavement may be attributed to weather variables such as air temperature, solar radiation, and wind [19].

4. HISTORY OF ASPHALT PAVEMENT TEMPERATURE PREDICTION MODELS

The prediction of asphalt pavement temperature may be separated into (1) numerical and finite element techniques; (2) theoretical and analytical approaches; and (3) statistical and probabilistic modeling based on the study methods and analysis tools used in the research [20].

Researchers have studied climatic variables' effects on asphalt pavement from an early stage. Moreover, the researchers who studied the temperature of the asphalt pavement focused on the distribution of temperature in various depths; theoretical frameworks based on the one-dimensional thermal driving model and the finite difference method (FDM) have been used to simulate the temperature distribution of the pavement structure [21].

In 1987, in the United States, the long-term pavement performance project (LTPP) measured asphalt pavement temperature [22]. The research focused on a novel data analysis strategy for pavement asphalt. Data, including atmospheric temperature and solar radiation, as well as their relationship with pavement temperature, have been made available, forming a critical database that facilitates and stimulates research in the field by using the regression method to develop models for predicting asphaltic temperature [22].

In the first stage (1950–1990), scientists focused on the fluctuation and distribution of temperatures. A limited number of studies utilized pitching techniques to estimate pavement temperatures. In the 1990s, Canadian and American researchers focused on utilizing a novel technique for analyzing data on asphalt paves. As a result, a valuable database is currently accessible to assist research on pavement temperatures based on many data and information on pavement temperatures and climatic factors, such as air temperature and solar radiation [23].

In that second step, however, most researchers used the reversal technique to build models to forecast the temperature of asphalt by focusing on the lowest and highest asphalt pavement temperatures throughout the service period using the Superpave method. Consequently, many studies have also begun to examine daily pavement temperature forecasts with somewhat varied changes and have been effectively applied in road engineering. The researchers employed statistical methods during a third phase, from 2000 to the present, to develop a regression prediction model in two applications, namely to correct deflection measurements in pavement layers with a back-calculation method and to simulate temperature fluctuation distributions in the structure of the asphalt [23–25]. The third phase of the study is heavily affected by the research results in the preceding phase, despite the significant expansion of the area of inquiry. To sum up, temperature prediction models have been enhanced and improved by the fast growth of the database in the 1990s up till now. At

present, the application of big data, artificial intelligence, and the likes has become prevalent in establishing temperatures and the variances in pavements.

5. DETERMINATION OF ASPHALT LAYER DEPTH TEMPERATURE

Three typical techniques are used to determine the temperature through the depth of an asphalt layer, including in-situ tests, the American Association of State Highway and Transportation Officials (AASHTO) method, and the BELLS model [25]. Another method is the indirect measurement, in this method, the temperature of an asphalt layer is measured every 1 to 1.5 hours using a thermometer when a hole to half the depth of the layer is perforated during Falling Wheel Deflectometer (FWD) testing [26]. Drilling the hole provides heat, and for this reason, the test result could be affected by the increased temperature between the instrument used for boring and the adjoining pavement layers, it is thus, recommended that at least 20 minutes of temperature readings should be carried out [25]. On the other hand, halting the FWD tests will decrease the test's effectiveness in detecting the pavement layers' temperature. The measurement of temperature at single points is another drawback of the direct measurement technique, expanding it across a stretch of the road that leads to severe uncertainties' [25, 27].

In addition, the pavement layer thicknesses typically fluctuate throughout the route, thus providing an additional source of inaccuracy for measuring the temperature at the middle depth of the asphalt layer. To develop dynamic modulus master curves of asphalt layers, using a direct measuring technique to estimate the pavement temperature during FWD testing is imperative, a simple method of testing pavement temperature is as demonstrated in Figure 2.

The pavement surface layer temperature is monitored to determine the temperature of the asphalt layer in the AASHTO technique. This is either determined by measuring the temperature at 25 mm depth or by the FWD infrared thermometer reading. Moreover, the prior mean air temperature for five days (i.e., before the FWD test) and the total asphalt layer thickness are revisited. The surface temperature is monitored with this information, and temperatures are calculated using the AASHTO graph at half depths and the bottom of the asphalt layer (AASHTO 1993). This technique defines the depth temperature of the asphalt layer as the average of the three above [26, 28, 29]. The climatic changes in the last five consecutive days before testing, which may influence the final temperature of the asphalt layer, are a significant drawback of the AASHTO approach [26]. In addition, no distinction is made between the positive temperature gradient at the beginning of the day, the surface temperature being higher than the depth, and the negative temperature gradient at the end of the day [26].

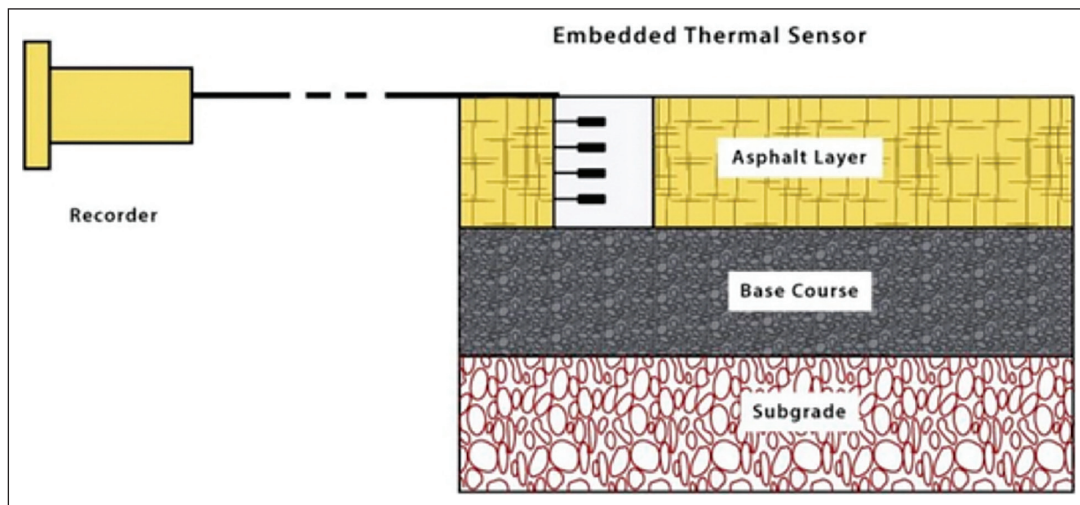


Figure 2. Representation of the method for measuring pavement temperature [2].

6. MAIN FACTORS CONTRIBUTING TO TEMPERATURE VARIATIONS OF ASPHALTIC PAVEMENT

Temperature is an essential indicator for determining the road surface temperature. The historical temperature condition shows that the current temperature of the pavement is a function of different factors and is also meaningful for decision making. However, to calculate the pavement temperature, there is still a debate on the temperature data to be selected. The temperature data of the past five days must be used if a result close to reality is to be obtained.

In addition, some prediction techniques for asphalt pavement temperatures require the previous day's temperature data. The sun's radiation may also raise the road surface temperatures and the temperature but will have an even more significant effect on the asphalt pavement temperature. A numerical method based on finite-difference modeling is proposed by [30], which evaluates temperature distribution in pavements depending on changes in the thermal environment. The model anticipates temperature variations in rates and depth during freezing and thawing cycles. However, the proposed model does not include surface cooling effects owing to precipitation, the influence of the tilt angle of the surface on surface boundary conditions, and internal heat stresses of the pavement due to different temperature levels.

Evaluated various computer algorithms for predicting the temperature of the asphalt-concrete pavement. The research compares the findings produced by the integrated Federal Highway Administration (FHWA) model with actual pavement temperatures [31]. The research shows that ignoring edge effects is not relevant for regular cross-sections but for the shoulders and extreme cross-sections. Researchers proposed an analytical method for examining rigid pavements exposed to temperature load in combination with finite-element algorithms. The pavement is idealized

as a thin isotropic platform sitting on an adjustable base of the Winkler type of foundation. The results produced from simulations for both linear and nonlinear temperature changes are given and contrasted. This research indicates that rigid pavement design cannot overlook temperature stresses [32]. Experimental and analytical research is given to create a technique for determining realistic stress caused by the thermal load. The research revealed that the overall temperature distribution throughout the concrete sheet depth is greater than the temperature difference between the extreme sheets [33].

Researchers have examined relationships between climatic variables and structural pavement characteristics in light of data obtained under the Long-Term Pavement Performance Seasonal Monitoring Program. Various statistical studies have been used to study the relationships between structural pavement characteristics and climate variables [33]. Changes to environmental variables may alter paved conditions and thus eventually affect the stiffness and degradation of pavement materials, thus affecting the performance in-service. These variables are always considered in pavement design and construction [34]. For example, the selection of bituminous binder grade is decided to match local temperature conditions to satisfy functional and structural needs [34, 35]. Despite the careful attention paid to environmental variables in pavements, difficulties arising from changes in those parameters are inevitable and frequently significant [36]. In its evaluation of material reactions and projections of long-term performance, the previous researchers examined the impact the environment has on pavement performance and documented effects on pavement environmental variables (e.g., temperature and humidity profiles) [36, 37].

In addition, a rise in the temperature ranges as a consequence of weather and climatic changes increases the thermal stress of asphalt layers and thus might worsen thermal

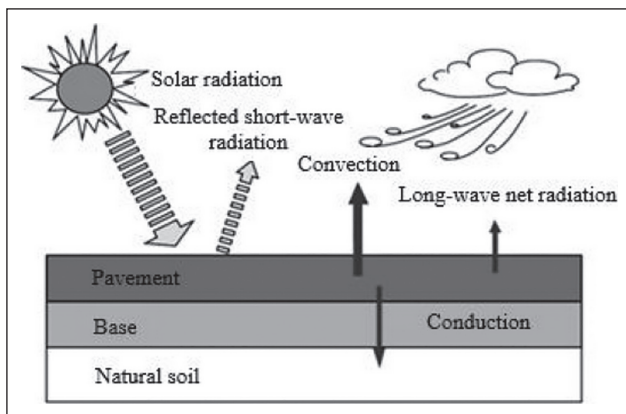


Figure 3. Pavement energy balance [39].

assumptions [37]. Moreover, greater temperatures may lead to a quicker (accelerated) aging of the asphalt layers and because of increased fracture, pavements may become more prone to cracking [37, 38]. Furthermore, low temperatures may lead to asphalt concrete hardening and result in thermal cracking on the road surface; low temperatures promote cracking processes, whereas high temperatures distort plastic deformation processes such as rutting [39].

7. ENERGY BALANCE IN FLEXIBLE PAVEMENTS

The thermal conditions directly influence the temperature profile of the asphalt pavement it is exposed to. The main methods of heat transmission are incident sunlight, heat, and radiation between the pavement's surface and the sky; heat transfer convection between the surface of the pavement and the fluid (air or water). The strength of direct and broad solar radiation depends on diurnal cycles, the sun's position in the sky, and the angle of incidence between the surface and the sun's rays. The pictorial example of the energy balance is shown in Figure 3.

The convective heat flow is determined by the speed and direction of the water. Generally, it is affected by the surface wind speed and direction the most. Whenever the thermal conductivity improves due to incredible wind speeds and wind directions occurring at the right moment, the convection heat flow increases. As a result, when the wind speed is relatively high and the temperatures of the wind are lower than the energy of the pavement surface, convective surface cooling occurs. A far crane is created by thermal and long-wave radiation. This is because profound temperatures are often lower than surface pavement temperatures, resulting in heat transfer in the far crane direction [40].

For the equilibrium of surface energy on a roadway, the sum of all heat gains across the road surface must equal all heat losses inside the pavement surface. The temperature differential determines the pattern of heat flow, convective heat, and thermal radiation between the pavement area and the bulk fluid or sky temperature. Convection and heat

transfer are both responsible for heat flow [41]. Suppose the temperature of the sky and the bulk temperature of the fluid are both lower than the temperature of the pavement surface. In that case, the surface cools, but the surface may also be heated by incoming solar radiation at the same time. As a result, the pavement is either heated or cooled, depending on the different heat fluxes involved.

It is possible to suppose that an adiabatic bottom surface exists for sufficiently broad pavement that does not need heat transfer between both the pavement and the sub-grade layers. The same is true for lateral pavement sides (paved edges) for appropriately significant horizontal expansion since increases in the vertical direction are considerably greater than changes in the horizontal direction at pavement edges. Heat transfer through pavement edge surfaces is unaffected [42, 43].

The convection of the heat conduction of the pavement structure and subgrade between the surface of the pavement and the surrounding environment. This is achieved using transmission media such as air or when water reaches the surface [39, 44]. On the other hand, temperature change was the most important factor for changing pavement performance in most studies on climate factors [45]. The causes underlying seasonal fluctuations and their effects on temperature changes are thus essential to understand [45–47]. It is also well-known that the reaction of pavement layers to traffic loads is strongly affected by environmental variables such as temperature and moisture. Any substantial temperature fluctuation may thus have a severe effect on the performance of the asphalt surface and the repair requirements [47].

Temperature, asphalt thickness, and binder qualities all influence whether the pavement cracks or not. Other variables such as aggregate quality, pavement age, pavement width, and friction between asphalt and base track influence thermal cracking severity if a vulnerable asphalt binder is employed. Temperature should be one of the significant factors in the asphalt pavement to prevent thermal cracking [48].

In a transient thermal examination followed by a quasi-static stress analysis, [49] analyses the thermoplastic response of a multi-faceted pavement construction at discrete time intervals using finite element methods. The research analyses the two- and three-dimensional cracking issues numerically. The possibility of heat fractures spreading through the asphalt overlay is evaluated using both a displacement formula and an energy balance concept based on a fracture-mechanics method.

A parametric study on variables leading to the thermal cracking of asphalt pavements [50] has been presented. A semi-analytical model has been constructed to address the multiscale nature of heat cracking pavement, including viscoelasticity effects. The research revealed material homogeneity, ductility, and frictional restriction on the contact

and cooling rate as the most significant factors [51]. Studied the effects of nonlinear temperature and wheel load on multi-faceted pavements with a plate consisting of one or more layers resting on a general elastic basis. The resulting bending stress is the amount of bending stress due to the load applied and a linear temperature gradient equivalent, plus the pure heat stress related to the nonlinear portion of the temperature distribution.

Presented research on thermal stress prediction in concrete pavement systems. The analysis is based on measured data on the actual test sections of concrete pavement [52]. The measured strains are divided into axial, curling, and nonlinear components, and each component is examined. The research shows that the curling component dominated cross-sectional stress while the nonlinear component reduced the maximum thermal stress by approximately 25%.

To assess pavement damage, [53] proposed a numerical method utilizing a 3D finite element analysis technique. Field temperature data was collected at 14 locations in the United States at various times of the day to calculate pavement stresses due to curling and wheel loads. A pavement fatigue algorithm was designed to provide comparable damage and effective temperature differentials [54]. Offered an analysis solution in a three-layer pavement system for the determination of slab temperature, subject to a regular change in ambient air or paved surface temperature. The thermal analysis is linked to plate theory and the Winkler foundation to enable curling stress and bending moments to be calculated. The analyses indicated that the distribution of pavement temperatures might be very nonlinear, mainly when the ambient air temperatures vary according to time. The research indicates that the frequency of temperature changes rather than amplitude affected estimated temperature profiles most, leading to thermal stresses in pavements.

8. ASPHALT PAVEMENT DESIGN INCORPORATING THE TEMPERATURE FACTOR

The characteristics of pavement materials, traffic, climate, and service results affect each other in the design process and determine the demand for a necessary mix of pavement structures [43]. The researchers [55] put forward a computer method that uses the Temperature Equivalency Factors concept [56] and introduces the Temperature Factor as a significant factor in the asphalt pavement construction method, which translates the design effect times of the axle load into a standard reference temperature.

Before then, generally, the average temperature in the asphalt design technique was dominant, the number of axle loads was realistic in time, and no comparable conversion was performed.

There are also various considerations for the temperature factors of various methods of asphalt pavement, such as taking into account the asphalt pavement experience at low and high temperatures and the associated prediction formula.

When the temperature is gradient, the weighted average temperature is calculated as a pavement temperature based on various pavement temperature depths. According to a more precise technique for considering the non-uniform temperature distribution, the asphalt pavement thickness may be split into multiple levels in the depth of the scope. Analysis indicates that the technique of division level and the method of the asphalt pavement's equivalent temperature provide comparable findings [55–57].

9. THE EFFECT OF TEMPERATURE ON STRUCTURAL PERFORMANCE OF ASPHALT PAVEMENT

The change in asphalt mixing would substantially influence the asphalt pavement's structural capacity and its performance, and asphalt mixture depends on the temperature. It is continuously changing within a day or even a year. Thus the temperature may in the following aspects influence the structural bearing capacity of the asphalt pavement:

- Higher stress is transferred to the base and subbase by the asphalt mixture modulus reduction. Material characteristics of the foundation, however, are linked to stress.
- The base material is consolidated under high stress, particularly granular material, although the cohesive ground will become more susceptible. Consequently, the temperature of the asphalt mixture directly influences the material characteristics of the base and base.
- The asphalt mixture module is linked directly to the temperature. The module decreased progressively as the temperature improved, which may cause the structural bearing capacity to be lowered.
- Temperature-change stress: according to a microscopic mechanical model, the contact force between granular base granules would rise in the event of an increase in temperature, resulting in increased volume strain. According to findings from the study by [58], the temperature on the modulus is more critical with a greater degree of compaction and lower starting volume stress levels.
- The rise of the asphalt pavement structure temperature will decrease the top layer pore-water tension.

It may lead to water transfer to the top layer, which reduces pore water pressure. Effective base stress or soil base stress will be reduced. At the same time, the material modulus is reduced. A brief summary of the effect of the extreme thermal effect on pavements is presented in Table 1 and the preventive measures are presented in Table 2.

The findings indicated that the impact of temperature on the asphalt-paved structural bearing capacity is very complex, and it is difficult for the individual component to be distinguished from complicated variables. Asphalt pavement structural bearing capacity changes with the change in temperature. This implies that the stress distribution of

Table 1. Summary of common causes of temperature and effect on pavements

S/No	Causes	Types of effect on pavement
1	Extreme high temperature	Portions of the pavement heat disproportionately
2	Temperature variations	Temperatures alteration or cycle rapidly
3	Less rain and more sunshine	Pavements deteriorate from oxidation effect
4	Ice cold	Pavement (frost heave) melts, thus causing deterioration
5	Freezing temperature	Freezing temperatures can lead to a freezing of water trapped under the pavement, resulting to deterioration
6	Temperature variations	Pavement is exposed to excessive or prolonged heat or cold that leads to quick deterioration especially during cold seasons

Table 2. Methods to protect pavements from adverse thermal effects

S/No	Preventive measure	Explanation
1	Conducting routine inspections	Even the supreme paved roads exhibit aging signs like temperature cracks after a while; keeping eyes on the pavement all year round may help discover areas of concern that may become more problematic. Take notice of cracks, in particular during extremely high temperatures and shallow temperatures in rainy seasons.
2	Preventative maintenance adoption:	While not all pavement damage can be prevented, preventive maintenance is crucial for extending the life span of pavements. Fill or seal small cracks and apply suitable surface treatments to maintain the pavements in an excellent form.
3	Correct deficiencies as early as possible:	Once a major flaw has been discovered, it is appropriate to select the most suitable patches and work with a contractor to fix the damage. It is advised not to wait until the damage gets serious – keeping the damaged pavement in place is a safety risk, and the expenditure only rises as the deteriorations persist.
4	Get the design and construction right as the first step	The design and construction stages are the first stages that need to be gotten right in order to keep pavements in their proper place for the design life before deteriorations. A great deal of preventive work must be done when pavement longevity is to be prioritized.

the pavement changes at various times, even at the same loads. Therefore, the asphalt pavement deterioration model changes with time and temperature effect [58–60].

Find in Table 1 below the summary of common causes of temperature ad effects on pavements.

10. SUMMARY OF THE MECHANISM OF PAVEMENTS' REACTIONS TO THERMAL VARIATIONS

Pavement surfaces resist tremendous impact from vehicles, trucks, and trailers daily. Given the resilience of the pavement, it may seem odd that just temperature changes can cause severe structural damage to roadways and parking lots. However, changes in the weather represent a significant danger to both asphalt and concrete. Temperature changes cause the pavement to expand and contract, which leads to cracks that proliferate if not repaired. Such cracks are not just a tiny annoyance but may develop into warped, uneven surfaces that are a safety risk to vehicles and pedestrians in a facility. These risks are particularly apparent when seasons change due to the possibility of abrupt temperature changes. However, high temperatures may lead to cracking on their own at either end of the range. Therefore,

it is essential to be particularly attentive at the summer and winter levels. An awareness of how the pavement responds to variations in temperature may help create a maintenance plan to avoid developing unattractive and hazardous pavement faults. This article discusses the factors leading to a cracking temperature and the measures taken to safeguard the pavement [60].

11. PAVEMENT PROTECTION FROM WEATHER EFFECTS

Temperature variation that leads to pavement deterioration in the true sense of practice is inevitable, but can, however, can minimize with the correct pouring and maintenance; however, the pavement may be protected against the temperature variations as presented in Table 2.

12. CONCLUSION

In conclusion, highlights of the significant areas presented and discussed in the study above are listed here. The study's objective was to discover several ways the asphalt temperature might be estimated to help road design engineers overcome the problems and minimize the dangers

of changing temperatures. The conclusion is that analytical techniques offered simple answers but needed precise boundaries. In addition, the above study concluded that temperature has a reasonably substantial effect on the asphalt pavement layer's mechanical and physical material characteristics. It has effectively examined the existing techniques of monitoring temperature and temperature prediction models for pavement construction. Thus, it may be inferred that since the middle of the last century, experts have been trying to forecast asphalt pavement temperatures. However, these models have unique flaws and strengths, and some prediction models are excessively complicated and demand the usage of several factors. Furthermore, heat transfer studies between the ambient and pavement temperatures are thus strongly suggested, considering the impacts of temperature on pavements.

DATA AVAILABILITY STATEMENT

The authors confirm that the data that supports the findings of this study are available within the article. Raw data that support the finding of this study are available from the corresponding author, upon reasonable request.

CONFLICT OF INTEREST

The authors declare that they have no conflict of interest.

FINANCIAL DISCLOSURE

The authors declared that this study has received no financial support.

PEER-REVIEW

Externally peer-reviewed.

REFERENCES

- [1] Abaza, K. A. (2011). Stochastic approach for design of flexible pavement. *Road Materials and Pavement Design*, 12(3), 663–685. [\[CrossRef\]](#)
- [2] Adwan, I., Milad, A., Memon, Z. A., Widyatmoko, I., Ahmat Zanuri, N., Memon, N. A., & Yusoff, N. I. (2021). Asphalt pavement temperature prediction models: A review. *Applied Sciences*, 11(9), 37–94. [\[CrossRef\]](#)
- [3] Airey, G. (2011). Factors affecting the rheology of polymer modified bitumen (PMB). *Polymer Modified Bitumen* 4(7), 238–263. [\[CrossRef\]](#)
- [4] Al-Abdul Wahhab, H., I. Asi, S. Ali, S. Al-Swailmi, & A. Al-Nour. (2004). Pavement stripping in Saudi Arabia: Prediction and prevention. *The Journal of Engineering Research*, 1(1), 38–45. [\[CrossRef\]](#)
- [5] Barzegari, S., Stoffels, S. M., & Solaimanian, M. (2017). Novel application of reclaimed asphalt pavement in construction of new cold mix pavements. *Airfield and Highway Pavements*, 90–101. [\[CrossRef\]](#)
- [6] Ali, H. A., & Lopez, A. (1996). Statistical analyses of temperature and moisture effects on pavement structural properties based on seasonal monitoring data. *Transportation Research Record: Journal of the Transportation Research Board*, 1540(1), 48–55. [\[CrossRef\]](#)
- [7] Chen, L, Chen, J., Chen, T., Lecher, T., & Davidson, P. (2019). Measurement of permeability and comparison of pavements. *Water*, 11(3), 444–454. [\[CrossRef\]](#)
- [8] Barry, K., Daniel, J., & Boisvert, D. (2014). Forensic analysis of long term aged hot mix asphalt field cores containing reclaimed asphalt pavement. *Asphalt Pavements*, 1189–1197. [\[CrossRef\]](#)
- [9] Cannone Falchetto, A., Moon, K., & Wistuba, M. (2016). Strength size effect on small asphalt mixture specimens at low temperature. *Functional Pavement Design*, 1767–1776. [\[CrossRef\]](#)
- [10] Chaturabong, P., & Bahia, H. U. (2016). Effect of moisture on the cohesion of asphalt mastics and bonding with surface of aggregates. *Road Materials and Pavement Design*, 19(3), 741–753. [\[CrossRef\]](#)
- [11] Ahmed, T., Lee, H., & Baek, C. (2015). Evaluation of laboratory and field warm mix asphalt mixtures with high contents of reclaimed asphalt pavement. *Bituminous Mixtures and Pavements VI*, 623–627. [\[CrossRef\]](#)
- [12] Ma, X., Leng, Z., Wang, L., & Zhou P. (2020). Effect of reclaimed asphalt pavement heating temperature on the Compactability of recycled hot mix asphalt. *Materials*, 13(16), Article 3621. [\[CrossRef\]](#)
- [13] Chen, X., Wei, W., & Liu, M. (2012). Characteristics of temperature variation in seasonal snow in the western Tianshan mountains, China. *Meteorological Applications*, 20(4), 457–465. [\[CrossRef\]](#)
- [14] García-Casuso, C., Lapeña-Mañero, P., Blanco-Fernández, E., Vega-Zamanillo, Á., & Montenegro-Cooper, J. M. (2020). Laboratory assessment of water permeability loss of Geotextiles due to their installation in pervious pavements. *Water*, 12(5), Article 1473. [\[CrossRef\]](#)
- [15] Ghabchi, R., Singh, D., & Zaman M. (2014). Evaluation of moisture susceptibility of asphalt mixes containing RAP and different types of aggregates and asphalt binders using the surface free energy method. *Construction and Building Materials*, 7(3), 479–489. [\[CrossRef\]](#)
- [16] Gopalakrishnan, K., Kim, S., Ceylan, H., & Kaya, O. (2015). Use of neural networks enhanced differential evolution for backcalculating asphalt concrete viscoelastic properties from falling weight deflectometer time series data. *Bituminous Mixtures and Pavements*, 6(8), 679–686. [\[CrossRef\]](#)
- [17] Huang, W., Li, B., & Wang, P. (2016). Low temperature cracking of modified asphalt mixtures as related to binder characteristics. *Functional Pavement Design*, 7(9), 403–409. [\[CrossRef\]](#)

- [18] Imanbayev, Y. (2017). High temperature transformation of tar-asphaltene components of bituminous sand bitumen. *Juniper Online Journal Material Science*, 1(1), 23–45. [CrossRef]
- [19] Li, H. (2016). Thermal resistance pavements and thermal properties. *Pavement Materials for Heat Island Mitigation*, 9(4), 97–133. [CrossRef]
- [20] Kandhal, P., & Koehler, W. (2019). Effect of rheological properties of asphalts on pavement cracking. *Asphalt Rheology: Relationship to Mixture*, 9(9), 99–117. [CrossRef]
- [21] Sivapatham, P., & Simmleit N. (2019). Impact of seasonal fluctuations and provenience of bitumen on lifetime of asphalt pavement. *Bituminous Mixtures and Pavements VII*, 2(9), 88–92. [CrossRef]
- [22] Kodippily, S., Tighe, S. L., Henning, T. F., & Yeaman, J. (2016). Evaluating pavement performance through smart monitoring – effects of soil moisture, temperature and traffic. *Road Materials and Pavement Design*, 19(1), 71–86. [CrossRef]
- [23] Paul, B., Choudhury Dibakar, R., Rajdeep, R., Abhisek, R., & Sayak, B. (2020). An ecofriendly substitute of asphalt binder – Review. *International Journal of Chemical and Environmental Sciences*, 1(3), 64–69. [CrossRef]
- [24] Li, H. (2016). Permeable pavements and permeability. *Pavement Materials for Heat Island Mitigation*, Chapter 4, Elseiver, 79–96. [CrossRef]
- [25] Khadrawi, A. F., Al-Shyyab, A., & Abo-Qudais, S. A. (2020). Transient thermal behavior of hot-mix asphalt pavement. *Applied Mechanics and Materials*, 1(2), 400–407. [CrossRef]
- [26] Ravnikar Turk, M., & Tušar, M. (2016). *Effect of ageing on the low temperature properties of bitumen*. Proceedings of 6th Eurasphalt & Eurobitume Congress, 4(8), 34–48. [CrossRef]
- [27] Li, H., Harvey, J. T., Holland T. J., & Kayhanian, M. (2013). The use of reflective and permeable pavements as a potential practice for heat island mitigation and stormwater management. *Environmental Research Letters*, 8(1), 015-023. [CrossRef]
- [28] Qian, G., Zheng, J., & Wang, Q. (2008). Calculating thermal stresses of asphalt pavement in environmental conditions. *Pavements and Materials*, 4(6), 234–241. [CrossRef]
- [29] American Association of State Highway and Transportation Officials. (1993). AASHTO Guide for Design of Pavement Structures. American Association of State Highway and Transportation Officials.
- [30] Tiza, M. (2021). Evaluation of thermal effects on slag cement concrete's strength properties. *Journal of Cement Based Composites*, 3(3), 11–15. [CrossRef]
- [31] Sakib, N., Bhasin, A., Islam, M. K., Khan, K., & Khan, M.I. (2019). A review of the evolution of technologies to use sulphur as a pavement construction material. *International Journal of Pavement Engineering*, 22(3), 392–403. [CrossRef]
- [32] Solatifar, N., Abbasghorbani, M., Kavussi, A., & Sivilevičius, H. (2018). Prediction of depth temperature of asphalt layers in hot climate area. *Journal of Civil Engineering and Management*, 24(7), 516–525. [CrossRef]
- [33] Zhang, Y. H., & Wang, F. Z. (2011). Effect of emulsified asphalt on temperature susceptibility of cement asphalt mortar. *Advanced Materials Research*, 3(6), 124–127. [CrossRef]
- [34] Tari, Y., & Wang, M. (2015). *Probabilistic data-driven assessment of pavement management systems*. Conference: Structural Health Monitoring 2015. [CrossRef]
- [35] Teltayev, B., Kaganovich, Y., & Amirbayev, Y. (2014). Evaluation of low temperature stability of bitumen and hot mix asphalt pavement. *Asphalt Pavements*, 5(7), 1557–1565. [CrossRef]
- [36] Moghadas Nejad, F., Azarhoosh, A., Hamed, G. H., & Roshani, H. (2013). Rutting performance prediction of warm mix asphalt containing reclaimed asphalt pavements. *Road Materials and Pavement Design*, 15(1), 207–219. [CrossRef]
- [37] Vasenev, A., Hartmann, T., & Dorée, A. G. (2012). Prediction of the in-asphalt temperature for road construction operations. *Computing in Civil Engineering*, 3(4) 34–43. [CrossRef]
- [38] Vujovic, S., Haddad B., Karaky, H., Sebaibi, N., & Boutouil, M. (2021). Urban heat island: Causes, consequences, and mitigation measures with emphasis on reflective and permeable pavements. *Civil Engineering*, 2(2), 459–484. [CrossRef]
- [39] Romaniuk, N., Little, L., Arguelles, F. A., Babadagli, T., & Ozum, B. (2013). *Effect of bitumen viscosity and bitumen-water interfacial tension on the efficiency of steam assisted bitumen recovery processes*. SPE Western Regional & AAPG Pacific Section Meeting 2013 Joint Technical Conference.
- [40] Chintakunta Reddy, S. (2016). *Sensitivity of thermal properties of pavement materials using mechanistic-empirical pavement design guide* [Unpublished Master Thesis]. Iowa State University.
- [41] Díaz-Sánchez, M. A., & Timm, D. H. (2015). Influence of sustainable technologies on in-place thermal properties of asphalt pavements. *Airfield and Highway Pavements*, 6(8), 536–547. [CrossRef]
- [42] Islam, R., Mannan, A., Rahman, T., & Tarefder, A. (2014). Simplified thermal stress model to predict low temperature cracks in flexible pavement. *Pavement Materials, Structures, and Performance*, 6(8), 234–250. [CrossRef]
- [43] Hui, L. (2016). Pavement thermal modeling. *Pave-*

- ment Materials for Heat Island Mitigation, 5(5), 239–262. [CrossRef]
- [44] Tiza, M., Mogbo, N., Duweni, E., & Asawa, I. (2020). Recycled asphalt pavement: A systematic literature review. *Journal of Modern Technology and Engineering* 5(3), 242–254.
- [45] Blab, R. (2018). Multiscale modeling for performance prediction of asphaltic materials. *Advances in Materials and Pavement Performance Prediction*, 5(7), 5–15. [CrossRef]
- [46] Han, J., Shaopeng, W., Zhiyi, H., Dehong, Z., & Fujian, L. (2012). Research on low temperature rheological behavior of aging resistant bitumen and mixture. *Sustainable Construction Materials*, 6(9), Conference Paper. [CrossRef]
- [47] Kim, S.-M., & Nam, J. H. (2010). Measurements and experimental analysis of temperature variations in portland cement concrete pavement systems. *Road Materials and Pavement Design*, 11(3), 745–771. [CrossRef]
- [48] Marciales, A., & Babadagli, T. (2014). Selection of Optimal solvent type for high temperature solvent applications in heavy-oil and bitumen recovery. *Energy Fuels*, 10(2), 345–365. [CrossRef]
- [49] Wu, S., Feng, Y., & Wong, A. (2004). Selected rheological properties of tall oil pitch binder for asphaltic road pavement construction. *International Journal of Pavement Engineering* 5(3), 175–182. [CrossRef]
- [50] Zaghoul, S., & Saeed, N. (2017). The use of falling weight Deflectometer in asphalt pavement construction quality control. *Quality Management of Hot Mix Asphalt*, 5(9), 66–76. [CrossRef]
- [51] Yavuzturk, C., Ksaibati, K., & Chiasson, A. D. (2005). Assessment of temperature fluctuations in asphalt pavements due to thermal environmental conditions using a two-dimensional, transient finite-difference approach. *Journal of Materials in Civil Engineering*, 17(4), 465–475. [CrossRef]
- [52] Yuan, H., Han, D., & Zhang, W. (2015). The effect of pressure and temperature on bitumen saturated carbonate. *SEG Technical Program Expanded Abstracts*, 5(6), 34–40. [CrossRef]
- [53] McBee, W. C., Sullivan, T. A., & Saylak, D. (2018). Recycling old asphaltic pavement with sulfur. *Recycling of Bituminous Pavements*, 5(9), 123–129. [CrossRef]
- [54] Ravnikar Turk, M., & Tušar, M. (2016). Effect of ageing on the low temperature properties of bitumen. Proceedings of 6th Eurasphalt & Eurobitume Congress, 4(5), 34–50. [CrossRef]
- [55] National Precast Concrete Association. (2018). *Reducing shrinkage cracking*. National Precast Concrete Association.
- [56] Xu, W., Jimenez-Bescos, C., Pantuna, C. A. J., Calautit, J., & Wu, Y. A coupled modelling method for the evaluation of the impact of pavement solar collector on urban air temperature and thermal collection. *Future Cities and Environment*, 7(1), 1–16. [CrossRef]
- [57] Choi, G. Y., Kim, H. S., Kim, H., & Lee, J. S. How do pavement and planting strategies affect microclimate conditions and thermal comfort in apartment complexes? *International Journal of Climate Change Strategies and Management*, 13(2), 97–119. [CrossRef]
- [58] McDonald, T., & McDonald, P. (2010). *Guide to pavement maintenance*. iUniverse.
- [59] Wambold, J. C. (1989). *Pavement friction measurement normalized for operational, seasonal, and weather effects*. Federal Highway Administration and Pennsylvania Transportation Institute
- [60] Pavement Interactive. (Dec 17, 2020). *Pavement interactive*. <https://pavementinteractive.org/>



Review Article

A review on engineering biocomposites and natural fiber-reinforced materials

Ataberk BAYSAL¹, Paşa YAYLA^{*1}, Halit Süleyman TÜRKMEN²

¹Department of Mechanical Engineering, Marmara University Faculty of Engineering, İstanbul, Türkiye

²Department of Aeronautical Engineering, İstanbul Technical University, Faculty of Aeronautics and Astronautics, İstanbul, Türkiye

ARTICLE INFO

Article history

Received: 26 June 2022

Accepted: 06 September 2022

Key words:

Biocomposites, biopolymers,
green composites, natural fibers

ABSTRACT

Fiber-reinforced polymer composites are well-studied and established products, and today they are being used in different industrial and non-industrial areas. However, the increased interest in recyclability and the concerns about climate change caused materials scientists to look for a non-petroleum-based alternative to synthetic fibers and polymers. Since the beginning of this century, natural fibers and biopolymers have attracted increasing interest each year for composite applications. Thanks to this interest, studies on natural fibers and biopolymers have increased significantly. Despite the high number of studies on natural fibers and natural fiber-reinforced polymers (NFRP), there are gaps in the literature. This work reviews studies on natural fibers, biopolymers, and biocomposites with their advantages, disadvantages, and limitations. Studies that focus on the ways to reduce or eliminate these disadvantages and limitations have also been looked at. Also, current challenges and future perspectives for natural fibers, biopolymers, and NFRPs have been discussed.

Cite this article as: Baysal, A., Yayla, P., & Türkmen, HS. (2022). A review on engineering biocomposites and natural fiber-reinforced materials. *J Sustain Const Mater Technol*, 7(3), 231–249.

1. INTRODUCTION

Fiber-reinforced polymers (FRP) have replaced conventional materials since the mid-last century. This replacement was mainly due to their superior mechanical properties compared to traditional materials, such as steel and aluminum. Composite materials have a more specific strength and higher fatigue resistance than steel and aluminum and are lighter than conventional materials [1].

Today, FRPs have many applications in various industrial areas, such as the automotive, aviation, and defense industries. While composite materials solved many prob-

lems for these industries, they created new ones for the environment. Better mechanical properties with composite materials alone are not enough to solve today's problems. Better specific strength, higher fatigue resistance, and weight reduction do not solve the environmental issues associated with FRPs.

In the present century, thermoset polymers reinforced with synthetic fiber composites are being questioned due to problems related to environmental issues [2]. Due to thermoset polymers' nature, synthetic fibers with thermosets render FRP impossible to recycle. This causes irreversible problems for the environment.

*Corresponding author.

*E-mail address: pasa.yayla@marmara.edu.tr



However, the substitution of natural fiber-reinforced polymers (NFRP) for the traditional (FRP) is not due to only environmental reasons. Natural fiber-reinforced polymer composites present the same or comparable mechanical properties to fiber-reinforced polymer composites with lower density [3]. Natural fibers (hemp fiber 1.48 g/cm³, flax fiber 1.4 g/cm³, kenaf fiber 1.45 g/cm³, jute fiber 1.46 g/cm³, banana fiber 1.35 g/cm³) are lighter than their synthetic counterparts (glass fiber 2.54 g/cm³, carbon fiber 1.75–2.00 g/cm³), this aspect makes the NFRPs favorable against FRPs in areas where weight reduction is essential. Natural fibers with very low densities, such as hemp, can be used in non-critical areas where solid mechanical properties are not needed [4].

In addition to the low-weight characteristics of natural fibers, NFRPs can be produced at a lower cost when compared with polymer composites with synthetic fibers. The automotive industry, where lower cost and lower weight are critical, started using natural fibers at the beginning of this century [4]. Furthermore, the aviation industry, another area where cost and weight reduction are essential to compete, started using natural fibers as a reinforcing material for polymer matrix composites [5].

Even though natural fibers bring new characteristics to the table, such as environmental friendliness, it comes with some drawbacks too. As they are crop-based materials that grow naturally on the soil, the mechanical properties of natural fibers depend upon the harvesting region, the soil condition, harvesting time, and the intensity of sunrays and rain [5, 6].

The compatibility between natural fiber and matrix polymer of NFRPs is poor [7]. This causes lower mechanical properties than expected due to the non-uniform dispersion of fiber in the matrix and low stress transfer between the matrix and the fiber.

Most polymers, especially thermoplastic ones, which are widely used with natural fibers due to their recyclability, are hydrophobic, in contrast to natural fibers, which are hydrophilic [5]. The hydrophilic characteristic of a natural fiber creates another problem: water or moisture absorption. They also have poor fire resistance [8].

Although their use in composite materials has increased over time, the subject of natural fibers as reinforcement materials is still a new topic and developing field. Therefore, research on natural fibers should be reviewed and summarized to guide future studies. In this paper, the studies on natural fibers and biocomposites are thoroughly reviewed and classified according to their content and purpose. Reviewed studies are arranged to create an orderly explanation of the subject in question.

This study aims to review the pros and cons of natural fibers and the studies that have been done to mitigate these disadvantages. First, an introduction to biocomposites is presented, and the classification of natural fibers is

explained. After that, the natural fibers' sources and macrostructure are explained, and the effects of surface modification on natural fibers are reviewed. In addition, the mechanical performance of surface-modified and non-surface-modified natural fibers is also reviewed. The last part, before the conclusions, explains the topic of green composites and potential areas for utilizing them.

2. BIOCOMPOSITES

Composite materials must consist of at least two or more materials. Biocomposites, a subcategory of composites, are no exception. However, the requirement of combining at least two materials is not enough on its own for biocomposites. For a material to be called a biocomposite, at least one of the materials that form the composite must be a natural material [3]. Composite materials made from natural fiber-reinforcements (hemp, jute, rami, etc.) and petroleum-derived polymer matrices can be labeled as biocomposites. Composite materials that consist of synthetic fiber-reinforcements and natural-based polymer-biopolymer matrices like PLA are also called biocomposites. If both the reinforcement and the matrix materials are naturally based, the material is considered biocomposite too, but to emphasize the material's biodegradability, they are classified as green composites [9].

Natural and synthetic fibers can be utilized in a single matrix to increase the performance of the biocomposite. The composite materials composed of this combination are called hybrid composites [10].

There are various reasons for using natural fiber-reinforced polymers over synthetic fiber-reinforced polymers. Aside from the low-cost and low-density benefits of biocomposites, biodegradability will become an essential feature of these materials as global environmental issues worsen. Biopolymers or biocomposites may be a long-term solution to 21st-century environmental problems (such as climate crisis, waste plastic pollution, etc.) [9].

2.1. Green Composites

Green composites are a subcategory of biocomposites. Green composites can be defined as fully biodegradable composite materials. A combination of natural fibers with natural polymers or biopolymers can be called a green composite [11]. It is critical to distinguish biocomposites from green composites; every green composite can be labeled as a biocomposite, but the reverse is not always achievable. Although hemp-polypropylene natural fiber reinforced polymer is a biocomposite, it is not a green composite due to polypropylene's nondegradability. Due to the degradable hemp and PLA, Hemp-PLA is both a biocomposite and a green composite.

The most crucial advantage of green composite is its biodegradable nature. This characteristic only makes green composites unrivaled against other synthetic or natural fiber-re-

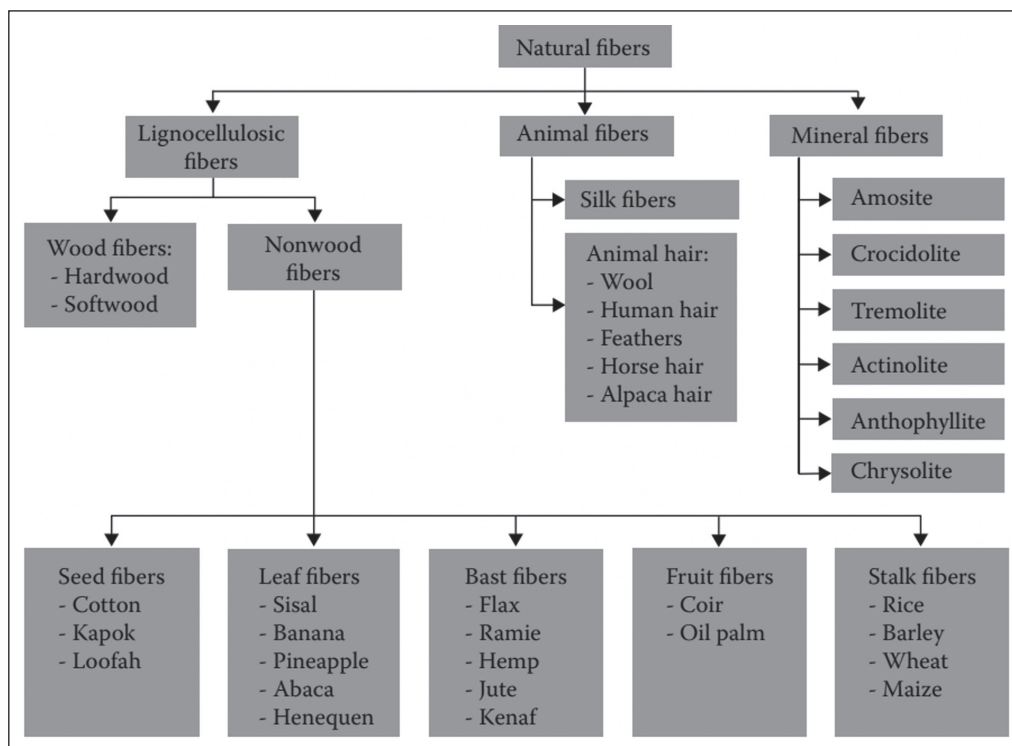


Figure 1. Classification of natural fibers [14].

inforced petroleum-derived polymers as an environmentally friendly alternative. In addition to this aspect, producing biodegradable polymers from renewable resources like animals, plants, and microbes through biochemical reactions offers lower reliance on petroleum-derived polymers, thus lower petroleum usage [11]. Increased use of green composites will help the struggle against environmental issues like climate crisis and plastic waste due to excessive usage of non-biodegradable and non-recyclable polymers [12].

2.2. Natural Fibers

Fibers can be divided into two categories: synthetic and natural fibers. Natural fibers can also be subdivided based on their origins, like animal, mineral, and plant (cellulosic/lignocellulosic). Most natural fibers are planted (lignocellulosic), like cotton, jute, flax, hemp, ramie, etc. These fibers have mainly lignified secondary cell walls, which give mechanical stability to the plant body [13]. The classification of natural fibers is shown in Figure 1. Some of the most popular plant (lignocellulosic) fibers are shown in Figure 2.

There can be significant differences between the different types of natural fibers. For example, their density, length, diameter, and mechanical properties can vary greatly. Although this difference might seem a disadvantage, it allows the engineers and designers to choose different materials with different physical and mechanical properties suitable for the design requirements. The physical and mechanical properties of various natural fibers are shown in Table 1.

2.2.1. Sources of Natural Fibers

As shown in Figure 1, natural fibers are classified based on their origin, the part of the plant, animal, and mineral from which they are derived. Animal and mineral fibers are obtained from animals and minerals, respectively.

There are two types of wood fibers, hardwood, and softwood. Wood fibers are extracted from wood using various methods, but for natural fiber-reinforced polymer applications, wood flour is more widely used than wood fiber due to its low price and ease of processing with conventional polymers.

Seed fibers, cotton, kapok, loofah, etc., are obtained from the seeds of these plants. Leaves of monocotyledonous plants are used to obtain leaf fibers, such as sisal, banana, pineapple, abaca, henequen, etc. Bast fibers, which include flax, ramie, hemp, jute, kenaf, etc., are collected from the stems' inner bark, called phloem, of the dicotyledonous plants. Fruit fibers are the fruits of plants that bear the name. Stalk fibers of straw fibers, rice, barley, wheat, maize, etc., are the stalks of their plants [13]. The production of some plant (lignocellulosic) fibers and the largest producer countries is shown in Table 2.

Plant (lignocellulosic) fibers are more popular than animal and mineral-based natural fibers among all these natural fibers. Cotton (seed fiber), flax, jute, ramie, and kenaf (bast fibers) are plant fibers' most popular and most researched fibers.

According to Townsend [17], world fiber production in 2018 was approximately 110 million, including 32 million

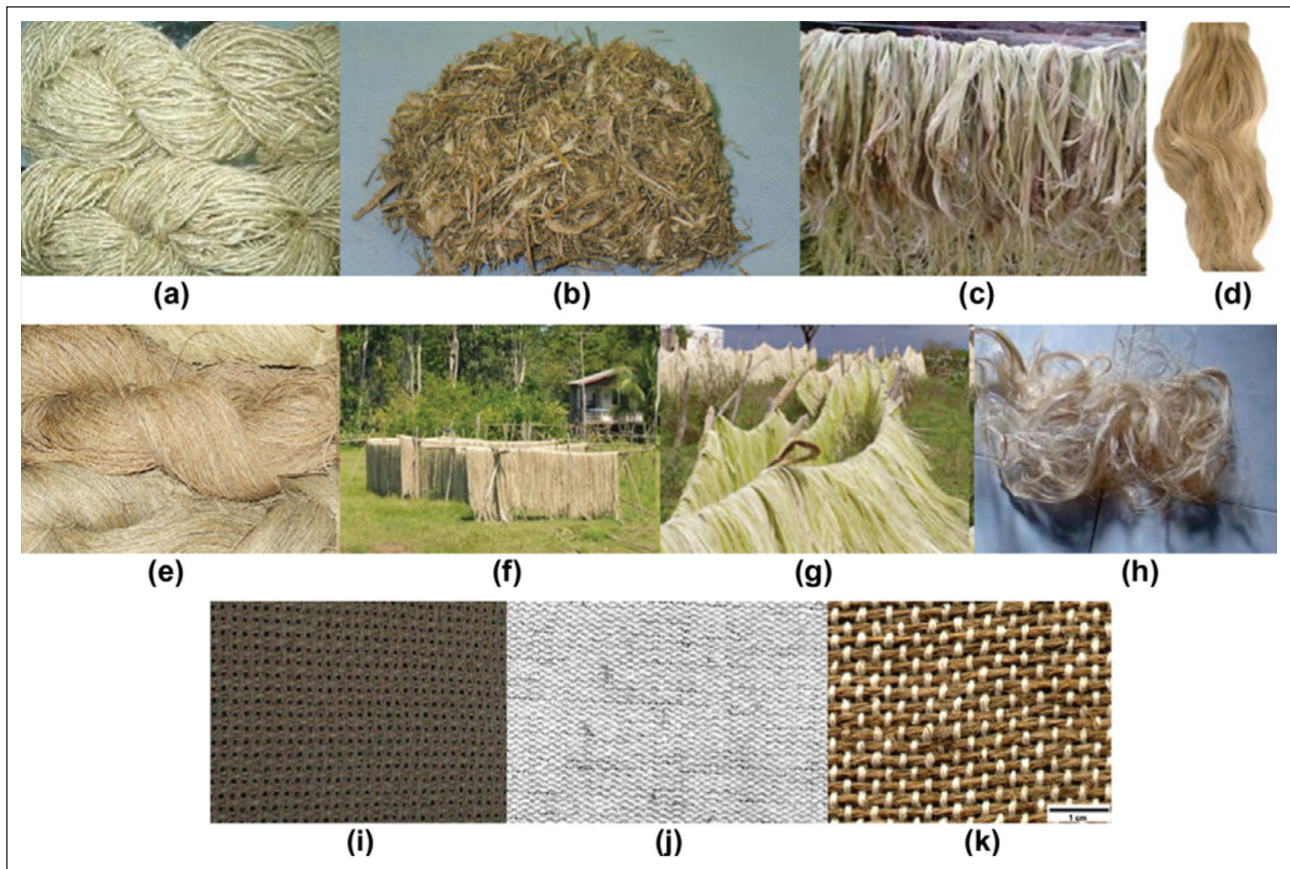


Figure 2. Plant-based natural fiber-reinforcements, (a) Banana; (b) sugarcane bagasse; (c) curaua; (d) flax; (e) hemp; (f) jute; (g) sisal; (h) kenaf. The typical pattern of reinforcements used in the hybrid LC-based biodegradable composite synthesis. (i) Jute fabric; (j) ramie-cotton fabric; (k) jute-cotton fabric [15].

tons of natural fibers (Fig. 3). Cotton accounted for 80% of natural fiber production by weight, and jute production was approximately 3 million tons in 2018, with wool and coir each accounting for about 1 million tons.

Unlike synthetic fibers, natural fibers do not get manufactured at a fiber production plant. Instead, they come from "natural" sources, as the name implies. This brings biodegradability and new factors that can affect the fiber properties that synthetic fibers do not have. These factors are shown in Table 3.

One of the most critical factors in Table 3 is the harvesting time because the harvesting time of the plant would significantly affect the structure of fibers and their physical and chemical composition. Because of this, the best harvesting time for the desired natural fiber mechanical and chemical composition, which are the essential aspects in defining the fibers' overall qualities, must be determined [6, 14].

2.2.2. Chemistry of Natural Fibers

A single natural fiber is between 1 and 50 mm in length, and the diameter of a fiber is around 10–50 μm . The fiber cell wall is composed of two main parts: the primary wall and the second wall. The primary wall's main purpose is to

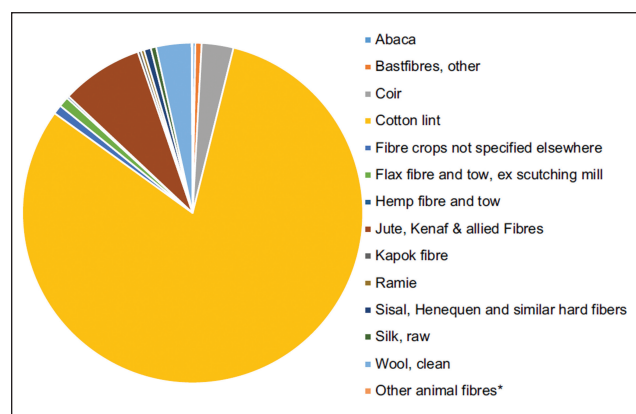


Figure 3. World natural fiber production in 2018 [17].

control the fibers' growth direction and rate. The secondary wall provides mechanical strength to the fiber, composed of three main layers, S1, S2, and S3 [13]. The three-dimensional structure of fiber and a fiber's typical cross-section is shown in Figure 4.

The major constituents of natural plant fibers are cellulose, hemicellulose, and lignin. Natural fibers also include

Table 1. Physical and mechanical properties of some natural fibers [16]

Fiber type	Density [g/cm ³]	Length [mm]	Diameter [μm]	Tensile strength [MPa]	Tensile modulus [GPa]	Specific modulus (Approx.) (E/ρ) [GPa.cm ³ .gr ⁻¹]	Elongation [%]
Abaca	1.5	–	–	400–980	6.2–20	9	1.0–10
Alfa	0.89	–	–	35	22	25	5.8
Begasse	1.25	10–300	10–34	222–290	17–27.1	18	1.1
Bamboo	0.6–1.1	1.5–4	25–40	140–800	11–32	25	2.5–3.7
Banana	1.35	300–900	12–30	500	12	9	1.5–9
Coir	1.15–1.46	20–150	10–460	95–230	2.8–6	4	15–51.4
Cotton	1.5–1.6	10–60	10–45	287–800	5.5–12.6	6	3–10
Curaua	1.4	35	7–10	87–1150	11.8–96	39	1.3–4.9
Flax	1.4–1.5	5–900	12–600	343–2000	27.6–103	45	1.2–3.3
Hemp	1.4–1.5	5–55	25–500	270–900	23.5–90	40	1–3.5
Henequen	1.2	–	–	430–570	10.1–16.3	11	3.7–5.9
Isora	1.2–1.3	–	–	500–600	18–20	14	5–6
Jute	1.3–1.49	1.5–120	20–200	320–800	8–78	30	1–1.8
Kenaf	1.4	–	–	223–930	14.5–53	24	1.5–2.7
Nettle	1.4–1.55	–	–	650	38	25	1.7
Oil Palm	0.7–1.55	–	150–500	80–248	0.5–3.2	2	17–25
Piassava	1.4	–	–	134–143	1.07–4.59	2	7.8–21.9
PALF	0.8–1.6	900–1500	20–80	180–1627	1.44–82.5	35	1.6–14.5
Ramie	1.0–1.55	900–1200	20–80	400–1000	24.5–128	60	1.2–4.0
Sisal	1.33–1.5	900	8–200	363–700	9.0–38	17	2.0–7.0

Table 2. Production amount and producer countries of some plant fibers [13]

Plant (lignocellulosic) fibers	Type	Worldwide production amount (10 ³ tons)	Countries
Abaca	Leaf	70	Philippines, Ecuador, Costa Rica
Pineapple	Leaf	74	Philippines, Thailand, Indonesia
Sisal	Leaf	378	Tanzania, Brazil
Coir	Fruit	100	India, Sri Lanka
Cotton	Seed	25000	China, India, USA
Oil Palm	Fruit	40	Malaysia, Indonesia
Flax	Bast	830	Canada, France, Belgium
Hemp	Bast	214	China, France, Philippines
Jute	Bast	2300	India, China, Bangladesh
Kenaf	Bast	970	India, Bangladesh, USA
Ramie	Bast	100	China, Brazil, Philippines, India
Bagasse	Grass	75000	Brazil, India, China
Bamboo	Grass	30000	India, China, Indonesia

a small amount of pectin and wax. The amount of cellulose will vary depending on the type and age of the plant. The differences between the different natural plant fibers' cellulose, hemicellulose, and lignin values are shown in Table 4.

Cellulose microfibrils have a diameter between 10–30 nm. They act as the reinforcement material and remain

embedded in the hemicellulose/lignin matrix, which is responsible for providing mechanical strength to the fibers. These microfibrils are linked together to form the cellulose fibers, the main constituent of most plant-based natural fibers. The second most abundant natural fiber constituent in cell plant walls is hemicellulose. Lignin is another signifi-

Table 3. Factors related to the production of natural fibers affect fiber properties [14]

Stage	Factors affecting fiber properties
Plant growth	Plant species
	Crop cultivation
	Crop location
	Fiber location in plants
	Climate
Harvesting	Fiber ripeness, which affects;
	Cell Wall thickness
	iber coarseness
	Fiber-structure adhesion
Fiber extraction	Decortication process
	Type of retting method
Supply	Storage conditions
	Age of fibers

cant component of the plant cell wall that provides strength, rigidity, and protection against microbial pathogens of lignocellulosic-based natural fibers cell walls [13].

2.2.3. Polymers and Biopolymers

Thermosetting polymers (thermosets) are widely used with natural fibers to produce biocomposites. Thermosets commonly used as matrix material in biocomposites are polyester resin, epoxy resin, and vinyl ester resin [18]. Due to their chemical composition, thermosets are non-recyclable and non-biodegradable materials. Biocomposites are preferred because of their environmentally favorable properties like recyclability and biodegradability, but thermosets render them unusable as the environmental problems due to the excessive use of non-recyclable polymers increase, the use of thermoset biocomposites decreases. However, to

address these environmental problems, there are efforts for thermoset biopolymers from vegetable oils, e.g., castor oil, soybean oil, rapeseed oil, etc. [13].

Linear chain molecules characterize thermoplastic polymers. The most crucial aspect of thermoplastic polymers is that they can be repeatedly melted or reprocessed. This characteristic makes the thermoplastic polymers favorable to use over the thermoset polymers as a matrix material in biocomposites. The degree of crystallinity of the thermoplastic is affected by the cool-down time because of its reusability. This is because the polymer chains need time to get organized in the orderly pattern of the crystalline state; too quickly of a cooling rate will not allow crystallization to occur [1].

On the other hand, too slow of a cooling rate may cause thermal degradation in the polymer. Thermoplastics with different cool-down times may show different mechanical behaviors under static or dynamic loads. This makes the temperature and cool-down time control very important during reprocessing. Commonly used thermoplastic polymers as matrix materials in biocomposites are polypropylene (PP), polyethylene (PE), low melt poly(ether-sulfone) (PES), and polyethylene terephthalate (PET).

For a biocomposite to be classified as a green composite material, it must consist of a biodegradable and biobased reinforcement material with a biodegradable and biobased matrix material. Conventional thermosets and thermoplastics are not enough for a composite material to be considered a green composite. In order to achieve complete biodegradability, biopolymers or biobased polymers must be used as matrix materials. Only biodegradable and biobased polymers can be defined as biopolymers. Due to the action of microorganisms over a determined time and in a specific environment, the material undergoes a degradation process; this material's ability is called biodegradability [13].

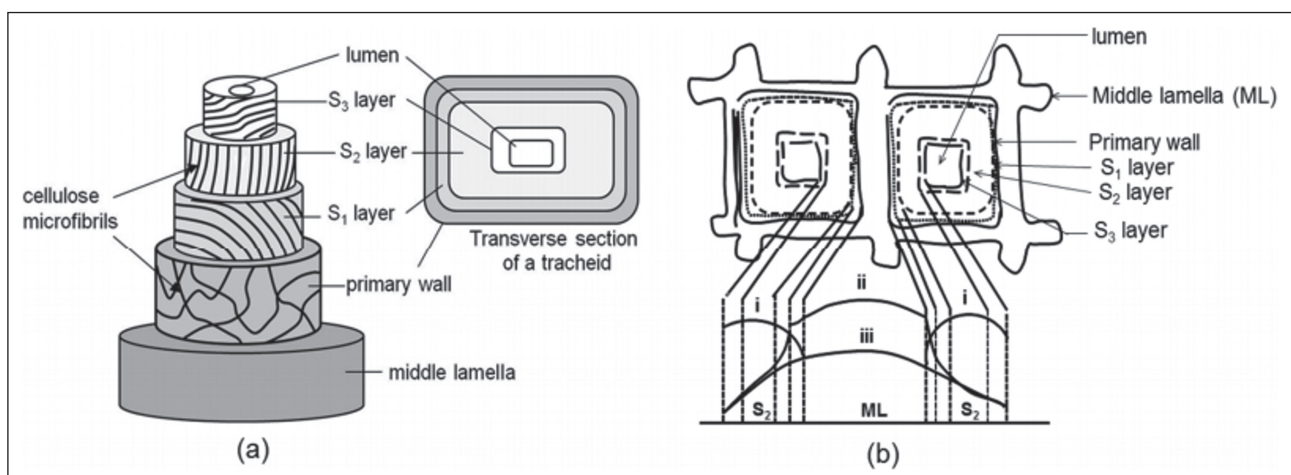


Figure 4. (a) Three-dimensional structure of the secondary cell wall of a xylem cell (b) the relative amounts of cellulose, hemicellulose, and lignin across a cross-section of two wood cells (i: cellulose, ii: lignin, iii: hemicellulose) [18].

Table 4. Composition of some natural fibers [16]

Fiber type	Cellulose [wt%]	Hemicellulose [wt%]	Lignin [wt%]	Pectin [wt%]	Waxes [wt%]	Micro-fibril angle [deg]	Moisture content [wt%]
Abaca	56–63	20–25	7–13	1	3	–	5–10
Alfa	45.4	38.5	14.9	–	2	–	–
Begasse	32–55.2	16.8	19–25.3	–	–	–	–
Bamboo	26–65	30	5–31	–	–	–	–
Banana	63–67.6	10–19	5	–	–	–	8.7–12
Coir	32–43.8	0.15–20	40–45	3–4	–	30–49	8
Cotton	82.7–90	5.7	<2	0–1	0.6	–	7.85–8.5
Curaua	70.7–73.6	9.9	7.5–11.1	–	–	–	–
Flax	62–72	18.6–20.6	2–5	2.3	1.5–1.7	5–10	8–12
Hemp	68–74.4	15–22.4	3.7–10	0.9	0.8	2–6.2	6.2–12
Henequen	60–77.6	4–28	8–13.1	–	0.5	–	–
Isora	74	–	23	–	1.09	–	–
Jute	59–71.5	13.6–20.4	11.8–13	0.2–0.4	0.5	8	12.5–13.7
Kenaf	31–72	20.3–21.5	8–19	3–5	–	–	–
Nettle	86	10	–	–	4	–	11–17
Oil Palm	60–65	–	11–29	–	–	42–46	–
Piassava	28.6	25.8	45	–	–	–	–
PALF	70–83	–	5–12.7	–	–	14	11.8
Ramie	68.6–85	13–16.7	0.5–0.7	1.9	0.3	7.5	7.5–17
Sisal	60–78	10.0–14.2	8.0–14	10	2	10–22	10–22

Biopolymers can be classified into two main categories. The first category is biopolymers made from natural raw materials (biobased) and biodegradable. The most popular biopolymer, PLA (Polylactide acid), is considered in this category along with other biopolymers, such as PHAs (polyhydroxyalkanoates), starch, and chitosan [19]. The second category belongs to biopolymers made from fossil resources but biodegradable, such as PCL (polycaprolactone), PBS (polybutylene succinate), and PBAT (Polybutylene adipate terephthalate) [13].

2.2.4. Macrostructure of Natural Fibers

Natural fibers used in NFRPs can be divided into three categories according to their fiber orientation: non-woven, woven fabric, and unidirectional (UD). Non-wovens are mainly produced with randomly oriented short fibers. Felts, a non-woven type, use randomly oriented short natural and polymer fibers as reinforcement and matrix materials. Felts have excellent sound absorption and thermal insulation properties due to their high thickness values. However, unlike other NFRP types, felts have lower strength than woven fabrics and UD.

The second type is woven fabrics. This type of fabric is generally used for composite applications where the composite is produced by combining natural fiber fabrics with polymer pellets or films. Depending on the needs, they can

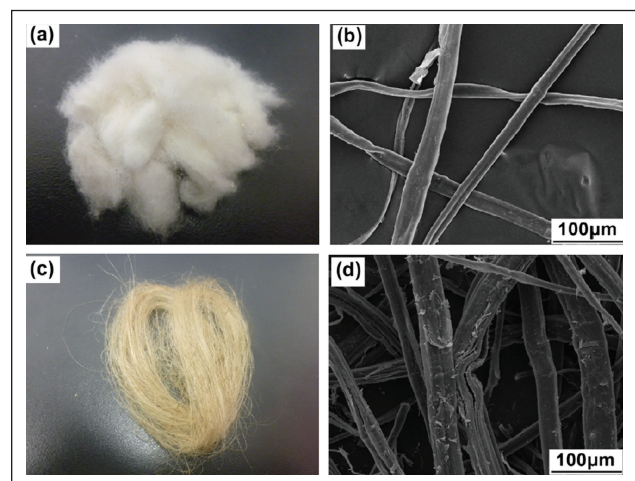


Figure 5. Photos and micrographs of NHF (a, b) and SHF (c, d) [27].

be produced in bi-directional or multidirectional form. These fibers are easy to produce and are used to obtain high mechanical strength in multiple directions. However, this multidirectional fiber structure might create extra weight than felts and UD.

Unidirectional (UD) fibers' structure is similar to the woven ones with a difference: all-natural fibers run in a

single, parallel direction. UD s show the best mechanical performance under loads with the same direction as their fibers. In addition, UD s are lighter than their woven counterparts. These properties allow for more precise production with even lighter weights. However, UD s are not appropriate for parts where a great anisotropic strength property is required.

Two of the most popular natural fibers are hemp and flax [20]. Therefore, the macrostructure of natural fibers is explained in this section with hemp and flax fibers studies.

Numerous studies focus on hemp fiber-reinforced polymers and flax-reinforced polymers. In the case of hemp fiber-reinforced non-wovens, most studies focused on their superior noise reduction properties [21–23]. The works of Nick et al. [21], Yilmaz et al. [22], and Oldham et al. [23] utilize non-wovens in their felt forms, where their sound absorption properties are most robust, but their mechanical strength values are lowest. Numerous studies exist for woven hemp fiber-reinforced polymer biocomposites [24–28]. Corbin et al. [24] have studied the effects of weave patterns and features on hemp fabrics and have concluded that high-performance woven hemp fabric composites made from low-twisted roving can be obtained. The study presented by Bonnafous et al. [25] compared the damage mechanisms in woven hemp fiber composites and glass fiber composites; they established that the damage development of these two composites is different. Hasan et al. [26] studied the mechanical performance of hemp/glass woven fabric hybrid composites treated with greenly synthesized silver nanoparticles. Berhanu et al. [27] have studied the sliding behavior of woven hemp fabric reinforced biocomposites and have established good compatibility between the woven hemp fabric and polypropylene. Baghei et al. [28] have studied the characterization of biocomposite reinforced with woven hemp fabrics and lyocell fabrics. They have used polylactic acid (PLA) as matrix material; PLA is a filament produced using natural resources. Thus the biocomposite in this study can be classified as a green composite. It should be noted that the performance of this green composite was lower than its lyocell reinforced counterpart.

However, the composites with woven fiber are mainly manufactured with polymer pellets and resins as thin plates [24–27]. This feature seriously limits the sound absorption capability of hemp fibers but increases their mechanical strength remarkably. Even the woven hemp reinforced biocomposites with polymer fiber matrix are investigated for superior mechanical properties and water absorption characteristics instead of poor noise reduction performance [28].

As mentioned, non-woven NFRPs are weaker than their woven counterparts, considering their mechanical performance. To use the felts in the areas where high mechanical strength is needed, they must be hot-pressed and formed as biocomposite plates. Hargitai et al. [29] have worked on hemp-PP and flax-PP non-wovens to find the optimal re-

inforcement to matrix ratio for best mechanical strength values. They have concluded that 50 % by weight is the optimal value for hemp fiber-reinforced PP felts. The studies of Shahzad [30] and Stelea et al. [31] have also focused on the characterization of hemp-PP felts by testing them as plates. Chen et al. [32] have compared the mechanical performance of hemp-PP non-woven to bagasse-PP, kenaf -PP, and ramie-PP non-wovens. They revealed that the hemp-PP composites, compared to other biocomposites, featured similar tensile and flexural modulus values with better thermal properties [32]. It should also be noted that there are also studies on the mechanical strength of unpressed hemp fiber-reinforced felts, but their mechanical properties are inferior compared to their hot-pressed counterparts [33].

For flax-reinforced biocomposites, the studies for non-woven flax composites also focus on sound absorption and thermal insulation properties [34–36]. Rasyid et al. [34], Velayutham et al. [35], and Muthukumar et al. [36] studied the sound absorption and acoustic performance of non-woven flax fiber fabrics. They have established that the sound absorption performance of flax fibers is good due to the macrostructure of the natural fibers [34, 35] and can be improved with the addition of low-melt PET [36]. However, since the flax fibers are mechanically stronger than hemp fibers, as established by Pil et al. [37], Shahria et al. [38], and Maity et al. [39], the emphasis is on the mechanical strength of non-woven flax fiber-reinforced polymers. Maity et al. [39], John et al. [40], Omrani et al. [41], Bachmann [42], and Alimuzzaman [43] have studied the mechanical performance of flax fiber reinforced biocomposites by using characterization tests and by employing different techniques and methods to increase its performance, such as surface modification. Compared with hemp felts, flax fiber-reinforced biocomposites show better mechanical performance in their felt forms but with high material deformation [41]. Due to the high mechanical strength of their fibers, non-woven flax fibers may even be used as structural building materials [44, 45]. Woven flax fibers have higher mechanical properties than non-woven flax fibers [46] and woven hemp fibers [47].

Unidirectional flax fibers, like all-UD fibers, perform best when the load is in the same direction as the fibers. Depending on the load, their mechanical performance may be better or worse than their woven counterparts [48]. There are numerous studies that focus on the polyesters [49], polylactic acid (PLA) [50], polypropylene (PP) [51, 52], bio-based resins [53], and geopolymers [54] that are UD flax fibers reinforced.

Hybrid biocomposites reinforced with two different types of fibers or reinforced with the different fiber orientations of the same fibers are also possible to produce. Due to their higher mechanical performance, flax fibers are mostly combined with glass fibers [55] or carbon fibers [56]. However, they can also be combined with other natural fibers, including hemp fibers [57, 58], to preserve their recyclabil-

ity and to be able to classify them as biocomposites [38]. However, hemp fibers are not as strong as flax fibers, and because of this, the most used synthetic fiber for hybrid hemp fiber composites is glass fibers [26, 59].

Limitations of Natural Fibers

Natural fibers have higher moisture absorption than synthetic fibers due to their hydrophilic nature. The long-term effect of moisture absorption is developing micro-cracks, thus lowering the mechanical properties of NFRP significantly [1, 5, 29]. However, there are some contradictory research results about the effect of moisture in the short term. For example, Hargitai et al. [29] proposed that wetting the hemp fiber-reinforced polypropylene fiber composite increases the impact strength but decreases the bending properties. On the other hand, Munoz et al. [60] have studied the water absorption of flax fiber-reinforced bio-epoxy composite and concluded that water absorption increases tensile strength but reduces the flexural properties, similar to those proposed by Hargitai et al. [29]. Even though the impact strength aspect has positive effects in the short term, moisture, and water absorption, wear down the mechanical properties of natural fibers by creating micro-cracks or fiber swelling and weaken the NFRP structurally [4].

Another problem with natural fibers is that they have limited thermal stability. The temperature of natural fibers should not exceed 200 °C. Beyond this temperature, the fibers will degrade, and the mechanical properties of the natural fibers will be significantly reduced. Several studies found that this thermal stability problem depends on the lignin rate of natural fiber [4]. Manfredi et al. [61] proposed that the decomposition of the lignin starts at 200 °C, which is the main reason for natural fiber's thermal problems. Kumar et al. and Sarkar et al. [62, 63] proposed that lower lignin content in the natural fiber causes degradation to begin at a higher temperature. This means that there are differences between different natural fibers in the aspect of thermal stability. Due to this characteristic, Manfredi et al. [61] proposed that flax fiber has the best thermal resistance since its lignin content is the lowest among natural fibers.

Regarding the dependence on harvesting time, Pickering et al. [6] have found a significant increase in the average tensile strength of hemp fiber during the growth period from 99 days to 114 days and reaches optimum average tensile strength at 114 days. Das et al. [64] have found that the optimum days of growth for jute fibers should be 120 days; beyond 120 days, tensile strength reduces significantly.

2.3. Surface Modification of Natural Fibers and Polymers

The problems mentioned in the previous section are severe limitations to developing and applying natural fibers. However, especially in the last ten years, much progress has been made to reduce or, if possible, eliminate these prob-

lems. The most important limitations are dependence on harvesting region and time, poor compatibility with the polymer matrix, the tendency to moisture absorption, and thermal stability issues. Each of these limitations became the subject of different studies, and efforts have been made to find a solution to these problems.

The problems and the solutions and solution proposals to these problems have been thoroughly investigated, and these findings will be explained in a detailed manner with different studies to introduce the solutions for these disadvantages to make biocomposites more favorable.

Various researchers proposed that surface modification must be used to increase poor compatibility with polymer matrix. Surface modification of NFRPs not only increases the poor compatibility problem of natural fibers but also solves other essential issues of biocomposites, such as decreasing water hydrophilicity and increasing thermal stability by removing lignin and hemicellulose. However, different views on surface modification should be applied to different natural fibers. Due to these significant advantages and differences in the application of surface modification, this topic will be investigated thoroughly.

Wu et al. [65] have proposed that applying magnesium hydroxide (MH) as the surface modification significantly increases the rupture and tensile strength of kenaf fiber. First, the surface of kenaf fibers has treated with a five wt% alkali solution, then modified with MH. According to Wu et al. [65], these mechanical properties improved interfacial compatibility between kenaf fibers and polyester resin after modifying the surface of kenaf fibers with MH. In addition to improved mechanical properties, kenaf fiber-reinforced polymer composites with MH modification showed excellent thickness swelling and water absorption with deficient water intake, thus improving another problem of NFRPs.

Suizu et al. [66] have suggested that mercerization of ramie fiber-reinforced biopolymer composites increases the fracture strain of ramie fibers, thus improving the toughness of the green composite significantly. In addition to the toughness, mercerized ramie fibers absorb almost twice as much impact energy as the green composite using untreated ramie fiber reinforcement. Other than mechanical properties, water absorption was also studied by Suizu et al. [66], and they found that the impact energy of the ramie fiber-reinforced biopolymer composite with mercerization increased as the water content increased. However, the article also indicates that this increase in impact properties is due to softening of the ramie fiber reduces the deformation resistance and the strength of the composites. Also, they have established that, even though low water addition (2 wt% to 5 wt%) increases the composites' impact energy. It can be anticipated that the impact energy and general mechanical properties of the composite would decrease with further increased water content. This finding on water absorption coincides with Hargitai et al. [29] and Munoz et al. [60].

Qiu et al. [67] have worked on surface modification of hemp fiber-reinforced unsaturated polyester composites to increase the composite's mechanical properties by improving the interfacial adhesion. They have proposed that treating hemp fibers with 1,6-diisocyanatohexane (DIH) and 2-hydroxyethyl acrylate (HEA) significantly increases the tensile strength, flexural modulus of rupture and flexural modulus of elasticity, water absorption resistance, and dramatically improves the interfacial adhesion between hemp fiber and UPE.

Lu et al. [68] have worked on the effect of 5 wt% alkalis and 5 wt% silane treatments on the thermal stability of hemp fiber. They have proposed that both treatments effectively removed pectin and wax, along with partial removal of lignin and hemicellulose, which increased the mechanical properties and adhesion with the polymer matrix. It is worth noting that while both treatments improved the thermal stability of the hemp fiber, alkali-treated fibers showed higher thermal stability compared with the silane treatment results.

Oh et al. [69] have modified the surface of hemp fibers using five wt% alkali solution and oils (soybean and corn) on hemp-PP composites. They have found that alkali treatment removed the non-cellulose parts, such as lignin and hemicellulose, thus reducing the fiber diameter of hemp fibers. Higher temperatures during the surface treatment process mean better removal of non-cellulose parts. However, when the fiber was treated with alkali solution at temperatures higher than 100 °C, the tensile strength was decreased due to the accelerated cellulose hydrolysis. Cellulose hydrolysis occurs at higher temperatures and causes the cellulose to be decomposed by alkali into aldehydes and acetone. This causes a reduction in tensile strength and poor mechanical performance overall. Alkali-treated hemp fibers treated with soybean and corn oil also have increased water resistance and interfacial performance. Even though both oils have increased the compatibility between hemp fiber-reinforcement and PP matrix, soybean has performed better than corn oil, thus making soybean a better choice. The paper concluded that 100 °C is the optimum temperature for maximum lignin and hemicellulose removal without damaging the cellulose part of the fiber to increase the overall mechanical performance of hemp fibers.

There are different results on the alkali treatment of hemp fibers, however. According to Islam et al. [70], alkali treatment removes lignin and hemicellulose, resulting in better-separated fibers with cleaner surface topography and better thermal stability. However, they have also found that the fiber's tensile strength was reduced due to the removal of lignin and degradation of the cellulose chains. It is worth noting that at the surface treatment stage of this paper, hemp fibers were treated with five wt% alkali solution at 120 °C for 60 minutes, which further proves the argument made by Oh et al. [69] that when fiber treatment

temperature is higher than 100 °C, alkali removes cellulose along with excessive amounts of lignin and hemicellulose. Väisänen et al. [71] also proposed that the alkali treatment of hemp fibers reduces tensile strength slightly. They treated the hemp fibers with ten wt% alkali solution at 95 °C for 60 minutes. They have established that the main reason for this reduction is the removal of lignin and degradation of cellulose chains, the same as Islam et al. [70]. However, Väisänen et al. [71] suggested that the main reason for this contradiction in the effect of alkali treatment on natural fibers is the longer treatment time and relatively high concentration of the alkaline solution (NaOH) used in the current study in terms of increasing or decreasing the tensile strength. It is also worth noting that previous research made by various researchers [65–70] has used five wt% surface treatment solution utmost, thus proving the point of Väisänen et al. [71] in using excessive rate (10 wt%) of alkali solution.

There are various types of surface modification or surface treatment methods mentioned above. According to surveys, one of the most effective surface treatment chemicals is maleic anhydride grafted polypropylene (MAPP). Unlike other surface treatments applied to natural fibers, MAPP is added to the polymer matrix in this study to polypropylene (PP). Sullins et al. [72] have worked on the effects of alkali treatment on hemp fiber and MAPP treatment on PP pellets. Three different composites have been used: only alkali treated, only MAPP treated, and both alkali and MAPP treated hemp-PP composites. Both surface treatments have increased hemp-PP composite's tensile and flexural properties by having excellent interfacial adhesion with no apparent gaps between the fiber and matrix. A critical aspect of this work is that only MAPP-treated hemp-PP composites showed better tensile and flexural properties than only alkali-treated and both MAPP and alkali-treated hemp-PP composites. This paper indicates that instead of treating the surface of hemp fiber reinforcement, better results can be achieved with the MAPP treatment of the PP matrix. In addition to the significant increase in mechanical properties and better interfacial adhesion, Bledzki et al. [73] and Schirp and Stender [74] have established that the application of MAPP reduced the water uptake of NFRPs significantly, thus strengthening the idea of using untreated fibers with thermoplastic polymers with maleic anhydride grafted polymer (MAH) or when used with polypropylene, MAPP addition.

Niu et al. [75] have worked on hemp fiber-polypropylene composites' mechanical properties and thermal stability with MAH addition. They also used maleic anhydride grafted styrene-(ethylene-co-butylene)-styrene copolymer (SEBS-MAH) and maleic anhydride grafted Poly (ethylene octane) (POE-MAH) as a compatibilizer to improve the fiber-matrix interactions. They found that all composites containing compatibilizers showed higher storage modulus and interfacial adhesion between hemp fiber and PP

matrix than total composites. The addition of PP-MAH increased the tensile flexural strengths of the composite. It is also worth noting that the addition of SEBS-MAH and POE-MAH elastomer remarkably increased the notched and unnotched impact strengths, thus proving itself a valuable compatibilizer for areas with strong impact resistance is needed.

Another study on PP-MAH or MAPP is the paper by Merotte et al. [76]. This study used four non-woven biocomposites; flax-PP, flax-MAPP, hemp-PP, and hemp-MAPP. A critical aspect of this work is that they used PP and MAPP fiber instead of the usual PP and MAPP pellet or powder. They used a fiber-matrix ratio of 50 wt% at all these four composites. As expected, hemp fibers exhibited poorer tensile properties but showed better interfacial shear strength with PP and MAPP than flax. Both hemp and flax fiber have shown better tensile strength and tensile modulus values with MAPP fiber matrix than pure PP fiber.

Yan et al. [77] have compared two different types of hemp fibers: noil hemp fibers (NHF) and scutched hemp fibers (SHF). SHF is mechanically degummed raw material for textile hemp fiber production, and NHF is a by-product of textile hemp fiber production from SHF. It is the over-degummed hemp fiber with a much smaller diameter and length. These two types of hemp fibers are very different from each other visually, as shown in Figure 5. The NHF reinforced PP matrix composites and SHF reinforced PP matrix composites have their surface treated with MAPP, and the results have been compared with the NHF-PP and SHF-PP composites without surface treatment. They have found that most of the pectin, hemicellulose, and lignin were removed during the degumming process of noil hemp fibers. Due to this removal, NHF has performed better thermally when compared with SHF. They have also established that MAPP significantly improved the hemp fiber-PP adhesion, which leads to significantly better tensile strength, flexural strength, and impact strength by increasing the fiber-resin adhesion. The positive effects of MAPP coincide with the findings of Sullins et al., Bledzki et al., Schirp et al., Niu et al., and Merotte et al. [72–76].

Talla et al. [78] have worked on hemp-Polyethylene terephthalate (PET) composites. PET has been compounded with Polycaprolactone (PCL) to reduce the melting point of PET, and hemp fibers have been treated with an alkali solution to increase their thermal stability to be able to use PET and hemp fiber together. The results from pure hemp-PET composite have been compared with hemp-PET composite with additives such as clay grade Cloisite 30B, pyromellitic dianhydride (PMDA), and glycidyl methacrylate (GMA). The results have shown that melt-processed PET can be a suitable matrix for hemp-thermoplastic polymer composites. Hemp and PET, without any additives, can have a good bonding interface, thus making rearing coupling agents optional. With some trade-off between the mechanical and

structural properties, hemp-PET composites can be used without any added chemical and can be used instead of the widely popular hemp-PP. However, it should be noted that hemp fibers have been treated with an alkali solution to increase the fiber's thermal performance to match it with PET's thermal degradation ($T_m > 200$ °C), so the hemp fiber-reinforced composite is not 100% chemical-free.

2.4. Impact Performance of Biocomposites

Studies in the literature so far are mainly about improving tensile and flexural strength, with only a few studies on impact strength using surface modification. Although the tensile and flexural strengths are essential parameters to determine the mechanical characteristics of an NFRP, they are not sufficient alone. Impact behavior should always be considered, especially for composite materials, since composites react differently to impacts when compared with conventional materials, and most composite materials are used in areas where high impact strength is needed; in addition to that, impact performance is an essential indication of the overall strength of the composite materials [79]. Because of these requirements, papers and studies focusing on the impact properties of NFRP must be surveyed thoroughly too. For this reason, the focus of the following studies will be on the impact performance of natural fiber-reinforced biocomposites.

The Charpy impact behavior of gigantic bamboo fibers reinforced with epoxy composites was studied by Glória et al. [80]. They employed bamboo fibers with no surface modification as the matrix and DGEBA epoxy resin as the reinforcement material. Charpy impact testing was performed on 10%, 20%, and 30% bamboo fiber-reinforced composite biocomposites. According to the findings of this study, the Charpy toughness of biocomposites increases with increasing bamboo fiber density. This work shows that the Charpy toughness of biocomposites increases with increasing bamboo fiber density. However, they also note that this increase in Charpy toughness is relatively smaller than the other natural fibers due to defects introduced in the giant bamboo fiber during extraction by a manual cut of the hard culm with a razor blade, thus rendering the use of bamboo fibers ineffective at the areas where strong impact toughness is needed.

As in the previous study, Assis et al. [81] have worked on the Charpy impact behavior of natural fibers without surface modification as reinforcement and DGEBA epoxy resin as a matrix with triethylenetetramine (TETA) as a hardener. This study used banana fibers with 10%, 20%, and 30% in volume as natural fiber reinforcement instead of bamboo fibers. They have established that as banana fiber volume increased, the Charpy toughness of biocomposite increased significantly. This increase in toughness is apparently due to the low banana fiber/epoxy matrix interfacial shear stress. This results in higher absorbed energy because of a longitudinal propagation of the cracks throughout the

interface, which generates larger rupture areas than a transversal fracture. They have concluded that banana fibers have the best impact characteristics compared with other fibers. However, low banana fiber/epoxy matrix interfacial strength will be a significant problem and a limiting factor for other mechanical performance characteristics such as tensile, bending, and shear.

Pereria et al. [82] have worked on the Charpy impact behavior of epoxy matrix composites with jute fibers. They have used aligned jute fibers without surface modification as reinforcement material and DGBEA epoxy resin as a matrix material with TETA as a hardener. Similar to previous papers with giant bamboo fibers [29] and banana fibers [30], this paper also used three different biocomposites with 10%, 20%, and 30% in volume as a natural fiber matrix. They have found that jute fibers have performed well at the Charpy impact test. Similar to the previous results, impact toughness was measured as a function of fiber, so composites with a higher volume of jute fibers showed better impact characteristics than the lower volume of jute fiber composites. Pereria et al. also note that even though jute fibers have good impact properties, they underperform compared to banana fiber-reinforced biocomposites [80, 81].

In addition to these studies, previously surveyed papers from Suizu et al. [66] too, have focused on the impact properties of green composites with mercerized ramie fibers. Niu et al. [75] have worked on hemp-PP composites and proposed that with the addition of SEBS-MAH and POE-MAH, the impact strength of the composites increased significantly. Another study on hemp-PP composites that has tested the impact properties is the paper published by Yan et al. [77]. They have established that with the addition of MAPP, the impact strength of the composite increased. From the studies of Niu et al. and Yan et al. [75, 77], the conclusion can be drawn that with the correct chemical additions, impact strength enhanced-hemp fibers can compete against jute and banana fibers, which have higher impact resistance than pure hemp fibers [81, 82].

Thanks to the data and results from previous studies, recent studies on the impact performance of biocomposites and green composites are focused on the different areas with different natural fibers. Reddy et al. [83] studied the mechanical and wear performance of three different epoxy biocomposites reinforced with different natural fibers (Tapsi, Abolition Indicum, and Prosopis). They have concluded that Abolition Indicum has shown better impact properties among the biocomposites.

Al-Oqla et al. [84] have studied the flexural and impact performance of LDPE reinforced with green olive leaves. The increase in impact performance of the biocomposite with adding olive leaves indicates that olive leaves can be considered a low-cost and eco-friendly alternative reinforcement material.

The studies of Hassan et al. [85] and Liang et al. [86] focused on the impact performance of green composites. Hassan et al. [85] studied green composites' acoustic, mechanical, and thermal properties reinforced with three types of fiber wastes: cotton fly, coconut/coir husk, and sugarcane, with green epoxy resin as matrix material. They found an increase in impact performance with all natural fiber additions, with the cotton fiber reinforced green composite performing the highest. The study of Liang et al. [86] has worked on the impact performance of PLA reinforced with sisal fibers. However, it should be noted that sisal fiber was treated with an alkali solution before blending with PLA. They have also found increased impact performance with the addition of sisal fibers. They have also established that long-sisal fiber reinforced green composites have performed better than their short-sisal fiber reinforced counterparts.

2.5. Hybrid Biocomposites

As mentioned before, for a material to be considered a composite material, it should consist of at least two different materials; this means that there is a possibility of manufacturing a composite material that consists of more than two different types of materials if it is feasible to use. These materials are called hybrid composites. Such examples may be suitable for this definition; a composite material with two reinforcement materials and a polymer matrix or one reinforcement material with two polymer matrices. However, even though there are unlimited possibilities that can be created by using this formula, there are few real-world applications with acceptable results.

Petrucci et al. [87] have used various hybrid composite laminates based on basalt fibers combined with flax, hemp, and glass fibers. They have manufactured three different hybrid composites using EC360 epoxy as a matrix material: GFB, which consists of glass fiber, flax fiber, and basalt fiber; GHB, which contains glass fiber, hemp fiber, and basalt fiber; FHB, with flax fiber, hemp fiber, and basalt fiber, respectively. Their mechanical tests have shown that in terms of flexural performance, GFB has performed the best, followed by FHB and GHB, respectively. This order is also preserved in the case of post-impact flexural loading, suggesting that the addition of glass fiber offers a much better result in the presence of flax fibers than in the presence of hemp fibers. This formula also increases the impact toughness of composite by adding basalt fibers.

Another study on natural and glass fiber-reinforced polymer hybrid composites was carried out by Kong et al. [88]. They have used regenerated cellulose fiber with glass fiber as reinforcement material and epoxy resin as a matrix material. They have established that the natural fiber must be sandwiched between the glass fiber layers to maximize the toughness of hybrid composite material. Clark and Ansell [89], which is considered one of the first studies on a

hybrid glass fiber/natural fiber composite, found that sandwiched jute fibers between glass fibers maximize the toughness of hybrid composite, which is the source of the claim made by Kong et al. [88].

Sanjay and Yogesha [90] have established various advantages of hybrid composites against pure glass fiber or pure natural fiber composites, but the problem with hybrid composites is not due to their compatibility between synthetic and natural fibers; instead is due to using synthetic fibers in the composite.

Due to the general characteristics of synthetic fibers, hybrid composites with synthetic fibers are non-biodegradable, non-recyclable, and non-green, thus rendering compositely unusable in the areas where using biodegradable or recyclable materials is compulsory due to regulations [4]. No matter how good hybrid composites are, this problem prevents the wide use of synthetic fibers with natural fibers.

Due to some obligations to use biodegradable and recyclable materials in specific industries (especially in the automotive industry), natural fiber's use has increased significantly over the last 20 years. Thermoplastic polymers reinforced with natural fibers are only recyclable [4]. However, to manufacture a fully biodegradable composite material, matrix material should be biodegradable (biopolymer), just like the natural reinforcement fiber.

Various studies used a biodegradable matrix (biopolymer), as mentioned by Mitra [11]. Considerable studies have been made on green composites with natural fibers and biopolymers such as starch, polylactide (PLA), polycaprolactone (PCL), and Poly(3-hydroxybutyrate-co-3-hydroxyvalerate) (PHBV). Even though they have environmental advantages, Mitra [11] also noted that these biopolymers have tensile and flexural strengths lower than 100 MPa, limiting their usage in high-strength applications.

The application areas of green composites are extensive [91]. They can be used for environmental concerns and sustainability [92, 93] or as construction materials [94]. The production of green composites can also be achieved with significantly different materials, as long as they are recyclable and biodegradable [95, 96]. The study by Scaffaro et al. [97] shows a wide variety of areas for the use of green composites. They used PLA-based green composites reinforced with agricultural and marine wastes and studied the possibility of three-dimensional printability of these green composites. They have established that with a slight difference in molecular weight and filler aspect ratio, it is possible to 3D print the biocomposite. Another study by Leow et al. [98] utilized spent coffee grounds as reinforcement materials. They established that with the addition of spent coffee grounds and acetone, the performance of the composite material increased. Kamble et al. [99] have worked on green composites reinforced with waste cotton fibers. The increase in performance of an epoxy matrix with reinforcement

indicates that waste cotton fibers are an environmentally friendly and economical alternative to synthetic fiber reinforced composites.

The increased concern for the environment heightens the search for sustainable and environmentally friendly materials for various applications. When a wide variety of application areas and types of reinforcement materials are considered, green composites may be an answer to this search [100, 101].

2.6. Performance and Degradability of Green Composites

Various studies focused on using and performing natural fiber-reinforced and biopolymer matrix biocomposites, with their specific name, green composites. The study by Stapulionienė et al. [102] used short hemp fibers (20–30 mm in length) as reinforcement material with PLA fibers as matrix material. They have found that the direction of fibers at the stress direction may significantly influence the mechanical properties. However, this study's most important result is the possibility of successfully using hemp and PLA fibers together.

Song et al. [103] have also worked on hemp-PLA fiber green composites. The degummed and surface-treated hemp fibers are mixed with PLA fiber to create fiber pellets; then, fiber pellets are mixed with PLA pellets. Thus, composite pellets were created. Hemp-PLA fiber composite pellets have been manufactured from these composite pellets with the help of injection molding. After the mechanical tests, they concluded that this process increases the mechanical properties with the help of PLA fibers and silane treatment.

Mukherjee and Kao [104] proposed that both PLA and natural fibers are hydrophilic so that this property will facilitate better adhesion. However, they have found poor adhesion between natural fiber and PLA, probably due to debonding during mechanical testing or poor approximation during composite production. The hydrophilicity of PLA means that, as seen in natural hydrophilic fibers, PLA is also subjected to water or moisture absorption. The surface modification increases the interfacial adhesion and eliminates the natural fiber and PLA's water or moisture absorption problems. Therefore, it is essential to compete with synthetic and other natural fibers with synthetic polymers without compromising the biodegradability of these two materials.

It is also worth mentioning that degradability features are essential to compete with sustainability issues. For example, Shibata et al. [105] have worked on the degradability of biodegradable polyesters reinforced with abaca fibers and found from the soil-burial test that the composites containing untreated abaca fibers have shown the highest weight loss after being soil-buried for 24 weeks, thus indicating the highest biodegradability when compared with treated abaca fibers.

3. CONCLUSIONS, CHALLENGES, AND FUTURE PERSPECTIVES

In this work, the studies on natural fibers and natural fiber-reinforced polymers have been reviewed. The micro-and macrostructure of natural fibers has been explained. The advantages and the limitations of natural fibers have been discussed, and the methods used to eliminate these limitations have been examined.

It can be seen from this review that natural fibers can replace synthetic fibers as the primary reinforcement materials for composites. Despite their limitations, their advantages of recyclability and degradability make them a critical part of environmental issues. Also, it has been seen that with the help of correct surface modification, limitations of natural fibers, namely, moisture absorption, poor compatibility, and low thermal stability, can be reduced to acceptable levels or, if possible, wholly eliminated.

These aspects make natural fibers and biocomposites a critical material for composite materials and the environment. This importance will be increased with new natural fibers, biopolymers, and methods for producing these natural fibers and biopolymers.

However, there are still challenges for natural fiber-reinforced polymers to be utilized in areas with high safety standards, such as the cabin interior of commercial aircraft. Poor fire resistance of natural fibers is a big concern for this area. There is also the issue of the degradability of natural fibers and biopolymers. This might be considered an advantage for parts with a short life span or those used as consumables, but this aspect might be a disadvantage for long-life span parts. The degradability of the NFRP must be examined and correctly understood to predict a part's life limit appropriately, whether structural or not.

As an alternative to petroleum-based synthetic polymers, biopolymers can be enhanced. More natural materials can be introduced as resource materials to minimize reliance on petroleum and expand the range of biopolymer resources. These new natural resources can help achieve thermoplastic biopolymers' objectives with improved fire resistance and strength.

In addition, there is a gap in the literature on the aging of biocomposites subjected to different service environments. The studies must cover this area to increase the possible service areas of biocomposites. For example, a study that includes an aging test at cryogenic temperatures may enable biocomposites for deep-space applications.

For the implementation of large-scale production of NFRPs, different and more efficient production methods must be studied. Biocomposites can be produced with the same production methods as traditional synthetic composites. However, novel production methods must be introduced to NFRPs for mass production. Additive manufacturing of NFRPs can be an alternative to traditional composite production methods.

There are many areas for the potential use of biocomposites. More studies on NFRPs are needed to fill the literature gap about biocomposites and make them available for more areas and industries. The areas mentioned above and the challenges that come with them are the future of biocomposites and green composites.

DATA AVAILABILITY STATEMENT

The authors confirm that the data that supports the findings of this study are available within the article. Raw data that support the finding of this study are available from the corresponding author, upon reasonable request.

CONFLICT OF INTEREST

The authors declare that they have no conflict of interest.

FINANCIAL DISCLOSURE

The authors declared that this study has received no financial support.

PEER-REVIEW

Externally peer-reviewed.

REFERENCES

- [1] Chawla, K. K., (2015). *Composite materials science and engineering* (3rd ed). Springer.
- [2] Monteiro, S. N., Lopes, F. P. D., Ferreira, A. S., & Nascimento, D. C. O. (2009). Natural-fiber polymer-matrix composites: cheaper, tougher, and environmentally friendly. *The Journal of The Minerals, Metals & Materials Society*, 61(1), 17–22. [\[CrossRef\]](#)
- [3] Joshi, S. V., Drzal, L. T., Mohanty, A. K., & Arora, S. (2004). Are natural fiber composites environmentally superior to glass fiber reinforced composites? *Composites Part A: Applied Science and Manufacturing*, 35(3), 371–376. [\[CrossRef\]](#)
- [4] Ahmad, F., Choi, H. S., & Park, M. K. (2015). A review: natural fiber composites selection in view of mechanical, light weight, and economic properties. *Macromolecular Materials and Engineering*, 300(1), 10–24. [\[CrossRef\]](#)
- [5] Arockiam, N. J., Jawaid, M., & Saba, N. (2018). Sustainable bio composites for aircraft components. *In Sustainable Composites for Aerospace Applications* (pp. 109–123). Woodhead Publishing. [\[CrossRef\]](#)
- [6] Pickering, K. L., Beckermann, G. W., Alam, S. N., & Foreman, N. J. (2007). Optimising industrial hemp fibre for composites. *Composites Part A: Applied Science and Manufacturing*, 38(2), 461–468. [\[CrossRef\]](#)
- [7] Wang, Y. N., Weng, Y. X., & Wang, L. (2014). Characterization of interfacial compatibility of polylactic acid and bamboo flour (PLA/BF) in biocomposites. *Polymer Testing*, 36, 119–125. [\[CrossRef\]](#)
- [8] Kozłowski, R., & Władysław-Przybylak, M. (2008). Flammability and fire resistance of composites rein-

- forced by natural fibers. *Polymers for Advanced Technologies*, 19(6), 446–453. [CrossRef]
- [9] Mohanty, A. K., Misra, M., & Drzal, L. T. (Eds.). (2005). *Natural fibers, biopolymers, and biocomposites*. CRC Press.
- [10] Guna, V., Ilangovan, M., Ananthaprasad, M. G., & Reddy, N. (2018). Hybrid biocomposites. *Polymer Composites*, 39, E30–E54. [CrossRef]
- [11] Mitra, B. C. (2014). Environment friendly composite materials: biocomposites and green composites. *Defence Science Journal*, 64(3), 244–261. [CrossRef]
- [12] La Mantia, F. P., & Morreale, M. (2011). Green composites: A brief review. *Composites Part A: Applied Science and Manufacturing*, 42(6), 579–588. [CrossRef]
- [13] Ray, D. (Ed.). (2017). *Biocomposites for high-performance applications: Current barriers and future needs towards industrial development*. Woodhead Publishing.
- [14] Campilho, R. D. (Ed.). (2015). *Natural fiber composites*. CRC Press. [CrossRef]
- [15] Majeed, K., Jawaid, M., Hassan, A., Abu Bakar, H., Abdul Khalil, P. S., Salema, A. A., & Inuwa, I. (2013). Potential materials for food packaging from nanoclay/natural fibres filled hybrid composites. *Materials & Design*, 46, 391–410. [CrossRef]
- [16] Barbero, E. J. (2017). *Introduction to composite materials design*. CRC Press.
- [17] Townsend, T. (2020). World natural fibre production and employment. In *Handbook of Natural Fibres* (pp. 15–36). Woodhead Publishing. [CrossRef]
- [18] Wei, L., & McDonald, A. G. (2016). A review on grafting of biofibers for biocomposites. *Materials*, 9(4), Article 303. [CrossRef]
- [19] Ilyas, R. A., Sapuan, S. M., Kadier, A., Kalil, M. S., Ibrahim, R., Atikah, M. S. N., & Ibrahim, M. I. J. (2020). Properties and characterization of PLA, PHA, and other types of biopolymer composites. In *Advanced processing, properties, and applications of starch and other bio-based polymers* (pp. 111–138). Elsevier. [CrossRef]
- [20] Faruk, O., Bledzki, A. K., Fink, H. P., & Sain, M. (2012). Biocomposites reinforced with natural fibers: 2000–2010. *Progress in Polymer Science*, 37(11), 1552–1596. [CrossRef]
- [21] Nick, A., Becker, U., & Thoma, W. (2002). Improved acoustic behavior of interior parts of renewable resources in the automotive industry. *Journal of Polymers & the Environment*, 10(3), 115–118. [CrossRef]
- [22] Yilmaz, N. D., Powell, N. B., Banks-Lee, P., & Michielsen, S. (2013). Multi-fiber needle-punched non-woven composites: effects of heat treatment on sound absorption performance. *Journal of Industrial Textiles*, 43(2), 231–246. [CrossRef]
- [23] Oldham, D. J., Egan, C. A., & Cookson, R. D. (2011). Sustainable acoustic absorbers from the biomass. *Applied Acoustics*, 72(6), 350–363. [CrossRef]
- [24] Corbin, A. C., Soulat, D., Ferreira, M., Labanieh, A. R., Gabrion, X., Malécot, P., & Placet, V. (2020). Towards hemp fabrics for high-performance composites: Influence of weave pattern and features. *Composites Part B: Engineering*, 181, Article 107582. [CrossRef]
- [25] Bonnafous, C., Touchard, F., & Chocinski-Arnault, L. (2011). Damage mechanisms in hemp-fibre woven fabric composite, and comparison with glass-fibre composite. *Polymers and Polymer Composites*, 19(7), 543–552. [CrossRef]
- [26] Hasan, K. F., Horváth, P. G., Zsolt, K., Kóczán, Z., Bak, M., Horváth, A., & Alpár, T. (2021). Hemp/glass woven fabric reinforced laminated nanocomposites via in-situ synthesized silver nanoparticles from *Tilia cordata* leaf extract. *Composite Interfaces*, 29(5), 503–521. [CrossRef]
- [27] Berhanu Yallew, T., Kumar, P., & Singh, I. (2015). Sliding behaviour of woven industrial hemp fabric reinforced thermoplastic polymer composites. *International Journal of Plastics Technology*, 19(2), 347–362. [CrossRef]
- [28] Baghaei, B., & Skrifvars, M. (2016). Characterisation of polylactic acid biocomposites made from prepregs composed of woven polylactic acid/hemp-lyocell hybrid yarn fabrics. *Composites Part A: Applied Science and Manufacturing*, 81, 139–144. [CrossRef]
- [29] Hargitai, H., Rácz, I., & Anandjiwala, R. D. (2008). Development of hemp fiber reinforced polypropylene composites. *Journal of Thermoplastic Composite Materials*, 21(2), 165–174. [CrossRef]
- [30] Shahzad, A. (2013). A study in physical and mechanical properties of hemp fibres. *Advances in Materials Science and Engineering*, 2013, Article 325085. [CrossRef]
- [31] Stelea, L., Filip, I., Lisa, G., Ichim, M., Drobotă, M., Sava, C., & Mureşan, A. (2022). Characterisation of hemp fibres reinforced composites using thermoplastic polymers as matrices. *Polymers*, 14(3), Article 481. [CrossRef]
- [32] Chen, Y., Sun, L., Negulescu, I., Wu, Q., & Henderson, G. (2007). Comparative study of hemp fiber for non-woven composites. *Journal of Industrial Hemp*, 12(1), 27–45. [CrossRef]
- [33] Stapulionienė, R., Vaitkus, S., & Vėjelis, S. (2017). Investigation of mechanical properties of composite made from hemp and polylactide. In *Key Engineering Materials* (Vol. 721, pp. 63–67). Trans Tech Publications Ltd. [CrossRef]
- [34] Rasyid, M. A., Salim, M. S., Akil, H. M., Karger-Koc-

- sis, J., & Ishak, Z. M. (2019). Non-woven flax fibre reinforced acrylic based polyester composites: the effect of sodium silicate on mechanical, flammability and acoustic properties. *Express Polymer Letters*, 13(6), 553–564. [CrossRef]
- [35] Velayutham, T., Manickam, R. K., Sundararajan, P., Chung, I. M., & Prabakaran, M. (2021). A study on the effect of natural regenerated and synthetic non-woven fabric properties on acoustic applications. *Journal of Natural Fibers*, [E pub ahead of print] doi: 10.1080/15440478.2021.1929645 [Cross-Ref]
- [36] Muthukumar, N., Thilagavathi, G., Neelakrishnan, S., & Poovaragan, P. T. (2019). Sound and thermal insulation properties of flax/low melt PET needle punched non-wovens. *Journal of Natural Fibers*, 16(2), 245–252. [CrossRef]
- [37] Pil, L., Bensadoun, F., Pariset, J., & Verpoest, I. (2016). Why are designers fascinated by flax and hemp fibre composites? *Composites Part A: Applied Science and Manufacturing*, 83, 193–205. [CrossRef]
- [38] Shahria, S. (2019). Fabrication and property evaluation of hemp–flax fiber reinforced hybrid composite. *Cellulose*, 7(2), 17–23. [CrossRef]
- [39] Maity, S., Gon, D. P., & Paul, P. (2014). A review of flax non-wovens: Manufacturing, properties, and applications. *Journal of Natural Fibers*, 11(4), 365–390. [CrossRef]
- [40] John, M. J., & Anandjiwala, R. D. (2009). Chemical modification of flax reinforced polypropylene composites. *Composites Part A: Applied Science and Manufacturing*, 40(4), 442–448. [CrossRef]
- [41] Omrani, F., Wang, P., Soulat, D., Ferreira, M., & Ouagne, P. (2017). Analysis of the deformability of flax-fibre non-woven fabrics during manufacturing. *Composites Part B: Engineering*, 116, 471–485. [Cross-Ref]
- [42] Bachmann, J., Wiedemann, M., & Wierach, P. (2018). Flexural mechanical properties of hybrid epoxy composites reinforced with non-woven made of flax fibres and recycled carbon fibres. *Aerospace*, 5(4), Article 107. [CrossRef]
- [43] Alimuzzaman, S., Gong, R. H., & Akonda, M. (2013). Non-woven polylactic acid and flax biocomposites. *Polymer Composites*, 34(10), 1611–1619. [CrossRef]
- [44] Claramunt, J., Ventura, H., Fernández-Carrasco, L. J., & Ardanuy, M. (2017). Tensile and flexural properties of cement composites reinforced with flax nonwoven fabrics. *Materials*, 10(2), Article 215. [CrossRef]
- [45] Gonzalez-Lopez, L., Claramunt, J., Hsieh, Y. L., Ventura, H., & Ardanuy, M. (2020). Surface modification of flax non-wovens for the development of sustainable, high performance, and durable calcium aluminate cement composites. *Composites Part B: Engineering*, 191, Article 107955. [CrossRef]
- [46] Phongam, N., Dangtungee, R., & Siengchin, S. (2015). Comparative studies on the mechanical properties of nonwoven and woven-flax-fiber-reinforced Poly (butylene adipate-co-terephthalate)-based composite laminates. *Mechanics of Composite Materials*, 51(1), 17–24. [CrossRef]
- [47] Awais, H., Nawab, Y., Anjang, A., Akil, H. M., & Abidin, M. (2020). Mechanical properties of continuous natural fibres (jute, hemp, flax) reinforced polypropylene composites modified with hollow glass microspheres. *Fibers and Polymers*, 21(9), 2076–2083. [CrossRef]
- [48] Goutianos, S., Peijs, T., Nystrom, B., & Skrifvars, M. (2006). Development of flax fibre based textile reinforcements for composite applications. *Applied Composite Materials*, 13(4), 199–215. [CrossRef]
- [49] Charlet, K., Jernot, J. P., Gomina, M., Bizet, L., & Bréard, J. (2010). Mechanical properties of flax fibers and of the derived unidirectional composites. *Journal of Composite Materials*, 44(24), 2887–2896. [CrossRef]
- [50] Couture, A., Lebrun, G., & Laperrière, L. (2016). Mechanical properties of polylactic acid (PLA) composites reinforced with unidirectional flax and flax-paper layers. *Composite Structures*, 154, 286–295. [CrossRef]
- [51] Tanguy, M., Bourmaud, A., Beaugrand, J., Gaudry, T., & Baley, C. (2018). Polypropylene reinforcement with flax or jute fibre; Influence of microstructure and constituents properties on the performance of composite. *Composites Part B: Engineering*, 139, 64–74. [CrossRef]
- [52] Mak, K., & Fam, A. (2020). The effect of wet-dry cycles on tensile properties of unidirectional flax fiber reinforced polymers. *Composites Part B: Engineering*, 183, Article 107645. [CrossRef]
- [53] Loong, M. L., & Cree, D. (2018). Enhancement of mechanical properties of bio-resin epoxy/flax fiber composites using acetic anhydride. *Journal of Polymers and the Environment*, 26(1), 224–234. [CrossRef]
- [54] Alzeer, M., & MacKenzie, K. (2013). Synthesis and mechanical properties of novel composites of inorganic polymers (geopolymers) with unidirectional natural flax fibres (phormium tenax). *Applied Clay Science*, 75, 148–152. [CrossRef]
- [55] Zhang, Y., Li, Y., Ma, H., & Yu, T. (2013). Tensile and interfacial properties of unidirectional flax/glass fiber reinforced hybrid composites. *Composites Science and Technology*, 88, 172–177. [CrossRef]
- [56] Sarasini, F., Tirillò, J., D'Altilla, S., Valente, T., Santulli, C., Touchard, F., & Gaudenzi, P. (2016). Damage tolerance of carbon/flax hybrid composites sub-

- jected to low velocity impact. *Composites Part B: Engineering*, 91, 144–153. [CrossRef]
- [57] Chaudhary, V., Bajpai, P. K., & Maheshwari, S. (2018). Studies on mechanical and morphological characterization of developed jute/hemp/flax reinforced hybrid composites for structural applications. *Journal of Natural Fibers*, 15(1), 80–97. [CrossRef]
- [58] Boccarusso, L., De Fazio, D., & Durante, M. (2021). Production of PP composites reinforced with flax and hemp woven mesh fabrics via compression molding. *Inventions*, 7(1), Article 5. [CrossRef]
- [59] Shahzad, A. (2011). Impact and fatigue properties of hemp–glass fiber hybrid biocomposites. *Journal of Reinforced Plastics and Composites*, 30(16), 1389–1398. [CrossRef]
- [60] Munoz, E., & García-Manrique, J. A. (2015). Water absorption behaviour and its effect on the mechanical properties of flax fibre reinforced bioepoxy composites. *International Journal of Polymer Science*, 2015, Article 390275.
- [61] Manfredi, L. B., Rodríguez, E. S., Wladyka-Przybylak, M., & Vázquez, A. (2006). Thermal degradation and fire resistance of unsaturated polyester, modified acrylic resins and their composites with natural fibres. *Polymer Degradation and Stability*, 91(2), 255–261. [CrossRef]
- [62] Kumar, A. P., Singh, R. P., & Sarwade, B. D. (2005). Degradability of composites, prepared from ethylene–propylene copolymer and jute fiber under accelerated aging and biotic environments. *Materials Chemistry and Physics*, 92(2–3), 458–469. [CrossRef]
- [63] Sarkar, S., & Adhikari, B. (2001). Jute felt composite from lignin modified phenolic resin. *Polymer Composites*, 22(4), 518–527. [CrossRef]
- [64] Das, B. K., Ray, P. K., & Chakravarty, A. C. (1983). 37—The properties of jute fibres at different stages of plant growth. *Journal of the Textile Institute*, 74(6), 367–373. [CrossRef]
- [65] Wu, Y., Xia, C., Cai, L., Garcia, A. C., & Shi, S. Q. (2018). Development of natural fiber-reinforced composite with comparable mechanical properties and reduced energy consumption and environmental impacts for replacing automotive glass-fiber sheet molding compound. *Journal of Cleaner Production*, 184, 92–100. [CrossRef]
- [66] Suizu, N., Uno, T., Goda, K., & Ohgi, J. (2009). Tensile and impact properties of fully green composites reinforced with mercerized ramie fibers. *Journal of Materials Science*, 44(10), 2477–2482. [CrossRef]
- [67] Qiu, R., Ren, X., Fifield, L. S., Simmons, K. L., & Li, K. (2011). Hemp-fiber-reinforced unsaturated polyester composites: Optimization of processing and improvement of interfacial adhesion. *Journal of Applied Polymer Science*, 121(2), 862–868. [CrossRef]
- [68] Lu, N., Oza, S., & Ferguson, I. (2012). Effect of alkali and silane treatment on the thermal stability of hemp fibers as reinforcement in composite structures. *In Advanced Materials Research* (Vol. 415, pp. 666–670). Trans Tech Publications Ltd. [CrossRef]
- [69] Oh, J. T., Hong, J. H., Ahn, Y., & Kim, H. (2012). Reliability improvement of hemp based bio-composite by surface modification. *Fibers and Polymers*, 13(6), 735–739. [CrossRef]
- [70] Islam, M. S., Pickering, K. L., & Foreman, N. J. (2011). Influence of alkali fiber treatment and fiber processing on the mechanical properties of hemp/epoxy composites. *Journal of Applied Polymer Science*, 119(6), 3696–3707. [CrossRef]
- [71] Väisänen, T., Batello, P., Lappalainen, R., & Tomppo, L. (2018). Modification of hemp fibers (*Cannabis Sativa L.*) for composite applications. *Industrial Crops and Products*, 111, 422–429. [CrossRef]
- [72] Sullins, T., Pillay, S., Komus, A., & Ning, H. (2017). Hemp fiber reinforced polypropylene composites: The effects of material treatments. *Composites Part B: Engineering*, 114, 15–22. [CrossRef]
- [73] Bledzki, A. K., Reihmane, S. A., & Gassan, J. (1998). Thermoplastics reinforced with wood fillers: a literature review. *Polymer-Plastics Technology and Engineering*, 37(4), 451–468. [CrossRef]
- [74] Schirp, A., & Stender, J. (2010). Properties of extruded wood-plastic composites based on refiner wood fibres (TMP fibres) and hemp fibres. *European Journal of Wood and Wood Products*, 68(2), 219–231. [CrossRef]
- [75] Niu, P., Liu, B., Wei, X., Wang, X., & Yang, J. (2011). Study on mechanical properties and thermal stability of polypropylene/hemp fiber composites. *Journal of Reinforced Plastics and Composites*, 30(1), 36–44. [CrossRef]
- [76] Merotte, J., Le Duigou, A., Kervoelen, A., Bourmaud, A., Behloul, K., Sire, O., & Baley, C. (2018). Flax and hemp non-woven composites: The contribution of interfacial bonding to improving tensile properties. *Polymer Testing*, 66, 303–311. [CrossRef]
- [77] Yan, Z. L., Wang, H., Lau, K. T., Pather, S., Zhang, J. C., Lin, G., & Ding, Y. (2013). Reinforcement of polypropylene with hemp fibres. *Composites Part B: Engineering*, 46, 221–226. [CrossRef]
- [78] Talla, A. F., Mfoumou, E., Jeson, S., Pagé, J. S. Y. D., & Erchiqui, F. (2013). Mechanical and structural properties of a novel melt processed PET–hemp composite: Influence of additives and fibers concentration. *Journal of Reinforced Plastics and Composites*, 32(20), 1526–1533. [CrossRef]
- [79] Brostow, W., & Hagg Lobland, H. E. (2010). Brittleness of materials: implications for composites and a relation to impact strength. *Journal of Materials Sci-*

- ence, 45(1), 242–250. [CrossRef]
- [80] Glória, G. O., Margem, F. M., Ribeiro, C. G. D., Moraes, Y. M. D., Cruz, R. B. D., Silva, F. D. A., & Monteiro, S. N. (2015). Charpy impact tests of epoxy composites reinforced with giant bamboo fibers. *Materials Research*, 18, 178–184. [CrossRef]
- [81] Assis, F. S., Monteiro, S. N., Margem, F. M., & Loiola, R. L. (2014). Charpy toughness behavior of continuous banana fiber reinforced epoxy matrix composites. *Characterization of Minerals, Metals, and Materials*, 2014, 499–506. [CrossRef]
- [82] Pereira, A. C., Monteiro, S. N., de Assis, F. S., Margem, F. M., da Luz, F. S., & de Oliveira Braga, F. (2017). Charpy impact tenacity of epoxy matrix composites reinforced with aligned jute fibers. *Journal of Materials Research and Technology*, 6(4), 312–316. [CrossRef]
- [83] Reddy, P. V., Reddy, R. S., Rajendra Prasad, P., Mohana Krishnudu, D., Reddy, R. M., & Rao, H. R. (2022). Evaluation of mechanical and wear performances of natural fiber reinforced epoxy composites. *Journal of Natural Fibers*, 19(6), 2218–2231. [CrossRef]
- [84] Al-Oqla, F. M. (2021). Flexural characteristics and impact rupture stress investigations of sustainable green olive leaves bio-composite materials. *Journal of Polymers and the Environment*, 29(3), 892–899. [CrossRef]
- [85] Hassan, T., Jamshaid, H., Mishra, R., Khan, M. Q., Petru, M., Novak, J., Choteborsky, R., & Hromasova, M. (2020). Acoustic, mechanical and thermal properties of green composites reinforced with natural fibers waste. *Polymers*, 12(3), Article 654. [CrossRef]
- [86] Liang, Z., Wu, H., Liu, R., & Wu, C. (2021). Preparation of long sisal fiber-reinforced polylactic acid biocomposites with highly improved mechanical performance. *Polymers*, 13(7), Article 1124. [CrossRef]
- [87] Petrucci, R., Santulli, C., Puglia, D., Nisini, E., Sarasini, F., Tirillò, J., & Kenny, J. M. (2015). Impact and post-impact damage characterisation of hybrid composite laminates based on basalt fibres in combination with flax, hemp and glass fibres manufactured by vacuum infusion. *Composites Part B: Engineering*, 69, 507–515. [CrossRef]
- [88] Kong, K., Hejda, M., Young, R. J., & Eichhorn, S. J. (2009). Deformation micromechanics of a model cellulose/glass fibre hybrid composite. *Composites Science and Technology*, 69(13), 2218–2224. [CrossRef]
- [89] Clark, R. A., & Ansell, M. P. (1986). Jute and glass fibre hybrid laminates. *Journal of Materials Science*, 21(1), 269–276. [CrossRef]
- [90] Sanjay, M. R., & Yogesha, B. (2017). Studies on natural/glass fiber reinforced polymer hybrid composites: An evolution. *Materials Today: Proceedings*, 4(2), 2739–2747.
- [91] Das, P. P., & Chaudhary, V. (2021). Moving towards the era of bio fibre based polymer composites. *Cleaner Engineering and Technology*, 4, Article 100182. [CrossRef]
- [92] Rafiee, K., Schritt, H., Pleissner, D., Kaur, G., & Brar, S. K. (2021). Biodegradable green composites: It's never too late to mend. *Current Opinion in Green and Sustainable Chemistry*, 30, Article 100482. [CrossRef]
- [93] Vázquez-Núñez, E., AVECILLA-Ramírez, A. M., Vergara-Porras, B., & López-Cuellar, M. D. R. (2021). Green composites and their contribution toward sustainability: a review. *Polymers and Polymer Composites*, 29(Suppl 9), S1588–S1608. [CrossRef]
- [94] Koppaathy, S. D. S., & Netravali, A. N. (2021). Green composites for structural applications. *Composites Part C: Open Access*, 6, Article 100169. [CrossRef]
- [95] Ilyas, R. A., Zuhri, M. Y. M., Aisyah, H. A., Asyraf, M. R. M., Hassan, S. A., Zainudin, E. S., ... & Sari, N. H. (2022). Natural fiber-reinforced polylactic acid, polylactic acid blends and their composites for advanced applications. *Polymers (Basel)*, 14(1), Article 202. [CrossRef]
- [96] Mann, G. S., Singh, L. P., Kumar, P., & Singh, S. (2020). Green composites: A review of processing technologies and recent applications. *Journal of Thermoplastic Composite Materials*, 33(8), 1145–1171. [CrossRef]
- [97] Scaffaro, R., Maio, A., Gulino, E. F., Alaimo, G., & Morreale, M. (2021). Green composites based on PLA and agricultural or marine waste prepared by FDM. *Polymers*, 13(9), Article 1361. [CrossRef]
- [98] Leow, Y., Yew, P. Y. M., Chee, P. L., Loh, X. J., & Kai, D. (2021). Recycling of spent coffee grounds for useful extracts and green composites. *RSC Advances*, 11(5), 2682–2692. [CrossRef]
- [99] Kamble, Z., Behera, B. K., Mishra, R., & Behera, P. K. (2021). Influence of cellulosic and non-cellulosic particle fillers on mechanical, dynamic mechanical, and thermogravimetric properties of waste cotton fibre reinforced green composites. *Composites Part B: Engineering*, 207, Article108595. [CrossRef]
- [100] Gholampour, A., & Ozbakkaloglu, T. (2020). A review of natural fiber composites: Properties, modification and processing techniques, characterization, applications. *Journal of Materials Science*, 55(3), 829–892. [CrossRef]
- [101] Nawab, Y., Kashif, M., Asghar, M. A., Asghar, A., Umair, M., Shaker, K., & Zeeshan, M. (2018). Development & characterization of green composites using novel 3D woven preforms. *Applied Composite Materials*, 25(4), 747–759. [CrossRef]
- [102] Stapulionienė, R., Vaitkus, S., & Vėjelis, S. (2017). Investigation of Mechanical Properties of Composite Made from Hemp and Polylactide. *In Key Engi-*

- neering Materials* (Vol. 721, pp. 63-67). Trans Tech Publications Ltd. [\[CrossRef\]](#)
- [103] Song, Y., Liu, J., Chen, S., Zheng, Y., Ruan, S., & Bin, Y. (2013). Mechanical properties of Poly (lactic acid)/hemp fiber composites prepared with a novel method. *Journal of Polymers and the Environment*, 21(4), 1117–1127. [\[CrossRef\]](#)
- [104] Mukherjee, T., & Kao, N. (2011). PLA based biopolymer reinforced with natural fibre: a review. *Journal of Polymers and the Environment*, 19(3), 714–725. [\[CrossRef\]](#)
- [105] Shibata, M., Ozawa, K., Teramoto, N., Yosomiya, R., & Takeishi, H. (2003). Biocomposites made from short abaca fiber and biodegradable polyesters. *Macromolecular Materials and Engineering*, 288(1), 35–43. [\[CrossRef\]](#)